Electron Correlations in the 2D Multilayer Organic Metal κ-(BEDT-TTF)$_2$I$_3$ in Magnetic Fields

Habilitation

submitted by

Dr. Eduard Balthes

3. Physikalisches Institut
Universität Stuttgart
Germany

Preface

This work presents quantum oscillation experiments in quasi-twodimensional multilayer organic metals. They show that low integer Landau level filling factors ν are present in the two-dimensional organic metal κ-(BEDT-TTF)$_2$I$_3$ and give strong indications for the existence of the fractional filling factor ν = ½ in this material. By this the work shows the presence of electron localisation and electron correlation in a bulk metallic two-dimensional system. These effects are found in the normal conducting state of the organic superconductor κ-(BEDT-TTF)$_2$I$_3$.

The revolutionary discovery of the integer as well as the fractional quantum Hall effect in two-dimensional semiconducting single-layer systems invoked, i.a., the questions, whether these effects may also be present in other types of conductors and, especially, whether they may also occur in bulk three-dimensional crystals. Strong efforts were made to produce bilayer two-dimensional semiconductors, to control their interlayer coupling as well as electron tunnelling, to increase step by step the number of involved layers with the aim to realise the quantised Hall effects in 'bulk' multilayer and, finally, in 'infinite-layer' systems. Furthermore strong efforts are made in semiconducting two-dimensional systems to realise carrier densities above 10^{11}/cm^2 with mobilities exceeding 10^7cm^2/Vs.

κ-(BEDT-TTF)$_2$I$_3$ is a metallic compound with a very high electron density of $2*10^{19}$/cm^2 and a very high carrier mobility reaching about $5*10^8$cm^2/Vs. From its structural principle this organic material represents a system of 10^5 coupled metallic multilayers, which can be synthesised in very high purity and can be produced as three-dimensional bulk single crystals. Despite of this, the material shows strongly two-dimensional electronic properties under certain experimental conditions, as found in the frame of this work. In contrast to the characteristic situation in semiconducting two-dimensional systems, where (correlated) electrons move on a single quantised orbit, the strongly correlated carriers in κ-(BEDT-TTF)$_2$I$_3$ move on various quantised orbits with even very different filling factors. These are the main conditions under which the above mentioned filling factors are found in κ-(BEDT-TTF)$_2$I$_3$.

Besides these characteristics, the present two-dimensional organic metal holds a number of further peculiarities, which may represent a challenge for the understanding of possible fractional filling factors and quantum limit in a macroscopic multilayer crystal with two-dimensional electronic properties.

In addition, the present work resumes experiments on the influence of low-dimensionality onto the electronic properties of a number of low-dimensional multilayer organic conductors.

Stuttgart, March 2004 *Eduard Balthes*

——— * ———

dedicated to Beate Baßfeld

Contents

List of Most Important Symbols and Abbreviations

1- ... 3D	one- ... three-dimensional
1- ... 3DES	one- ... three-dimensional electronic system
2DEG	two-dimensional electron gas
a	gauge vector potential
A	vector potential
A_0	scalar potential
A"	curvature of the Fermi surface
A_F	extremal area of the cut of the Fermi surface perpendicular to the magnetic field
A_{Max}, A_{Min}	extremal areas (maximal or minimal) of the Fermi surface
A_n	cross-sectional area of the *n*-th Landau cylinder
A_p	quantum oscillation amplitude of the p^{th} harmonic of the fundamental frequency *F*
B	magnetic field
$\hat{B}$	magnetic field direction
BCS	Bardeen-Cooper-Schrieffer theory for superconductivity
B_{MB}	magnetic breakdown field
B_n	magnetic field for the *n*-th LL
BEDO-TTF	bis(ethylenedioxy)tetrathiafulvalene
BEDT-TTF	bis(ethylenedithio)tetrathiafulvalene (organic electron donor molecule)
BEDT-TSF	bis(ethylenedithio)tetraselena-fulvalene)
α–, β–, κ–(...)	different structural phases of the same stoichiometry
C	weight factor in the CND
CDW	charge-density wave
CND	'coupled network description' of magnetic breakdown phenomena
CF	composite fermion
CSLG	Chern-Simons-Landau-Ginzburg description
CT	charge-transfer (salts)
D	Landau level degeneration factor
D	density of states
DEs	(anomalous) damping effects of quantum oscillation amplitudes
dHvA	de Haas-van Alphen
DMET	dimethyl-ethylenedithio-diselenedithiafulvalene
DOS	density of states
DP	Dingle plot

EC	electron correlation
E_C	Coulomb energy
EDT-TTF	ethylenedithiotetrathiafulvalene
E_F	Fermi energy
E_g	gap energy
EL	electron localisation
E_n	energetic eigenstate to the quantum number *n*
ES	edge states
E_Z	Zeeman energy
F	fundamental frequency of a quantum oscillation
$\bar{F}$	average quantum oscillation frequency
FBZ	first Brillouin zone
F_j	quantum oscillation frequencies corresponding to different closed orbits in *k*-space
FQHE	fractional quantum Hall effect
FS	Fermi surface
g	g-value of electrons
h*; *ħ	Planck constat; 'Dirac *h*'
IQHE	integer quantum Hall effect
k; $\mathbf{k}_x$, $\mathbf{k}_y$, $\mathbf{k}_z$	wave vector; in components
$\mathbf{k}_B$	Boltzmann constant
$\mathbf{k}_F$	Fermi wave vector
$\mathbf{K}^s$	Knight shift
L	system size
l_0	magnetic length, cyclotron radius (definition for semiconductors) ≡ average distance between two electrons at a given magnetic field
LC	Landau cylinder
$L_{d,//}$	drift length (intraplane)
LK	Lifshitz-Kosevich theory
LL	Landau level
L_{QP}	size of a quasiparticle ≡ localisation length
$\mathbf{m}_e$	free electron mass
$\mathbf{m}_{eff}$	effective electron mass
m*, $\mathbf{m}_j$*	reduced effective electron mass ($m^* = m_{eff} / m_e$); for the QO frequency F_j
M; $\tilde{M}$	magnetisation; oscillating
MB	magnetic breakdown
MBE	molecular beam epitaxy
MI	magnetic interaction

MOSFET	metal-oxide-semiconductor field effect transistor
MDT-TTF	methylenedithiotetrathiafulvalene
n	Landau level index; Landau level filling factor (spin degenerate)
$\mathbf{n_{Fj}}$	ibid., for different quantum oscillation frequencies F_j
$\mathbf{n_e}$	electron concentration
$\mathbf{N_e}$	total number of carriers
OCP	one-component-plasma
p	harmonic index of an oscillation frequency; amplitude for magnetic breakdown
$\wp$	statistical phase factor
P	flux probability for magnetic breakdown
q	amplitude for Bragg reflection
Q	flux probability for Bragg reflection
Q1D; Q2D	quasi-one/twodimensional
QI	quantum interference
QL	quantum limit
QO	magneto-quantum oscillation
$\mathbf{R_C}$	cyclotron radius (definition for free electrons; metals) ≡ localisation length
$\mathbf{R_H = R_{xy}}$	Hall resistance
$\mathbf{R_K}$	von Klitzing constant
$\mathbf{R_T}$, $\mathbf{R_D}$, $\mathbf{R_S}$, $\mathbf{R_{MB}}$	amplitude reduction factors (considering temperature, Dingle temperature, spin, magnetic breakdown)
$\mathbf{R_{xx}}$	diagonal resistance
S	spin splitting factor
SdH	Shubnikov-de Haas
SDW	spin-density wave
$t_\perp; t_{//}$	electronic transfer integrals perpendicular and parallel to the conducting planes
TCNQ	tetracyano-p-quinodimethane
$\mathbf{T_D}$	Dingle temperature
TMTSF	tetramethyltetraselenafulvalene
TLL	Tomonaga-Luttinger liquid
TTF	tetrathiafulvalene
TSF	tetraselenafulvalene
$\mathbf{U_H}$	Hall voltage
U(**r**)	potential
$\mathbf{v_F}$	Fermi velocity
$\mathbf{V_g}$	gate voltage
$\mathbf{z_j}$	complex coordinate
$\boldsymbol{\gamma}$	Onsager phase factor ≡ Maslov constant
$\boldsymbol{\Delta}$	energetic gap, energy difference
$\boldsymbol{\varepsilon_0}$	vacuum dielectric constant
$\boldsymbol{\varepsilon_r}$	dielectric constant in material
Φ_m	magnetic flux at filling factor $1/m$
Φ_0	magnetic flux quantum
Θ	angle between the magnetic field orientation and the normal to conducting planes
$\mu, \tilde{\mu}, \tilde{\mu}_{Fj}$	chemical potential; oscillating, with the quantum oscillation frequency F_j
μ_e	electron mobility
μ^R, μ^L	chemical potential at the sample edges
$\boldsymbol{\nu}$	Landau level filling factor (considering Zeeman spin splitting)
ν_{Lj}	dto., for a single layer L_j
ν_{tot}	dto., for a complete multilayer system
$\boldsymbol{\rho}$	resistivity
$\boldsymbol{\rho_{xx}}$	diagonal resistivity
$\boldsymbol{\rho}_{xy}$	Hall resistivity
$\boldsymbol{\sigma}$	conductivity
$\boldsymbol{\sigma_{xx}}$	diagonal conductivity
$\boldsymbol{\sigma}_{xy}$	Hall conductivity
$\boldsymbol{\tau}$	average carrier scattering time
$\boldsymbol{\Phi}, \boldsymbol{\Phi}_0$	magnetic flux; quantised
$\boldsymbol{\omega_C}$	cyclotron frequency
$\Omega; \widetilde{\Omega}$	thermodynamic potential; oscillating
$\boldsymbol{\xi}$	localisation length
$\boldsymbol{\Psi}$	wave function
$\boldsymbol{\nabla}$	differential operator

1. Introduction

The start for the development of organic conductors and superconductors may be dated to 1954, when *Akamatu et al.* realised a conductivity of $\sigma \approx 0.1 \mathrm{Scm}^{-1}$ in a perylene-bromine salt [1,2]. With that synthesis of the first conducting organic material without any metal atoms included, the class of '*synthetic metals*' was introduced. The next great progress was made by the synthesis of the electron acceptor TCNQ [3,4] and the electron donor TTF (see Fig. 1.1, also for the abbreviations used in the following) [5]. From these two constituents a TTF-TCNQ charge-transfer (CT) complex was synthesised by a diffusion method and it showed anisotropic, i.e., quasi-onedimensional (Q1D) metallic properties [6,7]. This material exhibits a conductivity $\sigma \approx 10^4 \mathrm{Scm}^{-1}$ at 60K (comp. with Cu: $\sigma \approx 10^6 \mathrm{Scm}^{-1}$ at 300K). Below 60K, however, the TTF-TCNQ salt undergoes a phase transition to a Peierls insulator [8].
As pointed out by *Fröhlich*, a 1D metal is on principle unstable against lattice distortion, so that a concomitant gap may open at the Fermi level [9] and therefore a variety of very different ground states are possible: **a)** In the presence of interactions, the aforementioned instability may result in a charge-density or spin density wave (CDW or SDW), respectively [8,10]. These collective phenomena indeed may describe the ground state of several Q1D organic conductors [11]. **b)** Alternatively to the density-wave state even a superconducting transition may occur [12]. **c)** In the presence of disorder the carriers may localise in a so-called Mott-insulating phase [13]. **d)** As soon as strong electron interactions are present in a strictly 1D system, the carriers may no longer obey Fermi liquid theory [14,15], but instead a so-called Tomonaga-Luttinger liquid [16,17] may develop. Indeed, the subsequently synthesised Q1D organics show a variety of different ground states. These are determined not only by the above mentioned conditions a) - d), but also by the 'design' of donor and acceptor molecules and furthermore by external parameters, i.e., temperature, pressure and magnetic fields (see, e.g., [18,19,20,21] for density-wave states, e.g. [22,23,24,25] for non-Fermi-liquid behaviour; cons. Refs. therein).
The synthesis of Q1D organics was extremely pushed by the vision of room temperature superconductivity based on an idea of *Little* [26,27], which is an extension of the BCS theory for conventional superconductivity developed by *Bardeen*, *Cooper* and *Schrieffer* [28]. Little's ideas suggests that a pairing of electrons might be possible via their coupling to highly polarisable side-chains in a polymeric material. Since the characteristic excitation energy of such an 'excitonic' mechanism exceeds that for lattice vibrations by about two orders of magnitude, a tremendous increase of the superconducting transition temperatures T_c seemed to be in prospect. In 1979 the first Q1D organic superconductor $(TMTSF)_2PF_6$ was presented, which belongs to the so-called *Bechgaard* salts based on the planar donor molecule TMTSF (see Fig. 1.1) [29] and is synthesised by electrocrystallisation. This material with a T_c = 0.9K needs application of pressures of about 6.5kbar to suppress an insulating transition at about 12K, which otherwise would result into a SDW state [30]. The subsequent efforts led to a number of organic superconductors by replacing the anion PF_6 by SbF_6, AsF_6, TaF_6, ReO_4, FSO_3, and ClO_4. However from these materials only the ClO_4 salt ($T_c \approx 1$K) is an ambient pressure superconductor [31] (for an insight to the development of organic superconductors see, e.g., [30,32,33,34,18,35,36,37,25]). Subsequent pressure studies showed that the superconducting state in these materials adjoins an insulating SDW state (see, e.g., [18]).

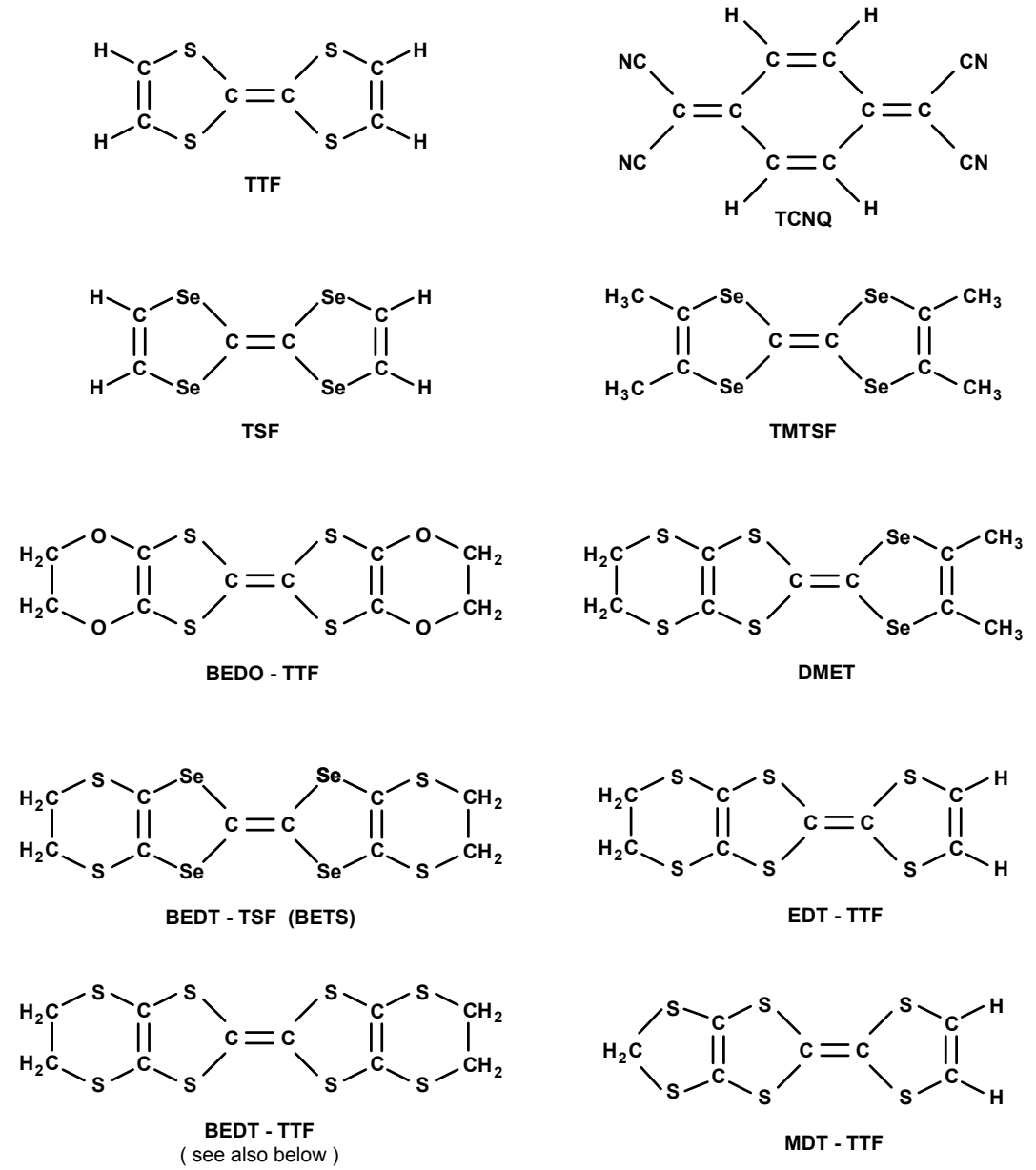

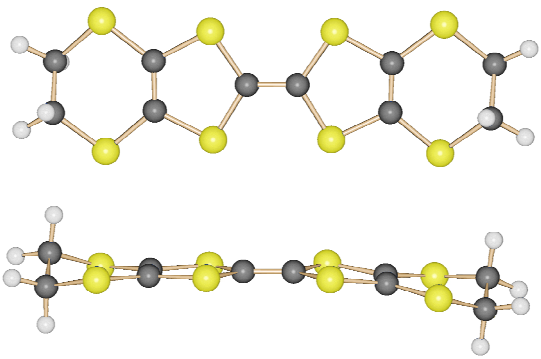

Fig. 1.1: Selection of most important organic constituents in the history of organic conductors with the following abbreviations:

TTF	tetrathiafulvalene
TCNQ	tetracyano-p-quinodimethane
TSF	tetraselenafulvalene
TMTSF	tetramethyltetraselenafulvalene
BEDO-TTF	bis(ethylenedioxi)tetrathiafulvalene
DMET	dimethyl-ethylenedithio-diselenedithiafulvalene
BETS-TTF	bis(ethylenediselena)-tetrathiafulvalene
BEDT-TTF	bis(ethylenedithio)tetrathiafulvalene
EDT-TTF	ethylenedithiotetrathiafulvalene
MDT-TTF	methylenedithiotetrathiafulvalene

However, it turned out that the superconducting transition temperatures in the Q1D TMTSF salts remained limited to $\lesssim$ 3K and that the pairing mechanism is most likely different from that proposed by Little.
Especially in order to enhance T_c, but also to avoid the 1D Peierls instability, strong efforts were made to enhance the dimensionality of the systems from Q1D to Q2D electronic systems. This was realised during the late 1970's and 80's by the 'design' of nonplanar donors, reduction of the molecular weight, widening of the lattice constants and also by the synthesis of various donors and acceptors which allow a reduction of disorder during electrocrystallisation. The further development of these low-dimensional conductors and superconductors in the following decades is based on the characteristic that this class of CT complexes crystallises in *alternating sheets* of organic donor monolayers separated by acceptor monolayers[1]. By the electrocrystallisation process materials can be synthesised, which on the one hand yield 3D bulk 10^5-layer single crystals (with even up to 0.5-1mm thickness), but on the other hand show *low*-dimensional electronic properties.

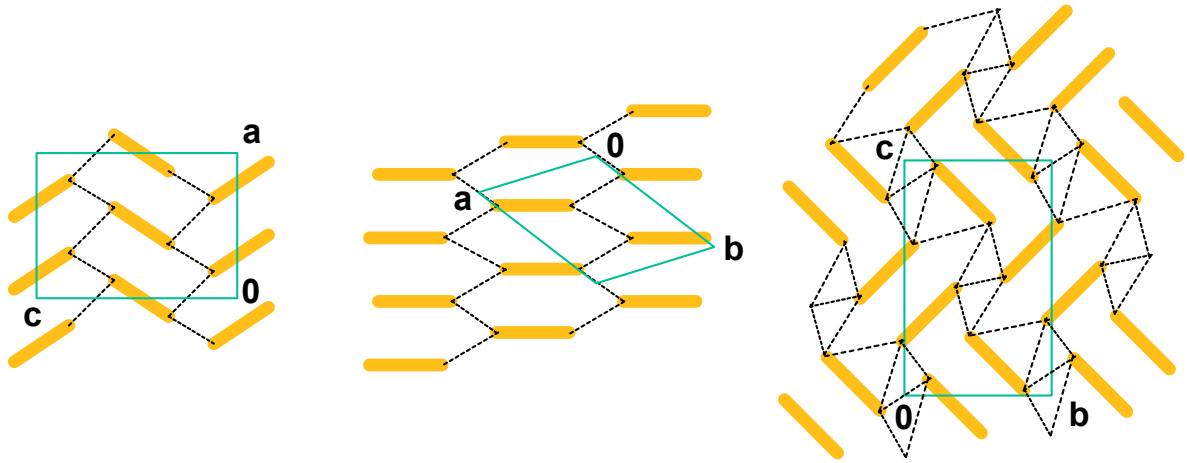

α-structure (Q2D) | β-structure (Q2D) | κ-structure (pronounced ... strongly 2D)

Fig. 1.2: Schematic illustration of three of the most represented structures (α, β and κ) of low-dimensional organic conductors including their unit cells. Top view on a single conducting layer (the acceptor layers are skipped for clarity). Thick orange lines symbolise donor molecules in a view along the central C = C bond (comp. Fig. 1.1), so that these molecules stand upright out of the plane. Dashed lines indicate the (simplified) π-orbital overlap, whose network hints to the main orientation of electronic transport. This results in quasi-2D (**left** and **centre**) or, more or less pronounced 2D transport (**right**).

These properties are determined a priori by 'internal' parameters, as, e.g. **i)** the charge-transfer between donor and acceptor molecules and **ii)** the allocation pattern of the donors within their successive layers, including dimerisation effects (see. Fig. 1.2). Both these conditions determine the conduction mechanism by the band filling. The latter circumstance is of additional importance, since the distances of the outer atoms of neighbouring donor molecules may be less than the van der Waals radii (of 3.6 - 4Å) [2], so that a π-orbital overlap enables an electronic transport within this so-called conducting plane. Thus the allocation pattern of donor molecules prescribe the possible *network of orbital overlap* and, in consequence, the *dimensionality* of in-plane electronic transport. Here the

[1] Indeed, within the organic conductors the *organic* constituents of these CT complexes play in general the role of a *donor* and, moreover, in most cases the *counter ions* are *inorganic*.
[2] The van der Waals radii depend on the atoms involved.

separating (low-conducting) acceptor layer comes into play and its influence on the interlayer component of transport determines the resulting dimensionality of electronic transport in the bulk single crystal. By a variation of donors, acceptors as well as their combinations, a wide variety of Q1D, Q2D and, in rare cases even strongly two-dimensional (2D) organic conductors were synthesised in the last decades. Figure 1.1 shows a selection of the most important constituents from a meanwhile huge number of organic donors. The variety of different structures are distinguished by a prefix, i.e., α-, β-, κ-, λ-, Θ-, ... where the first three are most represented to date (see Fig. 1.2). In general α-phases show Q2D behaviour with clear influences of one-dimensionality, β-phases show Q2D, whereas κ-phases exhibit more or less pronounced 2D electronic behaviour.

One of the most successful donors in the production of meanwhile more than 60 organic superconductors [34,38,39,35,36,25] is BEDT-TTF, which was first synthesised by *Mizuno et al.* ([40,41], see Fig. 1.1). The first BEDT-TTF-based organic superconductor was $(BEDT\text{-}TTF)_2ReO_4$ ($T_c \approx 2K$ at 4.5kbar [42]). It was the start of a series of meanwhile more than 40 BEDT-TTF-based superconductors, from which the κ-structure $(BEDT\text{-}TTF)_2X$-salts held for a long time the highest superconducting transition temperatures, i.e., $T_c \approx 10.4K$ for $X = Cu(NSC)_2$ [43,44], $T_c = 11.6K$ for $X = Cu[N(CN)_2]Br$ [45] and $T_c = 12.8K$ for $Cu[N(CN)_2]Cl$ at 0.3kbar [46]. This highest T_c was recently overcome by β'-$(BEDT\text{-}TTF)_2ICl_2$ with $T_c \approx 13.5K$, however at 82kbar [47]. Furthermore a number of derivates of BEDT-TTF have been synthesised, as, e.g., DMET, MDT-TTF, BEDO-TTF, BEDT-TSF and EDT-TTF (see Fig. 1.1), whose superconducting CT salts, however, have in general lower T_c than the BEDT-TTF-based superconductors [48,49,50,51,52,53,37,25].

In these layered organic CT salts the bulk superconducting state is established by a tunnelling of Cooper pairs via the intrinsic Josephson effect (see, e.g., Refs. [54,55,56]). The vortex-state properties were found to be considerably different from those of the so-called Abrikosov vortex lattice, including, e.g., lattice melting phenomena and even new thermodynamic phases such as vortex-glass states (see, e.g., [57,58,59] and Refs. therein). The relation of these layered organic superconductors to the well-known high-T_c cuprates by their layered structure concomitant with Q2D electronic properties, directs attention to the nature of superconductivity in the organics. This question is still in controversial discussion, since a variety of experiments support either BCS or unconventional pairing. It is understood as a sign for unconventional behaviour i.a., that in some experiments a so-called Hebel-Schlichter peak [60] as expected in nuclear-magnetic relaxation experiments at about $0.85*T_c$ is absent, while an excessive peak occurs, however at $0.5*T_c$ [61,62,63]. Furthermore, the proximity of antiferromagnetic ordering and superconductivity in TMTSF- and some BEDT-TTF - based superconductors arises the question on a pairing mechanism by spin fluctuations [32,64,65,66]. Moreover, some optical experiments report a strongly anisotrope superconducting gap even with the indication for nodes in the superconducting order parameter. Further indications for non-BCS behavior is suggested, e.g., by some B_{c2} experiments [67,68]. Controversial results are obtained by London penetration depth measurements, where a part of them suggest unconventional pairing (see, e.g., Refs. [69,70,71,72,73,74]), whereas others propose conventional BCS-pairing (see, e.g., Refs. [75,76,77,78,79,80,81]), however with a tendency to enhanced coupling. Furthermore, a number of results from, e.g., specific heat, surface impedance, $B_c(T)$, $T_c(p)$ as well as tunnelling experiments, as well as a conventional isotope effect (regarding the *entire* donor molecules) and a conventional dependence of T_c from unit cell volumes, support rather BCS behaviour. Even if contradictory results still stimulate the discussion, in general the superconducting mechanism in the organics is understood as BCS-like, however with a considerably enhanced coupling [82].

Besides this, a series of further peculiarities attract interest onto organic conductors, e.g., field-induced superconductivity, the coexistence of antiferromagnetism and superconductivity, the influence of charge ordering onto superconductivity, the investigation of scattering and screening mechanisms in the Shubnikov phase by Haas-van Alphen (dHvA) and Shubnikov-de Haas (SdH) experiments between B_{c1} and B_{c2}. Furthermore also normal-conducting properties of these organics achieve high interest, as, e.g., the presence of ferroelectric phases, the synthesis of low-dimensional magnetic materials, organic molecular magnets as well as magnetic conductors and especially the various influences of low-dimensionality onto the electronic systems (for an insight see [37,25] and Refs. therein).
The wide variety of their low-dimensional electronic properties stimulated Fermi surface (FS) investigations on the organic CT salts [83,58,84,37,25]. For this purpose, dHvA and SdH experiments can be used as most powerful tools due to the very high crystal quality of these organics, which may result in the detection of magneto-quantum oscillations (QOs) even above 0.8T (see Ch. 5). This very favourable circumstance makes QO experiments a very suited for detailed FS investigations over a wide magnetic field and temperature range.
It was found by QO measurements that tight-binding Hückel calculations yield in general surprisingly correct band structures. However, results from QO investigations indicate also clearly that corrections have to be made concerning, e.g., the presence of small closed pockets on the FS which are not found in the calculations (see, e.g. Ch. 5), the size of gaps between successive trajectories in *k*-space, the presence of superstructures or hidden 1D open trajectories, which may act as electron reservoirs and therefore influence the electronic properties of low-dimensional systems. Furthermore dHvA and SdH investigations on low-dimensional organic metals allow the verification of the standard theories for QOs in 3D metals [85,86,87] as well as for 2D systems [88,89,90,91] and show their application and their limits (see, e.g., Ch. 5). Besides this the interplay of fermiology and low-dimensionality can be studied in QO experiments. These features manifest themselves, i.a., by oscillations of the chemical potential, in the carrier tunnelling between closed and open sheets of the FS (the so-called magnetic breakdown), in quantum interference effects between different carrier trajectories (see Chs. 4 and 5) or in interplane transport effects. These studies are very stimulating for the progress in the theoretical understanding of the electronic properties of low-dimensional systems (see, e.g., [88,89,90,91,92,93,94,95,96,97,98]).
Furthermore, QO experiments are found to be a very powerful tool to distinguish between quasi-2D and strongly 2D systems by the determination of the corrugation of the FS and the quantification of the interlayer transfer integral. This characteristic is of special importance for the focus of the present work (see Ch. 5).

During the 1980's a strong interest on two-dimensional electronic systems (2DESs) came up with the discovery of the integer quantum Hall effect (IQHE) by *von Klitzing et al.* [99] (resumed in Ch. 4). The coincidence of this pioneering finding in 2D semiconductors with the progress in synthesis of low-dimensional organic conductors stimulated the research on these organics in high magnetic fields. In the early 80's this could be done only on the quasi-*one*dimensional TMTSF salts, since pronounced 2D systems were not yet realised within the organic CT salts. A decisive step was achieved by magnetotransport experiments on the Q1D organic material $(TMTSF)_2PF_6$, whose metallic state was stabilised by pressures above 6.5kbar. At high fields applied along the lowest-conductive crystallographic *c*-direction, structures equidistant in $[1/B]$ were observed in magnetoresistance which remember to SdH oscillations [100]. A closer view on these oscillations revealed however that the 'oscillation frequency' itself is *temperature* dependent and that the oscillations occur only above a certain *threshold* field. This is in contrast to the behaviour of SdH oscillations

and showed that they cannot be attributed to the presence of a small pocket on the FS. The search for their origin was additionally stimulated by the detection of Hall steps in the Q1D organic conductor $(TMTSF)_2ReO_4$ [101,102], which represent the first detection of the IQHE in a 3D bulk material[3]. Subsequently such peculiar effects were subject of detailed investigations and were also found in further $(TMTSF)_2X$ salts (e.g., with X = ClO_4 and AsF_6) [102,103,104,105,106,107,108,109,110,111]. A theoretical description of this peculiar behaviour of Q1D organics was developed in terms of so-called field-induced spin density waves (FISDW) [112] and refined in Refs. [113,114,115,116,117,118,119,120] (see also [34] for an insight). As already mentioned, the metallic state in the Q1D Bechgaard salts has to be stabilised by an increase of dimensionality via the application of high pressure. However, as aforementioned, this still Q1D electronic system is very sensitive to external parameters as, e.g., magnetic fields. Application of a magnetic field forces the electrons to move along the open 1D wavy trajectories. This causes an oscillation in the perpendicular direction and as the field is increased, the motion becomes more and more one-dimensional. This makes the system more and more unstable against density-wave transitions and finally magnetic fields induce transitions to SDW states as described above. Within this approach it was shown that in the presence of a FISDW *no extended states* are present at Fermi energy, which explains perfectly the observation of Hall steps as well as dips in the SdH signals. In later experiments a further apparent complication was found by the observation of sign-reversed quantised Hall steps were found in $(TMTSF)_2X$ salts, which were proposed to be explained by the coexistence of two successive SDWs in these materials [121,105,104,109,110,122].
These investigations of the FISDW states show that the mechanism leading to the IQHE in Q1D organics is very different from the effects beyond the IQHE in 2D semiconductors.

During the 1980's the interest on low-dimensional electronic systems was concentrated to 2D systems not only by the discovery of the IQHE [99] but especially by the discovery of the fractional quantum Hall effect (FQHE) by *Tsui, Störmer* and *Gossard* [123] (resumed in Ch. 4). Within this highly active field of research very elegant explanations for these effects were found by *Laughlin* [124,125], which identified these effects as a result of two-dimensionality and attribute them to electron localisation in high magnetic fields at low temperatures [126,127,125,128]. Furthermore it was found, i.a., that the IQHE may be understood in a single-particle picture (i.e., noninteracting particles), whereas the occurrence of the FQHE requires strong electron correlation in a 2DES.
One of the most stimulating questions which accompanied the progress in the explanation of both effects in 2D semiconductors was to ask whether electron localisation and strong electron correlation is restricted to 2D single-layer semiconducting systems or whether they may also occur in other 2D systems as, e.g., organic metals. During the same decade the dimensionality of layered organic conductors was enhanced from 1D systems to quasi-2D systems. The continued effort in the progress on donor molecules and the synthesis of new structures resulted in the production of more and more pronounced 2D systems, from which a few show even strongly 2D behaviour. Within this objective a number of Q2D organic were synthesised precedent to this work. It was a very favourable circumstance that one of the most promising candidates for twodimensionality, κ-$(BEDT\text{-}TTF)_2I_3$, could be produced as very high quality single crystals and, within the frame of the present work, this material turned out to represent the actually strongest 2DES within its class of materials. It was therefore that this work was mainly concentrated on the search for results of two-dimensionality in this material, especially for indications for electron localisation and electron correlation effects. For reasons described below, quantum oscillation experiments

[3] R_{xy} indeed exhibits Hall plateaux, while however R_{xy} does not drop to zero during the Hall steps.

were found to be the most powerful tool for this research and indeed, the existence of low integer Landau level filling factors ν (i.e., ν = 1, 2, 3, 4) is found and even the very special fractional filling factor ν = ½ seems to be present in κ-(BEDT-TTF)$_2$I$_3$. These results prove that both, electron localisation and electron correlation, which are beyond the IQHE and the FQHE, respectively, may also occur in 2D organic metals.

Chapter 2 briefly resumes different ways to realise 2DESs and introduces to some of the fundamental differences between 2D semiconductors and 2D multilayer organic metals. Chapter 3 introduces to the theoretical descriptions of magneto-quantum oscillations in 3D and 2D metals and includes a number of corrections which may be required by fermiological peculiarities, low-dimensionality, etc. . In Ch. 4 the description of both, IQHE and FQHE is resumed, focusing on electron localisation and electron correlation effects and the way in which they may influence QO experiments. Detailed investigations on κ-(BEDT-TTF)$_2$I$_3$ are discussed in Ch. 5. They show the above mentioned filling factors ν = ½, 1, 2, 3, 4 and further effects of two-dimensionality in this material. Chapter 6 resumes the actual state of research on other Q2D and pronounced 2D organic metals on the search for comparable effects and further influences of two-dimensionality in this class of materials.

2. The Realisation of Two - Dimensional Electronic Systems

The present chapter recalls the most important material-specific conditions which are necessary to enable the quantised Hall effects to occur in semiconductors. Furthermore it comprises methods to realise a two-dimensional electronic system (2DES)[1] in different material classes, in which the IQHE and FQHE may also be present.
One of the decisive requirements to a material exhibiting the quantised Hall effects is the two-dimensionality of its electronic system, i.e. the restriction of the electron motion to a 2D layer with a finite spatial extent of their wave function in the third dimension. The methods by which such conditions are realized, is briefly summarized in the following (for details see [129,130,131,132].

2D electronic systems may be created in different materials. An almost ideal 2DES is given on the surface of liquid helium, where electrons approach the He surface from above being attracted by the electric polarization of the He atoms. Since the 1s orbitals of He are completely filled and the 2s state is of too high energy, the electrons cannot penetrate the surface. The electron density can be controlled by a metal electrode below the surface and a positive voltage [133]. By this a dimple on the He surface is formed below each bound electron. The dimples are independent at sufficiently low electron concentrations n_e, they overlap at increasing n_e accumulating electrons on the dimple bottom and finally, as n_e is further increased the electrons from the dimple bottom escape to the metal electrode. This limits the variation of the carrier concentration within about 10^5 - 10^9 cm $^{-2}$ and, due to this, the resulting 2DES behaves classically.

Higher carrier densities are reached in so-called metal-oxide-semiconductor field effect transistors (MOSFETs) [129,134,130]. These systems consist of metal-oxide- semiconductor sandwich (see Fig. 2.1), where a 2DES is generated as follows. A semiconductor (*p*-Si) with a planar interface is covered by a thin insulating film (SiO_2) and a metal gate electrode.

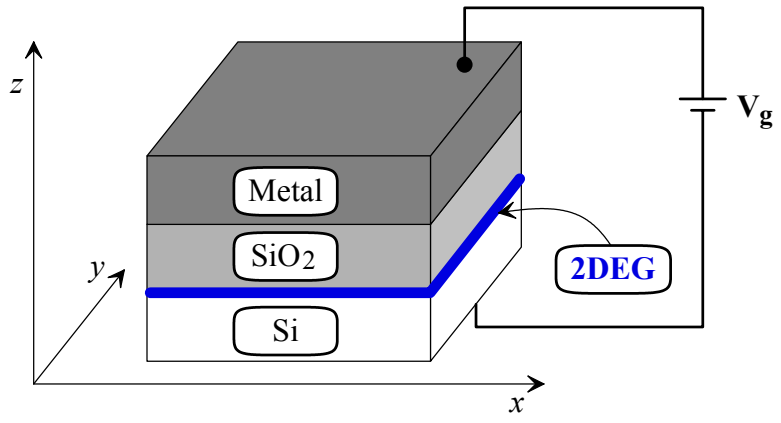

Fig. 2.1: Schematic picture of a metal-oxide-silicon structure with the position of the induced 2DEG at the interface between the Si and the SiO_2 layer (thick blue line).

[1] A 2DES is also frequently named a 2DEG (2D electron gas), which points out that the carriers are considered to be non-interacting.

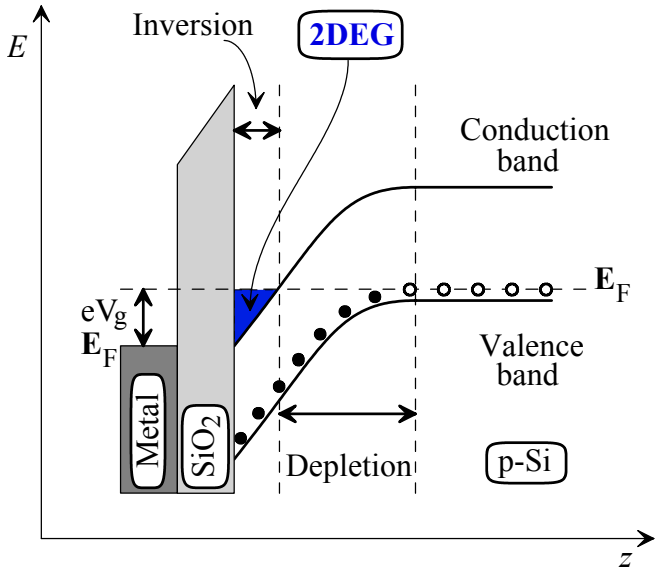

Fig. 2.2: Energy levels in a MOSFET, where a sufficiently high $V_g > 0$ bends the conduction band of p-Si such that a 2DEG is induced in an inversion layer (open circles: neutral acceptors, filled circles: negatively charged acceptors).

A gate voltage V_g between the metal electrode and the Si/SiO_2 interface bends the initially unoccupied conduction band of p-Si (see Fig. 2.2). At sufficiently high V_g the bottom of the conduction band dips below the Fermi energy E_F in a thin plane ($\approx$ 2.5 - 5nm) parallel to the 2D SiO_2 interface. In this region the conduction band becomes occupied by electrons and the system forms a so-called inversion layer ('inversion', since here the charge carriers are electrons, whereas the doping is *p*-type). At low temperatures ($k_BT \ll \Delta E$, the subband spacing) the electrons are trapped in the lowest subband, so that the system becomes a single layer 2DEG. Therein the electron number n_e can be varied by the gate voltage, so that $n_e \approx 0 - 10^{13}$ cm^{-2} can be reached. However only the region $n_e \approx 10^{11}$-10^{13} cm^{-2} is of importance for IQHE studies, since impurity effects are too strong at too low electron densities. MOSFETs have the advantage that n_e can be easily varied but the disadvantage, that crystal discontinuities at the interface and impurities trapped in the SiO_2 layer limit the electron mobility to $\mu_e \leq 10^5$ cm^2 (Vs)$^{-1}$. This is sufficient to realise the IQHE, but insufficient to generate the electron correlation which is required for the occurrence of the FQHE.
The mobility increase required for the presence of the FQHE can be achieved by the creating a 2DEG in a semiconductor heterostructure which consists of a semiconductor-semiconductor interface. Such a material was proposed in 1969 [135] first synthesised in 1978 [136] and in 1979 identified as 2DEG [137]. A well-known class of heterostructures is based on GaAs/$Al_xGa_{1-x}As$ ($x \leq 1$) where the lattice constants of both, GaAs and $Al_xGa_{1-x}As$, match very good to each other. This results in an interface, a so-called heterojunction, which is nearly free of disorder. Now the band gap of the $Al_xGa_{1-x}As$ alloy increases by the Al concentration x and is therefore wider as that of GaAs (see Fig. 2.3). When the alloy layer is doped by donors, the carriers in the vicinity of the heterojunction move across the interface to occupy the low-lying band edge states of the GaAs conduction band. The resulting electric field bends the energy bands of both neighbouring materials at their interface such that the GaAs conduction band is pushed below E_F. Hereby a 2DEG of about 10nm thickness is generated parallel to the heterojunction. During the last two decades the synthesis of heterostructures strongly developed, e.g. by starting from different semiconductors (III-V and

II-IV materials) varying the doping of the two layers and introducing a spacer material between the successive layers (along the dashed line in Fig 2.3) [138,139,140].

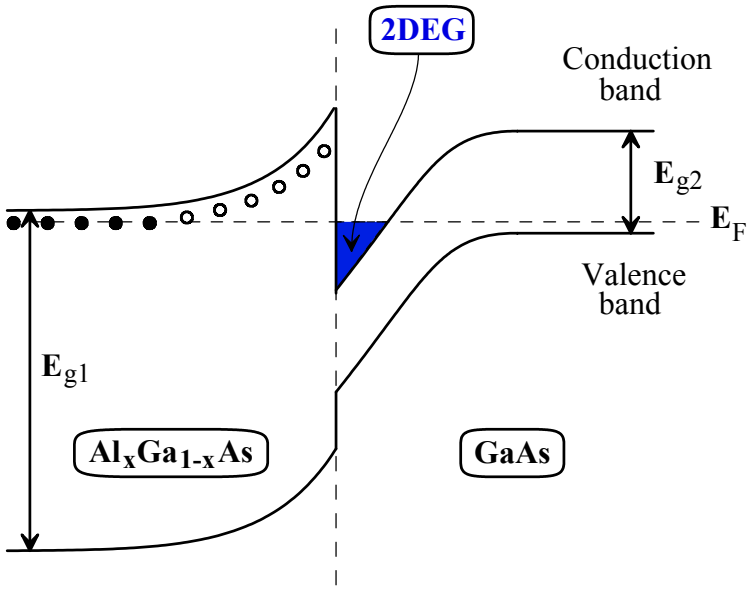

Fig. 2.3: Energy levels in a doped heterojunction with the generation of a 2DEG.

By the latter procedure the electrons become spatially well-separated from the donors, so that scattering is minimised and very high electron mobility (meanwhile up to $\mu_e \approx 2 \bullet 10^7$ cm^2 (Vs)$^{-1}$ [132]) can be reached. The FQHE was first measured in GaAs/$Al_{0.3}Ga_{0.7}As$ heterostructure with $n_e \approx 10^{11}$ cm^{-2} and $\mu_e \approx 10^5$ cm^2 (Vs)$^{-1}$ [123].
Whereas the advantage of heterostructures with respect to MOSFETs is their high quality and their quite high mobility, the electron density, however, can be varied only in a relatively narrow range between about $n_e \approx 10^{11}$ cm^{-2} and $n_e \approx 10^{12}$ cm^{-2}.
Heterostructures can be grown layer by layer by molecular beam epitaxy (MBE). By this, single layer as well as multilayer 2D electron gases can be realised. This method allows to choose the thickness as well as the electron concentration of every heterojunction. In a multilayer it enables to control interlayer coupling and electron tunneling between the successive 2D layers. This is of special importance for the generation of the IQHE and FQHE in multilayer systems. It should be emphasised that the single- as well as multilayer systems are generally regarded as 2DESs, but in fact they are all quasi-2D systems, since the finite width of the electron layer allows a finite motion perpendicular to the layer.
Moreover in multilayer 2DESs, the 2D electronic properties, i.e., the presence of the quantised Hall effects are found to persist when interlayer coupling and even interlayer electron tunneling occur (for details see Sec. 5.5. ff.).

It turned out that the upper mobility bound $\mu_e \approx 10^5$ cm^2 (Vs)$^{-1}$ reached by MOSFETs is just the optimum for the IQHE but not sufficient for the FQHE. Especially for the occurrence of the FQHE, high sample quality, high electron concentration and high mobility are required. These conditions are not only given in heterostructures but may be also reached (or even unified) in 2D layered organic metals.

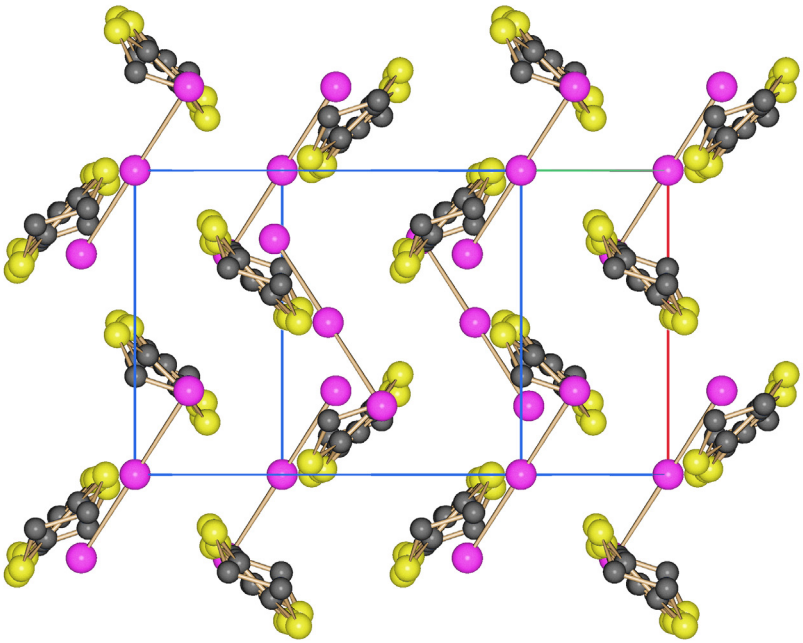

Fig. 2.4.a (top): View on a conducting BEDT-TTF (b,c) plane of κ-(BEDT-TTF)$_2$I$_3$ with a sheet of linear I$_3$ molecules on top of it and one below, respectively.

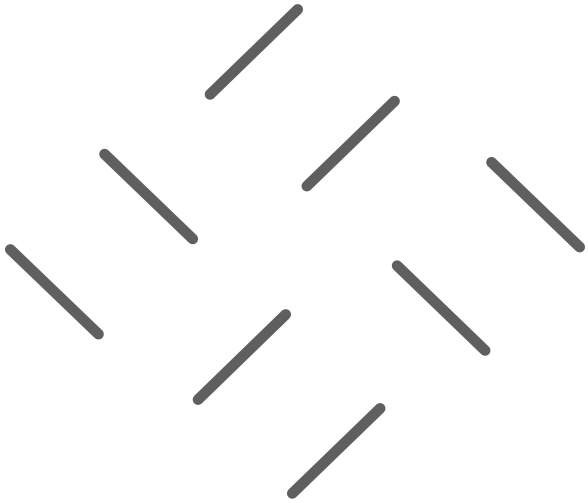

Fig. 2.4.b (centre): Schematic orientation of the BEDT-TTF dimers nearly perpendicular to each other.

Fig. 2.4.c (bottom): Single BEDT-TTF layer with indicated network electronic transport by S-S orbital overlap (dashed lines).

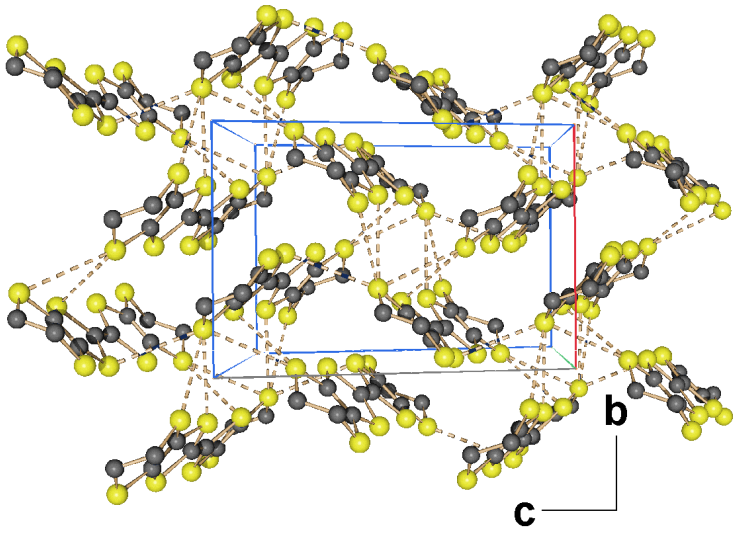

Since the basics on the synthesis of organic metals and superconductors are already briefly discussed in Ch. 1, in the following it is illustrated how especially a 2DES can be realised in multilayer organic metals. As mentioned in Ch. 1, these materials are grown by electrochemical synthesis [141] and crystallise in donor layers with the thickness of a single donor molecule length. These sheets are separated by monolayers of anion molecules, neighboured by the next donor monolayer and s.o., alternating (see Figs 2.4a and 2.5a).
One condition for the realisation of a 2DES is a high electronic isotropy within the conducting donor planes. Therefore the orbital overlap between neighouring donor molecules should form a network of electronic transport which is as isotrope as possible. This can be best reached by the choice of the non-planar BEDT-TTF as donor molecules and the crystallisation in a so-called κ-structure, where these donor molecules build dimers and neighbouring dimers are oriented nearly perpendicular to each other [142]. The resulting transport network (sketched by dashed lines) in Fig 2.4.a hints to the high electronic isotropy within the conducting BEDT-TTF (b,c)-planes. The conduction in the perpendicular a*-direction is influenced by size, shape and electronic properties of the anions. Here it turned out that the I_3 molecule provides low interlayer coupling and, presumably since I_3 is small and linear, it allows a very good orientation of the BEDT-TTF molecules in the neighbouring donor plane. The resulting organic superconductor κ-(BEDT-TTF)$_2I_3$ ($T_C \approx 4K$ [143,144, 145]) turned out to be in its normal conducting state the to-date strongest 2DES within this class of material. This can be expressed by the ratio of transfer integrals perpendicular and parallel to the conducting planes $t_\perp / t_\parallel < 10^{-4}$ [146] while the in-plane anisotropy is nearly 1 in the entire temperature range between room temperature and the superconducting transition [145,147]. The charge density of the 2DES can be illustrated by a side view of the unit cell and a scheme of the electron density (Figs. 4.5.a and b).

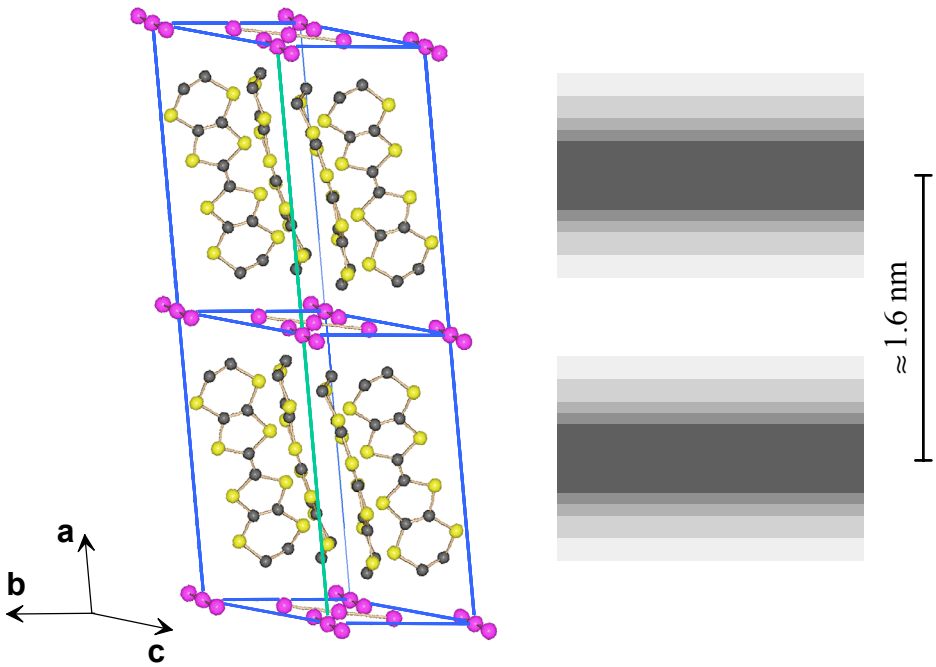

Fig. 2.5.a (left): Side-view on the conducting BEDT-TTF plane of κ-(BEDT-TTF)$_2I_3$ separated by I_3 sheets.
Fig. 2.5.b (right): Schematic illustration of the electron density on the BEDT-TTF molecules (increasing density with grey-scale darkness).

It was found by spin density measurements that the maximum charge density is located around the C = C double bond in the centre of the BEDT-TTF molecules [148] and decreases towards the donor/anion interface. This means that the maximum electron density is farest possible apart from the donor/anion interface which is a source of scattering.
One power of electrocrystallisation is that the local electric potential on the electrode, where the bulk crystals grow, cares for a strict alternation of donor and anion monolayers and, furthermore, minimises the incorporation of impurities into the crystal. However the ordered orientation of the end-standing CH_3 groups on the donor molecules can be hardly controlled by the growing parameters, since it is dominantly determined by the neighbouring anions. In some CT salts such a possible disorder strongly influences the electronic properties, however in κ-(BEDT-TTF)$_2$I$_3$ no CH_3 disorder is found. These briefly sketched pecularities may illustrate, why organic metals can be grown very pure, resulting in high electron mobilities and how strongly 2DES can be realised in this class of materials. In κ-(BEDT-TTF)$_2$I$_3$ the in-plane mobility was estimated as $\mu_e \approx 5 \cdot 10^8$ cm^2(Vs)$^{-1}$, which is considerably higher than the electron mobility in heterostructures. The typical electron density for κ-structured BEDT-TTF salts is $n_e \approx 10^{14}$ cm^{-2} per layer (for estimations see appendix A). A typical crystal of the size 1.0 x 2.0 x 0.25 mm^3 consists of about 10^5 layers. Its electronic properties are determined by the bulk electron concentration which is in the order of $n_e \approx 10^{17}$ per crystal, or, $n_e \lesssim 7 \cdot 10^{20}$ cm^{-3} (see appendix A). This is considerably higher as in multilayer heterostructures.
It should be mentioned that κ-(BEDT-TTF)$_2$I$_3$ shows metallic intra- but also interlayer transport [145], as a number of quasi-2D and 2D organic metals do [83]. Despite of this, it shows the presence of typical strong 2D properties at high magnetic fields and low temperatures, i.e. the presence of integer Landau level filling factors in the quantum limit and indications for the existence of fractional filling factors ν in a bulk metallic 10^5-layer system, whose electronic properties are surprisingly far away from the typical materials where the FQHE is expected and usually observed.
These integer and fractional ν are observed in κ-(BEDT-TTF)$_2$I$_3$ by SdH experiments and are interpreted as hints to the presence of electron correlation and electron localisation. For the discussion of the results it seems indicated to recall briefly the basics of the behaviour of electrons in strong magnetic fields (Ch. 3) as well as selected properties of semiconducting 2D systems in the IQHE and FQHE region (Ch. 4).

3. Electrons in Strong Magnetic Fields

The behaviour of electrons in strong magnetic fields is widely discussed in standard condensed matter textbooks, in more detail in Ref. [87], but also in well-known reviews on the quantised Hall effects (see, e.g., [130,127,149,150]). Therefore the present chapter is restricted to recall the most important details of this subject which are necessary for the discussion of the experiments.

3.1. Landau Quantisation and Magneto - Quantum Oscillations (QOs)

The motion of a free electron with the effective mass $m_{eff} = m^* m_e$ in an uniform magnetic field $\mathbf{B} = \nabla \times \mathbf{A}$ (where $\mathbf{A}$ is the vector potential) can be expressed by the Schrödinger equation

$$H\,\psi = \frac{1}{2\,m_{eff}} \left(\frac{\hbar}{i} \nabla - \frac{e}{c} A \right)^2 \psi \;=\; E\,\psi \tag{3.1}$$

If $\mathbf{B}$ is collinear to the z coordinate ($\mathbf{B}$ = (0, 0, B_z)) the solution in k-space represents an electron motion which is quantised in the (k_x,k_y) plane perpendicular to $\mathbf{B}$ by a quantisation of ($k_x^2 + k_y^2$), while the motion along $\mathbf{B}$ expressed by k_z remains unaffected by quantisation. The electrons condense onto Landau levels (LLs) which are the eigenvalues of Eq. (3.1), i.e.,

$$E_n = (n + \gamma)\,\hbar\omega_c + \frac{\hbar^2}{2\,m_{eff}} k_z^2 \qquad \text{with} \qquad \omega_c = \frac{e}{m_{eff}} B\,, \tag{3.2}$$

where $\hbar\omega_c$ is the cyclotron energy determined by the cyclotron frequency ω_c [151,152]. γ is the Onsager phase factor[1], which is exactly ½ for a parabolic band (i.e., free electrons), but in general γ departs slightly from ½ by an energy and field dependent amount [153]. Such departure hints to the presence of electron correlation. n counts the energy eigenstates with n=0,1,2,3, ... and n likewise represents Landau level index, however starting with 1,2,3, ... , as well as the LL filling factor (see Sec. 4.1, Fig. 4.2) [2].

In an infinitely thin 2D system k_z vanishes, so that the electron states in k-space are concentric Landau circles which are determined only by ($k_x^2 + k_y^2$). A real 2D single layer system of finite thickness (like, e.g. a 2D semiconducting device) would be described in k-space by a so-called pancake with a finite 'thickness' in k_z-direction. For a system of free electrons however, the quantisation results in a set of Landau *cylinders*, where k_z is not affected by B and is therefore free. The occupation of these cylinders by electrons is determined by system specific properties and forms the shape of the Fermi surface (FS), which encloses the occupied states. For a perfect 3D system the FS is a sphere [154,155], whereas in the more general case of an anisotrope 3D system the FS is an ellipsoid (see Fig. 3.1).

The number of electrons condensed to every successive LL is given by the degeneration factor

[1] also known as Maslov constant

[2] The situation in high fields, where the innermost LL with n = 1 is the only occupied state below the FS is called quantum limit (QL).

$$D = \frac{e}{h} B V, \tag{3.3}$$

which can be calculated either for a bulk sample of volume V or for a single layer system with a certain area S (by replacing V by S). It should be noticed that D is controlled by the magnetic field, not by the system's fermiology, i.e., every successive occupied LL contains the same number of electrons.

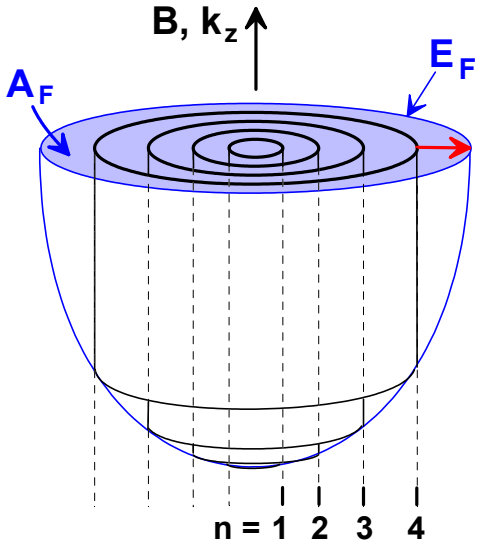

Fig. 3.1: Schematic illustration of a set of Landau cylinders counted by the LL index n in a Fermi surface (FS) (dotted line) of a 3D system. The cut perpendicular to the **B** direction reveals the actual extremal area A_F of the FS and the Fermi energy E_F.

The area A_n in k-space perpendicular to B encircled by the n-th Landau cylinder (LC) is given by

$$A_n = (n + \gamma) \frac{2\pi e}{\hbar} B \tag{3.4}$$

[156,85,154]. As soon as B is raised, A_n increases until it parts company with the FS and the electrons have to be redistributed onto the LCs below the FS. This occurs when the area of the outermost LC reaches the extremal area A_F of the FS perpendicular to B. Further increase of B reproduces this feature equidistantly in [1/B] with a spacing

$$\Delta\left[\frac{1}{B}\right] = \frac{1}{B_{n-1}} - \frac{1}{B_n} = \frac{2\pi e}{\hbar A_F}. \tag{3.5}$$

Variation of the eigenstates with B (see. Eq. (3.2)) and redistribution of the electrons when a LC leaves the FS leads to oscillations of the thermodynamic potential

$$\tilde{\Omega} = \left(\frac{e}{2\pi c\hbar}\right)^{3/2} \frac{2 k_B T B^{3/2} V}{|A''|^{1/2}} \sum_{p=1}^{\infty} \frac{R_T(p) * R_D(p) * R_S(p)}{p^{3/2}} \cos\left[2\pi p\left(\frac{F}{B} - \frac{1}{2}\right) \pm \frac{\pi}{4}\right] \tag{3.6}$$

where $A'' = |\partial^2 A/\partial k^2|_{k=k_F}$ is the local curvature of the FS, R_j are damping factors (discussed below), p is the harmonic index and

$$F = \frac{\hbar}{2\pi e} A_F \quad [\text{Tesla}]; \qquad A_F = \pi |\boldsymbol{k}_F|^2. \tag{3.7}$$

F is the fundamental oscillation frequency of these so-called magneto-quantum oscillations (QOs) [157,85,86,87]. These oscillations of Ω result in QOs in a series of thermodynamic and transport properties which are obtained by partial derivative of $\widetilde{\Omega}$. The best-known are QOs of the magnetisation $\widetilde{M}$, i.e., the de Haas-van Alphen (dHvA) effect and QOs of the conductivity $\tilde{\sigma}$ (or the resistivity $\tilde{\rho}$, respectively), which is the Shubnikov-de Haas (SdH) effect. $\widetilde{M}$ is obtained by

$$\tilde{M}_{//} = -\left(\frac{\partial \Omega}{\partial B}\right)_{T,\mu} \qquad \text{and} \qquad \tilde{M}_{\perp} = -\frac{1}{B}\left(\frac{\partial \Omega}{\partial \Theta}\right)_{T,\mu,B} \tag{3.8}$$

as

$$\tilde{M}_{//} = -\left(\frac{e}{c\hbar}\right)^{3/2} \frac{2F k_B T V}{(2\pi B|A''|)^{1/2}} \sum_{p=1}^{\infty} \frac{R_T(p) * R_D(p) * R_S(p)}{p^{3/2}} \sin\left[2\pi p\left(\frac{F}{B} - \frac{1}{2}\right) \pm \frac{\pi}{4}\right] \tag{3.9a}$$

and

$$\tilde{M}_{\perp} = -\frac{1}{F}\frac{\partial F}{\partial \Theta}\tilde{M}_{//} \tag{3.9b}$$

for the components parallel and perpendicular to B. This is known as the Lifshitz-Kosevich (LK) formula which describes the expected quantum oscillation amplitude. It should be emphasised that the LK formula is valid for 3D metals where the chemical potential is constant and where the total number of carriers N_e is conserved. The sign in the oscillatory part introduces a phase and is " - " when the extremal area A_F of the FS is a maximum and " + " when it is a minimum (see Fig. 3.5.a). The amplitude reduction factors $R_T(p)$, $R_D(p)$, $R_S(p)$, respectively are discussed in detail in [87] (see also Refs. therein) and their meaning is therefore only briefly sketched here.

3.2 Reduction of Quantum Oscillation Amplitudes by Phase Smearing Effects

3.2.1 Finite Curvature of the Fermi Surface of a 3DES

As already mentioned in context with Eq. (3.9), the standard LK formula is valid for QOs in 3D metals. The corresponding background is that the actual position of E_F for the various allowed k_z in a 3D system is defined by a number of Landau cylinders inside the FS or even by all of them (see Fig. 3.1). However the determination of their contribution to the magnitude of QOs by integration over k_z reveals a destructive interference for all those k_z values where E_F varies with k_z. Thus after integration the only persisting contributions come from the extremal areas, where $\partial E_F/\partial k_z \equiv 0$ [87]. These may be maximal (A_{Max}) or minimal areas (A_{Min}) of the FS, i.e., bellies or constrictions of the FS (see Fig. 3.5.a or, e.g., as known

from Cu [158]). The contribution of A_{Max} and A_{Min} to the oscillation amplitudes is of different phase, which is considered by the above mentioned sign in the last term of Eq. (3.9). The remaining contribution from the extremal areas is damped by the local curvature of the FS, A'' along k_z, which enters into the denominator of Eq. (3.9). This makes straightforward to see that in a 2D system where A'' vanishes, the standard 3D LK formula is expected to diverge and to lose its application.

3.2.2 Effect of Finite Temperature

Due to the temperature-induced broadening of the Fermi distribution function the Fermi level E_F is broadened at finite T, so that the redistribution of electrons to the lower lying LCs inside the FS happens within a widened field range. This ends up in a reduction of the QO amplitudes by the factor

$$R_T(p) = \frac{\alpha p m_{eff} T/B}{\sinh(\alpha p m_{eff} T/B)} \quad \text{with} \quad \alpha = \frac{2\pi^2 m_e k_B}{\hbar e} = 14.69\ [\tfrac{\mathrm{T}}{\mathrm{K}}]\,. \tag{3.10}$$

Here from the reduced carrier effective mass $m^* = m_{eff}/m_e$ can be obtained by a fit of the temperature dependence of the QO amplitudes to Eq. (3.10). This can be done independently for the p-th harmonic of a QO frequency and, moreover, for carriers moving on different closed orbits in k-space.
In addition Eq. (3.10) holds an important possibility to control the application and limits of the standard 3D LK formula (Eq. 3.9) to quasi two-dimensional (Q2D) electronic systems or 2DES, respectively. For this purpose Eq. (3.10) is converted into

$$\frac{\ln(A_p/T(1-\exp(-2\alpha p m_{eff} T/B)))}{T} = b = -\frac{\alpha p}{B} m_{eff}\,, \tag{3.12}$$

which means that a plot of the implicit amplitudes A_p versus temperature should be a straight line whose gradient contains m^*. In reversal, deviations from the expected straight line show that the standard 3D LK theory for QOs has lost its application.

3.2.3 Effect of Finite Relaxation Time

Due to the presence of impurities and crystal defects the electrons of a real system have a finite relaxation time τ. Via the Heisenberg uncertainity principle this leads to a Lorentzian broadening of the Landau levels. Under the assumption of an energy independent τ, *R.B.Dingle* showed that the problem can be solved by projection of the broadened LLs to a broadened Fermi energy in conjunction with sharp LLs. This means that broadened LLs act similarly as a broadened E_F, i.e., a finite temperature. Therefore the measure for broadening was defined as a temperature equivalent, the so-called Dingle temperature T_D (see Eq. (3.14). By a Fourier transform the oscillation amplitude for the p-th harmonic A_p is obtained as

$$A_p(B) = A_{p,0}\,\frac{TB^{-n}R_D(p)}{\sinh(\alpha m_{eff} pT/B)}\,, \tag{3.12}$$

where A_p represents the undamped amplitude and depends on the QO detection method as n does (n = -1/2 for dHvA torque experiments, whereas n = +1/2 for SdH measurements). R_D is the Dingle damping factor with

$$R_D(p) = e^{-(\alpha p m_{eff} T_D/B)} = e^{-(\pi p/\omega_c \tau)} \triangleq \sqrt{n_{e,unscattered}} \ . \tag{3.13}$$

R_D represents the square root of the number of unscattered electrons which have passed p cyclotron orbits without being scattered [159]. T_D can be understood as the temperature by which an *ideal* reference crystal has to be heated with respect to the actual temperature T in the measurement in order to produce the same reduced QO amplitudes as the *real, imperfect* crystal at the same T. T_D can be estimated independently for the electrons moving on every successive closed orbit by a fit of the field dependence of the QO amplitudes to Eq. (3.12) and τ is obtained therefrom by

$$\tau = \frac{\hbar}{2\pi k_B T_D} \ . \tag{3.14}$$

It should be stressed that Eq. (3.12) holds a powerful possibility to control the validity of the standard 3D LK for quasi-2D and 2D systems and its limits by conversion into the form

$$\frac{\ln\left(A_p B^n \sinh\left(\alpha p m_{eff} T/B\right)\right)}{1/B} = d = -\alpha p T_D \tag{3.15}$$

with α and n as given above. A plot of the implicit amplitudes A_p versus $1/B$, the so-called Dingle plot (DP), should be linear according to the 3D LK formula with a gradient containing T_D. However in the presence of magnetic breakdown between neighbouring trajectories of the FS, the DP should be sublinear, deviating towards lower values at high B (see Sec. 3.4.2).
The DP is very sensitive to system specific peculiarities of the FS, as, e.g., to FS instabilities or to a so-called warping (i.e., corrugation) of the FS (see Sec. 3.5.2). In the latter case the QO amplitudes are damped at certain field values, which are exactly equidistant in 1/B (see Fig 3.5 and its discussion). This can be observed as equidistant local minima in the DP.

3.2.4 Effect of Electron Spin

In magnetic fields the energetic position of the Landau levels E_n are corrected by the interaction energy between the magnetic field and the orientation of the spin magnetic moment which lifts the spin degeneracy. By this E_n is modified to

$$E_n = (n+\gamma)\,\hbar\frac{eB}{m_{eff}} \pm \frac{\hbar}{4}\frac{g\,e\,B}{m_e} \tag{3.16}$$

The first term is the cyclotron energy and the second term is the Zeeman spin splitting (Δe_s). It contains the g-value of the electrons averaged over the closed electron trajectory in k-space [160]. A superposition of the contributions of LLs of different spin orientation to the QOs is considered by

$$R_s(p) = \left|\cos\left(\tfrac{1}{2} p \pi g m_{eff}(\Theta)\right)\right| \tag{3.17}$$

which enters into the LK formula (Eq. (3.9)) as the spin dependent amplitude reduction factor [161,162]. As shown by Eq. (3.16), the Zeeman term is determined by the free electron mass, whereas the cyclotron energy is given by m_{eff}, which is angular dependent. At certain angles Θ_i, where ΔE_{Ze} is a multiple of $\hbar\omega_C$, the successive spin states cannot be observed, since each of the two spin states of a LL matches exactly with the spin-reversed state of a neighbouring LL. At other angles Θ_j, however, where $\Delta E_{Ze} = ((2n+1)/2)\,\hbar\omega_C$, the successive spin states are best resolved, so that the double set of oscillations is observed (provided that $\hbar\omega_C$; $\Delta E_{Ze} > k_B T$). In the Fourier spectrum this leads to an enhancement of the amplitudes of the even harmonics (i.e., p=2, 4, 6,...) and the absence of the fundamental frequency and its odd harmonics (i.e., p=1, 3, 5,...). The angles Θ_j where this occurs are called spin zeros. Knowing m_{eff} from a fit to Eq. (3.10) the electron g-value can be determined from the sequence of spin zeros Θ_j.
It is noteworthy that according to Eq. (3.17) R_S and therefore the position of the Θ_j is very sensitive to changes of gm_{eff}. By detection of the successive Θ_j at different magnetic fields this can be utilised to verify whether m_{eff}, or, respectively, m_{eff} is magnetic field dependent or not.
For cases where QOs cannot be detected over a sufficiently wide angular range, another method allows the g-value determination and holds even more information. Equation (3.16) can be read in the sense that Zeeman splitting shifts the field position where the n-th LL intersects the FS (i.e., $E_n \equiv E_F$) by its contribution to the total energy. This shift in B where g contributes to, is a phase factor which added to the QO sequence. The field positions B_n, where n-th LL reaches the FS is given by

$$\frac{F}{B_n} = (n+\gamma) \pm S \quad \text{with} \quad S = \tfrac{1}{4} g m_e \,, \tag{3.18}$$

where F is the QO frequency and $\gamma \approx ½$ is the Onsager phase factor. Under favourable circumstances this allows the determination of the g-value, which is of importance when in a 2D system at high magnetic fields the possibility for the occurrence of skyrmions has to be examined (see Sec. 5.8.4). Furthermore a more exact γ-value can be extracted, which may give hints to the presence of electron correlation).

3.3 The Shubnikov-de Haas (SdH) Effect

Oscillations of the field dependence of the resistivity by *Shubnikov* and *de Haas* in 1930 on Bi were in fact the first observation of quantum oscillations [163]. The theoretical background was developed by *Adams* and *Holstein* in 1959 [164] and was rather complex, since scattering in magnetic field had to be considered. A few years later the problem could be simplified by *Pippard* [165] with the argument that the scattering probability is proportional to the number of destination states in which electrons can be scattered. This probability which determines the scattering time τ and the resistivity ρ, oscillates in conjunction with the oscillating density of states $D(E_F)$ at E_F. In Ref. [164] it could be shown that even very different scattering mechanisms as, e.g., phonon or ionised impurity scattering, act in a quantitatively very similar way, which simplifies the problem.
For electrons moving on a single closed orbit on a spherical FS of a 3DES, to which a magnetic field is applied along the z-direction and an electric field along the x-direction, the diagonal conductivity $\sigma_{xx}(B)$ was obtained as

$$\sigma_{xx}(B) = \sigma_0(B)\,[1 + \Delta\tilde{\sigma}_1(B) + \Delta\tilde{\sigma}_2(B)]\,. \tag{3.19}$$

σ_{xx} consists of the classical background resistivity σ_0(B) and two oscillating components

$$\Delta\tilde{\sigma}_1(B) = \frac{5}{2}\sigma_0(B)\left(\frac{\hbar\omega_c(B)}{E_F}\right)^{\frac{1}{2}}\left[\frac{1}{2}\left(\frac{\hbar\omega_c(B)}{\delta E}\right)^{\frac{1}{2}} - \left(\frac{1}{2} + \frac{\delta E}{\hbar\omega_c(B)}\right)^{\frac{1}{2}}\right] \tag{3.20}$$

and

$$\Delta\tilde{\sigma}_2(B) = \frac{3}{2}\sigma_0(B)\left(\frac{\hbar\omega_c(B)}{E_F}\right)\left[\frac{1}{2}\left(\frac{\hbar\omega_c(B)}{\delta E}\right)^{\frac{1}{2}} - \left(\frac{1}{2} + \frac{\delta E}{\hbar\omega_c(B)}\right)^{\frac{1}{2}}\right]^2 . \tag{3.21}$$

$\Delta\tilde{\sigma}_1(B)$ represents the contributions coming from inter-LL scattering, whereas $\Delta\tilde{\sigma}_2(B)$ is the contribution from intra-LL scattering. At low fields, where a number of LLs are inside the FS, $\Delta\tilde{\sigma}_1(B)$ dominates, whereas in field regions, where only a few LLs are within the FS, $\Delta\tilde{\sigma}_2(B)$ becomes dominant. Both terms are determined by the cyclotron energy and E_F. However a decisive variable is δE, which denotes the energy difference between E_F and the energetic state on the outermost LL (i.e., the LL being closest to the FS) with $k_z = 0$. When the field is increased and the outermost LL reaches the FS, δE vanishes[3], so that the SdH oscillations would tend to diverge. However, broadening and collisions avoid a divergence of $\Delta\tilde{\sigma}$.

It should be stressed that in a spherical FS the Landau cylinders intersect the FS 'smoothly' (see Fig. 3.1), which means that electron states from higher to lower $|k_z|$ are emptied, ending up with $k_z = 0$ (see [3]). This means that the electron occupation of the outermost LL is lowered smoothly, which limits the QO amplitudes. As will be shown later, in the 2D FS of a bulk metal, where the FS itself is a cylinder, the vanishing of δE occurs *instantaneously* for all k_z, so that much higher SdH oscillation amplitudes with a rich harmonic content are expected in such a 2D system. For real conditions a formula for the oscillating part of the conductivity was obtained as

$$\frac{\Delta\tilde{\sigma}}{\sigma_0} = \frac{5}{2}\left(\frac{p\,\pi\,e\,B}{\hbar A"}\right)^{\frac{1}{2}} \sum_{p=1}^{\infty} \frac{R_T(p) * R_D(p) * R_S(p)}{p^{3/2}} \sin\left[2\pi p\left(\frac{F}{B} - \frac{1}{2}\right) \pm \frac{\pi}{4}\right] \tag{3.22}$$

with the same amplitude reduction factors R_T, R_D, R_S as discussed in Sec. 3.2, except for the exponent n in R_D as discussed with Eqs. (3.12) and (3.15). This means that SdH measurements can be used just as dHvA experiments for fermiological investigations and for the estimation of m^*, T_D, τ as well as the electron g-value. This is in agreement with the general experience made in the investigations of a series of conventional metals [87] as well as organic metals [25,37], even though especially the Fermi surfaces of the latter materials typically consist of several orbits, whereas the description for the SdH effect discussed here is made for a single orbit [4].

Furthermore it should be mentioned, that organic metals are relatively high conductive, so that in pulsed magnetic fields the experimental technique itself may introduce subtle

[3] This energetic state on the outermost LL can be imagined as the equator line of a spherical FS when the field is in polar orientation.

[4] One of the possible complications in the presence of several orbits may be a nontrivial background magnetoresistivity.

problems, e.g., by eddy currents. These are induced by the strong $\partial B/\partial t$, and moreover, eddy currents may themselves oscillate because of the dHvA oscillations of M. By this the dHvA effect may influence the SdH effect in pulsed fields, but also vice versa. Namely, when a pickup coil is used to detect the dHvA effect, SdH oscillations may enter the obtained signal through eddy current effects [87]. Furthermore, in some cases the dissipation of eddy currents may heat the sample.

In a survey, the SdH effect was found to be a comparably powerful tool for Fermi surface investigations as the dHvA effect. The standard SdH formalism however was made for a 3DES with a constant chemical potential and for a system where the total number of electrons is conserved. Strong deviation from this formalism are expected for 2D systems, where an amplification of the QO amplitude is expected. This amplification should be stronger with increasing field, since $\hbar\omega_c$ is in the numerator of Eqs. (3.20) and (3.21) and since the LL degeneration increases with field.
A further increase of the oscillation amplitude is expected when only a few LLs are inside the FS since according to Eq. (3.21) the amplitude is then proportional to $(\hbar\omega_c)^2$ instead of $\hbar\omega_c$.

3.4 Departures from the Standard LK Theory for 3DES

The derivation of the standard LK formula (Eq. (3.9)) is based on several simplifying assumptions. It is assumed, e.g., 1) that the magnetic field in the material is not considerably modified by magnetisation, 2) that the carriers move on a closed orbit in k-space without a possibility to tunnel to a neighbouring trajectory, 3) that the chemical potential is practically fix, i.e. the system is a 3DES and 4) that the electronic system is a metal where carriers are free and the absolute number of carriers N_e is conserved. The latter assumption means that as soon as N_e is varied by effects as, e.g. phase transitions or electron localisation, the QO amplitudes show deviations from the LK formula.
These most important corrections (in view of the experimental results) are sketched in the following and experimental features are recalled by which their occurrence may be recognised in QO experiments.

3.4.1 Magnetic Interaction (MI)

The derivation of Eq. (3.9) is based on the assumption that the magnetic field in the sample B_i is the applied external field B_{ext}, i.e., that the oscillating magnetisation $\widetilde{M}$ of the sample is negligible. At high field and low temperatures however it is possible that $\widetilde{M}$ caused by the redistribution of electrons to lower LLs feeds back onto the field during the oscillation cycle itself, so that B_i may be changed. This effect is called magnetic interaction (MI) or Shoenberg-effect and was first reported 1962 by *Shoenberg* on noble metals [166], followed by *Plummer* and *Gordon* [167] and *Condon* [168].
If the magnitude of $\widetilde{M}$ is so high as to cause an oscillating B_i during every oscillation cycle, shape and magnitude of the QOs are influenced and the field and temperature dependence of the QO amplitudes deviates from the expected behaviour in the standard LK formalism (Eq. (3.9)). In view of the QO experiments on κ-(BEDT-TTF)$_2$I$_3$, which state strong deviations in the field and temperature dependence of the SdH amplitudes under certain experimental

conditions (see Secs. 5.3 ff.), the main 'fingerprints' of MI are collected in the following which allow to distinguish, whether MI is their origin or not.

A quantity a for the feedback generated by MI to be significant is the inequality

$$a \equiv 4\pi \left| d\tilde{M} / dB \right| \geq 1 \tag{3.23}$$

A schematic illustration of the modification of the QOs, i.e., the significance of MI for different a is shown in the following Fig. 3.2 [87]. Figure 3.2.a starts from a simulated dHvA oscillation which is assumed to be a simple sine curve in the absence of MI, as plotted in reduced coordinates $y/a \sim M$ versus $x \sim B$.

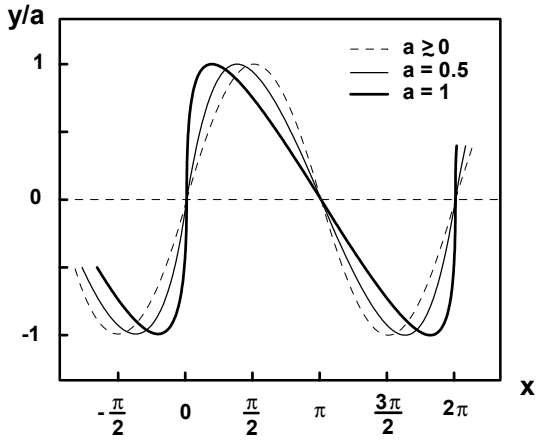

Fig. 3.2.a: Modification of a dHvA oscillation ($y/a \sim M$) within one oscillation period ($x \sim B$). Dotted line: dHvA signal (assumed to be sine-shaped in the absence of MI). Minor influence of MI, i.e., $a = 0.5$ and $a = 1$ change the shape of the dHvA signal [87].

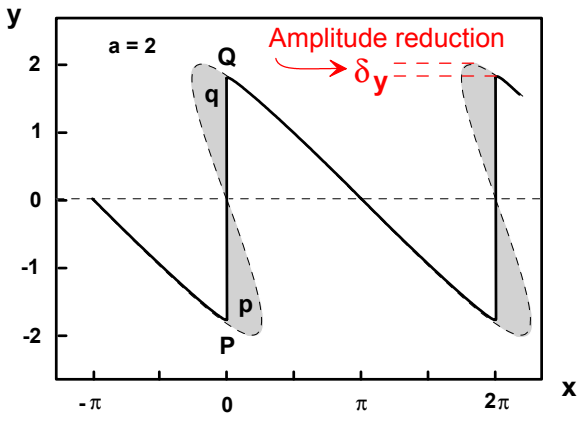

Fig. 3.2.b: For strong MI ($a > 1$) the $x(y)$-course becomes multivalued. The system takes an $x(y)$-, i.e., $M(B)$-course given by a Maxwell construction, where the areas **p** and **q** have to be identical. This results in a sawtooth shape of the QO and in an amplitude reduction by **δy**.

As soon as minor MI are introduced ($0 < a < 1$), the superposition between B_{ext} and $\widetilde{M}$ shifts the $x(y)$-curve as shown in Fig. 3.2.a into the x-, i.e., B-direction. This situation is recognisable in the Fourier spectrum by the presence of a large number of harmonics $n*F$ with enhanced amplitudes. Since this is driven by $\widetilde{M}$, the shift and therefore the amplitudes of the harmonics should strongly increase with field and especially with decreasing temperature. This feature is a precursor necessary to occur before strong MI are possible. In the presence of several QO frequencies F_j as given in the κ-phases of organic metals, combination and difference freqencies (i.e., $F_i \pm nF_k$, with $F_k < F_i$) of the fundamental frequencies are expected.

For strong MI (i.e., $a < 1$), a sawtooth shape of the oscillation is observed [169,170] and an amplitude reduction by **δy** is indicated (see Fig. 3.2.b). It is a matter of fact that the sawtooth is 'inverse', which means that its sharp drop is on the low-field flank of an oscillation[5]. For completeness it should be mentioned, that the sample may break up into so-called Condon domains [168], if the magnitude of MI is further increased.

[5] This orientation of the sawtooth is in contrast to the situation where the chemical potential oscillates: there the sharp drop of the sawtooth is on the high-field flank of a QO (see Fig. 3.7).

In general it can be recorded that an amplitude *reduction* by MI announces itself by a preceding strong enhancement of the harmonics at high B and especially at low T. Furthermore, when $\widetilde{M}$ is 'smooth', i.e., hardly angular dependent, the action of MI, when present, must also be hardly angular dependent.

Besides MI a further effect may occur which modifies the QO amplitudes and spectra with respect to the standard LK formalism (Eq. (3.9)). This effect, known as magnetic breakdown (MB), is described in the following Sec. 3.4.2 . Since both, MI and MB, manifest themselves by partially very similar experimental features (e.g., occurrence of difference and combination frequencies between F_3 and F_2), a collection of distinguishing features is given at the end of Sec. 3.4.2 .

3.4.2 Magnetic Breakdown (MB)

The derivation of the LK formula (Eq. (3.9) is based on the assumption that the electrons move on a closed orbit in k-space. Depending on the band structure, however, individual closed and/or open orbits can lie close to each other, i.e., separated by a finite energy gap E_g. Enabled by an increasing B, the electrons may tunnel through the potential barrier and thus leave their initial trajectory. This effect is known as magnetic breakdown (MB), by which new closed orbits may be realised, while the QO amplitudes of the left orbits are damped with increasing field. MB was first observed by *Shoenberg* [171] and *Priestly* [172]. Stimulation for its understanding was given by *Cohen and Falicov* [173], *Blount* [174] as well as *Pippard* [175,176,165,177]. An overview is provided by Ref. [87].
The description of the MB can be illustrated by Fig. 3.3 according to Ref. [178] on a FS which is very similar to that of the k-phases of organic metals.

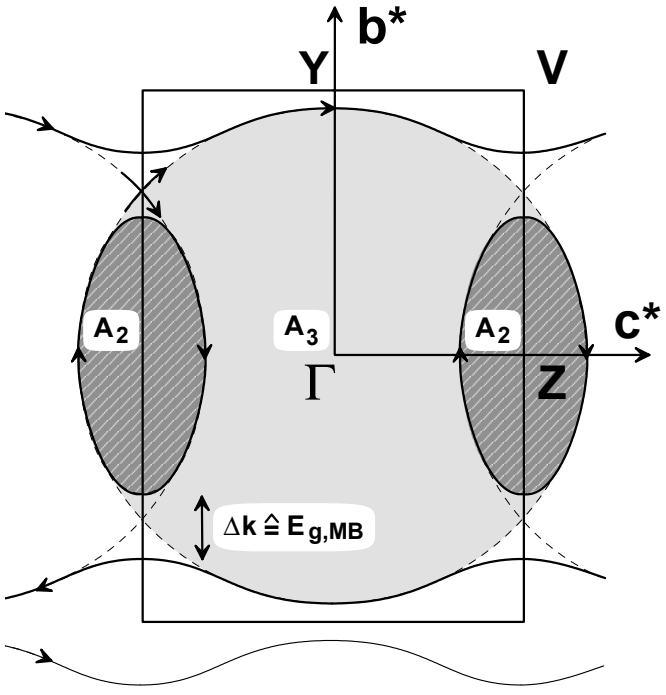

Fig. 3.3.a: Cut of the FS with a closed orbit around A_2 separated from the open 1D trajectory by an energy gap $E_{g,MB}$. At sufficiently high fields the electrons from both trajectories may tunnel the gap (as shown by arrows in one of the gaps), thus closing the trajectory around A_3. For clarity the gap width is grossly exaggerated compared to the real FS of κ-(BEDT-TTF)$_2$I$_3$.

Fig. 3.3.b: Schematic illustration of an 1D coupled network of trajectories in real space (see Refs. [175,165]).

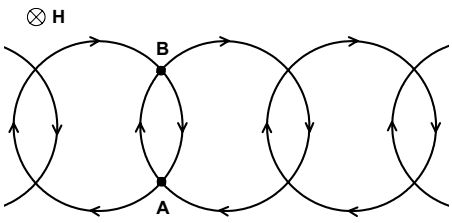

The cut of this FS consists of a closed 2D trajectory encircling A_2, as well as an open one-dimensional (1D) trajectory. Therefore at low fields the QO frequency F_2 corresponding to A_2 is the only observed frequency[6] [179]. Both trajectories are separated from each other by a Δk which corresponds to an energy gap $E_{g,MB}$. In the gap region the passing electrons of both trajectories can undergo either Bragg reflection or tunnelling to the neighbouring orbit, so that in the latter case the orbit around A_3 becomes closed and the corresponding frequency F_3 arises. According to the following so-called Blount criterion [174], tunnelling should dominate when

$$\hbar\omega_C = \hbar\frac{eB_{MB}}{m_{eff}} \geq (E_{g,MB})^2 / E_F \,. \tag{3.24}$$

This equation relates also the gap energy with the so-called magnetic breakdown field B_{MB}. Different approaches to the estimation of B_{MB} were proposed in Ref. [180] and by various other authors (for Refs. see [178]), ending up in very similar results for B_{MB}.
In the gap region the probabilities for both, tunnelling or Bragg reflection, are controlled by the applied field B as well as the MB field, resulting in the probabilities P for MB and Q for Bragg reflection with

$$P = e^{-(B_{MB}/B)} \quad \text{and} \quad Q = (1 - e^{-(B_{MB}/B)}) \quad \text{with} \quad P + Q = 1 \,. \tag{3.25}$$

The 'loss' and 'gain' of electrons on each orbit can be calculated by multiplying an assumed initial number of electrons by P or Q for every time when they pass a gap or when they are reflected. This has to be done until the carriers have passed one complete closed orbit. However for a correct quantitative description it has to be considered, that the trajectories leave the first Brillouin zone, i.e., that the corresponding particle exchange also contributes to the amplitudes. But this consideration expands the problem by arising complex questions on the quantisation due to the lattice structure coinciding with that by the magnetic field. *Pippard* solved this complication by introduction of the so-called coupled network description (CND) [175,176]. He projected the problem to a coupled network of possible trajectories in real space (see Fig. 3.3.b), where the MB and Bragg reflection probabilities are transferred into switching probabilities at the junctions of this coupled 'electrical network'. Detailed analysis (see also [180,87]) reveals the 'magnetic breakdown reduction factor'

$$R_{MB} = (ip)^{n_1} q^{n_2} \,, \tag{Eq. (3.26)}$$

which has to be introduced to the LK formula (Eq. (3.9)) for each possible closed trajectory. $p=(P)^{1/2}$ and $q=(Q)^{1/2}$ represent the amplitudes of the propagating electron wave functions for MB and Bragg reflection, respectively. n_1 is the number of branches, where MB occurs, n_1 is the number at which Bragg reflection takes place during one orbit. The phase factor i considers the possibly different phases of non-equivalent paths, by which an orbit is realised. If the same orbit is realised by a number C of equivalent paths, this 'weight factor' C has to be multiplied to Eq. (3.26). The introduction of the MB by Eqs. (3.24)-(3.26) to the field dependent reduction factor R_D (Eq. (3.13)) of the LK formula allows in reversal the estimation of B_{MB} and $E_{g,MB}$, respectively.
Within the MB region, i.e., when the gap between two neighbouring orbits is indeed tunnelled but not yet overcome, the probability for Bragg reflection at one of the gaps is still non-vanishing. This manifests itself by the occurrence of combination and difference

[6] The notation for A_j and F_j are chosen as to be the same as in the experiments on κ-(BEDT-TTF)$_2$I$_3$ discussed in Ch. 5 .

frequencies between the two fundamental frequencies (here F_2 and F_3) [178]. The most relevant QO frequencies F_j are illustrated in Fig. 3.4 by their enclosed areas A_j in k-space.

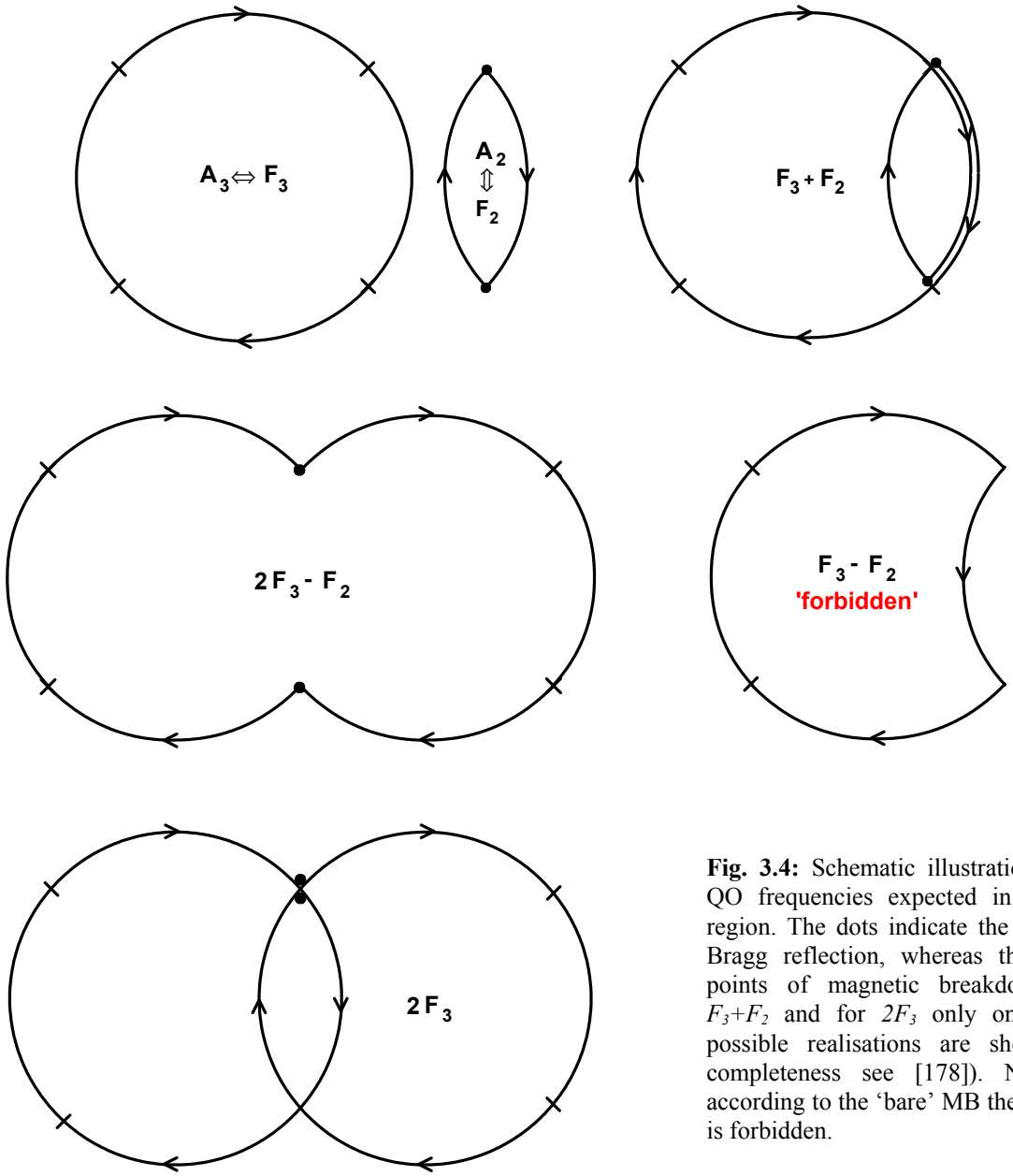

Fig. 3.4: Schematic illustration of the QO frequencies expected in the MB region. The dots indicate the points of Bragg reflection, whereas the dashes points of magnetic breakdown. For F_3+F_2 and for $2F_3$ only one of the possible realisations are shown (for completeness see [178]). Note that according to the 'bare' MB theory F_3-F_2 is forbidden.

According to this the Fourier spectrum of the dHvA oscillations should consist of the fundamental frequencies F_2, F_3, their harmonics nF_j, the combination frequency F_3+F_2 as well as the difference frequency $2F_3$-F_2. It should be stressed that according to the CND description of the magnetic breakdown in a 3DES the difference frequency F_3-F_2 is forbidden due to the fact that it can be only realised by a reversal of the $\boldsymbol{k}$-direction in the gap region, for which the probability vanishes.
From Eqs. (3.25) and (3.26) it is straightforward to see that MB introduces only a smooth field dependent correction to the LK formula, which is determined by B_{MB}/B.

It should be also noted that the MB probabilities are not temperature dependent as long as $E_{g,\,MB} > k_B T$. For two organic metals, κ-(BEDT-TTF)$_2$I$_3$ (see Ch. 5) as well as (BEDT-TTF)$_4$[Ni(dto)$_2$] (see Sec. 6.2.1), it was found that in fact $E_{g,\,MB} \gg k_B T$ [146,181]. Furthermore, the MB probabilities for a cylindrical FS with a cut as shown in Fig. 3.3.a dependent only smoothly on the tilting angle Θ between $\hat{B}$ and k_z.

The occurrence of difference and combination frequencies in the MB region remembers to MI, where combination frequencies are also generated. Therefore the most important features are discussed in the following, which may help to trace back whether MI or MB are responsible for observed experimental features.

1) The **temperature dependence of the combination frequencies**.
As already mentioned, the MB probability is temperature independent, whereas MI is strongly field dependent. Therefore, in the presence of MB the temperature dependence of the 'mixed' frequencies F_3+F_2 and $2F_3-F_2$ should be only given by their respecting m^*_j (which are $m^*_{F3}+m^*_{F2}$ and $2m^*_{F3}-m^*_{F2}$, respectively). However in the presence of MI a strong temperature dependence of the amplitudes should be superimposed to this.

2) The **field dependence of combination frequencies.**
As mentioned in context with MB, frequency mixing should be restricted to the MB region, where $E_{g,MB}$ is not yet overcome. Therefore the amplitudes of combination frequencies induced by MB should decrease with increasing field. In contrast, MI, if present, strongly increases with field and this is just what would be expected for the amplitudes of the resulting difference and combination frequencies.

3) Fermiological features which determine the **spectral weight of difference and combination frequencies**.
Knowing the shape of the FS, especially in the gap region, the possibilities for frequency mixing can be assessed. For a FS as shown in Fig. 3.3, according to the LK theory expanded by the MB, combination frequencies (i.e., $F_3 + nF_2$) should be favoured with respect to difference frequencies (i.e., $F_3 - nF_2$), since the latter ones require a stronger change in the momentum Δk during the Bragg reflection at the gap as the former ones. Therefore the $F_3 + nF_2$ combination frequencies should have a higher spectral weight in the Fourier spectrum than the $F_3 - nF_2$ difference frequencies. In contrast, in the presence of MI, both, $F_3 \pm nF_2$ should have the same spectral weight for the same n.

These features may be utilised to distinguish between the possible occurrence of MB or MI, however keeping in mind that further deviations from LK behaviour may be produced by completely different effects, as, e.g. two-dimensionality of the electronic system.

Therefore the effects of quasi- and twodimensionality are discussed in the following two sections, starting with some principal properties of Q2D and 2D systems, which may even push the LK formalism to its limits. The influence of two-dimensionality onto the magnetic breakdown is described in Sec. 3.4.5 .

3.4.3 Effects of Quasi-Twodimensionality and Twodimensionality of the System

A Quasi-2D and 2D Fermi Surface in a Multilayer Metallic System

As already mentioned in the discussion of Eq. (3.2), the Landau-quantised states in an infinitely thin 2D system are concentric circles, since k_z vanishes. In a metallic multilayer system however, a motion along k_z is not only possible, but even free and, moreover, the motion is not influenced by a magnetic field oriented collinear to k_z. The resulting quantised states are concentric Landau cylinders. According to Eq. (3.2), the effective mass determines the contribution of k_z to the energy states. In a modestly anisotrope system this contribution is considerable and it is therefore called a *quasi*-2D system. Its typical FS is 'warped', i.e., corrugated along the k_z-direction as shown in Fig. 3.5.a .

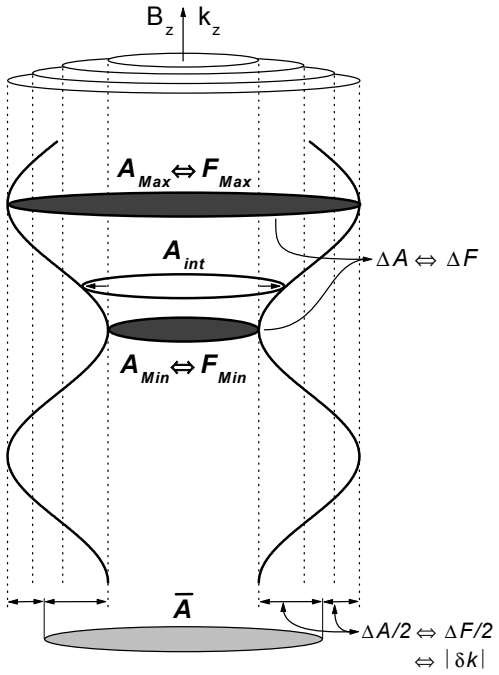

Fig. 3.5.a: Corrugated (i.e. warped) Fermi surface of a quasi-2D metallic multilayer system with the two remaining extremal areas A_{Max} and A_{Min} contributing to quantum oscillations (here $\bar{A} = (A_{Max} + A_{Min})/2$, details see text).

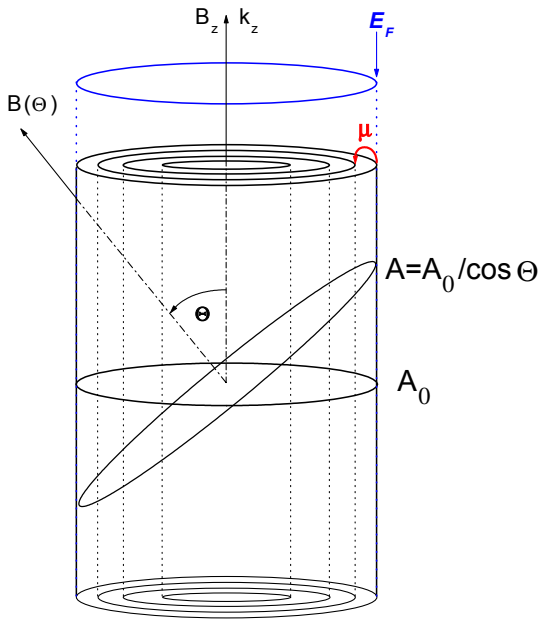

Fig. 3.5.b: Fermi surface (FS) of an ideal 2D electronic system of a multilayer metal, where k_z is not restricted. The actual position of μ is defined by the outermost occupied Landau cylinder. A cylindrical FS of a 2DES is characterised by $A(\theta) \sim F(\theta) \sim 1/\cos(\theta)$.

If however the system is strongly anisotrope, the contribution of k_z vanishes and the FS approaches an ideal cylinder (see Fig. 3.5.b). Both situations are responsible for deviations in the QO amplitudes from the standard 3D LK formalism (Eq. (3.9)), as will be sketched in the following.

Departures from the LK Formalism by a Warping of the FS

For the evaluation of a warped FS of a Q2D system it is useful to define a minimal area A_{Min} and a maximal area A_{Max} in k-space (see Fig. 3.5.a). In general the intercept between A_{Max} and A_{Min} is intersected by a number of LCs (dashed lines). Now, increasing the field means that the LCs within this intercept cross an intermediate extremal area A_{int} which varies its size from A_{Min} to A_{Max}. Since $A \sim F$, the varying A_{int} contributes with a varying frequency to the QOs. The superposition of these contributions coming from $A_{Min} < A_{int} < A_{Max}$ results in their destructive interference. The only remaining contributions to QOs originate from$A \equiv A_{Min}$ and $A \equiv A_{Max}$ themselves [7], which corresponds to the occurrence of two slightly different QO frequencies $F_{Min} \sim A_{Min}$ and $F_{Max} \sim A_{Max}$, respectively. The superposition of both these frequencies leads to a destructive interference at certain field values, i.e., the occurrence of so-called warping nodes[8] in the field dependence of the QO amplitudes (see simulation in Fig. 3.6).

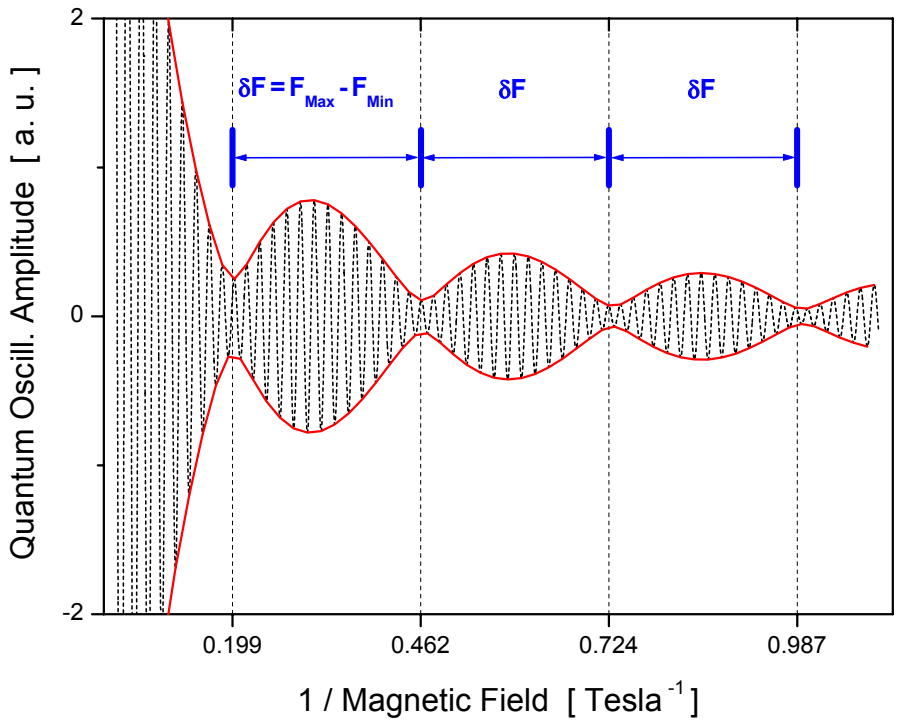

Fig. 3.6: Warping nodes generated by a corrugated FS as shown in Fig. 3.5.a with a warping frequency ΔF. In general, the two effective masses of the carriers which encircle A_{Min} and A_{Max} may be different. Since m_{eff} determines the QO amplitudes, this leads to different superposing amplitudes. Therefore the resulting amplitude in the warping nodes does not vanish for different m_{eff}, whereas it vanishes when the effective masses are identical.

The position of these nodes is exactly equidistant in $1/B$ and corresponds to the difference between the two superposing frequencies, i.e., $\Delta F = F_{Max} - F_{Min}$[9]. The ratio $\Delta F/F$ quantifies the

[7] As already mentioned in context with Eqs. (3.6) and (3.9), the contribution to the phase of the QOs coming from A_{Min} is a '+', whereas from A_{Max} it is a '-'.

[8] also called beating nodes

[9] The value of F counts the number of LCs inside the FS at 1T. Accordingly, ΔF counts the number of LCs between A_{Min} and A_{Max} at this field.

warping of the FS related to its diameter [10] in terms of a deviation of the FS from a perfect cylinder. ΔF is obtained by use of Eqs. (3.5) and (3.7) from the field intercept between two warping nodes, or, alternatively, ΔF can be read out from the local minima of a Dingle plot of the signal (plotted according to Eq. (3.15)), where exactly equidistant local minima are present. In the absence of such nodes, the maximal field intercept where warping nodes are absent allows to estimate at least an upper limit for the warping (see Sec. 5.3.1). From the amount of warping the interlayer transfer integral $t_\perp$ perpendicular to the conducting planes can be estimated. Assuming a cosine-shaped corrugation of the FS in k_z-direction the energy dispersion can be described by a cosine-modulation as

$$E(k) = \frac{\hbar^2}{2\,m_{eff}}\left(k_x^2 + k_y^2\right) + 2\,t_\perp \cos\left(k_z\,a\right), \tag{3.27}$$

where a is the spacing between the conducting planes [182,183,184]. The sum $(k_x^2+k_y^2) = \boldsymbol{k}_F^2$ is a measure for $t_{//}$. $t_\perp$ represents the warping of the FS and can be obtained from ΔA (see Fig. 3.5.a) via Eq. (3.7) in terms of a $|\delta k|$. With this the intrinsic two-dimensionality of an electronic system can be expressed by the ratio between the inter- and intralayer transfer integrals $t_\perp/t_{//}$, where $t_{//} = E_F/4$ in a 2D system.
It should be emphasised that according to the LK theory the warping nodes should occur at exactly the same field positions in dHvA and SdH experiments.

3.4.4 De Haas-van Alphen Effect in Two-Dimensional Electronic Systems

For a perfect 2DES the warping vanishes, so that the Landau-quantised states as well as the FS are perfect cylinders (see Fig. 3.5.b). In such a 2DES the actual position of the chemical potential μ is defined by the outermost occupied LC as long as $\hbar\omega_c \gg k_B T$. As soon as this LC passes the FS and is emptied, μ drops to the next lower lying LC and increases again with the area of this LC until its next drop. This means that in a 2DES μ oscillates sawtooth-like with the present QO frequency [185]. In contrast, a spherical Fermi surface of a 3D system is intersected by all LCs inside the FS (see Fig. 2.1), so that all of them define the actual position of μ. The contribution of the inner LCs to μ is non-oscillatory for the same reason as they do not contribute to QOs. The only oscillatory contribution to μ originates from the outermost LC as it leaves the FS. However since the curvature A'' of the FS is finite, this contribution is negligible, so that in a 3DES μ is practically fix.
For the derivation of the 3D LK formula a sum over all LCs inside the FS is required [186], whereas in the 2D case only the sum over the two outermost LCs is needed, since the inner ones are assumed not contribute to the oscillatory part of μ [88,89,90]. In consequence, in a 3DES the field dependence of the oscillation amplitudes is given by an exponential function (see Eq. (3.13)) entering the LK formula [186], whereas in the 2D case the field dependence is more complex. In contrast to the first description for an ideal 2DES at T=0K and with T_D=0K [185], the field dependence of the magnetisation of a real 2DES at finite T was obtained later (see Refs. [88,89,90]) as

[10] The correct quantity is $\Delta F/\overline{F}$ with $\overline{F}$ obtained from $\overline{A} = (A_{Max} + A_{Min})/2$ (see Fig. 3.4.a), however since mostly $\Delta F << F$, the simplification made in the text can be justified.

$$\widetilde{M}(B) \sim \left[\mu(B) + \hbar\omega_C A\left(n_F + \frac{\sinh\alpha}{2\sinh(x_F)}\right) - \hbar\omega_C\,(n_F^2+1) + k_B T \ln(2\cosh(x_F) + 2\cosh\alpha)\right]$$

$$\text{with}\quad A = \frac{\sinh x_F}{\cosh x_F + \cosh\alpha} = n_F - \frac{N\Phi_0}{VB};\qquad x_F = \frac{n_F\,\hbar\omega_C - \mu}{k_B T};\qquad \alpha = \frac{\hbar\omega_C}{2k_B T}\ . \quad (3.28)$$

n_F is the highest occupied LC and x_F is its contribution to M. An example for such a curve generated by numerical calculations is shown in Fig. 3.7 [90].

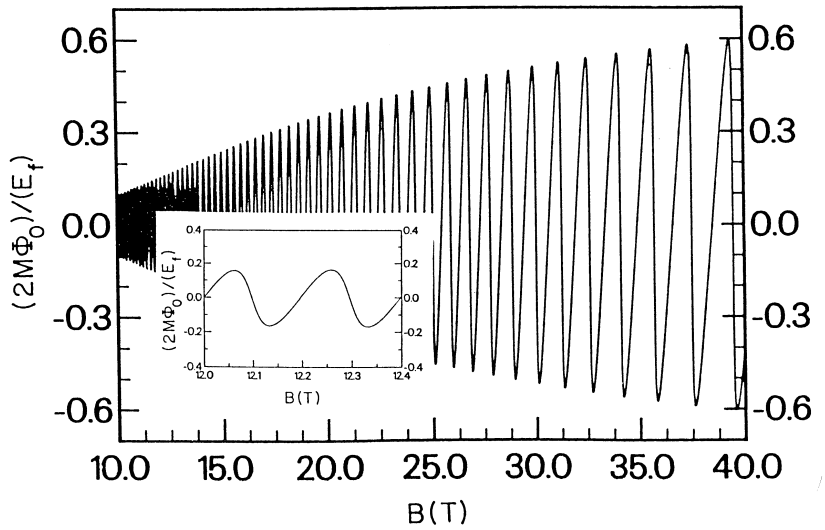

Fig. 3.7: Field dependence of the magnetisation (numerical according to Eq. (3.28)) with m_{eff}=0.3m_e, E_F=0.3eV, T_D=0K and T=10K (see Ref. [90]).

In contrast to the exponential field dependence of the QO amplitudes expected for the 3D case, this curve for a 2DES with an oscillating μ (called $\tilde{\mu}$ in the following) describes a sublinear increase of the amplitude with B. Equation (3.28) shows that $\widetilde{M}(B)$is driven by $\hbar\omega_c$ (which contains $m^*(\Theta)$) and k_BT. A consequence of this is that the resulting deviations from the LK formula are smoothly field and only weakly angle dependent.
A further result of $\tilde{\mu}$ is a sawtooth-shaped magnetisation curve (see inset of Fig. 3.7), which is here rounded off by effects of finite temperature. It is noteworthy that the steep flank of the sawtooth is on the high-field side of an oscillation when μ oscillates [88,187,91], whereas it is on the low-field side when the sawtooth is generated by MI instead of $\tilde{\mu}$ (see Fig. 3.2.b). When μ oscillates such a sawtooth-shaped magnetisation curve (including its orientation) is indeed observed in experiments on 2D semiconductors (see, e.g., Refs. [188,189]; consider the [1/B]-plotting in [189]). However it should be pointed out that the theoretical and experimental works quoted above consider only the simple situation of *one single* quantised orbit. The general case of *several* quantised orbits with *different* LL spacing is much more complex, since their density-of-states modulations *intersect* each other at the FS and therefore may prevent the development of a sawtooth - at least at actually available fields and temperatures. This latter situation is given in the 2D organic metal κ-(BEDT-TTF)$_2$I$_3$ (see Fig. 4.4 and Ch. 5).

A further influence of an oscillating μ manifests itself by a modification of the field positions of the spin-split quantum oscillations. A general treatment of this feature on the basis of experiments on the 2D organic metal κ-(BEDT-TTF)$_2$I$_3$ is given in [91] and will be discussed in Sec. 5.3.1 .

It should be noted that the description of the dHvA effect in 2DES recalled in this section is based on a conservation of the total number of carriers in the system contributing to QOs[11].

3.4.5 Influence of the Oscillating Chemical Potential on the Magnetic Breakdown

The description of conventional MB as discussed in Sec. 3.4.2, was derived initially for 3DES. The situation becomes more complex in a 2DES, where the chemical potential μ oscillates. In order to illustrate this, it is useful to switch from the picture in *k*-space (as used in Fig. 3.3.a) to an energetic picture as sketched in Fig. 3.8 .

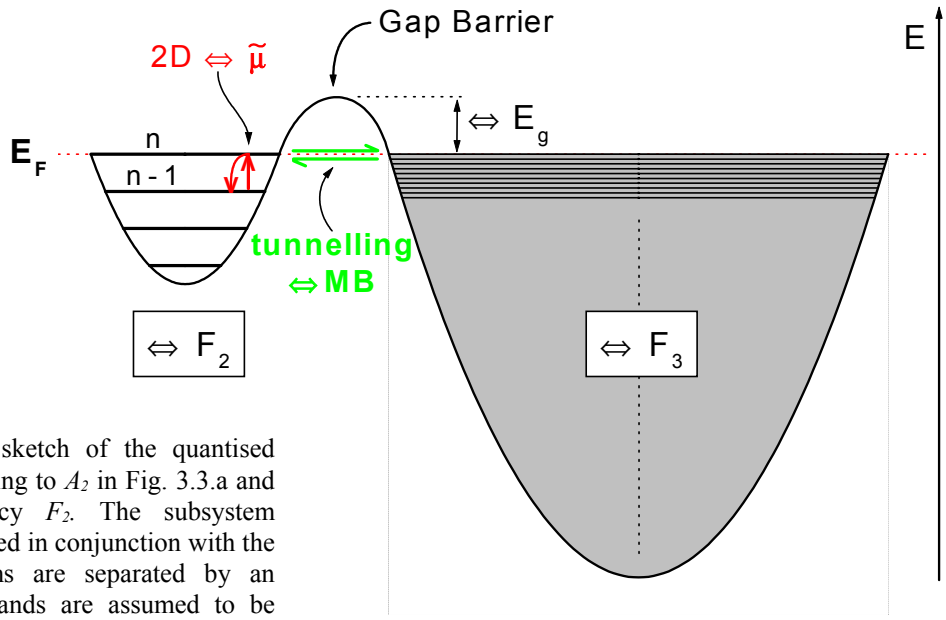

Fig. 3.8: Simplified sketch of the quantised subsystem corresponding to A_2 in Fig. 3.3.a and to the QO frequency F_2. The subsystem belonging to F_3 is closed in conjunction with the MB. Both subsystems are separated by an energetic gap. The bands are assumed to be parabolic.

Figure 3.8 shows a simplified energy scheme of the completely quantised subsystem corresponding to the extremal area A_2 in Fig. 3.3.a and to the QO frequency F_2. The subsystem representing F_3 is separated by a gap from the former one. It is Landau quantised in turn with the MB, so that an uniform electron distribution is still present (illustrated as grey-scaled background). In a 3DES, the chemical potential is practically fix, so that the electron density at E_F is only modulated by the broadened 3D electron density of the LL structure corresponding to F_2 (left part) and by the weakly modulated 3D electron density brought in by F_3. These (relatively moderate) modulations determine the tunnelling

[11] A 2D electronic system with a fixed number of electrons and an oscillating μ is also called a 'canonical ensemble' of electrons, whereas a 'grand canonical ensemble' is present in a 3D system where μ is fix.

probabilities and -directions in the gap and contribute to the MB and Bragg reflection probabilities discussed in Sec. 3.4.2. In a 2D system however the electron density is much sharper and, moreover, μ oscillates. This means that at low fields $B<B_{MB}$ μ is defined by the highest LL of the only quantised subsystem belonging to F_2. As the field is such increased that the LLs corresponding F_3 are sufficiently sharp, μ is defined alternately by the actual highest occupied LL provided by F_2 or F_3, respectively. The oscillation of μ changes the height and with of the gap and therefore the tunnelling probabilities. The modulation of this oscillation by F_2 and F_3 generates difference frequencies in the Fourier spectrum in the MB region, especially F_3-F_2, which is forbidden in the 'pure' MB when μ is fix (see Fig. 3.7) [190,191].
Briefly worded, the oscillation of μ in a 2DES modifies the Fourier spectrum in the MB region significantly. Before this can be compared with the spectrum of MB at fixed μ, it has to be considered that a further effect, namely quantum interference, may also influence the Fourier spectrum. This effect is described in the following, ending up with a comparison of the Fourier spectra of MB at fixed μ, at oscillating μ, as well as under the influence of quantum interference.

3.4.6 Modification of the QO Spectrum in the MB Region by Quantum Interference

The effect of quantum interference [192,193] can be illustrated by means of the coupled network description of orbits in real space [175,165,194] as reproduced in Fig 3.9. The points A and B within the network can be reached by different paths where electrons move in the same direction , e.g., C_2 and C_3. Two electron waves starting at A on the different paths C_2 and C_3 arrive with a phase difference in B, where they interfere. The phase difference is given by the enclosed area [192]. In *k*-space this corresponds to the difference between the extremal areas A_3 and A_2 (see Fig. 3.3.a) and represents a QO frequency F_3-F_2. This is one of the frequencies which may be generated by this so-called quantum interference (QI) effect. However, since no net current is circulating along the loop composed of C_2 and C_3, this motion does not result in a dHvA oscillation, so that in the dHvA spectrum a QI frequency on principle cannot be observed. However when a current is transported through the sample, the phase differences lying beyond QI may influence the magnetoresistance such that QI may observed in SdH experiments under appropriate conditions. When present in transport experiments, QI modifies the Fourier spectrum as shown in Sec. 3.4.7 .
In a stable FS the paths in *k*-space are not temperature dependent and the temperature dependence of the QO amplitudes of the *fundamental* frequencies (as given by m^*, see Eq. 3.10) is not considerably modified by QI. However it should be mentioned that for certain QI *combination* frequencies as e.g. $F_3 - 2F_2$, the effective masses $m^*_{F3-2F2} = m^*_{F3} - 2m^*_{F2}$ may be very small, so that the amplitudes of $F_3 - 2F_2$ can persist even up to $T \geq 4.2$K, where they may be even the only observed QOs [195].
It should not be suppressed that the conditions for QI are determined not only by semiclassical path differences as discussed here, but also by gap widths, or by the different effective masses and Fermi velocities of the electrons moving along the various trajectories. This implies that even in materials, which are very similar from the fermiological point of view, the conditions for QI may differ.

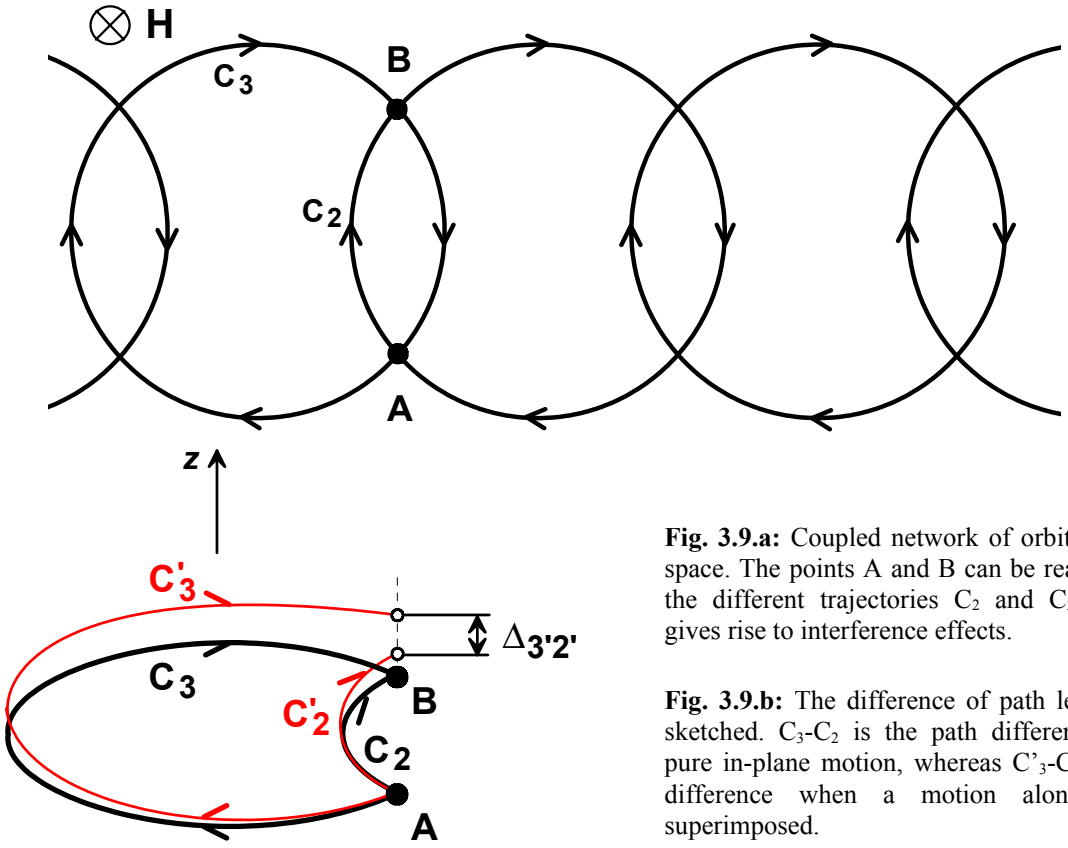

Fig. 3.9.a: Coupled network of orbits in real space. The points A and B can be reached by the different trajectories C_2 and C_3, which gives rise to interference effects.

Fig. 3.9.b: The difference of path lengths is sketched. C_3-C_2 is the path difference of a pure in-plane motion, whereas C'_3-C'_2 is the difference when a motion along z is superimposed.

In the following section the results of QI onto SdH oscillations are compared with the influence onto QOs coming from MB or an oscillating μ.

3.4.7 Comparison of the Fourier Spectra in the Presence of MB, an Oscillating Chemical Potential or QI

This section illustrates how Fourier spectra in the MB region might be modified by 'pure' MB in a 3DES, by an oscillating chemical potential in a 2DES or by QI. A number of authors have contributed to the understanding of MB (see, e.g., Refs. [171,172,173,174,175,176,165,177,178]) and to investigations of an oscillating μ as well as quantum interference in the MB region (see, for instance, Refs., [196,197,198,199,200,201,202,203,204,195,191,205,206,207,208,209,210,211,212,213], specified later).
Under very favourable circumstances the Fourier spectrum in the MB region might be a tool to recognise which of the above mentioned features are present in a material. However unfortunately a general unambiguous assignment between a Fourier spectrum and MB, with or without an oscillating chemical potential and with or without QI is unfortunately not given to date. Actually neither the experiments, nor the theoretical descriptions can be brought to a full general agreement. It would be beyond the scope of the present work to discuss these subjects in detail. Instead, a brief insight is given as far as necessary for the discussion of the experiments on κ-(BEDT-TTF)$_2$I$_3$ in Ch. 5. Furthermore some characteristics especially of an oscillating μ and QI are pointed out, which turned out to be at least a 'common denominator'

within the variety of experiments and the different theoretical approaches to these subjects. For clarity the insight starts, based on a study performed in Ref. [191] by experiments and numerical calculations on the organic metal κ-(BEDT-TTF)$_2$Cu(NCS)$_2$, which is closely related in many aspects to the material κ-(BEDT-TTF)$_2$I$_3$ discussed in Ch. 5, i.a., by their similar Fermi surfaces [214,143,144]. In Ref. [191] the influence on of a fixed vs. an oscillating μ on magnetisation is studied in the MB regime and furthermore the effects of QI on transport measurements are included.

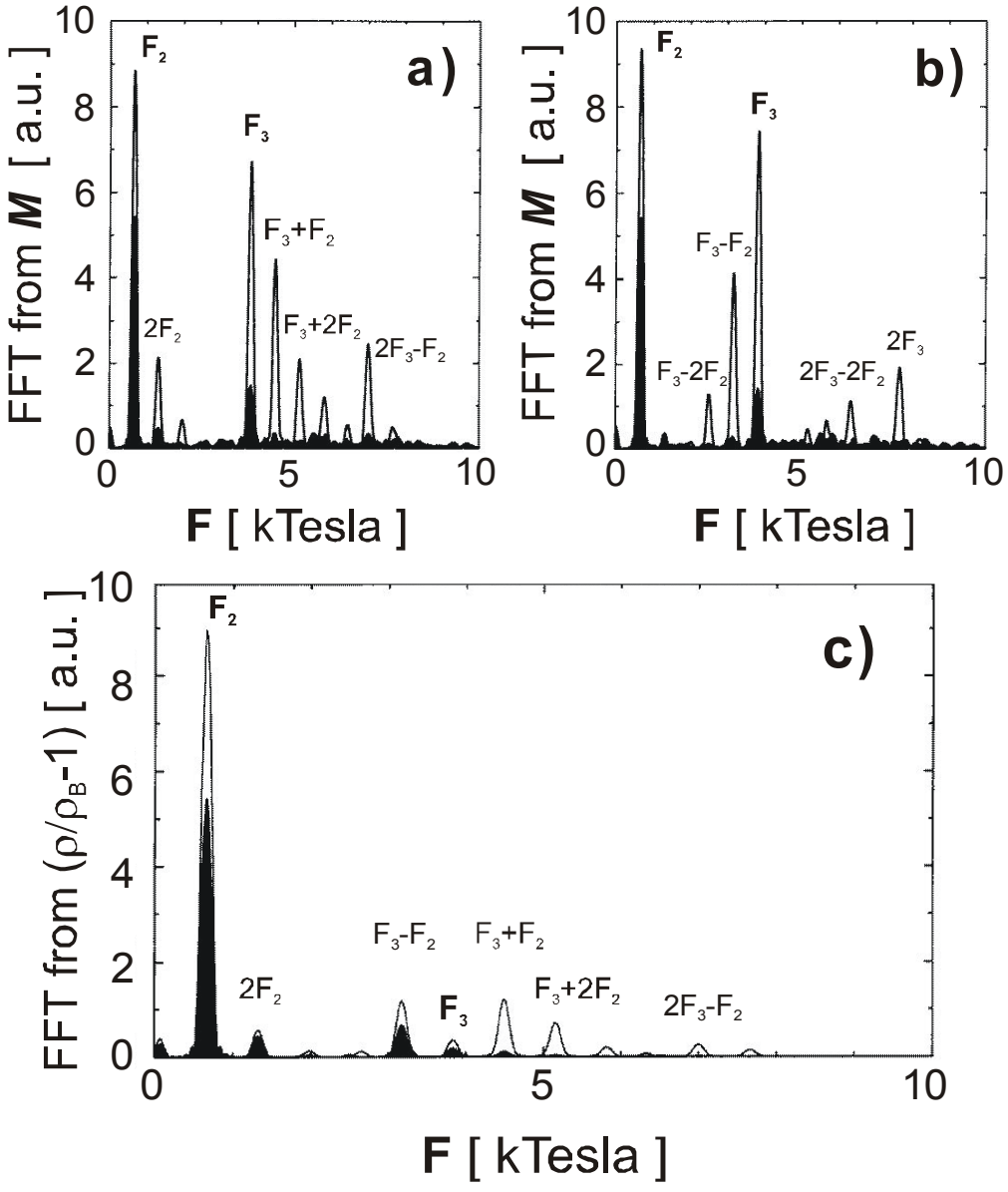

Fig. 3.10: Fourier spectra (numerical calculations) for magnetisation (parts a) and b)) and magnetotransport (part c)) on κ-(BEDT-TTF)$_2$Cu(NCS)$_2$ according to Ref. [191]. Filled areas represent the spectra at 1.4K while thin lines represent the spectra at 0.4K. **a):** 'Pure' magnetic breakdown with a fixed chemical potential μ ('3D CND approach'). **b):** MB in the presence of an oscillating μ ('2D approach'). **c):** Magnetotransport in a 2DES (oscillating μ) with quantum interference present.

As already mentioned in Sec. 3.4.2, the conventional coupled network description (CND) of magnetic breakdown in a 3DES is based on a fixed chemical potential and, furthermore, on an energy spectrum of the electrons, which is not influenced by the external magnetic fields

[173,174,175,176,165,177,178]. According to the CND, a typical Fourier spectrum in the MB region with *fixed* μ should consist of the fundamental frequencies denoted as F_2 and F_3 in Fig. 3.10.a [179], their harmonics, furthermore combination frequencies as F_3+F_2, F_3+2F_2 as well as allowed difference frequencies as $2F_3-F_2$ (see also Fig. 3.4 and Ref. [178]). However those difference frequencies which are connected with a reversal of momentum at the MB gap, especially F_3-F_2 and F_3-2F_2, are *forbidden on principle* in this picture. In contrast in a 2DES, i.e., with an *oscillating* μ, a dHvA Fourier spectrum in the MB region would be expected to tend to that shown in Fig. 3.10.b. It contains the fundamental frequencies and their harmonics, but contrary to Fig. 3.10.a it contains the 'forbidden' difference frequencies F_3-F_2 and F_3-2F_2, while the allowed combination frequencies F_3+F_2 and F_3+2F_2 are absent.
However, for reasons sketched in the following, it should not be suppressed here that it would be exaggerated to suggest that an unambiguous connection between a certain Fourier spectrum and an oscillating μ in the MB is actually available.

1) The spectral weights of the successive difference frequencies, for instance, are shown to vary with the MB gap width [202].

2) DHvA torque experiments on the same material κ-(BEDT-TTF)$_2$Cu(NCS)$_2$ as underlying to Fig. 3.10 were made by another group. As in Fig. 3.10.b they show F_3-F_2, but in contrast also F_3+F_2, both with even similar magnitudes in amplitude [213]. There however the result is explained by a 'coherent magnetic breakdown' model with a fixed μ, where the energy spectrum of the electrons is influenced by the external magnetic field. This results in Landau bands with both, oscillating bandwidth and oscillating band spacing, which generate such a Fourier spectrum.

3) In Refs. [203,204] a similar Fourier spectrum to those in Fig. 3.10.b and in Ref. [213] is explained by a recursive band structure model with fixed μ.

4) However, Refs. [202,206,208] explain such a Fourier spectrum again with oscillating μ (Refs. [202,206] by full 2D quantum numerical calculations, whereas [208] by extending the model introduced in Ref. [194]).

5) A similar FFT pattern is explained in Ref. [207] by a multiband model.

6) Additional aspects are introduced by Ref. [212] by a tight binding Hofstadter approach, which shows that the spectral weight of the frequencies F_3-F_2 and F_3+F_2 is even influenced by the spin *g*-value.

7) It was illustrated in Ref. [210] that in the same material κ-(BEDT-TTF)$_2$Cu(NCS)$_2$ μ is expected to oscillate not only with F_3-F_2, but also in the same order of magnitude with F_3+F_2, which is not observed in Fig. 3.10.b. In the same reference a Fourier spectrum very similar to that shown in Fig. 3.10.b is calculated for the material α-(BEDT-TTF)$_2$KHg(NCS)$_4$ assuming the case of $\tilde{\mu}$. However there the forbidden frequency F_3-F_2 also appears in comparative numerical calculations when a fixed μ is put in. The significant difference is that an oscillating μ 'amplifies' the amplitudes of difference frequencies as F_3-F_2 and F_3-2F_2, whereas a fixed μ 'amplifies' combination frequencies as F_3+F_2 and F_3+2F_2. This result would agree with parts b) and a) of Fig. 3.10. . However the authors of Ref. [210] come to the conclusion that the forbidden frequencies are generated by the interplay of two partially occupied bands near E_F rather than $\tilde{\mu}$.

8) Finally, a further point of discussion is given by dHvA measurements on the conventional 3D metal magnesium, where forbidden frequencies were observed, even though μ oscillations must be irrelevant [196].

The situation becomes even more complex when quantum interference (QI) is introduced. Figure 3.10.c reproduces the results of numerical calculations made for magnetotransport on κ-(BEDT-TTF)$_2$Cu(NCS)$_2$ in the MB region with oscillating μ and QI present [191]. Especially at low temperatures (thin lines in Fig. 3.10.c) the spectral weight of the occurring combination frequencies F_3+F_2 and F_3+$2F_2$ remembers to the case of 'pure' MB with fixed μ (comp part c) with part a) of the figure). However with QI the forbidden frequency F_3-F_2 is present with a similar spectral weight as F_3+F_2 (part c)). With QI the amplitudes of both, F_3-F_2 and F_3+F_2 at low T are even stronger than that of F_3 itself. These results are in agreement with SdH studies between 30T and 50T presented in the same reference.
However SdH studies on the same material made by another group [195] report on the occurrence of the forbidden frequency F_3-$2F_2$, which is absent in Fig. 3.10.c, whereas in return especially F_3-F_2,F_3+F_2 and F_3+$2F_2$ are absent in the study presented by Ref. [195].

The precedent aspects are collected to show that a unambiguous spectral 'fingerprint' of MB with fixed or oscillating μ and QI is not yet available. The results of theoretical approaches to these problems depend on the model used, whereas experimental results seem to depend on experimental parameters as fields, temperatures, scattering times, etc. .
For reasons of pragmatism at least a 'common denominator' is brought out in the following, which should be sufficient to assess whether $\tilde{\mu}$ and/or QI influence the experiments on κ-(BEDT-TTF)$_2$I$_3$ discussed in Ch. 5.

i) In the MB region an oscillating μ tends to support the occurrence of difference frequencies F_3-F_2 and F_3-$2F_2$ and to suppress combination frequencies F_3+F_2 and F_3+$2F_2$. In contrast, QI tends to suppress difference frequencies and to support combination frequencies. At temperatures which are sufficiently low that F_3 is observed a presence of QI without the occurrence of F_3+F_2 is not reported.

ii) At finite T and τ, an oscillating μ neither damps the amplitudes of F_2 and F_3 themselves nor changes the ratio of their amplitudes significantly (compare parts a) and b) of Fig. 3.10).

iii) QI is irrelevant, when even at low temperatures both, difference and combination frequencies have much lower amplitudes than F_3 and/or F_2 themselves. This means that most of the electrons may move along the closed orbits corresponding to F_3 and/or F_2, while only a small part is influenced by QI effects (see Figs. 3.3.a and 3.9).

iv) In the preceding discussion an oscillation of μ means that in the MB regime the chemical potential may oscillate with the QO frequency F_2, since the corresponding orbit is the only closed and Landau-quantised one. However as soon as the MB is completed, this μ oscillations with F_2 loose importance in favour of μ oscillations with F_3, since less and less electrons stay on the F_2 orbit, while the F_3 orbit is more and more populated and becomes fully quantised. Therefore μ oscillations with F_2 are restricted to the MB region.

v) The magnitude of μ oscillations is given by the effective magnetic field along the Landau cylinders. Therefore the influence of $\tilde{\mu}$ should depend only weakly and in any case *smoothly* on the tilting angle Θ between the magnetic field and the 2DES, i.e., the conducting plane of layered materials.

vi) For the same principle the influence of QI should be weakly and smoothly angle dependent, since the underlying path differences on cylindrical Fermi surfaces are only smoothly angle dependent within an order δΘ of degrees.

Since unfortunately an oscillating μ cannot be identified unambiguously by a clear spectral 'fingerprint', two different methods were introduced in Refs. [91,215] and [216], respectively, to detect μ oscillations. Furthermore the second of these methods is expanded in Ch. 5 where it reveals decisive new results.

The standard Lifshitz-Kosevich theory for quantum oscillations in 3D metals (Secs. 3.1 - 3.3) as well as all corrections to it as discussed in Secs. 3.4, including the theories for 2DES have the common assumptions that the electrons are noninteracting and that the total number of carriers N_e in a system contributing to quantum oscillations is conserved.
However it is well-known that in 2D electronic systems, which are exposed to high magnetic fields and low temperatures, electrons may be localised thus leading to the quantum Hall effects. The understanding of certain results of QO experiments carried out on the 2D organic metal κ-(BEDT-TTF)$_2$I$_3$ presented in Ch. 5 requires an insight to the understanding of the quantum Hall effects in Ch. 4.

4. The Quantised Hall Effects

As already mentioned earlier, conventional descriptions of quantum oscillations in 3D and even in 2D metals do not include the possibility that in 2D electronic systems electrons may be correlated as well as localised at high magnetic fields and low temperatures. Such electron localisation may occur in 2D systems of non-interacting carriers (as known from the IQHE), but also as a result of electron correlation (EC), as present in the FQHE.
In the present chapter it is not intended to reproduce a detailed review of the quantum Hall effects. This is already done extensively (see, e.g., Refs. [130,127,217,150]). However most of the work reviewed here is devoted to 2D systems based on *semiconductors*, whereas the experimental part of the work concentrates on a 2D *metal*. Therefore in the following especially those of the properties are discussed, which are most important for the understanding of the experiments on the 2D organic metal κ-(BEDT-TTF)$_2$I$_3$ presented in Ch. 5. In addition some aspects are worked in, which may illustrate, how electron localisation (EL) may influence QO experiments and which point out, where common features and significant differences of EC and EL in 2D semiconductors and in 2D multilayer organic metals may be.
It is noteworthy that a number of properties in the IQHE and FQHE are determined by the number of electrons, filling factors, carrier mobilities, dielectric constants, effective masses as well as the cyclotron radii. All these quantities may be very different in semiconductors and metals. It is, e.g., worth mentioning that the cyclotron radii[1] are

$$\ell_0 = \sqrt{\hbar/eB} \sim 1/\sqrt{B} \tag{4.1}$$

in a semiconductor (hopping motion), whereas

$$R_c = \frac{\hbar k_F}{eB} \sim 1/B \tag{4.2}$$

in a metal, where free electron motion is assumed. Furthermore, in a metal R_c is not universal, but depends on the Fermi wave vector k_F, i.e., the size A_F of a quantised orbit of an electron (as illustrated, e.g., in Fig. 3.1).
As already mentioned, nearly all calculations referred to here were carried out for 2D semiconductor devices. The influences of the above mentioned quantities onto the IQHE and FQHE may be a guide in the following as to stimulate to think over differences and similarities between the quantised Hall effects in 2D semiconductors and 2D metals.

4.1 The Integer Quantum Hall Effect (IQHE)

After the suggestion of *Ando et al.*, according to which the Hall resistivity ρ_{xy} may be quantised [218] and after plateau-like behaviour was observed in ρ_{xy} [219] and σ_{xy} [220], the quantum Hall effect at integer Landau level filling factors (IQHE) was discovered by *von Klitzing et al.* [99]. The IQHE is an exciting macroscopic result of a quantum phenomenon which was first observed in semiconducting two-dimensional electronic systems (2DES) in

[1] ℓ_0 is also called 'magnetic length', which is the average distance between two electrons at a given magnetic field.

high perpendicular magnetic fields at low temperatures (see Fig. 4.1). Under these conditions the Hall resistance R_H ($\equiv R_{xy} \equiv \rho_{xy}$) exhibits plateaux at integer multiples n of h/e^2, i.e., $\rho_{xy} = h/ne^2 = R_K/n$ with the *von Klitzing constant* $R_K = 25812.807 \pm 0.05\Omega$ [221,222]. By this ρ_{xy} was shown to be determined by universal constants (to an accuracy of 10^{-8}) without any influence of, e.g. sample impurity or system geometry.

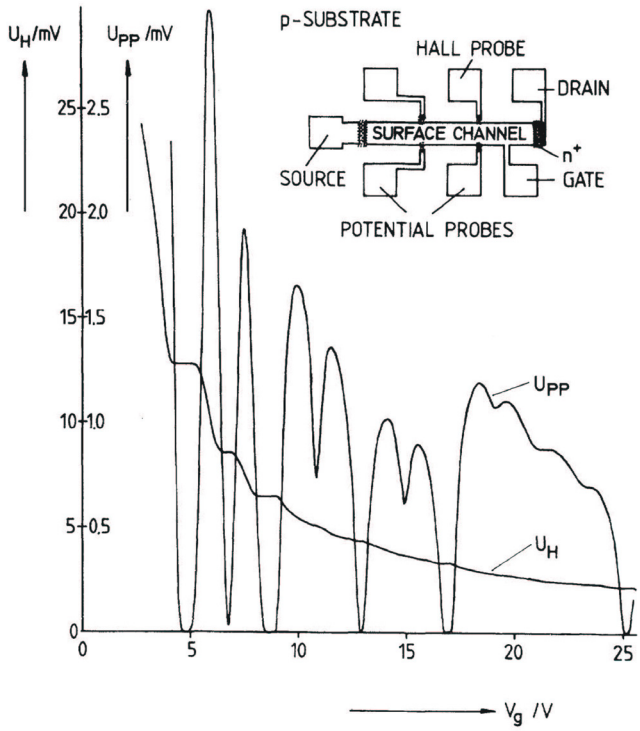

Fig. 4.1: Integer quantum Hall effect as detected by *von Klitzing et al*. (Ref. [99]) on a Si-MOSFET sample. U_H is the Hall voltage, whereas U_{PP} is proportional to the diagonal resistivity ρ_{xx}, i.e., the SdH signal. Further experimental parameters were B=18T, T=1.5K, source-drain current I=1μA. The Landau level filling factor was controlled by the gate voltage V_g (i.e. by the electron population in the 2DEG) rather than by a magnetic field variation. Both signals, U_H and U_{PP}, include spin as well as valley splitting.

Coinciding with the Hall plateaux the diagonal resistance ρ_{xx} tends to vanish (i.e., $R_{xx} < 10^{-10}\Omega$ [131]), thus indicating dissipationless current flow at integer Landau level filling factors n. Within the Hall plateau region both, ρ_{xx} and σ_{xx}, vanish, since $\sigma_{xx} = \rho_{xx}/\left(\rho_{xx}^2 + \rho_{xy}^2\right) \to 0$ provided that $\rho_{xy} \neq 0$ and $\sigma_{xy} = -\rho_{xy}/\left(\rho_{xx}^2 + \rho_{xy}^2\right) = -1/\rho_{xy}$. The filling factors n (later ν in the fractional effect) around which the successive Hall plateaux and resistance minima are centred, are given by the Landau level filling factor

$$\nu \equiv n = \frac{h\, n_e}{eB} \equiv \frac{n_e}{D};\ n = \text{integer}, \tag{4.3}$$

where n_e is the electron density and D is the Landau level degeneration factor as defined in Eq. (3.3). Both, n_e and D are expressed for a single layer 2D system. The most important aspects for the understanding of the FQHE are given in the following figures. Parts a) and b) of Fig. 4.2 show Landau quantisation in a perfect 2D system onto sharp Landau levels. In the presence of impurities (part c)) these energetic states are broadened to a density of states (DOS) as shown in part d). The presence of impurities, which results in a broadening of the DOS, is decisive for the understanding of integer Hall quantisation. At magnetic field positions where a LL is brought to the FS, the corresponding DOS represents free mobile carriers, the so-called extended states, which contribute to transport (see Fig. 4.3).

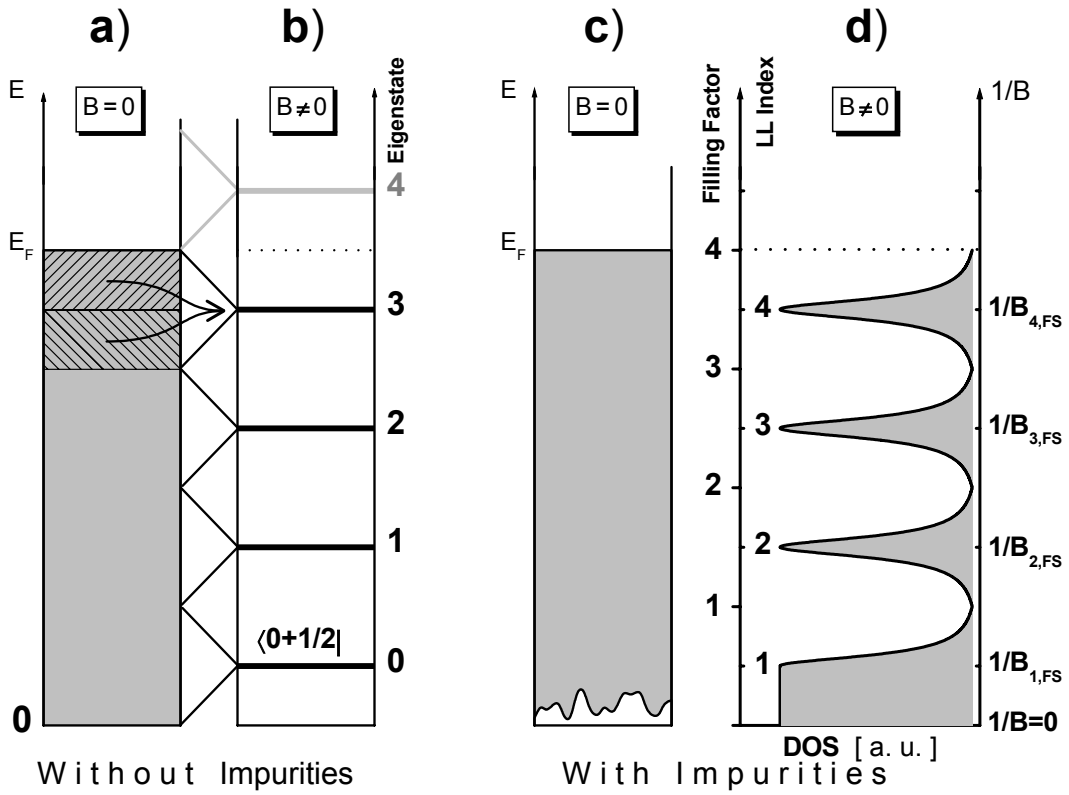

Fig. 4.2: Landau quantisation and density of states in a 2DES at $T = 0$ without and with impurities, respectively. **a):** Electron distribution (shaded) in a clean system at zero field. **b):** Condensation onto sharp energetic eigenstates (i.e. Landau levels) at nonvanishing B according to Eq. (3.2). Note that the counter starts with n=0 when the correct *energetic* position should be expressed. **c):** Electron distribution with random potential impurities (bottom of the potential pot) at zero field. **d):** Resulting *broadened* density of states (LL degeneration disregarded). The y-axis can be scaled in $1/B$, thus representing the LL filling factor n and the LL index. Note that contrary to b) n starts with n=1 when the *number of filled LLs* is expressed. Here n=4 is illustrated. The outermost y-axis shows the positions $1/B_{n,FS}$, where the n^{th} LL reaches the FS (coinciding with a ρ_{xx} maximum).

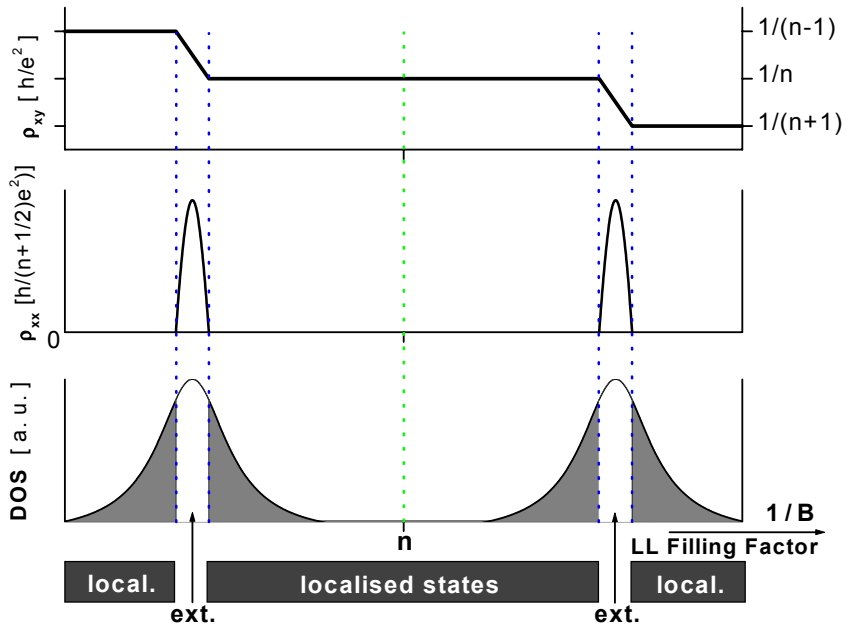

Fig. 4.3: Connection between the Hall plateaux, ρ_{xx} minima and the presence of localised states in the IQHE. The LL filling factor n is integer, when E_F is situated exactly midway between two adjacent Landau levels.

However at fields where the Fermi energy E_F lies between two adjacent LLs, the chemical potential either drops to the next lower LL when the system is clean, or is pinned to impurities when these are present. Caused by this, the actual DOS at the Fermi level contains only the carriers in the vicinity of impurities.
These carriers however are trapped to the impurities, so that they are localised. The DOS at the Fermi level is given by localised states as long as the Fermi level is pinned to the potential of localised impurities (shaded regions in Fig. 4.3). The role of the localised states in the IQHE is discussed in more detail in the following.

4.1.1 The Role of Localised States in the IQHE

The quantisation of ρ_{xy} in a 2DES can be understood as a result of the alternation of extended and localised states at the Fermi level when B is varied. This was proposed already in the original work [99] and is confirmed by different approaches to the IQHE. According to the *Kubo* formalism [223,224] it was found that at T=0K ρ_{xy} shows plateaux as long as the Fermi level lies within the regions of localised states (shaded areas in Fig. 4.3). *Aoki* found by numerical simulations that extended states are situated around the centre of a Landau level, whereas localised states are found on the tails of the LLs [126]. *Aoki* and *Ando* showed that the Hall plateau values are $|\sigma_{xy}| = n e^2/h$ and that in this region $\sigma_{xx} = 0$ [225]. *Prange* confirmed the connection between the occurrence of Hall plateaux and impurities. Moreover he showed that the current is carried exclusively by extended states, whereas localised ones do not contribute to transport [226].
Based on the Kubo formula, *Thouless* found that at integer n the Hall conductivity is unaffected by a weak variation of the impurity potential [227], which explains the perfect reproducibility of the Hall plateau values.
A further approach proposed by *Laughlin* is based on a gauge invariance argument [124] and accounts to the universal character of the IQHE. The author shows by a 'Gedankenexperiment' that the energies of localised electrons are stable against an adiabatic variation $\delta\Phi$ of the magnetic flux Φ. This generates the Hall plateaux around integer n. In the region of extended states however a Laughlin gauge transformation is only allowed when $\delta\Phi$ is an *integer* multiple of Φ, which means that the electron distribution maps into itself after the unitary gauge transformation. Laughlin's approach is based on this gauge invariance and moreover on the existence of a mobility gap, i.e., localised states.
Laughlin's work has been extended to the case of dirty systems [228] and, furthermore, the role of edge states was included by *Halperin* [229] (see Sec. 4.1.4).

4.1.2 Fundamental Difference Between Typical Semiconducting 2DESs and 2D Organic Metals

In a typical semiconducting 2DES, which exhibits the IQHE, all electrons move on the *same* quantised orbit in k-space. In consequence only a single QO frequency is present in the ρ_{xx} signal. Furthermore the regions of extended and localised states can be well separated, thus

defining clearly the regions where the IQHE plateaux are expected (see Fig. 4.3). However such a situation is not necessarily given in a 2DES.
In a 2D organic system as, for instance, κ-(BEDT-TTF)$_2$I$_3$, the FS is intersected by several bands, so that *different* quantised orbits are present (see, e.g., Fig. 3.3 and Ch. 5). This results in the coexistence of several different QO frequencies, whose successive DOS alters between extended and localised states as the field is varied (see Fig. 4.4). A cut through the DOS at arbitrary field (blue dashed lines) makes clear that the 'standard' situation in such a 2D system is a *coexistence of extended and localised states*.

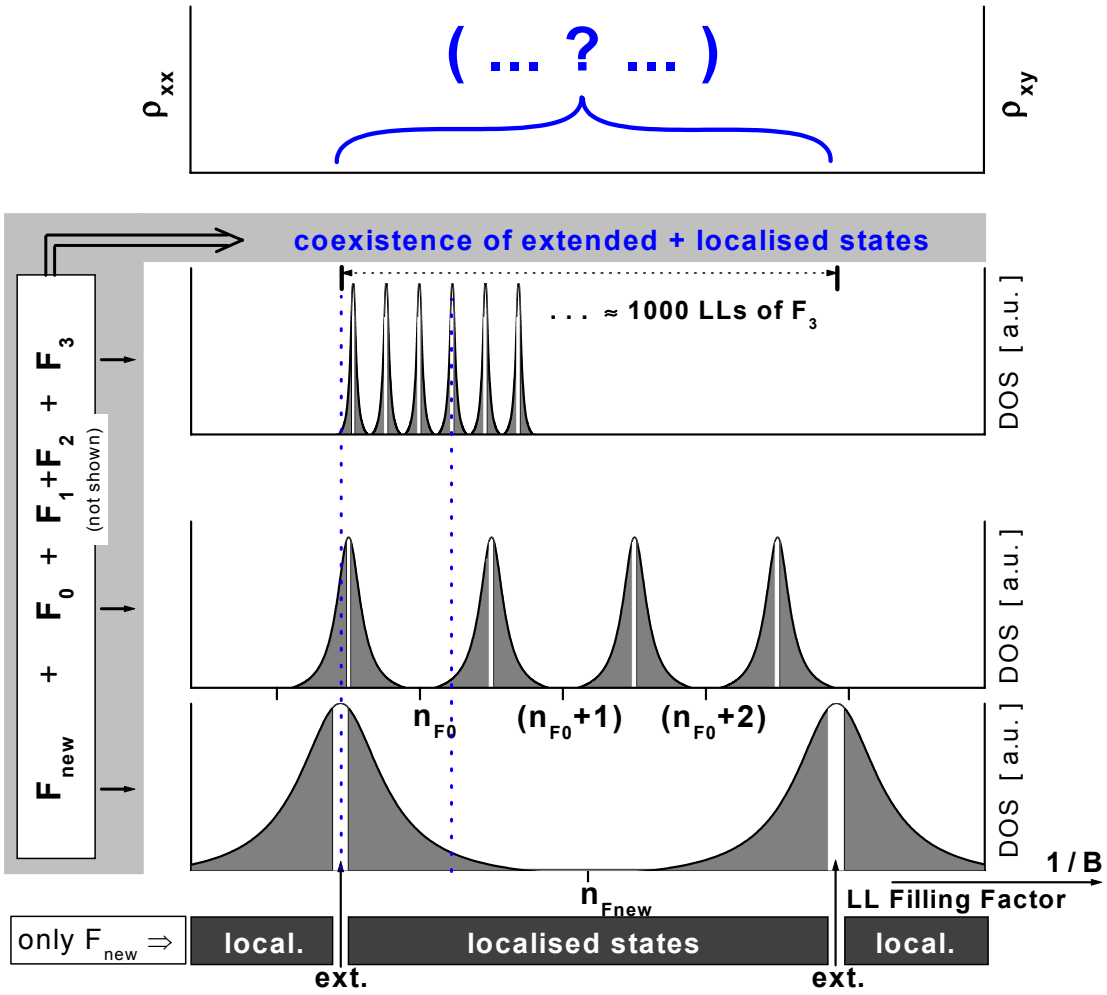

Fig. 4.4: Density of states versus *1/B* when several different quantised orbits are present. The shaded areas represent localised states within the different electron distributions. The notation F_j for the QO frequencies is chosen with reference to the experimental results on the 2D organic metal κ-(BEDT-TTF)$_2$I$_3$ discussed in Ch. 5. However, two of the occurring QO frequencies are omitted for clarity.

Since a theoretical description of such a rather complex situation is outstanding to date, a statement on the expected behaviour of Hall plateaux and ρ_{xx} cannot be given actually. It can be supposed that the contribution of the electrons on the different quantised orbits to the diagonal and the Hall resistivity is determined by

• the different filling factors ν_{Fj} of the successive Landau level structures, or, respectively the ratio $\hbar\omega_{C,F_j}/k_BT$.

• the effective masses, Fermi wave vectors and Fermi velocities,

• mobilities and scattering times of the different types of carriers

Despite this complication two central features are expected to be still given in such a 2D organic metal:

1) the presence of extended states,
2) a localisation of a part of the electrons in the vicinity of impurities trapped by their potential.

In view of this, Fig. 4.4 illustrates that as the field is varied the DOS at the Fermi level contains both, extended *and* localised states. The ratio of both varies with the DOS of the contributing LL structures, i.e., with the filling factors of the successive subsystems. In consequence the total number of mobile (here: metallic) carriers at the FS is *reduced* and, moreover, this number varies with Landau level filling.
It is therefore suggested to assume that such effects would influence magnetotransport and that they are therefore observable in SdH experiments on 2D organic metals.

4.1.3 Electron Localisation in the IQHE Regime - Microscopic Picture

An important precedent work on the understanding of localisation in 1D and 2D systems at B=0 has been provided by *Anderson* [230]. He starts from the simple picture where a low density of impurities (i.e., donors and acceptors) is randomly placed in a semiconductor and forms bound states there. At low temperatures carriers are localised around these impurities. As the density of impurities is enhanced such that impurity potentials and therefore carrier wave functions overlap, the situation changes in so far, that the idea of localisation has to be expanded. Under such conditions carriers may be almost free on an atomic scale (or, e.g., on the scale of a cyclotron radius), but they are localised on a larger scale due to the finite extent of their wave function. Such kind of localisation, where the wave function is spread over more than the average distance between impurities is called Anderson localisation. An important contribution for the understanding of Anderson localisation was given by a scaling theory [231]. Therein *Abrahams et al.* show that in a macroscopic 2D system at B=0 and T=0 all states are localised[2]. This shows that Anderson localisation cannot be straightforward related to the IQHE, since the latter effect requires extended states. The situation changes at B>0, where the system's symmetry breaks. *Aoki* showed that for σ_{xy}>0 at least one extended state must exist [127]. By numerical calculations it was found that the extended states are situated in the centre of a Landau band, whereas the localised ones are found on its tails [126].
A number of authors have studied the role of impurity potentials in the IQHE regime [232,233,234,235,236,237] and contributed to the following picture of electron localisation in the IQHE.

[2] This result was restricted to the case where electron interaction can be neglected.

A carrier motion in an impurity potential $U(\boldsymbol{r})$, which varies slowly along a length scale of the order of the cyclotron radius ℓ_0 (see Eq. (4.1)), can be reduced to a linear drift along the actual equipotential line $U(\boldsymbol{r})$ = constant. The state of an electron, which is by ΔE out of the centre of the Landau band, is localised on the equipotential line $U(\boldsymbol{r}) = \Delta E$ in the vicinity of the impurity (see Fig. 4.5). Based on the classical percolation model [238] it was found that the equipotential lines in a 2D random potential at $\Delta E \neq 0$ are closed curves of finite length and correspond to localised states. If the regions with $U(\boldsymbol{r}) > 0$ are represented as land and those with $U(\boldsymbol{r}) < 0$ as water, we obtain a set of islands when the Fermi level is situated at $\Delta E > 0$ and a set of lakes when $E_F = \Delta E < 0$ (see Fig. 4.5). However when the Fermi level is congruent with the centre of the Landau band, at least one extended coast line exists, on which a carrier can leave the impurity and thus contributes to macroscopic transport (red trajectories in Fig. 4.5). These delocalised drift trajectories in an external electric field were analysed by several groups [232,233,234,235] and the quantisation of σ_{xy} was reproduced.

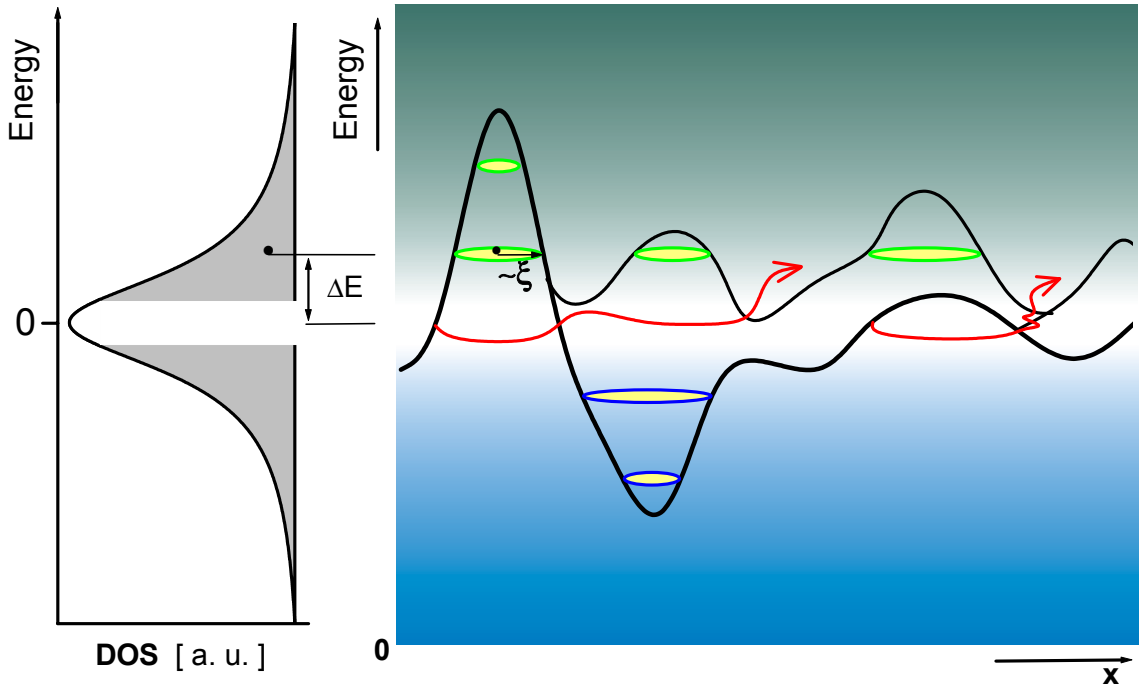

Fig. 4.5 left: Density of states (DOS) of one Landau band with extended states on its centre. Localised states are shaded. **right:** Topological sketch of a random impurity potential. A number of localised states (closed orbits) for $\Delta E \neq 0$ are selected. Extended states at the centre of the band are indicated by red trajectories.

The extent of the electronic wave function in dependence of ΔE, i.e., the localisation length ξ has been studied by several groups [239,240] starting from the suggestion that only the centre of the Landau band is extended, whereas the other states are exponentially localised [241]. The finite size calculations were done under neglect of electron interaction.
It was obtained that the localisation length $\xi(\Delta E)$ for the lowest Landau band is given by the equation

$$\xi(\Delta E) \sim |\Delta E - E_C|^{-\beta} \qquad \text{with} \qquad \beta = 2.3 \pm 0.1 \tag{4.4}$$

where E_c is the centre of the Landau band (set to zero in Fig. 4.5). As soon as ξ diverges in the centre of the Landau band, the state is regarded as extended. Moreover, Eq. (4.4) shows that carriers which are energetically far away from the centre of the Landau band are strongest localised. Furthermore the results show that in an infinitely large system there is only one extended state in centre of the band. However in finite systems of size L, all states with $L < \xi(\Delta E)$ can be considered as extended, which widens the region of extended states to a subband. (see Fig. 4.5).

4.1.4 The Role of Edge States in the IQHE

First interpretations of the IQHE assumed that the current is distributed over the entire surface of the 2D layer. However upon closer examination this assumption results in a paradox: According to the simple Landau quantisation picture, within the Hall plateau regions only localised states are at the Fermi surface. These states do not enable a transport, whereas a non-vanishing Hall current within the plateau regions *is* a transport. This means that the presence of a finite quantised Hall current requires the existence of extended states. These extended states are provided, i.a, at the edge of the 2DES by so-called edge states.
Some authors have pointed out that in fact the current must flow in the one-dimensional channel at the edge of a 2D layer [229,242,243,244,245]. As first *Halperin* [229] obtained this result by continuing *Laughlin's* gauge invariance description [124]. Halperin found that localised states do not play any role in the response to a change of the magnetic flux. This means that they are incompressible. If however a non-vanishing Hall current is present, it can only be realised by extended states, which respond to the magnetic flux (i.e. they are compressible). In particular the edge states at the FS have to be extended states. By this the edge state concept explains the existence of extended states which enable nonvanishing Hall currents in a situation where in the bulk sample only localised states are present at the Fermi surface.
The description of edge states is based on a single layer 2DEG as realised in a semiconductor, with all electrons being quantised on one single closed orbit. This 2DEG is confined to an electrostatic potential $V(x)$ which vanishes inside the sample and is infinite outside. First descriptions for a hard-wall, i.e., perfectly stair-like potential at the sample edge were replaced by a more realistic soft-wall potential profile [242], where $V(x)$ changes slowly with the length scale of the cyclotron radius ℓ_0. In this arrangement an eigenstate E_n is given by the sum of Landau energy and electrostatic energy and therefore the energy of all E_n is enhanced in the vicinity of the sample edges (see Fig. 4.6). Owing to this, even when the Fermi surface inside the 'bulk' 2D layer lies in a region of localised states, extended states are brought to the FS at the edges, where successive Landau levels cross the Fermi energy.
This causes that in a magnetic field applied perpendicular to such a 2DEG the electrons on both edges of the sample receive opposite velocities. For n filled LLs one obtains n quasi one-dimensional edge channels along the layer edges. Each of them carries a dissipationless current

$$I_n = \frac{e}{h}(\mu^R - \mu^L)\,, \tag{4.5}$$

which depends on the chemical potential difference between the right (μ^R) and the left sample edge (μ^L) in the semiconducting device [242]. For non-interacting electrons this net current would flow along the layer edges and the quantised Hall current would be just the difference between the two opposite edge currents.

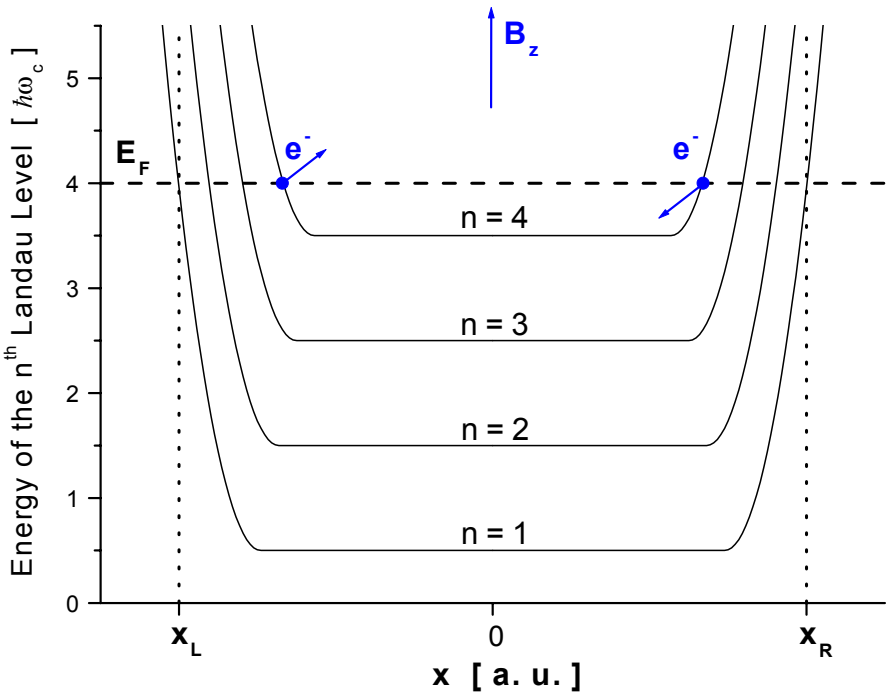

Fig. 4.6: Modification of the energy spectrum of a 2DEG of non-interacting electrons in an infinite soft-wall potential. x_L and x_R are the left and right sample edges, respectively. Edge currents (arrows) are induced by a present magnetic field $\boldsymbol{B} = B_z$.

It was also found in Ref. [242] that these results hold for the inclusion of random potential. An alternative approach to edge currents was performed in Ref. [244], which confirms the importance of edge states in the IQHE in general. Experiments on edge states are reported in Refs. [246,247,248,249]. Furthermore it has been proposed that edge currents might be observed also in magnetic susceptibility [250].
Further experiments on edge currents under different contact arrangements are reported for conventional four-probe Hall as well as quasi-Corbino geometry[3] in Ref. [251]. It was shown that in the presence of edge channels the contact arrangement plays a decisive role for any current to flow. At magnetic field values corresponding to one of the Hall plateaux an electric current through a 2DEG can only flow when both, source and drain, are situated within the narrow edge region and are contacted to the edge channels (see Fig. 4.7, left). As soon as one or both current contacts are not connected to the narrow region of edge channels (right part of Fig. 4.7) , the sample resistance diverges, since the current flow through the sample vanishes.

[3] The so-called Corbino geometry is given when circular contacts are arranged concentric on the sample.

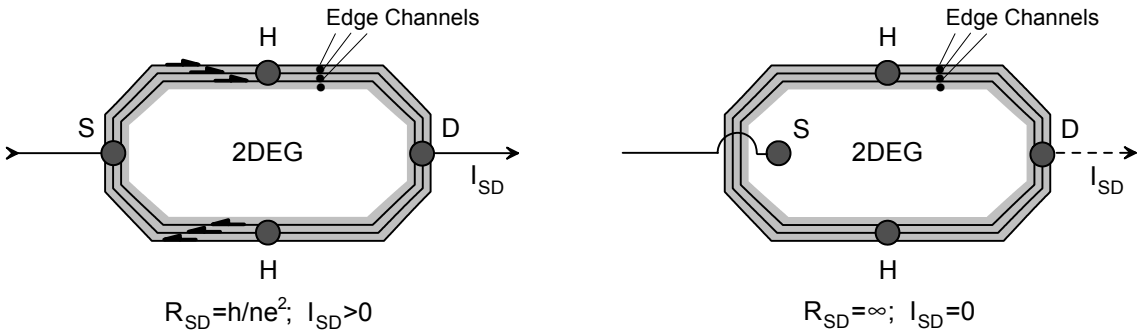

Fig. 4.7: Schematic illustration for the contact arrangements of source (S), drain (D) Hall contacts (H) (R_{SD} and I_{SD} are resistance and current between source and drain). The edge regions of the 2DEG, where the current flows (arrows), are shaded. The bulk, which is supposed to be free of current, is kept white. **left:** Standard Hall geometry, where S, D and H are on the same edge. **right:** One (or more) of the contacts is not at the edge. Thus a current flow in the Hall plateau is not possible.

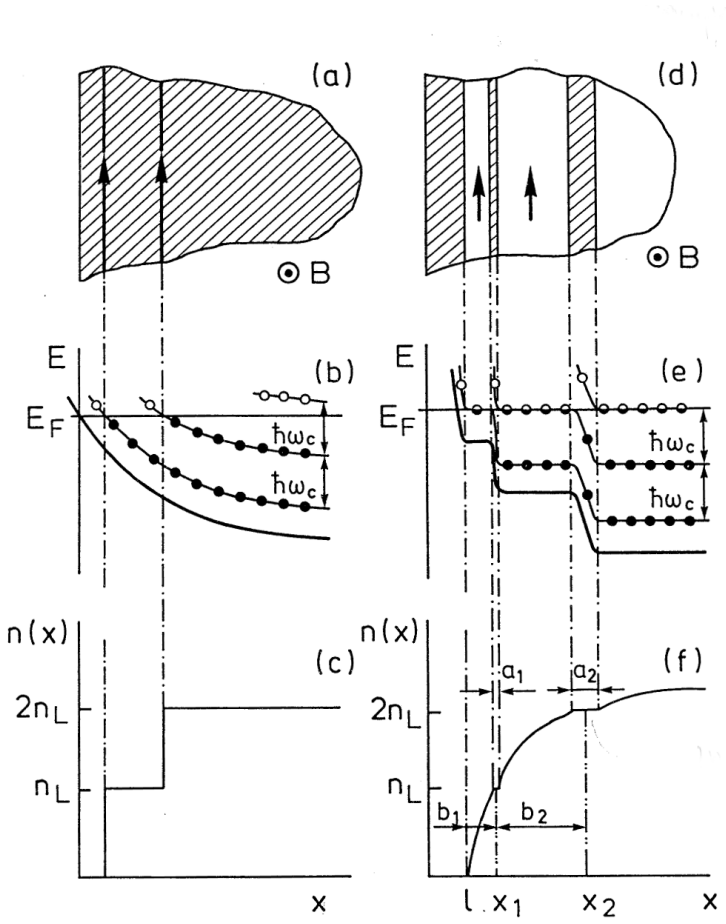

Fig. 4.8: Edge states in a 2DEG in the IQHE regime (according to Ref. [252]). **left:** In the single-electron picture. **a):** Top view on the left edge of a 2DEG. Arrows represent the current flow in the narrow edge channels. **b):** Landau level bending in the edge region according to Fig. 4.6 . Filled circles represent occupied states. **c):** Stair-like electron distribution near the boundary. **right:** The same in the self-consistent electrostatic picture. **d):** Top view on a 2DEG with incompressible (shaded) stripes and compressible (unshaded) stripes. **e):** Bending of the energy profile. **f):** Electron density vs. the distance to the middle of the depletion region.

So far the description is based on a simplified one-electron picture. The position of the edge channel is given by the intersection between Landau level energy and Fermi energy (see Fig. 4.8.b). The edge channel width corresponds to the spatial extent of the wave function on the Landau level, which is of the order of the magnetic length ℓ_0. In this description the edge channels are narrow (see Fig. 4.8.a). However this requires a stair-like change of the electron density at every edge channel (see Fig. 4.8.c). But in a real sample at zero field the electron density decreases rather gradually close to the surface. If such a gradual density profile at $B = 0$ should be changed into stair-like one at $B > 0$, this deformation would cost an extra amount of electrostatic energy. This disadvantage is overcome when partially filled Landau levels are spread on a spatially wider region on the FS (see Fig. 4.8.e). These partially filled LLs can take in charges without changing their energy, i.e., they are compressible. These widened intersection lines between the partially filled LLs and the Fermi energy form compressible edge stripes, which contain the extended states (see Fig. 4.8.d). In the regions between adjacent edge stripes, the Fermi level is situated between two LLs and the filling factor is integer. Adding a charge means that it has to occupy the next upper LL, which costs a finite energy. Therefore these states are incompressible (shaded in Fig 4.8.d). In this so-called self-consistent electrostatic picture (right part of Fig. 4.8), an alternation of compressible (i.e., current-carrying) and incompressible (current-free) stripes are aligned along sample boundary.

The role of edge states in the IQHE is tantamount to the question how much of the Hall current may be carried by them. The ratio between edge and bulk current has been calculated in Ref. [253]. It was found that for (realistic) soft-wall potential the bulk current dominates the edge current contribution, whereas only for the hard-wall case the edge currents dominate [254]. This means that for realistic situations the IQHE cannot be described exclusively by edge currents. It should be emphasised that the contribution of edge currents also depends on the total current I_{tot}. For $I_{tot} < 100$nA edge currents were found to be dominant [251] whereas for higher current densities the current penetrates into the bulk and the edge contribution finally becomes even unimportant. Correspondingly, it was demonstrated that a quantised Hall current occurs even in Corbino geometry, i.e., *without any edge* [255].

In conclusion the most important properties of edge states and edge currents are summarised in the following, which allow to assess the role of edge states in κ-(BEDT-TTF)$_2$I$_3$ (see Ch. 5):

1) Edge states are introduced to explain a non-vanishing Hall current in the Hall plateau regions, i.e. where extended states at the FS are not expected. However, as the edge state concept was proposed to explain extended states, it is rather unfavourable to describe localised states.

2) Edge currents are dissipationless and they are connected with the occurrence of a quantised Hall plateau.

3) Edge states can only occur when scattering between the edges is not possible. The condition beyond is that no electron may be transferred from one sample edge to the other. This implies that there are no extended states within the bulk of the sample which would allow such a transport.

4) Edge currents exist even when no external voltage is applied to the sample. Therefore it is expected that the effects of edge currents are also observed in magnetisation.

5) The filling factor regions ν in which edge states may occur, are given by

$$N - \frac{\ell_0}{W} < \nu < N\,, \tag{4.6}$$

where N is the number of edge states (N is just the actual number of LLs below the FS), ℓ_0 is the cyclotron radius and W is the sample width. Since ℓ_0 is a microscopic quantity, whereas W is macroscopic, edge currents may not occur in a continuous but only in a very limited filling factor region around integer $\nu \approx N$.

6) Edge currents are only weakly dependent on tilting the angle Θ between the magnetic field direction and the 2D plane out of the orientation normal to the plane.

7) The ratio between edge and bulk states is given by

$$\Re = \frac{\ell_0}{W}\,, \tag{4.7}$$

i.e., the cyclotron radius and the sample width. This ratio decreases with increasing magnetic field.

8) Edge states are able to carry only very limited currents. In 2D semiconductors they lose importance above about 100nA in favour of bulk currents and for I_{tot} >> 100nA their role in the IQHE tends to be negligible.

The 1D Chiral Tomonaga-Luttinger Liquid

As shown in the preceding, a (quasi) one-dimensional electron gas (1DEG) may be established at the edges of a 2D system, an effect which may lead to the occurrence of edge states. However under special circumstances the electron system becomes a perfectly 1DEG which cannot be described as a Fermi liquid any more, but represents a so-called Tomonaga-Luttinger liquid (TLL) [16,17]. If a 2D material provides an *ideal* edge and is brought onto a quantum hall plateau, this plateau is realised exactly up to the sample edge. Projected on Fig. 4.6, the ideal character of the sample means, that the Hall plateaux are *flat* up to the sample edges. In consequence edge states and edge stripes do not occur and when the magnetic field corresponds to a quantised Hall plateau value, i.e., there are no extended states at the FS inside the sample. The resulting 1DES on the sample edge represents a chiral one-dimensional TLL. It was shown that the system can be described by a boson operator, but not by Fermi liquid theory (see also Ref. [256]).
One of the most important properties of the TLL is that low-energy excitations of the system may exist only at the sample edge in terms of a carrier fluctuation at the edge itself. Regarding momentum distribution, the TLL shows no discontinuity at $\boldsymbol{k} \equiv \boldsymbol{k}_F$, which means, that the system has no Fermi surface.

In summary, the 1D chiral Tomonaga-Luttinger liquid is characterised by the following properties which are important for the assessment of its role in the experiments on the 2D organic metal κ-(BEDT-TTF)$_2$I$_3$ in Ch. 5:

i) The occurrence of a TLL requires ideal samples up to the sample edge without impurities, defects or carrier density fluctuations.

ii) In the presence of a TLL, the system cannot be described by Fermi liquid theory, especially:

iii) A Fermi surface is absent and therefore cannot be investigated.

In an organic metal the role of edge states is certainly influenced by several additional, even decisive conditions, as, e.g., cyclotron radii, different closed orbits on the FS, but also sample qualities at the edges. However in order to avoid needless repetition and for a better illustration, these are discussed with the experiments on the 2D organic metal κ-(BEDT-TTF)$_2$I$_3$ in Ch. 5 .

Up to now electron localisation and further results of two-dimensionality were illustrated as they occur in the integer IQHE, i.e., in a single-particle picture under neglect of electron correlation. The next sections describe the occurrence of electron localisation in the fractional IQHE as a result of electron correlation.

4.2 The Fractional Quantum Hall Effect

The present section recalls the most important basic information for the understanding of the fractional quantum Hall effect. Besides this, some selected topics are collected, which are important for the interpretation of the experiments on the 2D organic metal κ-(BEDT-TTF)$_2$I$_3$ in Ch. 5 . The focus is put on two features beyond the FQHE, i.e., electron correlation and electron localisation. Special weight is also put on the understanding of the FQHE in 2D *multilayer* systems.
It should be noted that most of the work on the understanding of the FQHE is done on *semiconductors*, where the effect is mainly observed. In contrast, the organic material κ-(BEDT-TTF)$_2$I$_3$ discussed in Ch. 5 is a *metal* and has moreover a rather complex electronic structure compared to the 'standard' FQHE devices. Thus it is straightforward to see that a number of even basic features of the FQHE possibly have to be thought over. This cannot be worked out in detail within the present work, so that in some aspects only a stimulation can be given. This is done to some extent in the following and with the discussion of the experiments in Ch. 5, as appropriate.

In 1981 *Tsui et al.* investigated a single-layer high mobility GaAs/Al$_x$Ga$_{1-x}$As heterostructure in high magnetic fields at low temperatures[4] on the search of a Wigner crystallisation, i.e., a crystalline ground state of a correlated electronic system, in which the potential energy dominates the kinetic energy [257]. In order to reach this imbalance of energies, the kinetic energy of the carriers can be minimised by limiting their motion within a 2D plane. In a single-layer 2D heterostructure an out-of-plane motion is prohibited on principle by the finite width of the 2DEG. The in-plane motion is limited as a by-product of Landau quantisation [151,152]. Under such conditions *Tsui et al.* discovered the fractional quantum Hall effect [123]. Besides the well-known Hall plateaux at integer filling factors $\nu_j \equiv n_j$, Hall plateaux were also present at fractional $\nu = 1/3$ and at lowest $T = 0.48$K also indicated at $\nu = 2/3$. In later experiments on higher mobility samples ($\mu_e \approx 10^6$ ... $2 \cdot 10^7$cm^2/Vs) a series of further fractional filling factors were observed (see Fig. 4.9) [258,132]. The Hall plateau widths are

[4] The experimental parameters in the first FQHE experiments were $n_e = 1.23 \cdot 10^{11}$/cm^2, $\mu_e = 9 \cdot 10^4$cm^2/Vs, T ≥ 0.48K, B ≤ 21T [123].

different at successive fractional ν and in conjunction, the minima in the diagonal resistance are differently pronounced, tending to zero resistance in the plateau regions.

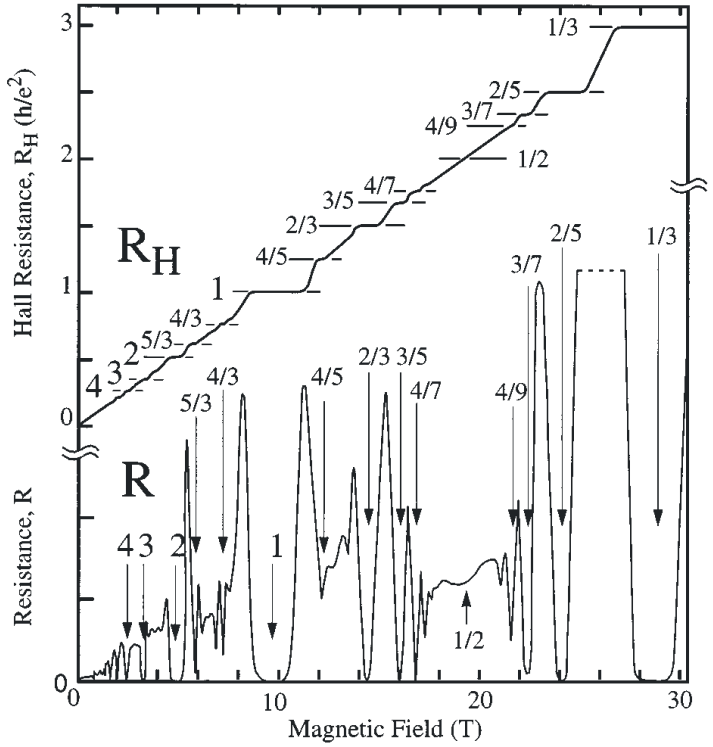

Fig. 4.9: Fractional quantum Hall effect as observed in a single-layer modulation-doped 2D GaAs/$Al_xGa_{1-x}As$ heterostructure with $\mu_e = 2 \cdot 10^7$ cm^2/Vs ([132], see also [258]).

$$\nu_j = \frac{1}{3}, \frac{2}{3}, \frac{4}{3}, \frac{5}{3},$$

$$\nu_j = \frac{1}{5}, \frac{2}{5}, \frac{3}{5}, \frac{4}{5}, \frac{7}{5}, \frac{8}{5},$$

$$\nu_j = \frac{2}{7}, \frac{3}{7}, \frac{4}{7}, \frac{5}{7}, \frac{10}{7}, \frac{11}{7}$$

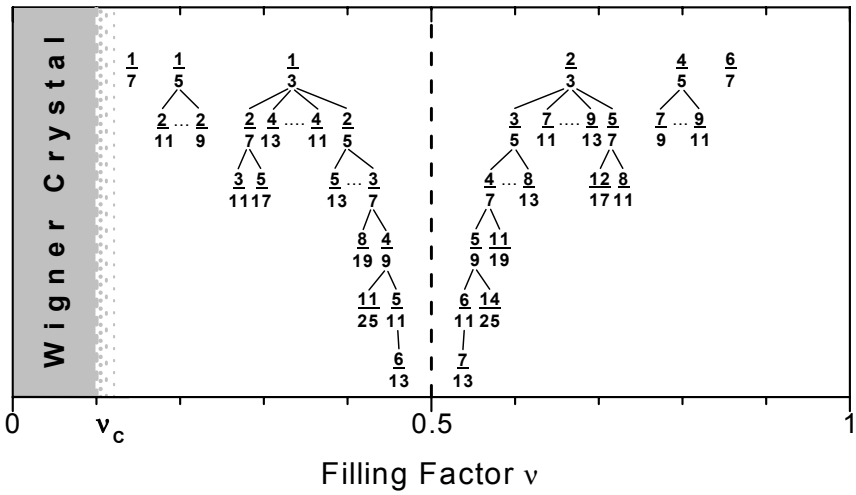

Fig. 4.10: Fractional filling factors ν ordered by their denominator (**left**) and by their hierarchy (**right**) after Ref. [259] (see also [260]). The hierarchy scheme is discussed in Sec. 4.2.6 whereas the transition to a Wigner crystal is sketched in Sec. 4.2.4.

A number of further experiments were carried out in GaAs/$Al_xGa_{1-x}As$ heterostructures [261,131,262,263,264]. Besides, the FQHE was also observed in high mobility Si-MOSFETs [265,266], *n*-type Si/SiGe heterostructures [267] and multiple quantum well heterostructures [268].
Among the fractional ν observed in detailed studies [269,270,271,272,273,258,274,275, 276,277,278,279] the most prominent ones are collected in Fig. 4.10. Further fractions *p/q* with q = 9, 11, 13 and even 15 were found in the SdH signal. The Hall resistance was found to be quantised to rational ν_j by

$$\rho_{xy} = \frac{h}{\nu_j e^2}. \tag{4.8}$$

It is common to the observed fractions that they occur nearly exclusively at odd denominator filling factors. A breaking of this rule has been detected by *Clark et al.* [273] and *Willett et al.* [258] who found the FQHE at ν = 5/2. However in a single-layer 2D system especially ν = 1/2 does not occur. At this special fraction ρ_{xy} follows exactly the classical Hall curve (see Fig. 4.9). However *Chakraborty et al.* predicted theoretically that ν = 1/2 should occur in multiple-layer rather than single-layer systems [280,281] and indeed *Eisenstein et al.* found ν = 1/2 to be realised in double-layer systems [282,283]. The background of this striking result will be discussed in detail in Sec. 4.2.8.

4.2.1 The Ground State

The observation of Hall plateaux and strong minima in the diagonal resistance, where ρ_{xx} even vanishes at certain rational ν, hints to the presence dissipationless currents, the existence of a gap and the occurrence of localised states. These states arise in a filling factor region, where a single-particle Landau level structure under neglect of electron correlation cannot generate localised states. These states and in conjunction the FQHE were shown to be generated by electron correlation. As the width as well as the variety of the FQHE plateaux increases with the carrier mobility, impurity potentials were supposed to be less important than electron interaction. This suggests to base the explanation of the FQHE on the description of a 2D correlated electronic system in an uniform positive background, where the impurities represent local perturbations. This system is exposed to low temperatures and such high fields, that the potential energy is lower than the cyclotron energy

$$\frac{e^2}{\varepsilon \ell_0} \lesssim \hbar\omega_c, \tag{4.9}$$

where $\ell_0$is the magnetic length (see Eq. (4.1)), ε is the dielectric constant ($\varepsilon \approx 12.9$ and $m^* \approx 0.067\ m_e$ in GaAs[5]). This inequality avoids Landau level mixing, i.e., the admixture of states in higher LLs, so that the system is in the so-called extreme quantum limit. Furthermore full spin polarisation is assumed.
The first studies of the ground state of such a system under Coulomb interaction between electrons was carried out by *Yoshioka et al.* by numerical calculations [284,285] (see Fig.

[5] It should be noted that in organic metals m^* is typically below 6 for different quantised orbits (see Chs. 5 and 6), the cyclotron radius R_c may be much bigger (see Fig. 5.31), whereas the dielectric constant is $8 \lessapprox \varepsilon \lessapprox 50$ [287] and might be even magnetic field dependent. This enhances the inequality in Eq. (4.9).

4.11). As one of the most important results they found a ground state with a significantly lower energy than that of a Hartree-Fock (HF) Wigner crystal. Furthermore the energies of the correlated ground state at certain filling fractions (i.e., $\nu = 1/3$; 2/5) are insensitive to the system size and, as found later, very similar to the infinite system results. Moreover, at these fractions a dip in the particle energy curve is indicated. This would mean that the compressibility

$$\kappa \sim \left(\frac{\partial E}{\partial \nu}\right)^{-1} \tag{4.10}$$

diverges with different signs when approaching to the dips from both sides and vanishes at these fractions. Therefore the system represents an incompressible state at these filling factors. This finding is important in connection with *Laughlin's* description of the ground state discussed later.

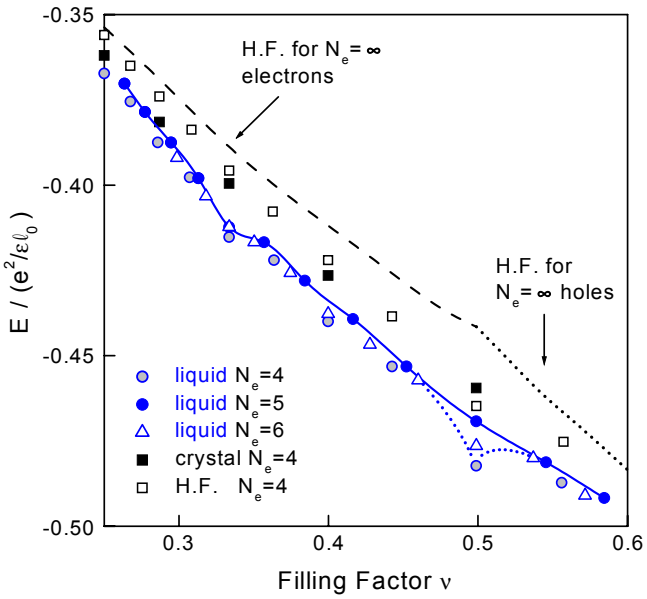

Fig. 4.11: Energies per particle for finite electron systems in a periodic rectangular geometry vs. filling factor of the lowest LL (according to Ref. [284]). The dashed and dotted lines result from Hartree-Fock (HF) approximation for an electron or hole crystal of infinite particle number [286]. Open circles, closed circles and open triangles are results for particle numbers N_e = 4, 5 and 6 for electron ($\nu < 1/2$) and hole states ($\nu < 1/2$). Closed squares show the crystal state energies and open squares the HF crystal states for N_e = 4. The solid line drawn through the N_e = 5 data is a guide to the eye. The crystalline and liquid state, respectively, are discussed in Sec. 4.2.2.

A dip in the ground state energies of the correlated system might be supposed also at $\nu = ½$. However a closer view reveals that there the energy is strongest system size dependent and is therefore an artefact of the very limited particle number.
It should be noted that the data for crystalline realisations of a ground state do not show any dips at fractional ν values. This underlines that they cannot represent the ground state, which 'prefers' certain fractional ν. Furthermore the data at low ν suggest that the energies of the Wigner crystal and the correlated state approach towards lower ν. Indeed the crystalline state was found to have lower energy at latest at ν < 1/70 (see Secs. 4.2.2 and 4.2.4).

4.2.2 Laughlin's Description of the ν = 1/3 Ground State

The work discussed yet describes some basic properties underlying to the FQHE. However the key of a microscopic understanding was given by *Laughlin,* who proposed to describe the FQHE in terms of a condensation of the electronic system into a novel liquid state of matter [125,288,289,290]. His description starts from a 2D electronic system where the carriers are correlated by logarithmic (i.e., 2D) Coulomb interaction. The magnetic field is assumed to be strong enough to generate ν = 1/3. The choice of an uniform neutralising background potential allowed to benefit from analogies to a 2D one-component plasma (OCP) [291]. *Laughlin* proposed a trial ground state wave function $\psi(x)$ for ν = 1/3, which consists of a product of *Yastrow*-type functions. It had to be optimised with respect to energy minimisation and symmetry. In order to describe a ground state which obeys Fermi statistics, Ψ has to be antisymmetric. This restricts its validity to filling factors with *odd* denominator. The resulting wave function at $\nu = 1/m = 1/3$ for N particles with complex coordinates $z = x + iy$ reads

$$\psi(z_1, ..., z_N) = \prod_{j<k}^{N} (z_j - z_k)^m \exp\left[-\frac{1}{4\ell_0^2} \sum_l |z_l|^2\right], \tag{4.11}$$

where all particles are in the lowest Landau level and fully spin-polarised. In analogy with the OCP it was shown that the states described by Eq. (4.11) stay liquid upon lowering ν until $\nu \approx 1/70$, whereas below the Wigner crystal state is favoured. This liquid nature can be also illustrated as shown in Fig. 4.12 by the correlation function *g(x)* [291,125,292].

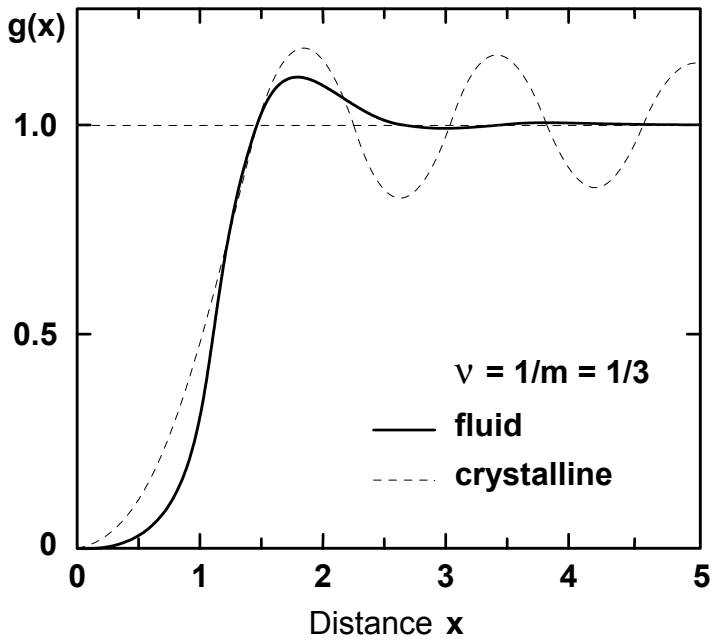

Fig. 4.12: Pair correlation function *g(x)* vs. a dimensionless particle distance $x = r/\sqrt{2m\ell_0}$ at ν = 1/3. The solid line shows the Laughlin state whereas the dashed line represents the Wigner crystal in Hartree-Fock approximation.

When one particle is assumed to be located at the origin, *g(x)* is the probability to find the neighbouring particle placed at a distance *x*, i.e., *g(x)* is a measure for charge separation in real space. For the Wigner crystal *g(x)* provides a clear short-range order for low particle distances (since *g(x)* decreases markedly, as x^2). For longer distances *g(x)* oscillates, which shows the presence of a long-range order. These are the characteristics of a crystalline

system. However in the Laughlin state *g(x)* provides an even better short-range order (since $g(x) \sim 1 - \exp(-x^2/2\ell_0^2) \sim x^{2m}$, whereas for longer distances *g(x)* shows no particular structure, i.e., a low long-range order. These properties are characteristic for a liquid state.

It should be noted that *g(x)* depends on the particle distance as well as the cyclotron radius, which both may be very different in 2D semiconductors and 2D metals. This may allow a different density of charge packing in the two classes of materials.

4.2.3 The Ground State Energy and the Energy Gap

In order to calculate the energy of the ground state, *Laughlin* used a modified 'hypernetted chain' theory introduced in Ref. [291] and obtained for the ground states at the special $\nu = 1/m$ [125]

$$E_{GS}(m=3) = (-0.4156 \pm 0.0012)\frac{e^2}{\varepsilon \ell_0} \quad \text{and} \quad E_{GS}(m=5) = (-0.3340 \pm 0.0028)\frac{e^2}{\varepsilon \ell_0}. \quad (4.12)$$

The ground state energies for various filling factors can be fitted to the following approximate formula:

$$E_{GS}(m) \simeq \frac{-0.814}{\sqrt{m}} \left[1 - \frac{0.230}{m^{0.64}}\right] \left(\frac{e^2}{\varepsilon \ell_0}\right). \quad (4.13)$$

It is noteworthy that the ground state energy is determined, i.a., by the dielectric constant ε as well as the cyclotron radius ℓ_0 which may be very different in semiconductors and metals (comp. Eqs. (4.1) and (4.2), for ε in organic conductors cons. Fn. 5 in Sec. 4.2.1). All calculations referred to in the following, were carried out for 2D semiconductor devices.
Haldane and *Rezayi* (Ref. [293]) calculated the ground state energy in spherical geometry by considering periodic boundary conditions [294]. They concluded that Laughlin's wave function indeed represents the exact ground state.
A number of groups have contributed to calculate the energy of the ground state using different methods, particle numbers and sample geometry. They obtained either perfect agreement with the results cited above or at most minor deviations to them. These deviations appear to be of minor importance from the viewpoint of this work, which focuses on the occurrence of fractional filling factors in a 2D metal instead of a semiconductor. Details of these calculations are found in [284,292,295,296,259,293,297,298,299,300,301].

Experimental access to the quasiparticle-quasihole energy gap is given by temperature dependence of the magnetoresistance, especially of the ρ_{xx} minima. In a semiconductor these properties show activated behaviour. Further access to the gap energy[6], is provided by microwave photoresistivity measurements. [270,265,302,303,304,305,306,307,308,309,310, 278].

[6] The gap energy is the energy required to generate a quasiparticle pair illustrated in Fig. 4.13c.

4.2.4 Transition From a Laughlin Liquid to a Wigner Crystal at Low ν

It was mentioned already in connection with Fig. 4.12 that the ground state in the FQHE is a quantum liquid state. It was also remarked that the 2D one-component plasma (OCP) undergoes a transition into a Wigner crystal at $\nu \lesssim 1/70$ [291].
In order to obtain the crystal energies which compete with the liquid state energies of a FQHE system, most calculations were carried out in the framework of Hartree-Fock (HF) approximation [284,286,292,311]. Monte Carlo results for the Laughlin liquid state were compared with the HF crystal energies in dependence of ν and a critical filling factor ν_c for a liquid-to-solid transition was estimated as $\nu_c \approx 1/10$ [292], which is very similar to Laughlin's value [125]. Slightly higher $\nu_c \approx 1/7$ were obtained in Refs. [312,313]. A number of experiments show that filling factors down to $\nu = 1/5$ and 2/11 [276], $\nu = 1/7$ [274,314] occur, thus giving an upper limit for ν_c.

A common conclusion of all calculations and experiments is that the Wigner crystal state adjoins the Laughlin liquid state at low filling factors $\nu < \nu_c$ (see Fig. 4.10). For $\nu > \nu_c$ however the liquid state is the more favourable one until it is destroyed at magnetic fields, which are too low to establish FQHE conditions.

4.2.5 Excited States: Quasiparticles and Their Main Properties

An important interpretation of Laughlin's ground state wave function for $\nu = 1/m$ (Eq. 4.9) was given by *Halperin* [128] (see also [297]). When the positions of N-1 electrons are fixed at Z_k, the wave function for the one remaining electron reduces to

$$\psi(z_1) = \prod_{k=1}^{M} (z_j - Z_k) \exp\left[-\frac{1}{4\ell_0^2} |z_1|^2\right]. \qquad (4.14)$$

According to the theory of functions a polynomial is completely determined by its zeros. The zeros of Eq. (4.14) can be identified with charges which repel the electron at z_1. In order to minimise energy, all zeros are distributed homogeneously in real space. *Halperin* observed that the zeros are allocated exactly at the particle positions. This means that at $\nu = 1/m$ every charge position is defined exactly by m zeros [128]. Moreover, these m zeros not only correspond to one electron charge, but, by $\nu = 1/m$, the number of zeros is identical to the number of flux quanta per electron. The analogy with the OCP gives strong support that this Laughlin ground state is a translationally invariant liquid state [125,291]. This means that at $\nu = 1/m$ the electronic states are extended states.
The creation of elementary excitations can be illustrated according to Refs. [125,128] by the following Fig. 4.13, which shows the situation around a liquid ground state of fractional $\nu = 1/m$, e.g., 1/3. Part a) of the figure shows the situation exactly at fractional $\nu = 1/m$. The position of every electron is defined by m zeros of Eq. (4.14) or m flux quanta, i.e., here by $m = 3\Phi_0$. The charges are distributed uniformly on the neutralising background as in an OCP. In this Laughlin liquid state the optimal ratio between charge and flux is realised and thus the energy is minimised. As the field is increased by adding, e.g., one flux quantum, the system tries to keep its favourable ground state (Fig. 4.13.b). Therefore it avoids an overall change, i.e., a *compression* of the favourable ratio between charge and flux.

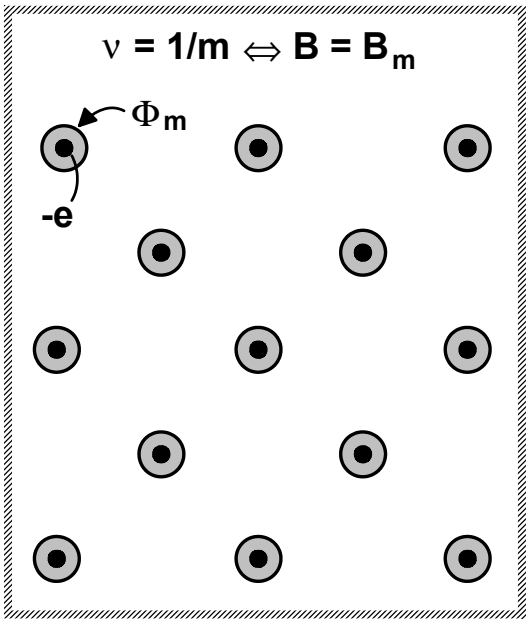

Fig. 4.13: Illustration of a correlated 2DES (schematic top view on a single layer) around fractional $\nu = 1/m$, e.g., 1/3. Full black circles represent electrons, grey-shaded areas represent the corresponding magnetic flux at ν, here $\Phi_m = 3\Phi_0$. The position of every electron is defined by m zeros of Eq. (4.11), i.e., here by m = 3 flux quanta Φ_0.

Fig. 4.13.a: Situation at $\nu \equiv 1/m$, i.e., $B = B_m$. The charges are distributed uniformly on the neutralising background. The optimal ratio between charge and flux is realised, which is inherent to the Laughlin liquid state.

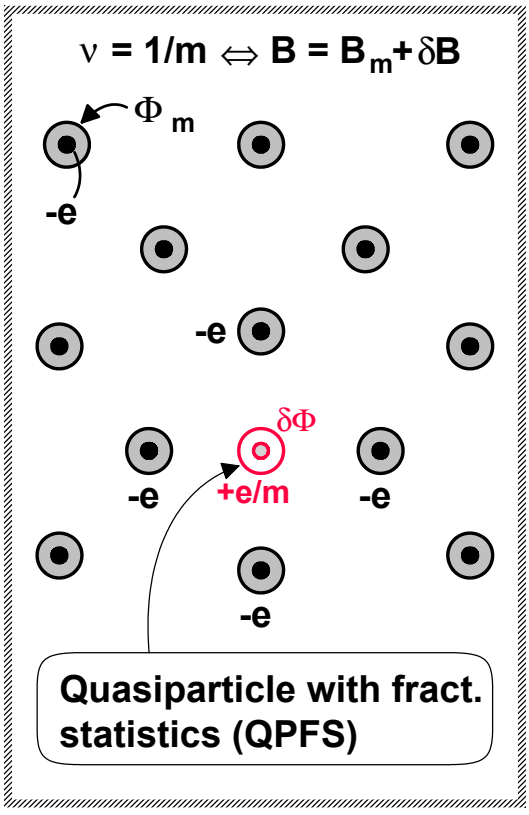

Fig. 4.13.b: Correlated 2DES at $B = B_m+\delta B$, i.e., one flux quantum is added to the system. One quasiparticle with fractional charge is generated.

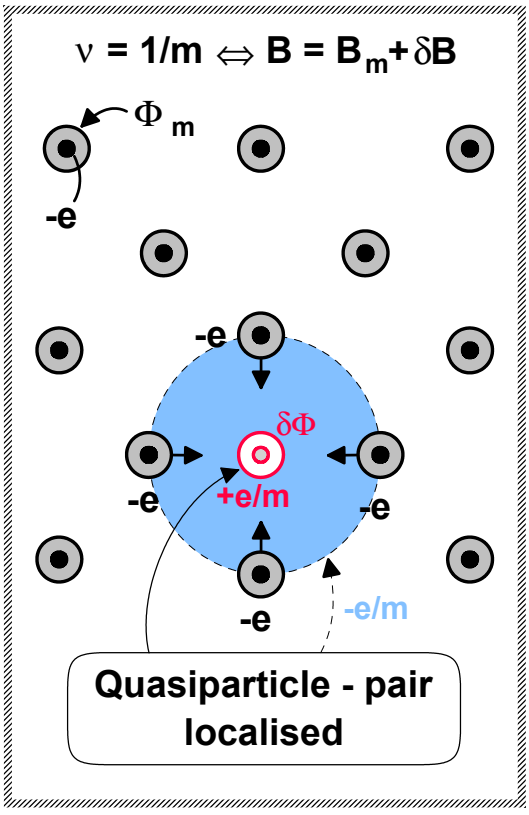

Fig. 4.13.c: Correlated 2DES at $B = B_m+\delta B$ after accumulation of a screening charge. The situation is symmetric with respect to the sign of the charges.

Instead, *one* single zero is generated formally in Eq. (4.14) and the flux is placed there. Since at $\nu = 1/m$ there are m zeros required to accommodate one charge, the corresponding single zero position is unoccupied and represents the lack of a charge of magnitude $+e/m$. This unoccupied charge position can be regarded as quasiparticle excitation with fractional charge ([125], see also [315,316,317,318,319]) i.e., as local charged perturbation. This quasiparticle (here it is a quasihole) is separated by a finite gap from the incompressible ground state.

Electron Localisation in the FQHE Region

After the generation of a quasiparticle (QP) with fractional charge $+e/m$ (see Fig. 4.13.b) the system minimises its total energy by keeping itself neutral on a mesoscopic scale. Therefore a negative counterpart charge of $-e/m$ in all is accumulated around the excitation until it is completely screened (Fig. 4.13.c)[7]. This screening object represents itself a quasiparticle of fractional charge. Up to now the generation of QPs was described for the situation $B \rightarrow B + \delta B$. In the symmetric case $B \rightarrow B - \delta B$ the created QPs have opposite sign but the same properties.
Experiments on the detection of QPs with fractional charges were carried out by a number of groups [310,320,321,322,323,324,325].
The quasiparticle excitations were shown to be allocated preferably at impurities [125] or at disorder sites. By this the QPs as well as the screening electrons are *localised* there. A further deviation of B from the value corresponding to $\nu \equiv 1/m$ results in the generation of further localised quasiparticle pairs which are expected to form a regular triangular lattice [128].
The role of the generated quasiparticles is to accommodate the flux difference which separates the system at *actual* internal magnetic flux from that of *optimum* flux at $\nu \equiv 1/m$ and to enable the major part of the system to stay incompressible. This procedure persists up to a critical flux value around fractional ν and is responsible for the occurrence of Hall plateaux.

By this process electron correlation in a 2D system may generate extended electronic states at low fractional ν. They are responsible for the ρ_{xx} minima in the FQHE. Around these fractions however, mobile as well as localised electrons were found to coexist, from which the localised carriers may not contribute to transport.

Fractional Statistics

The fact that the quasiparticle excitations generated around fractional $\nu = 1/m$ carry fractional charge $\pm e^* = \pm e/m$ [125,128,326] invokes questions on their further properties. It could be shown by *Arovas* in a gedankenexperiment that the interchange of two QPs of charge $|ve|$ leads to a Berry phase shift of $\Delta\varphi = \pi\nu$ introduced to their wave functions. For $\nu = 1$ the QPs would behave like fermions, however for fractional ν the QPs obey neither Fermi, nor Bose, but fractional statistics. This behaviour was also suggested in Ref. [327]. According to Wilczek this kind of particles can be called *anyons*, since for continuous ν any phase shift and therefore *any statistics* may be realised in a 2D system [328,329,326,315,330,331].

[7] The situation for $B \rightarrow \pm\,\delta B$ is symmetric, i.e., simply the sign of the generated quasiparticles/quasiholes in Fig. 4.13.c is changed for $\pm\,\delta B$.

One of the important results of fractional statistics is to determine the way in which quasiparticles pack in the 2DES [327,290]. This is done in dependence of the actual fractional ν and accounts, e.g., for the observed fractions 2/7 and 2/5 [327].

The Role of Impurities and Sample Inhomogeneities

The role of impurities in the FQHE was investigated by a number of groups [125,332,333,334,335]. As already pointed out in the original work [125], impurities and sample inhomogeneities lead to a broadening of the carrier bands which then consist of regions of extended and localised states. The FQHE is expected to be destroyed as soon as the zero-field scattering time $\tau < \hbar/\Delta$, where Δ is the quasiparticle energy gap.

The Size of Quasiparticles - Localisation Lengths

Important information on the size of quasiparticles and localisation lengths can be deduced from studies of the influence of impurities in the FQHE. It was found that the screening charge (see Fig. 4.13.c) which accumulates at an impurity, oscillates around the impurity on a characteristic length scale of

$$L_{QP} \approx \ell_0, \tag{4.15}$$

where ℓ_0 is the cyclotron radius in a semiconductor (see, e.g., [334]). This length scale L_{QP} can be understood as localisation length for those carriers which build the screening object. It means that those carriers can be considered as free as long as their motion is restricted to an area of radius below about ℓ_0 around the impurity. However since they are trapped to the corresponding area

$$S_{QP} \approx \pi (L_{QP})^2, \tag{4.16}$$

they have to be considered as localised on any larger length scale. This is expected to influence all experiments on longer length scales as, e.g., magnetotransport experiments and the result is indeed observed in the FQHE. The area S_{QP} can be interpreted as the size of a quasiparticle.
It should be recalled that the cyclotron radii ℓ_0 in semiconductors and the corresponding quantity $R_c$in metals may be very different quantities (see Eqs. (4.1) and (4.2)) and therefore localisation lengths and the size of quasiparticles may be very different in these classes of materials.
Furthermore it should be noted that the understanding of these quantities in multilayer systems is of course and additional challenge.

4.2.6 Hierarchy of Higher Order Fractions: From ν = 1/m to ν = p/q

The theory of Laughlin for the ground state and localised quasiparticle excitations is a successful description for the filling factors $\nu = 1/m$ (e.g., 1/3, 1/5). It should be kept in mind

that this approach was made to understand the FQHE in 2D semiconducting *single*-layer systems. It is furthermore assumed that all electrons are in the lowest Landau level and that their spins are completely polarised. The fact that the ground state wave function (Eq. (4.11)) must obey Fermi statistics, requires that m is odd. By electron-hole symmetry the description can be extended to $\nu = (1 - 1/m)$, e.g., 2/3, 4/5 (see Fig. 4.10 and Tab. 4.1).

The next step for the understanding of the realisation of more complex ν has been made by thinking over the role of spin polarisation. *Halperin* pointed out [128] that the electron g-value in GaAs is about 0.25 of the free electron value [336] and by comparison of Zeeman and cyclotron energy he argued that at moderate fields some of the spins may be reversed. Using the classical plasma approach [337,338,339,291], the filling factor region could be extended to fractions

$$\nu = \frac{2}{(m+n)}, \tag{4.15}$$

where, e.g., $m = 3$ and $n = 2$ would result in $\nu = 2/5$. Further investigations revealed that the 5/2 state is indeed spin unpolarised [340,295,300]. A later systematic calculation [341] showed that besides 5/2 also the 2/7 state is unpolarised, whereas the states at fractions 4/13, 4/11 and 4/9 are partially polarised (the latter fraction was observed in experiments and is reported in Ref. [261]).

The presence of the FQHE at a number of further ν with more complex fractions (see Figs. 4.9 and 4.10) asked to extend Laughlin's theory and to develop a hierarchy scheme for the filling fractions at which the FQHE and electron localisation may occur. Main efforts on this purpose were made by *Haldane* [259,342], *Halperin* [327], *Laughlin* [288,343] and *Jain* [344].
Haldane's approach is based on the idea that a first generation of quasiparticles at $\nu = 1/m$ (m = 3,5,7, i.e., first line in Fig. 4.10) is built by correlated electrons. These quasiparticles themselves can be understood as 'parent' states which *couple* and thus build the next generation of QPs (second line in Fig. 4.10). These again may couple and as the scheme is continued, a wide variety of fractions is realised. The sequence of possible filling fractions (see, e.g., Fig. 4.10) is given by

$$\nu = \cfrac{1}{m + \cfrac{\alpha_1}{p_1 - \cfrac{\alpha_2}{p_2 - \cfrac{\alpha_3}{p_3 - \ldots}}}} \tag{4.18}$$

where $m > 0$ is an odd or even integer for a Fermi or Bose system, respectively. The factors α_j are -1 for the creation of particles and +1 for holes, while p_j are even quantities. In this picture the elementary excitations obey Bose statistics. Considering particle-hole symmetry this formula holds for all filling fractions $0 < \nu < 1$ built on the lowest Landau level. Based on $m = 1$, however, Eq. (4.18) generates all odd denominator fractions with $0 < \nu < \infty$ (particle-hole symmetry included).
Halperin's hierarchial scheme [327] keeps very close to *Laughlin's* theory. The first set of quasiparticles at $\nu = 1/m$ (first line in Fig. 4.10) is generated as described in Sec. 4.2.5, restricting ν to $0 < \nu < 1/2$ with odd denominators (see Tab. 4.1). Particle-hole symmetry extends the fractions to $\nu = 1 - 1/m$. Inclusion of the second spin state allows certain fractions with $\nu = 1 + 1/m$. The coupling of electrons to pairs enables the realisation of $\nu = 1/p$ with

arbitrary p, including even values. Coupling between paired and unpaired electrons extends the ν region as shown in Tab. 4.1, where m (odd) controls the correlation between unpaired electrons, p (even) represents the correlated pairs and r (odd or even) introduces the electron-pair correlation.

Assumption	Possible Filling Factors		
System Spin - Polarized	$\nu = 1/m$	$\nu < 1/2$	m = odd
Electron - Hole Symmetry	$\nu = (1-1/m)$	$\nu < 1$	m = odd
Abrogation of Spin Polarization	$\nu = (1+1/m)$	$\nu > 1$	m = odd
Electron - Electron Pairs	$\nu = 1/q$	$\nu < 1$	q = arb.
Pairs + Single Electrons	$\nu = \frac{4m+p-4r}{mp-r^2}$		m = odd p = even r = odd/even
n - Tuplets of Electrons	$\nu = n^2/m$	ν = arb.	n, m = arb.
Inclusion of Higher Landau Levels	$\nu = p/q$	$\nu > 1$; arb.	p, q = arb.

Tab. 4.1: Extension of possible fractional filling factors ν from $\nu = 1/m$ to arbitrary $\nu = p/q$ according to the hierarchial scheme in Ref. [327].

This scheme can be extended to the generation of n-tuplets of electrons and ends up with $\nu = n^2/m$, which can, in principle, reach any rational filling factor, especially when higher Landau levels are included. In this picture the elementary excitations obey fractional statistics.

The following features are essential in the FQHE and in the above described hierarchial schemes.

1) The hierarchial schemes describe the FQHE in semiconducting *single*-layer 2D systems.
2) They allow indeed arbitrary ν in the liquid state above the critical value ν_c of Wigner crystallisation.
3) They 'propose' possible filling factors to the system and the system 'decides' whether they are sufficiently stable to be realised and in which Landau level occupation and spin conformation this can be done.
4) In both pictures the variety of possible ν is given by the coupling of electrons and/or quasiparticles.

From the experimental experience further characteristic properties of the FQHE states have been deduced:

5) The higher the carrier mobility is, the higher the variety of fractional ν is, where the FQHE occurs.

6) With increasing denominator value, both, the quantised Hall plateau width as well as the depth of the ρ_{xx} minima decrease.
7) The FQHE has a characteristic energy scale of a few degrees Kelvin.

It is straightforward to see that, provided that two-dimensionality is given, most of the characteristics are determined by system specific properties as, e.g., electron density, mobility, cyclotron radii and furthermore by scattering times, mean free paths of coherent motion gap energies and dielectric constants. All these quantities may be very different in 2D semiconductors and 2D metals, respectively.
It should be also noted that spin reversal depends on the spin interaction energy, which may be also very different in 2D semiconductors and metals.
Moreover, the above mentioned stability calculations were performed for finite systems containing only a few carriers, whereas metals have a huge number of electrons. This holds the possibility that in systems with a huge particle number complex coupling patterns may lead to stable states.

For these reasons the sequence of allowed ν in 2D metals might differ strongly from that observed in semiconducting 2D systems.

4.2.7 The Special Fraction ν = 1/2 in a Single-Layer 2DES: Composite Fermions

As already mentioned, *Laughlin's* description of the FQHE as well as the major part of the subsequent work concentrates on the treatment of filling factors with odd denominators. This is motivated by the fact that in experiments on single-layer 2DES odd denominator fractions are found to be strongly favoured. This is considered in the theoretical description by the requirement of antisymmetry of the wave functions of the first generation of quasiparticles. The same condition is also worked into the hierarchial schemes, thus leading to odd denominators also in higher order fractions (see Fig. 4.10 and Eq. (4.18)). However the possibility of even denominator filling factors is not excluded in these theories. Indeed minima in ρ_{xx} indicate the presence of $\nu = 3/4$ [270] and $\nu = 9/4$, 5/2 and 11/4 [273,345].
The most exciting even denominator filling factor is certainly $\nu = 1/2$. In this case a Laughlin-type wave function for a single-layer 2DES would describe a system obeying Bose statistics. Transport experiments on heterostructures show in the region of $\nu = 1/2$ dips in ρ_{xx} but no FQHE plateau (see, e.g., [258,264]). This finding invoked the question whether the occurrence of the FQHE at $\nu = 1/2$ either requires higher sample quality or whether the liquid state underlying to the FQHE can be ever established at $\nu = 1/2$ in a single-layer system. The question whether this liquid state is the stable ground state at $\nu = 1/2$ was followed by calculations of the ground state energies ([284,285], see also Fig. 4.11). Especially at this ν the ground state energies show system size dependence without tendency to convergence, thus leaving the question open. A number of further studies on the nature of the $\nu = 1/2$ state in a single-layer system were carried out (see, e.g., [128,346,337,347]). From isotropy arguments of the pair correlation function $g(\mathbf{r})$ it was concluded in Ref. [347] that at $\nu = 1/2$ the liquid state is *not* a stable ground state in a single-layer 2DES.

Composite Fermions

A decisive progress in the description of a half filled Landau level was achieved by a picture developed by different authors ([348,349,330,350,351,352,353] for a review see, e.g., [354]). It is based on the statistical transmutation of a system of electrons to one of *composite fermions*, which is reached by the introduction of a fictitious magnetic gauge field. The hamiltonian in this so-called Chern-Simons-Landau-Ginzburg (CSLG) description reads

$$H' = \frac{1}{2m}\sum_i \left[\boldsymbol{p}_i - \frac{e}{c}\boldsymbol{A}(x_i) - \frac{e}{c}\boldsymbol{a}(x_i)\right]^2 + \sum_i eA_0(x_i) + \sum_{i<j} U(x_i - x_j), \qquad (4.19)$$

where $\boldsymbol{A}$ represents the vector potential of the external magnetic field, A_0 is the scalar potential of the electric field and U represents the electron interaction term. The vector potential $\boldsymbol{a}(x)$ generates the fictitious magnetic gauge field and is given by the particle density $\rho(x)$ and the flux quantum in terms of

$$\nabla \times \boldsymbol{a}(x) = \wp \Phi_0 \rho(x). \qquad (4.20)$$

It contains a statistical phase factor $\wp$ which can be chosen as appropriate. The basic idea of the CSLG description of the FQHE is to attach the fictitious flux generated by $\boldsymbol{a}(x)$ to the electrons in the system and thus to transform electrons to composite particles consisting of charge and flux. Odd integer values of $\wp$, i.e., $\wp = (2k+1)$, attach an odd number of flux quanta to each electron, whereas even values ($\wp = 2k$) attach an even number of flux quanta to each electron. By interchange of such composites it can be shown that in the former case these composite particles behave as bosons, while in the latter case they behave as fermions. Therefore they are denoted as composite bosons and composite fermions, respectively.
At $\nu = 1/2$ (i.e., $k = 1$) there are two flux quanta attached to each electron. The orientation of the fictitious gauge field can be chosen to be opposite to the external magnetic field. Thus in a mean field approximation the fictitious field generated by $\boldsymbol{a}(x)$ cancels exactly the real external field $B_{ext,1/2}$, so that at $\nu = 1/2$ composite fermions 'feel' an effective field $B^*_{CF} \equiv 0$. By this vanishing of B^*_{CF} the CF picture illustrates why the FQHE is not observed at $\nu = 1/2$ in single-layer 2DES. As soon as the external field is varied from the value $B_{ext,1/2}$, the composite fermions (CFs) are exposed to a non-vanishing effective field, i.e., $B^*_{CF} \neq 0$. As the field is further varied, CFs show the IQHE, which occurs exactly at external field values where the FQHE of electrons is observed. This holds the considerable advantage to map the FQHE of electrons into the IQHE of composite fermions, viz, to turn the description from a many-particle problem of interacting particles to a single-particle problem of non-interacting CFs. This is indeed a very elegant simplification.
Composite fermions have a series of further very interesting properties, up to the fact that CFs themselves may couple and thus may lead to a FQHE of composite fermions [355].

Some of the most powerful features of the CF picture is to simplify the description of the FQHE in a single-layer 2DES and to illustrate why there the FQHE is not expected to occur at $\nu = 1/2$. However it has to be kept in mind that the CF picture, especially for $\nu = 1/2$ is developed just for single-layer 2DES. The situation may change drastically as soon as a 2DES consists of two or more layers.

4.2.8 The Special Filling Factors ν = ½ and ν = 1 in Multiple-Layer Systems

Most of the experimental and therefore also of the theoretical work on the FQHE was performed on single-layer 2DES based on semiconducting materials. The step from single-layer to double-layer and further to multiple-layer 2DES gave access to new exciting phenomena in the FQHE. After preceding theoretical studies of multilayer electron systems [356,357,358,359] outstanding works were presented by *Rezayi et al.* [360] and *Chakraborty et al.* [280,281]. These latter publications provide the theoretical description of the excitation spectrum in a double-layer 2DES of interacting electrons and predict the possible occurrence of new FQHE states, as, e.g., at ν = 1/2 in layered 2D systems. For such new states to exist *inter*layer electron-electron interaction is required to be comparable to *intra*layer electron-electron interaction. The length scale for the latter is the magnetic length ℓ_0 (see Eq. (4.1)[8]), so that interlayer separation is required to be of the same order as well.
The system is described in [280,281] in terms of the so-called *Visscher-Falicov* model [356] which assumes that equal electron densities are present in each plane. The two planes are coupled by Coulomb interaction, so that the twofold degeneracy of the states is lifted. The electrons are in their lowest subband, i.e., spin polarised. They may move freely in each plane, however in this first step of description, they are not allowed to tunnel between the layers. This latter condition allowed to describe the system by a simplified hamiltonian which conserves the total momentum as well as the electron number in each layer. In consequence the hamiltonian could be diagonalised and this simplification allowed to calculate the ground state and excitation spectrum of a two-layer 2DES of eight electrons in total at ν = 1/2 in each layer. It was found that

1) In contrast to the result for a single layer, a stable liquid ground state exists in a layered system at ν = 1/2 uniquely at a momentum $k = 0$.
2) The results are nearly independent from system size and geometry. This is in contrast to the results on the unstable single layer ν = 1/2 state.
3) An energy gap is present which separates a series of excited states from the ground state.
4) This gap of the ν = 1/2 double-layer FQHE state is found to be even larger than the gap of the ν = 1/3 single-layer state, so that under these conditions the FQHE at ν = 1/2 is expected to be even very stable in a double-layer.
5) The excitation spectrum for $k = 0$ and finite k, respectively, corresponds to the results for the Laughlin liquid state at ν = 1/3 [361] including indications for collective modes.

From these results it was concluded that in coupled multilayer 2DESs an incompressible liquid ground state exists at ν = 1/2 and that therefore the FQHE may be observed in such systems at half filling. Furthermore it was found that

6) The two lowest lying excitations can be interpreted as eigenmodes of the coupled double-layer system.
7) The number of excited collective modes was shown to be proportional to the number of layers N_L, so that for $N_L \rightarrow \infty$, i.e., in a superlattice, a band of excited states is generated.

[8] Note the difference between semiconductors and metals (Eq. (4.1) vs. (4.2)).

The answer to the question, why filling fractions which are 'forbidden' in single-layer systems may occur in multiple-layer systems, was illustrated by a contribution of *Yoshioka et al.* [362]. The authors employed the generalised Jastrow-type wave function [128] and outlined the possibilities of new FQHE states in double-layer systems. They pointed out that electron-electron interaction is not independent of the layer in which the electrons reside. Furthermore they showed this makes certain wave functions which are 'forbidden' in single-layer systems acceptable for double-layer systems.

In a number of subsequent works the role of interlayer Coulomb coupling was studied on double-layer systems and even finite interlayer tunnelling was introduced (see, e.g., [362,363,364,365,366,282,283]).
As long as the two layers are well-decoupled, the observed IQHE states in each layer are the same as in single-layer systems. The total system can be described either by the total filling factor ν_{tot}, or by those of the successive layers ν_{L1}, ν_{L2}, where

$$\nu_{tot} = \frac{hN_{tot}}{eB} = \nu_{L1} + \nu_{L2}\,. \tag{4.20}$$

This restricts the observation of the IQHE to even values of ν_{tot} when $\nu_{L1} = \nu_{L2}$ is odd or even (this situation is referred to as **a)** below). The same argument limits the variety of FQHE filling fractions to the sum of the allowed single-layer fractions.
The notation introduced by Eq. (4.20) holds even when the two layers are coupled but tunnelling is prohibited. However coupling introduces new allowed filling factors, as, e.g., $\nu_{tot} = 1$ realised by $\nu_{L1} = \nu_{L2} = 1/2$ (see above) and $\nu_{tot} = 1/2$ (see, e.g., Ref. [282]). When tunnelling is introduced, the above mentioned filling factor selection roles are lifted. States of symmetric and antisymmetric wave functions can be constructed, which are separated by a single-particle symmetric-antisymmetric tunnelling gap (Δ_{SAS}) [363,364,283]. From now it is more appropriate to describe the system by ν_{tot} instead of ν_{L1} and ν_{L2}, since the latter are no more conserved. For very strong tunnelling the system behaves as a bulk single layer (since only the lowest symmetric state is occupied) and both, IQHE and FQHE show their familiar single-layer spectra, however with respect to ν_{tot} instead of ν_{L1} and ν_{L2}, respectively.
The preceding aspects show that odd-filling IQHE states are very sensitive to interlayer effects. Therefore the role of interlayer coupling and tunnelling on the IQHE and FQHE in a semiconducting double-layer system can be illustrated by means of a phase diagram for the IQHE just at $\nu_{tot} = 1$ [364,283], which is shown in a revised version in Fig. 4.14. There the role of interlayer coupling is represented on the *y*-axis by the reciprocal *inter*layer Coulomb energy ($\varepsilon\, d/e^2$) rescaled by the *intra*layer Coulomb energy ($e^2/\varepsilon\ell_0$), whereas the single-particle tunnelling is represented on the *x*-axis by Δ_{SAS}, also rescaled by the intralayer Coulomb energy. The competition of interlayer Coulomb interaction (which generates interlayer collective phenomena) and single-particle interlayer tunnelling leads to the following situations:

a) *Well-decoupled layers without tunnelling.* This situation, where the $\nu_{tot} = 1$ IQHE is absent, is described above. In Fig. 4.14 this case is found collinear to the *y*-axis at sufficiently high $d/\ell_0 \gtrsim 2$.

b) *Coupled layers without tunnelling.* The $\nu_{tot} = 1$ IQHE is realised by $\nu_{L1} = \nu_{L2} = 1/2$ (see above) [280,362,363]. The FQHE at $\nu_{tot} = 1/2$ is present [282]. This case is illustrated by the *y*-axis for $d/\ell_0 \lesssim 2$.

c) *Coupled layers with finite tunnelling.* The ν_{tot} = odd IQHE occurs and can be generated either by pure Coulomb coupling or by single-particle tunnelling, respectively (see, e.g., Ref. [283]). This condition is represented by the whole area under the curves for finite Δ_{SAS} values. The FQHE at $\nu_{tot} = 1/2$ is present [366]. Under these conditions the IQHE is even more stable against coupling variations. This situation will be of special interest in connection with quantum oscillation experiments on the 2D multilayer organic metal κ-(BEDT-TTF)$_2$I$_3$ (see Sec. 5.8).

d) *Coupled layers with strong tunnelling.* This case is represented by the right margin of Fig. 4.14. The odd-value IQHE is present and the IQHE persists even for lower plane coupling up to a critical value. The system behaves like a bulk single-layer system (see, e.g., Ref. [282]) and is therefore expected to show the IQHE and FQHE as in single-layer systems, but with ν_{tot} as filling factor.
Of course, with too strong tunnelling the system becomes three-dimensional and the quantised Hall effects break down.

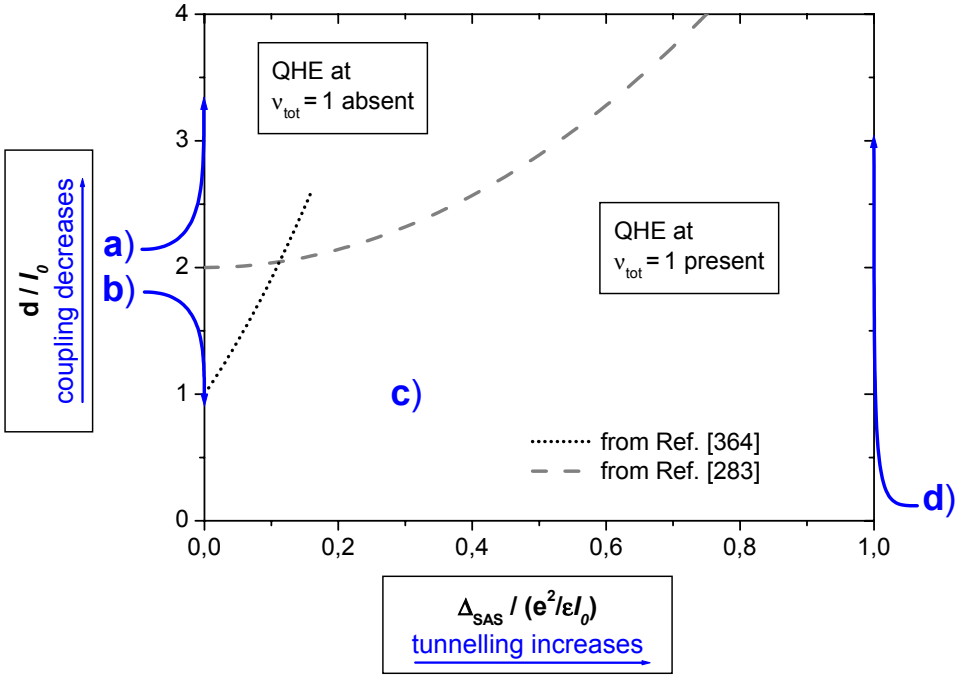

Fig. 4.14: Phase diagram for the occurrence of the IQHE at $\nu_{tot} = 1$ in a double-layer system. The influence of interlayer coupling (y-axis) and single-particle interlayer tunnelling (x-axis) results in the presence of the two phases. The dotted and dashed lines are calculated in Refs. [364] and [283] (consider the different conditions in both Refs., which however are not of importance in the present context). The cases **a) - d)** are discussed in the text.

Thus it can be summarised for IQHE and FQHE in double-layer systems:

i) The IQHE is realised for odd and even ν_{tot} values as soon as coupling (and tunnelling) is present.
ii) Under these conditions the FQHE is realised at $\nu_{tot} = 1/2$.
iii) If it is that the system is described by ν_{tot} rather than by the single-layer values ν_{Lj}, then interlayer tunnelling is clearly present.
iv) Both, Coulomb coupling and finite tunnelling stabilise the IQHE and FQHE in a double-layer system. With tunnelling the IQHE is even more stable than without tunnelling.

v) As tunnelling is increased, the layered 2DES shows the behaviour of a bulk single-layer 2DES.

All these multiple-effects are shown to influence IQHE and FQHE experiments and therefore may be observed also in other transport measurements.

4.3 Other Results of Two-Dimensionality: Skyrmions

In the preceding sections of the present chapter it is described, how a 2D system minimises its total energy around integer and fractional Landau level filling factors. The contribution of electron spin has been either disregarded or restricted to the case of sufficiently strong Zeeman splitting as to generate spin-flipped quasiparticles as described in Sec. 4.2.6. However a lower Zeeman energy gives the 2D system further possibilities to realise the minimum of total energy by deriving a benefit from spin correlation. This is done by minimising both, Coulomb energy $E_C = (e^2/\varepsilon_0\varepsilon_r\ell_0)$ and Zeeman energy $E_Z = g\mu_B B$. Since E_C is minimised by *lowering* the total spin whereas E_Z is lowered by *enhancing* the total spin, the minimum is found by setting both equal, i.e.,

$$\frac{e^2}{\varepsilon_0\varepsilon_r\ell_0} = g\mu_B B. \tag{4.21}$$

The conclusion of this equation is that the system will play with the local spin orientation in order to realise the total energy minimum. Illustrated on a completely spin-polarised system (e.g., spins parallel to $\boldsymbol{B}$, see Fig. 4.15), this results in the possibility to invert a spin at a certain position $\boldsymbol{r} \equiv 0$ (downward arrow in Fig. 4.15) and to generate a 'spin texture' around, where the spin orientation changes gradually from antiparallel orientation at the origin to the expected parallel orientation at sufficiently large $\boldsymbol{r}$.

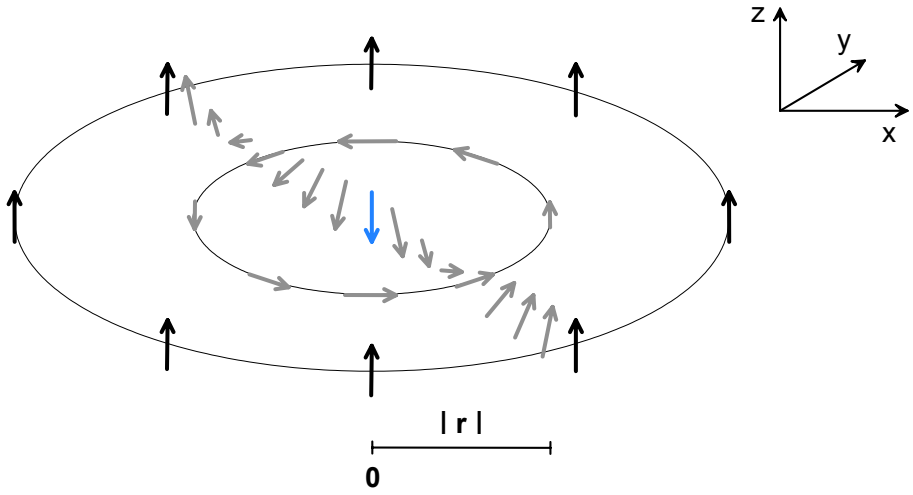

Fig. 4.15: Schematic illustration of a skyrmion, i.e., a 'charged spin texture excitation' in a 2D system. The skyrmion comprises all spins, which are declined from the totally spin polarised ground state (here: from the z-direction).

This object, which carries a charge of $\pm ve$, can be regarded as '*charged spin texture excitation*' and this quasiparticle is defined as '*skyrmion*' [9] [367,368,369,370]. For given ε_r and ℓ_0, the electron *g*-value decides if skyrmions may be generated or not and it marks roughly the field region, in which they are stable [368,369]. Especially, *g* determines the number of spins involved, as well as the size of a skyrmion. These quasiparticles are characterised by their quantum numbers *K* (i.e., the number of involved spins), *Q* (i.e., their total charge) as well as their angular momentum. It should be noted that these charged quasiparticles are localised at impurities.
Depending on the electron *g*-value in a 2D system, different cases can be distinguished:

1) Small *g*-value ($g \gtrapprox 0$): large skyrmions
In this case the gain in E_C is huge by lowering the total spin, whereas the cost in E_Z is finite due to the low *g*-value. Therefore large-*K* skyrmions are generated. The spin orientation around the spin flip changes only *gradually* (see Fig. 4.15). This spin texture can be described by the unit vector ***n(r)*** given by its components

$$n_x(r) = \frac{4\lambda x}{r^2 + 4\lambda^2}; \quad n_y(r) = \frac{4\lambda y}{r^2 + 4\lambda^2}; \quad n_z(r) = \frac{r^2 - 4\lambda^2}{r^2 + 4\lambda^2}, \tag{4.22}$$

where λ represents the size of the skyrmion.

2) Finite *g*-value $(0 < g \lesssim g_c)$: small skyrmions
In the case of an increasing *g*-value, each spin flip enhances the Zeeman energy considerably. Therefore the system tends to an equilibrium of E_C and E_Z (see Eq. (4.21)) at a low number of spin flips. This reduces the size of skyrmions with increasing *g*.

3) Limit of high *g*-value ($g \gtrsim g_c$): 'normal' quasiparticle excitations
As soon as *g* reaches and exceeds a critical value g_c (with $g_c \approx 0.054 e^2/(\varepsilon \ell_0 \mu_B B)$, see, e.g., [368,369]), skyrmions become 'normal' quasiparticle excitations as described in Secs. 4.2.2 ff.

The generation of skyrmions obeys a selection role regarding the filling factors, where these spin texture excitations are allowed to occur (see, e.g., Refs. [371]). A priori one might expect skyrmions around odd integer ν close to quantum limit[10]. However theoretical expectations [371] and experimental results [372] have shown that the low-energy spectrum at $\nu = 3, 5, \ldots$ does not contain any skyrmion-like structure, also ruling out such excitations near the filling fractions 3/5, 3/7, 5/7, etc. These studies leave the possibility for the generation of skyrmions near odd denominator fractions $\nu = 1/(2m+1)$. At special fractions, as, e.g., $\nu = 1/3$, even skyrmions of composite fermions are discussed [373].

Experimental verification for the occurrence of skyrmions can be achieved by electronic transport measurements [372,374], optical methods [375], hybrid methods [376,377,378,379,380,381,382] or, e.g., nuclear-magnetic resonance (NMR) experiments [383,384].

[9] The skyrmion was originally proposed by *T.H.R. Skyrme* as a model of a nucleon in terms of a soliton solution for a π-meson field.

[10] Of course skyrmions are prohibited around any even integer ν, since the system is already spin unpolarised there.

One of these methods, where skyrmions are identified in optically pumped NMR [383], is briefly quoted in the following. In these experiments the Knight shift (K^S) was investigated on multiple quantum wells at Landau level filling $0.66 < \nu < 1.76$ (see Fig. 4.16). The Knight shift signal is influenced by the electron spin polarisation and is therefore sensitive for deviations of the spin polarisation from the expected behaviour, which is filling factor, i.e., magnetic field dependent. The solid lines in Fig. 4.16 represent the behaviour as expected without the occurrence of skyrmions, i.e., the limit of large *g*-values (which is case 3) above). Below $\nu = 1$ the constant signal accounts for the fully polarised spin system. Above $\nu = 1$ the Knight shift decreases with decreasing total spin polarisation. As soon as skyrmions are generated around $\nu = 1$, the measured Knight shift signal (full circles) deviates from the expected solid curve. The bigger a skyrmion is, the more spins are involved and therefore the stronger the deviation from the solid curve is. In these experiments the skyrmions around $\nu = 1$ were found to comprise $K = 3.6$ (±0.3) spins in agreement with theoretical studies, which expect ($K = 3$)-skyrmions to be the most stable ones under these conditions.

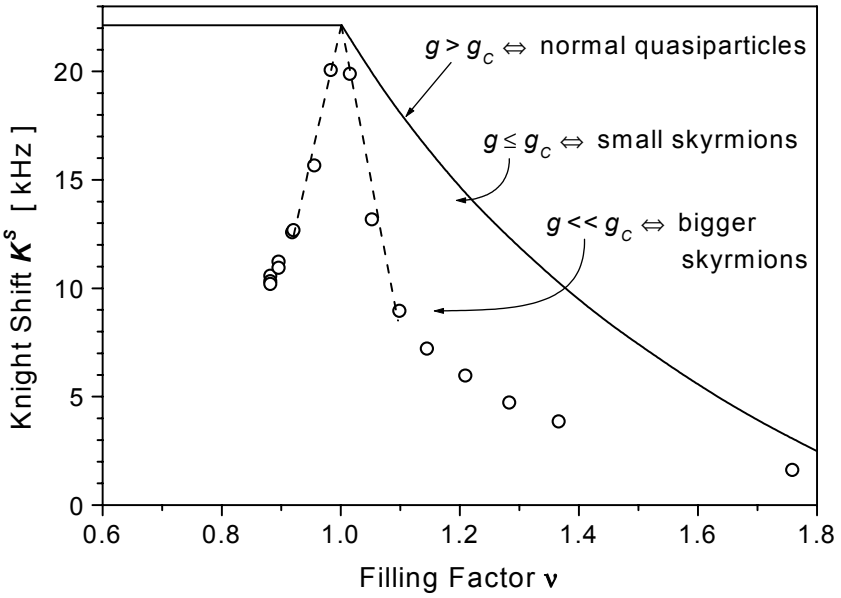

Fig. 4.16: Knight shift K^S in an *n*-doped multiple quantum well vs. filling factor ν (according to Ref. [383]). The solid lines represent the behaviour expected for large *g*-values ($g \gtrsim g_c$). The dashed line represents the behaviour expected for finite-size skyrmions comprising $K = 3.6$ spins.

Some of the most important properties of skyrmions are summarised in the following:

1) Skyrmions are localised charged spin texture excitations, which modify the total spin polarisation and lower the number of mobile charge carriers.
2) Their occurrence is restricted to $\nu = 1$ as well as odd denominator fractions $\nu = 1/(2m+1)$.
3) Their size, i.e., the number of involved spins decreases with increasing electron *g*-value.

4.4 Interjection

The preceding theoretical part concentrates on the description of the influences of two-dimensionality onto magnetotransport and thermodynamic properties of 2D electronic systems. Within this framework, Ch. 3 focuses on the description of quantum oscillations and involves tools which allow to distinguish between these influences of two-dimensionality and those arising from other effects. However there, electron localisation effects are disregarded.
Chapter 4 is devoted to the quantised Hall effects and focuses on the role of electron localisation in the IQHE and FQHE in single-layer and especially in multilayer 2D systems.
Unfortunately most of the work is done for semiconductor-based 2DESs. Within the reviewed literature there is no condition recognisable, which would restrict the occurrence of the quantum Hall effects and electron localisation to semiconductors. This stimulated our work on 2D and Q2D organic metals with the aim to observe low integer and, if possible, even fractional ν in a multilayer organic metal. The results are presented in the following chapters.

5. Electronic Properties of the 2D Multilayer Organic Metal κ-(BEDT-TTF)$_2$I$_3$

The following two chapters comprise investigations of electronic properties performed on different multilayer organic metals and superconductors, which exhibit two-dimensional (2D) and quasi-twodimensional (Q2D) electronic behaviour. Chapter 5 concentrates on quantum oscillation (QO) studied on the 2D normal conducting state properties of the organic superconductor κ-(BEDT-TTF)$_2$I$_3$, where influences of the two-dimensionality have been examined intensively. For comparison, effects of quasi-twodimensionality onto QO experiments of a number of further organic metals are presented in Ch. 6.

Quantum oscillation experiments were performed as de Haas-van Alphen (dHvA) as well as Shubnikov-de Haas (SdH) measurements. Therefrom, dHvA experiments were carried out mostly by torque technique whereas only to a minor part by field modulation and inductive techniques ([87], see also [385]). SdH experiments were carried out by standard four-probe method (see, e.g., [6b]), which prohibits influences of contact resistances onto potential detection. Different sample contacting methods were applied in order to avoid subtle contact effects. Annealed gold wires of 15 - 25μm thickness where applied either directly to the samples or on evaporated gold contacts. The wires were attached by gold, platinum or carbon paint, respectively. Low metallic contact resistances of about 2 - 5Ω (at room temperature) could be obtained, even if the evaporation of gold was refused (in order to save the sample surface from possible overheating). AC currents of frequencies between 90Hz and 4kHz were applied perpendicular and parallel to the conducting planes and were limited to 50 - 300μA, keeping the current well below values of about 3mA, where sample heating was found to set in at pumped ^{3}He temperatures. Quantum oscillation experiments were carried out on about 40 samples of different batches. The experimental conditions mentioned above were found to lead to consistent results.
High magnetic fields were provided by superconducting magnets (up to 10T), by steady resistive magnets (up to 28T, in a few measurements up to 36T) and by pulsed field magnets (up to 52T and 60T, respectively). Most of the QO measurements have been performed at the High Magnetic Field Laboratory MPI-FKF/CNRS Grenoble/France (GHMFL). They were completed by experiments at the pulsed field laboratory Laboratoire National de Champs Magnétiques Pulsés (LNCMP) Toulouse/France, the National High Magnetic Field Laboratory (LANL) Los Alamos/USA, the National High Magnetic Field Laboratory Tallahassee/USA and the Walther-Meissner-Institut in Garching/Germany.
Low temperatures down to 0.38K were realised by pumping on both, a ^{4}He bath cryostat and its ^{3}He insert, whereas temperatures down to 20mK were realised in a ^{3}He/^{4}He dilution refrigerator. Angle-dependent QO experiments at ambient pressure were carried out by mounting the samples on a rotatable sample-holder. SdH experiments at hydrostatic pressures up to 10kbar were carried out in a CuBe pressure cell.

The present chapter comprises the most important results obtained on the organic superconductor κ-(BEDT-TTF)$_2$I$_3$. The investigations presented here concentrate on the normal conducting state of this compound, which was found to realise the to date strongest 2D electronic system in its class of materials.

5.1 A Selection of General Electronic Properties of κ-(BEDT-TTF)$_2$I$_3$

Crystal Structure

The organic superconductor κ-(BEDT-TTF)$_2$I$_3$ was first synthesised by [143,144,386] by electrochemical methods. The crystal growth process was based on the supporting electrolyte (n-$C_4H_9)_4NI_3$, where a small amount of (n-$C_4H_9)_4NAuI_2$ was added in order to support especially the growth of κ-structured crystals. In contrast, the single crystals used for our investigations were synthesized as described in Ref. [141] without any AuI_2-based electrolyte. The obtained crystals have a typical size of $1 * 2 * 0.25mm^3$. The crystal structure of κ-(BEDT-TTF)$_2$I$_3$ is shown in Figs. 2.4 and 2.5. The structural data for crystals synthesised by different groups are shown in Tab. 5.1.

κ-(BEDT-TTF)$_2$I$_3$	**a** [Å]	**b** [Å]	**c** [Å]	**β** [Å]	**V** [Å^3]	**Ref.**
monoclinic P2$_1$/c (at 300K>T≥150K) P2$_1$ (at T< 150K)	16,39	8,47	12,83	108,56		[143][1]
	16,429	8,504	12,876	108,50	1 705,97	[145][2]
	16,433	8,500	12,871	108,51	1.704	[387][3]
	16,453	8,506	12,888	108,53	1.710	[387][4]

Tab. 5.1: Structure data of κ-(BEDT-TTF)$_2$I$_3$ obtained from crystals of different synthesis processes.

A comparison of the crystal data calculated by several groups reveals slight but significant differences, which may be attributed to the diverse underlying synthesis processes.
It should be noted that slightly different structures above and below about 150K are reported in [387] (see Tab. 5.1). This corresponds to a breaking of the c-axis symmetry at temperatures below about 150K. The structural phase transition coincides with an anomaly in the temperature dependent volume cell data at about 170K. From the absence of corresponding superlattice spots in the X-ray structure investigations the occurrence of a superlattice between 150K and 10K could be excluded. The phase transition proposed in [387] is in agreement with preceding resistivity and thermopower experiments [145,147] touched on below. Fermiologically this phase transition is found to cause the lifting of the degeneration between two bands, i.e., the opening of a gap (see Fig. 5.9), which can be tunneled by the magnetic breakdown at sufficiently high fields.
The highly conducting (b,c) planes of κ-(BEDT-TTF)$_2$I$_3$ are denoted as 2D planes in the following. It should be emphasised that a typical bulk single crystal contains about 10^5 successive conducting layers. This is a typical order of magnitude within these so-called

[1] with an amount of AuI_2-based electrolyte during the synthesis

[2] without AuI_2^-; there the space group P2$_1$/a was used, which means that the crystallographic a and c-direction are interchanged. The data shown in Tab. 5.1 are transferred to P2$_1$/c.

[3] with AuI_2^-

[4] without AuI_2^-

organic charge-transfer (CT) salts. In the framework of quantum oscillation experiments the present compound turned out to represent in fact a bulk multilayer organic metal with strongly 2D electronic properties (see Sec. 5.2 ff.).

Resistivity Measurements on κ-(BEDT-TTF)$_2$I$_3$ Single Crystals

Preceding measurements of the temperature dependence of the resistivity were carried out on single crystals between room temperature and 1.3K ([145], for details see [147]). In contrast to other κ-phase organic metals the present material was found to be a normal metal below room temperature (even below 350K, [388]) down to 4.2K, where the onset of the superconducting transition is observed in resistivity. A metal-metal transition occurs between 130K and 200K, whose transition temperature depends on the crystal axes. This transition may be attributed to the structural phase transition reported later in Ref. [387]. The high resistivity ratio of ρ(300K)/ρ(4.5K), reaching values op to $8 * 10^3$, reflects the high crystal quality [389].
The anisotropy of the resistivities reflected in the ratio of the interplane and in-plane resistivities (i.e., $\rho_{a^*}/\rho_{(b,c)}$) was studied on bulk single crystals by standard-four point method, whereas the in-plane anisotropy ρ_b/ρ_c was investigated on thin extended platelets in Ref. [147,145][5] by use of *Montgomery* method [390]. While the in-plane anisotropy was found to be only in the order of unity in the whole temperature range (300K - 10K), $\rho_{a^*}/\rho_{(b,c)}$ was found to reach high values, even up to 10^3. Figure 5.1 shows more recent anisotropy measurements [391].

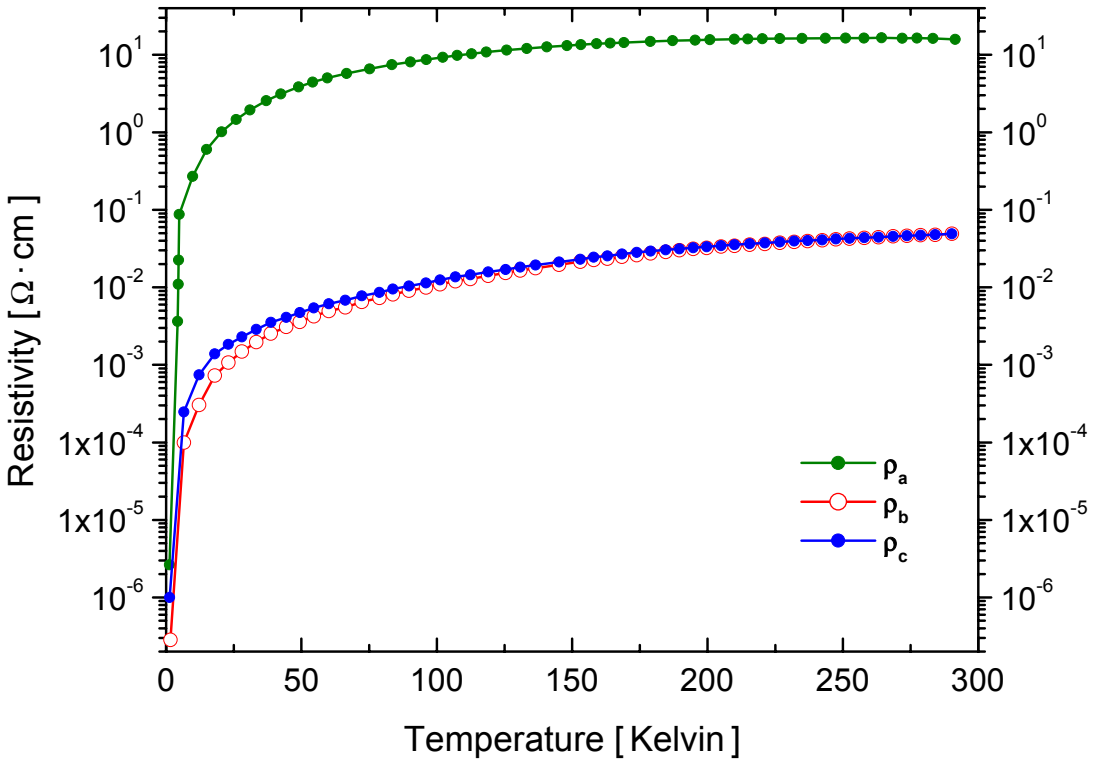

Fig. 5.1: Anisotropy of the resistivity of κ-(BEDT-TTF)$_2$I$_3$ single crystals [391].

[5] Please consider that the space group P2$_1$/a used in these references.

The interplane anisotropy is in accordance with the values reported in Ref. [143]. It indicates the pronounced two-dimensionality of the electronic system. However the value $\rho_{a^*}/\rho_{(b,c)}$ itself is not very suited to quantify the anisotropy exactly, since impurities and crystal defects may influence both, the interplane as well as the in-plane resistivities.
The pronounced quasi-twodimensionality indicated not only by the anisotropy of resistivity, but also by crystal and band structure calculations [143,387] was a strong motivation to quantify the two-dimensionality by more sensitive methods (see Sec. 5.2.2) and to investigate possible influences of two-dimensionality onto electronic properties of this material.

Thermopower Experiments at Zero Magnetic Field

Thermopower experiments at zero magnetic field were carried out by use of a slightly revised version of setup as proposed in Ref. [392]. The temperature range between 300K and 4.5K was covered by use of a ^{4}He flow cryostat. The results are plotted in Fig. 5.2 (see [145].

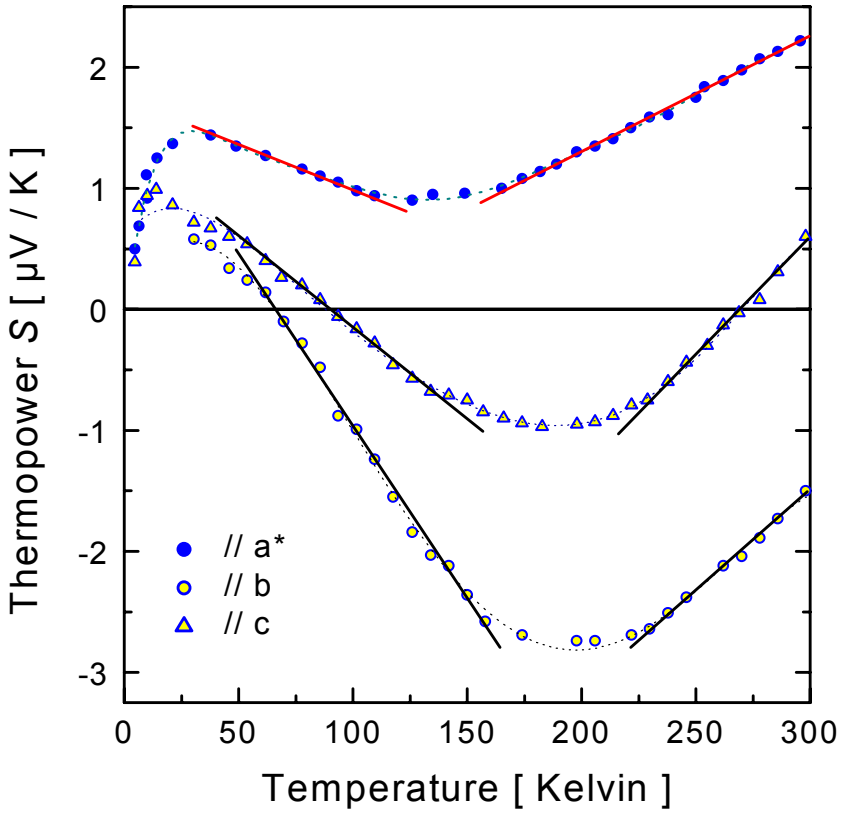

Fig. 5.2: Temperature dependence of the thermopower S of κ-(BEDT-TTF)$_2$I$_3$ single crystals along the different crystal axes. The direction a^* is oriented perpendicular to the 2D conducting planes ([145], where, however, the space group P2$_1$/a was used).

It is a matter of fact that a linearity of the thermopower $S(T)$ is characteristic for normal metallic behaviour. This means that κ-(BEDT-TTF)$_2$I$_3$ single crystals show metallic behaviour not only within the 2D conducting planes, but also perpendicular to them, i.e., along a^*. By the measurements plotted in Fig. 5.2 thermopower proves its well-known high sensitivity for phase transitions. $S(T)$ shows clearly the metal-metal phase transition by a change of the slopes of different linear $S(T)$ regions. Moreover, $S(T)$ reveals that this phase

transition occurs crystal axis dependent at temperatures between about 150K and 200K. These results are in good agreement with the phase transition proposed later on the basis of structure investigations at 295K, 150K and 10K, respectively ([387], see above).
It should be mentioned that the detected thermopower values are fairly low along each crystal axis and over the entire temperature range 300K > T > 4.5K. Below about 20K $S(T)$ tends to zero, the value expected for a superconductor.

Superconducting Properties

κ-(BEDT-TTF)$_2$I$_3$ is a strong type-II superconductor, as all organic metals to date. It was already mentioned that the superconducting transition occurs in resistivity typically at 4K (where resistivity vanishes) with an onset at about 4.2K [145], however in some cases even exceeding 5K. In AC-susceptibility the transition is observed at about 3.9K (see Fig. 5.3).

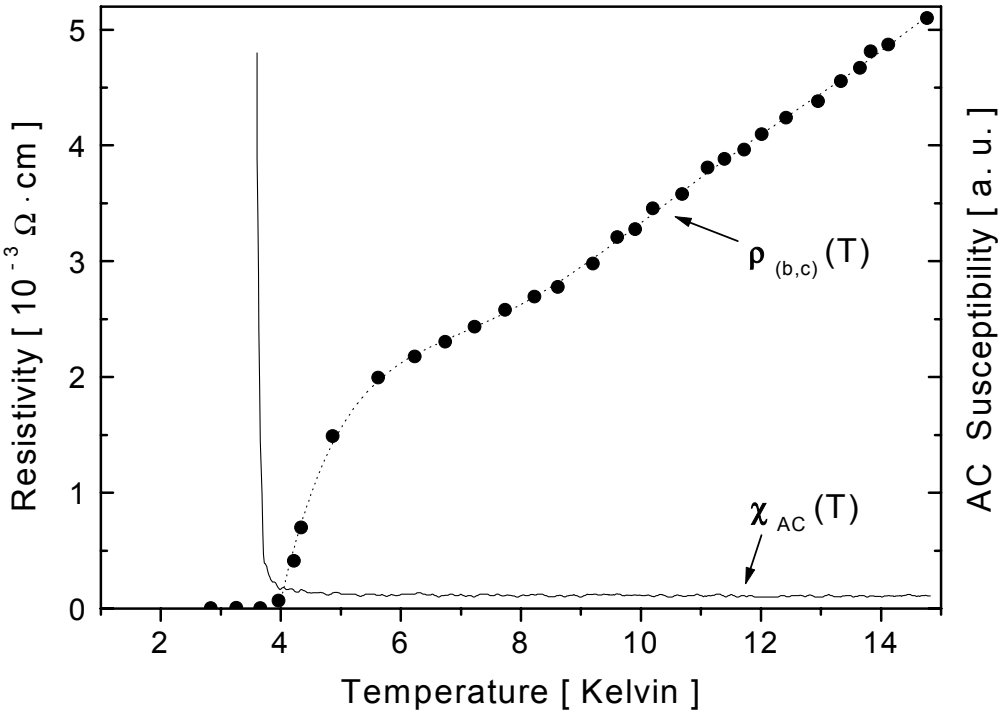

Fig. 5.3: Superconducting transition of κ-(BEDT-TTF)$_2$I$_3$ single crystals, as observed in resistivity ($\rho_{(b,c)}$) and AC-susceptibility (χ_{AC}).

The very sharp transition in AC-susceptibility shows that superconductivity spreads to the bulk within a very narrow temperature range, thus reflecting the very high crystal quality.
The superconducting and mixed-state properties of crystals from the syntheses described above were investigated in detail and are reported in Ref. [59]. Some of the results are shown in Tab. 5.2 and compared with those of other groups.

κ-(BEDT-TTF)$_2$I$_3$	B_{c1} [T]	$B_{c,th}$ [T]	B_{c2} [T]	ξ [nm]	λ [nm]	κ	Ref.
// (b,c) plane	$5 * 10^{-5}$	$7 * 10^{-3}$	7 6,8	41 35,9	70.000	675	[59] [143]
⊥ (b,c) plane	$4 * 10^{-3}$	$2 * 10^{-3}$	0,2 0,256	1,1 1,35	300	7	[59] [143]
anisotropy	$\frac{B_{c1,//}}{B_{c1,\perp}}$		$\frac{B_{c2,\perp}}{B_{c2,//}}$				
	$\approx 1{,}25 * 10^{-2}$		$\approx 2{,}86 * 10^{-2}$				[59]

Tab. 5.2: Extrapolated and calculated superconducting parameters for κ-(BEDT-TTF)$_2$I$_3$ with lower, thermodynamic and upper critical fields B_{c1}, $B_{c,th}$ and B_{c2}, respectively. ξ are the Ginzburg-Landau coherence lengths, λ the London penetration depths, and κ the Ginzburg-Landau parameters as obtained from $B_{c1}/B_{c2} = \ln\kappa/2\kappa^2$. The results reported in [59] were obtained by magnetisation, AC-susceptibility and specific heat measurements, whereas those from [143] were obtained from the half values of onset resistivities.

The difference between B_{c1} and B_{c2}, which results in a large Ginzburg-Landau parameter κ, shows that the material is a strong type-II superconductor. The coherence length $\xi_\perp$ perpendicular to the conducting planes is found to be less than the interlayer spacing. This is typical for organic superconductors and results in enhanced fluctuation effects, as observed, e.g., in Ref. [393]. In the wide mixed-state region flux pinning effects are expected to be rather weak in these very pure materials, whereas flux-flow and irreversibility effects are found to play an important role, as reported in [59].
It should be emphasized that from the very low ratios of $B_{c1,//}/B_{c1,\perp}$ and $B_{c2,\perp}/B_{c2,//}$ compared to other organic superconductors it was concluded in Ref. [59] that the superconducting properties of κ-(BEDT-TTF)$_2$I$_3$ show extreme two-dimensionality.
It is noted, that the nature of the superconducting state of these organic materials is still far from being understood. The continuous debate on conventional BCS-type or a more exotic mechanism is supported by a number of ambiguous or in some cases even contradictory experimental results (see, e.g., [37,25]). However, since the present work is dedicated to the complex *normal* state behaviour of organic metals, the detailed discussion on this point cannot be quoted here.

5.2 Fermiological Studies on κ-(BEDT-TTF)$_2$I$_3$ by Quantum Oscillation Experiments

It was already mentioned, that transport experiments as well as preceding band structure calculations gave hints to a pronounced two-dimensionality of the electronic system of κ-(BEDT-TTF)$_2$I$_3$. This motivated at first to detailed investigations of its Fermi surface by quantum oscillation experiments, followed by the search for influences of the pronounced two-dimensionality onto QOs (see Secs. 3.4.3 ff.). However from the obtained results it turned out that further, even more drastic effects of two-dimensionality have to be considered. The results are discussed in the following sections.

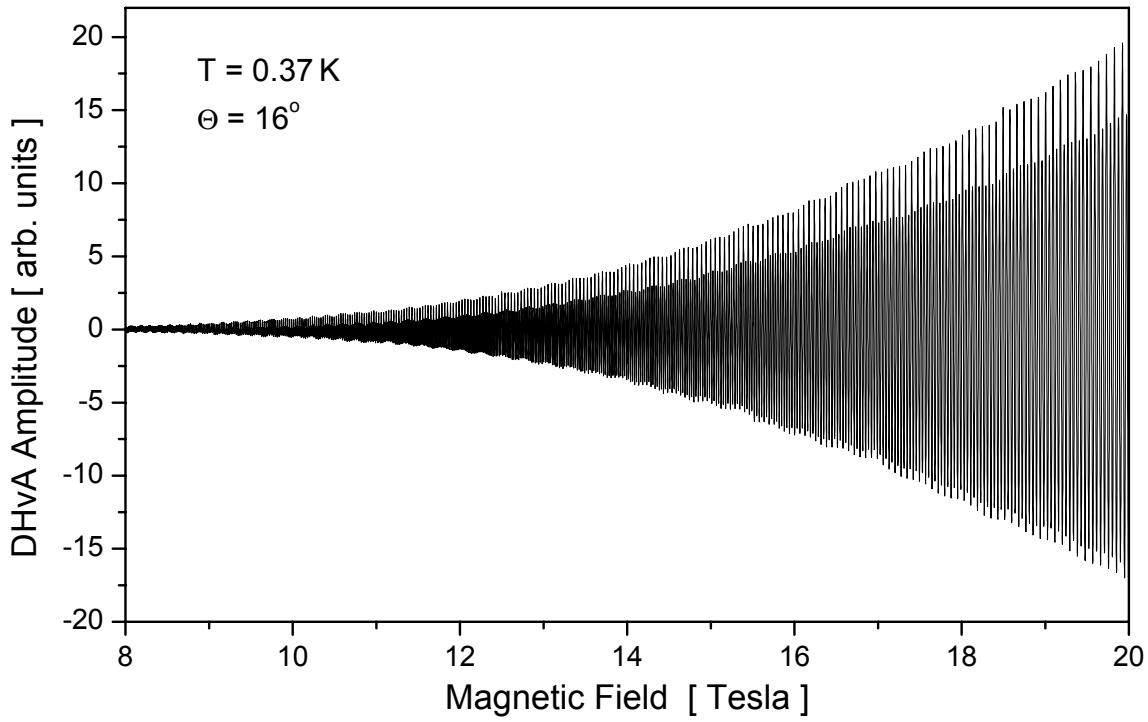

Fig. 5.4: De Haas-van Alphen torque signal (raw data) of κ-(BEDT-TTF)$_2$I$_3$ detected at Θ = 16° at 0.37K. A high frequency oscillation (denoted as F_3 in the following) is observed with a strong field dependence (the double-peak structure of the F_3 oscillations is caused by spin splitting). In the envelope of the signal a lower frequency oscillation can be recognized, called F_2 subsequently.

Fig. 5.5: Typical Shubnikov-de Haas signal (raw data) of κ-(BEDT-TTF)$_2$I$_3$ obtained at Θ = 0° at 30mK showing both, the F_2 as well as the F_3 oscillations.

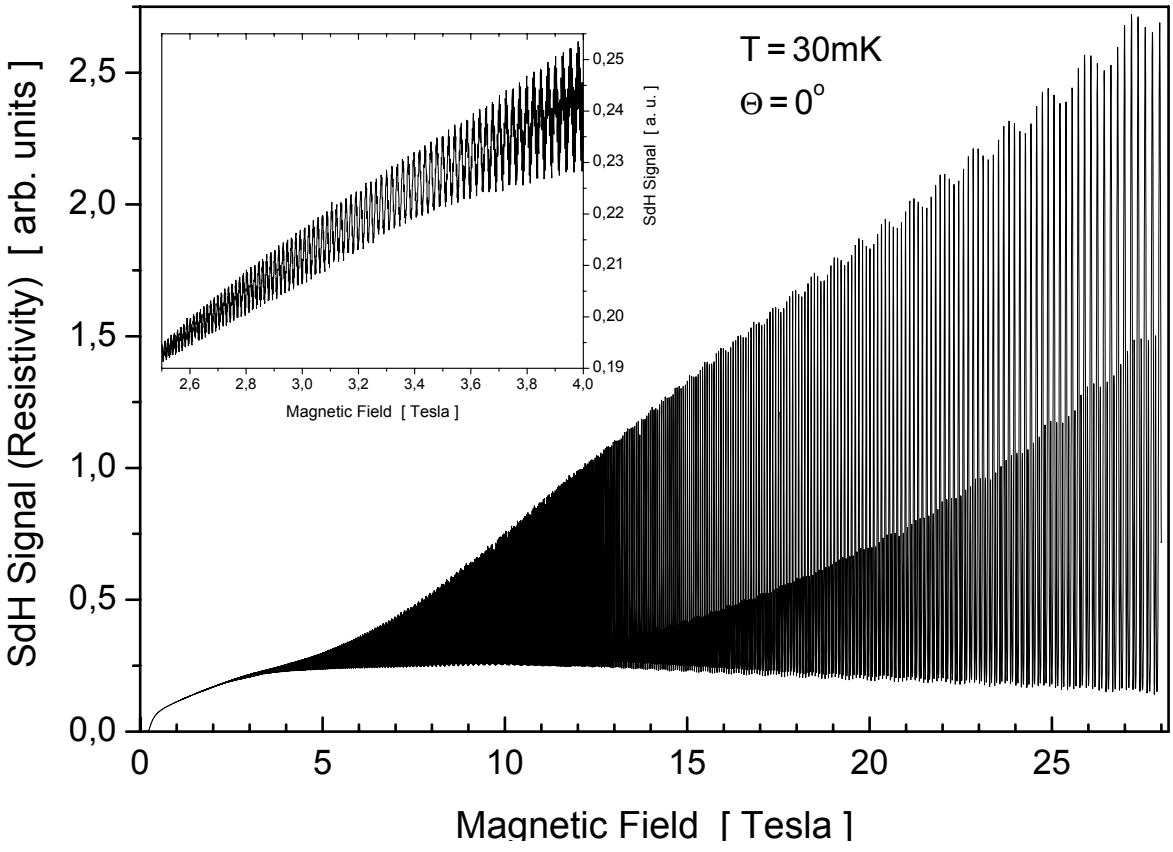

Quantum oscillations on κ-(BEDT-TTF)$_2$I$_3$ were first detected by dHvA technique above 8T [394]. In parallel, dHvA as well as SdH measurements were carried out as a starting point for the experiments collected here [395].
Figure 5.4 shows a dHvA torque signal detected at 0.37K and a tilt angle Θ between the magnetic field and the normal to the conducting (b,c) planes of 16°. In Figure 5.5 a typical SdH signal at Θ = 0° and T = 30mK is plotted. At 30mK SdH oscillations are observed above 0.8T at this angle, whereas at 0.4K they arise above 1.25T. At high fields the oscillatory part of the signal reaches even 90% of the background signal[6], which reflects the very good sample quality.

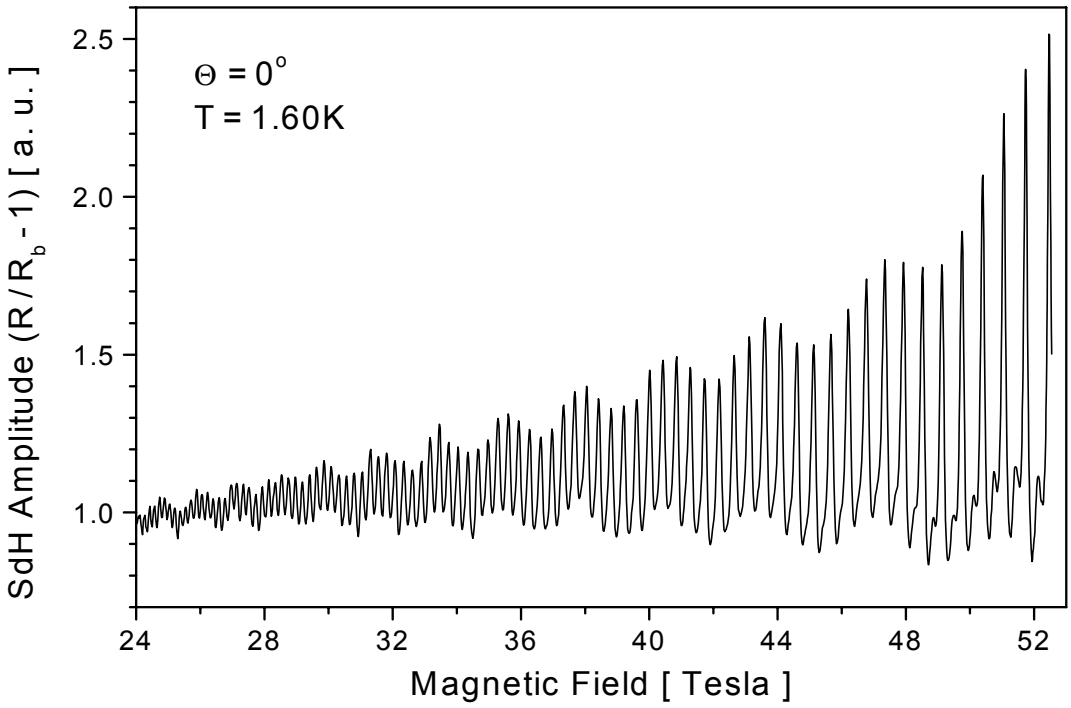

Fig. 5.6: SdH signal of κ-(BEDT-TTF)$_2$I$_3$ at Θ = 0° and 1.6K. The oscillation amplitudes of both, F_2 and F_3 increase steadily with field.

Figure 5.6 shows a SdH signal of κ-(BEDT-TTF)$_2$I$_3$ at Θ = 0° and 1.6K [396]. Both frequencies F_2 as well as F_3 are observed. It is noteworthy that their amplitudes increase continuously with field without indication of any beating node or saturation. This will be of special interest for the quantification of the anisotropy of the system (discussed in detail in Sec. 5.2.2).

A fast Fourier transform (FFT) of SdH signals is shown in Fig. 5.7. The prominent QO frequencies in the FFT are F_2 = 571T and F_3 = 3883T as well as their harmonics $n*F_j$. It should be noted that even $13*F_3$ is observed at high Fields. A rich harmonic content of the QOs is indeed expected in a 2DES (see Sec. 3.3), however it can only be observed when sufficiently high crystal quality is given.

[6] The ratio was estimated in conductivity in order to avoid possible artefacts in the background curve due to the low resistivity values.

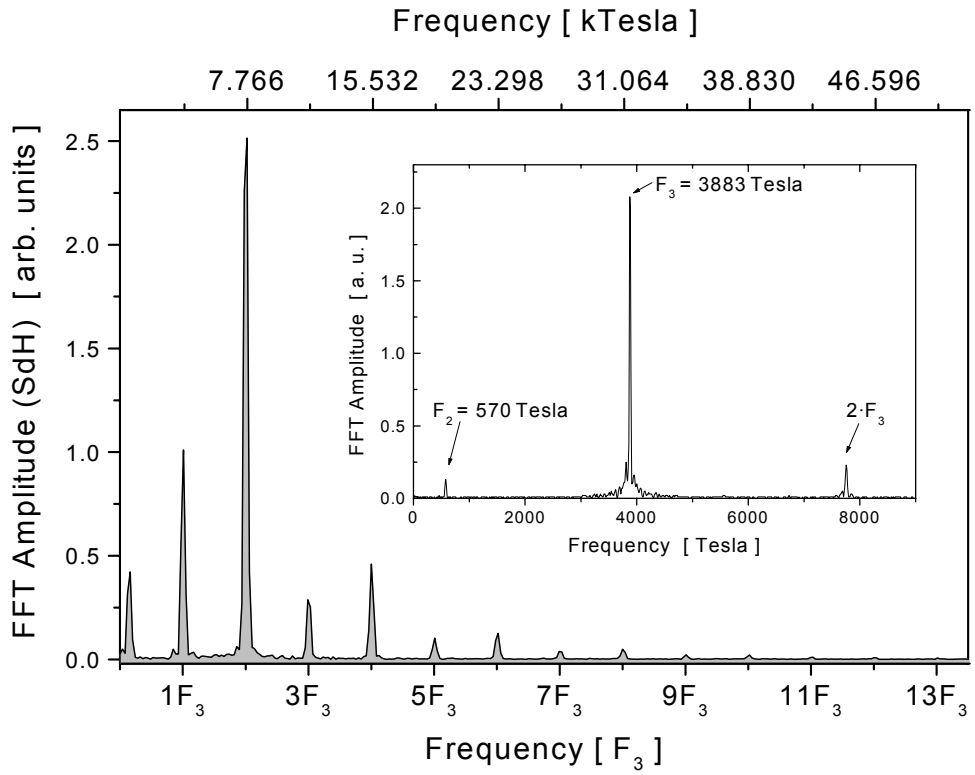

Fig. 5.7: Fast Fourier transforms (FFT) of SdH signals detected at 0.37K and Θ = 0°. The FFT in the inset is performed at an effective field B_{eff} = 8T, whereas the FFT in the main part is obtained at B_{eff} = 25T. The *x*-axis in the main figure is scaled to the value of the frequency F_3 = 3883T in order to illustrate the high harmonic content of the signal.

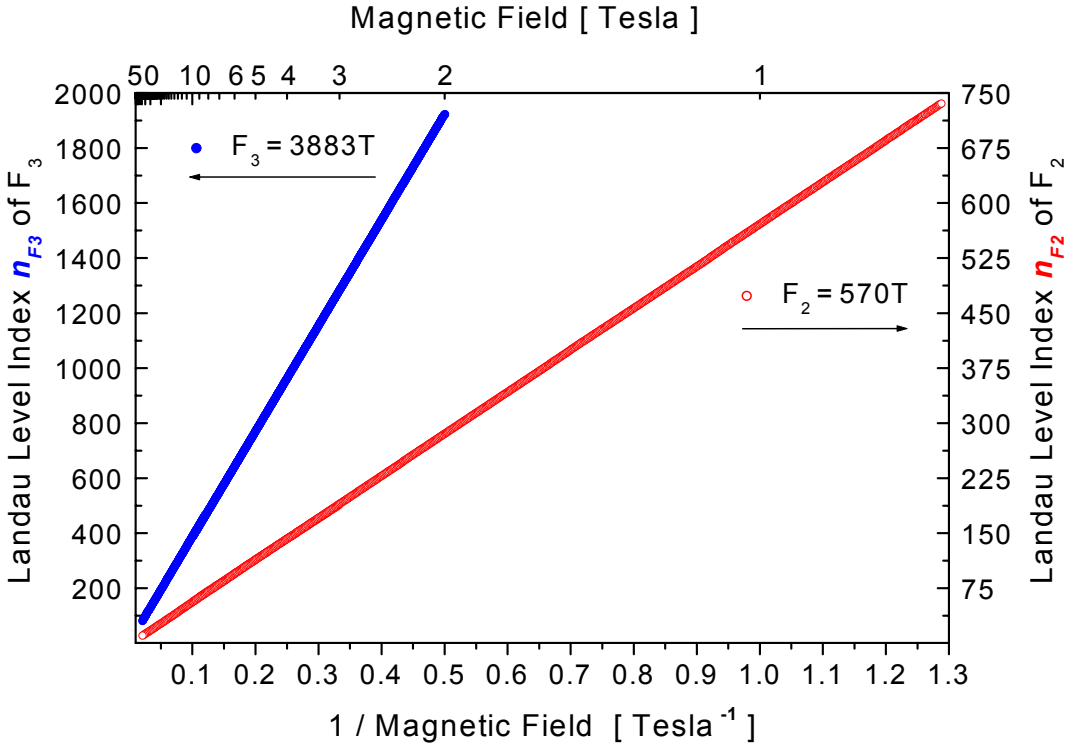

Fig. 5.8: Plot of the Landau level indices n_{F2} of F_2 and n_{F3} of F_3 for κ-(BEDT-TTF)$_2$I$_3$ versus 1/*B*. Every single circle represents the position of a Landau level.

Figure 5.8 shows a plot of the Landau level indices n_{Fj} of both QO frequencies F_j versus $1/B$. The values of n_{Fj} can be determined very precisely (with δn_{Fj} about ±1) by substituting the right part of Eq. (3.5) by Eqs. (3.4) and (3.7). From the slopes of the plots the exact values of the corresponding frequencies F_2 = 570T and F_3 = 3883T can be obtained according to Eq. (3.18) with a very high accuracy (±1T)[7] (see also [397,398,399]. Before discussing these frequencies it should be emphasized that Fig. 5.8 contains further important information. According to Eqs. (3.5) and (3.18) QOs should be equidistant in $1/B$ where B is the real internal magnetic field acting on the electrons. If the internal field corresponds indeed to the applied magnetic field, then a plot of the LLs vs. $1/B$ has to be *linear*. This is in fact the case in Fig. 5.8 even up to 52T and means that the steady magnetisation of the sample is negligible. This is in perfect accordance with the absence of any steady background in the raw dHvA torque signal plotted in Fig. 5.4.

From the obtained QO frequencies F_j the corresponding extremal closed areas A_j in k-space were determined by Eq. (3.7) and the results were compared to those obtained by band structure calculations. Figure 5.9 shows the band structure according to tight binding calculations reported in [143,387].

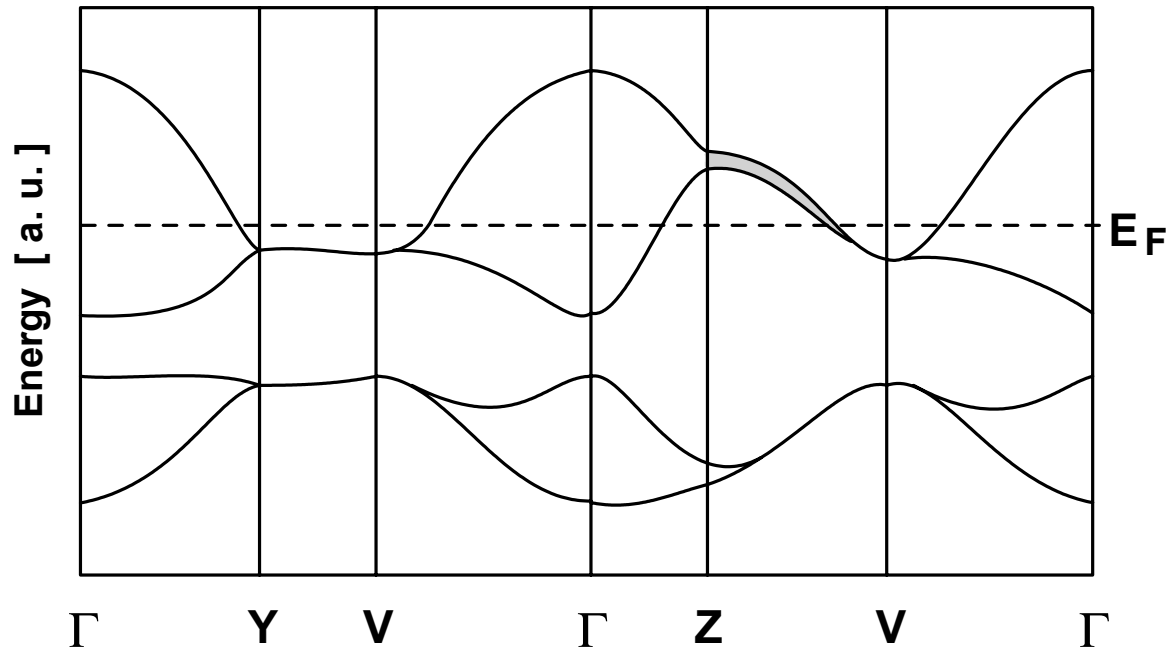

Fig. 5.9: Band structure of κ-(BEDT-TTF)$_2$I$_3$ as obtained by tight binding calculations in Refs. [143,387]. At 10K the degeneration of two bands between Z and V is lifted and a gap opens (shaded area). E_F represents the Fermi energy.

At room temperature the two bands between Z and V are degenerate due to the P2$_1$/c symmetry. At 10K this degeneration is lifted and a gap opens (grey shaded area). In κ-(BEDT-TTF)$_2$I$_3$ this gap is very narrow compared to related κ-structured organic metals

[7] It should be mentioned that experiments on crystals of different batches show quite different QO frequencies, exceeding by far the linewidth of the corresponding FFT peak (e.g., for F_3 values between 3811T and 3963T are found on samples from different batches). This peculiarity is typical for organic metals and may be attributed to slight variations in structural details. In the following, error bars of QO frequency values are skipped, since they are of minor interest in the context.

(see, e.g., [387]). A cut of the band structure at the Fermi energy E_F shows the trajectories in k-space on the Fermi surface (see Fig. 5.10, according to [143,387]). For these κ-phase materials the FS is expected to consist of two extremal areas. One of them is a closed lens-shaped orbit around Z which encircles the extremal area A_2 and corresponds to the QO frequency with F_2 = 570T. The second one, a circular orbit covering A_3 corresponds to F_3 = 3883T and is only closed as the gap between V and Z is overcome by the magnetic breakdown (MB, see Sec. 3.4.2) at sufficiently high magnetic fields.

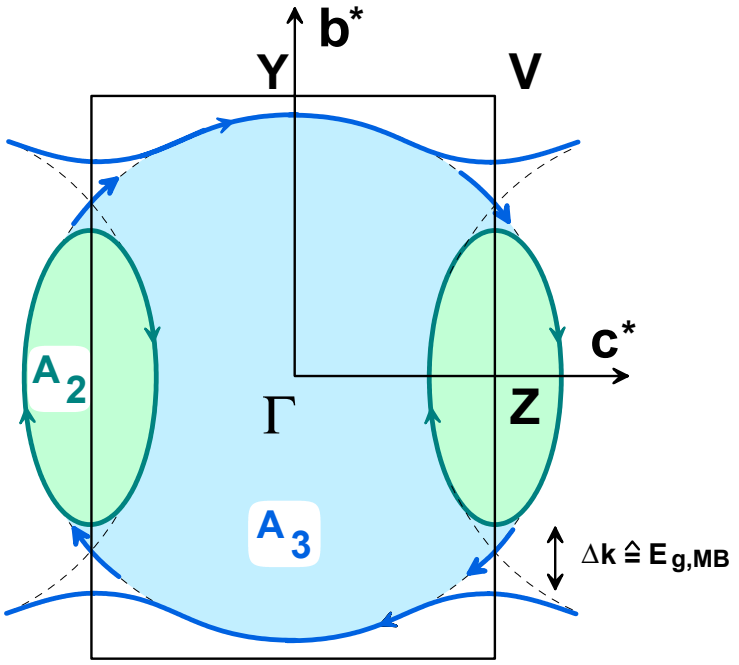

Fig. 5.10: Fermi surface of κ-(BEDT-TTF)$_2$I$_3$ according to [143,387]. The closed orbit encircling A_2 corresponds to the QO frequency with F_2 = 570T, whereas the circular orbit covering A_3 is only closed as the gap between V and Z is overcome by MB. A_3 corresponds to F_3 = 3883T.

In later SdH experiments in pulsed fields a further QO frequency of about 100T was detected [146,400,401][8]. The presence of a frequency F_1 is not indicated in band structure calculations. However this is not surprising, since not all structural details can be considered in such calculations[9]. Possible realisations of F_1 are discussed in [146,402], however the origin of F_1 could not yet be clarified.

From the values of the QO frequencies a set of fermiological data on κ-(BEDT-TTF)$_2$I$_3$ can be derived (see Tab. 5.3). These are the corresponding extremal areas A_j of the orbits in k-space (as obtained by help of Eq. (3.7)), the average Fermi wave vectors $\boldsymbol{k}_{F,j}$ for the successive orbits, as obtained by the simple relation $A_j = \pi(\boldsymbol{k}_{F,j})^2$, as well as the part of the first Brillouin zone (FBZ) which is covered by an orbit.

[8] The frequency F_1 was not further investigated in detail, since it was found to play no special role in the context of the influences of two-dimensionality reported here. Therefore F_1 occurs in the following discussion, if at all, only for completeness.

[9] Usually in band structure calculations structural details as, e.g., the position of CH_2 end groups on the BEDT-TTF molecules at low temperatures, etc. cannot be completely considered. Furthermore, the calculations are simplified by symmetry considerations, so that the calculated topology of a FS has a finite resolution. Under such conditions especially *small* pockets on the FS might be disregarded.

κ-(BEDT-TTF)$_2$I$_3$	A_j [nm^{-2}]	$k_{F,j}$ [nm^{-1}]	**Part of the FBZ** [%]
F_3 = 3883T	37,0 36,3 *)	3,4 3,4 *)	100 100 *)
F_2 = 570T	5,44 5,08 *)	1,3 1,3 *)	14,7 14 *)
(F_1 = 100T)	(0,95)	(0,55)	(2,6)

Tab. 5.3: Fermiological data of κ-(BEDT-TTF)$_2$I$_3$ as obtained by quantum oscillation experiments, i.e., the values for the extremal areas A_j and the part which they represent on the first Brillouin zone and the average Fermi wave vectors $k_{F,j}$. Theoretical values*) at 10K taken from [387] are included for comparison.

It is notable that the data obtained by quantum oscillation experiments correspond very well with the theoretical data determined by band structure calculations based on the 10K structure [387].

5.2.1 Further Fermiological Properties of κ-(BEDT-TTF)$_2$I$_3$

Magnetic Breakdown

As already mentioned in Sec. 5.1 and discussed with Fig. 5.9, the band structure derived from the room temperature structure suggested that the two bands between the points Z and V in Fig. 5.9 are degenerate, so that the F_3 orbit around A_3 is completely closed without any gap. In contrast, 10K data (quoted in Figs. 5.9 and 5.10) show a gap between these orbits, which was estimated to be in the order of 20-30meV [387]. In first dHvA measurements on this material, the question on the existence of the gap could not be answered, since at 8T, where dHvA oscillations appeared, the high frequency oscillation was *already present*. Thus the magnetic breakdown field B_{MB} could not be estimated and therefore the gap (see Eqs. (3.24)-(3.26)) could not be determined. This field value of 8T, where F_3 is already present in the I_3 salt [395a], is considerably lower than $B_{MB} \approx 30$T observed on κ-(BEDT-TTF)$_2$Cu(NCS)$_2$ [403,198,404,199,201][10]. Therefrom it was suspected that the gap might be even completely closed in κ-(BEDT-TTF)$_2$I$_3$.
In preceding SdH experiments on κ-(BEDT-TTF)$_2$I$_3$ at 0.4K a magnetic breakdown field B_{MB} of about 2.5T was determined [146]. Therefrom a gap value $E_g \lessapprox 3.2$meV was estimated according to Eq. (3.24). In later SdH experiments at 20mK F_3 was observed already beginning from 2T (see plots of the LLs of F_3 in Fig. 5.8). From these results the gap can be redetermined as about

$$E_g \lessapprox 3\,\text{meV} \,. \tag{5.1}$$

This gap value is considerably higher than $k_B T \approx 1.7 * 10^{-3}$meV, which means that the magnetic breakdown itself does not contribute to the temperature dependence of the QO amplitudes of the involved QO frequencies F_2 and F_3, respectively.
The gap value in the present I_3 salt is also considerably lower than $E_g \approx$ 9-11meV[10] determined for κ-(BEDT-TTF)$_2$Cu(SCN)$_2$ and moreover the present gap is by about one order of magnitude lower than the value of 20-30meV proposed by band structure calculations for the 10K structure [387]. In consequence this means that in κ-(BEDT-TTF)$_2$I$_3$ the shape of the large orbit enclosing A_3 is closest to an ideal circle, which ensures a nearly isotropic carrier motion within the 2D (b,c) conducting planes. This is an important condition for strongly 2D electronic properties.

Electron *g*-Values, Dingle Temperatures T_D and Carrier Scattering Times τ

The electron *g*-value for the carriers contributing to F_3 was first determined by dHvA measurements at 11T and reported in Ref. [395a]. As usual within QO experiments, *g* was extracted from the spin damping factor R_s of the LK Formula (Eq. (3.17)), which allows to deduce a value for $g_* m^*$ from the angular positions of so-called spin zeros [87]. Thus, from 5 observed spin zeros $g_{F3*} m_{F3}^* = 8.63$ was ascertained and with the known carrier effective mass $m_{F3}^* = 3.8$ (see Sec. 5.3) a value of $g_{F3} = 2.27$ was obtained for the F_3 orbit [395a]. This value for $g_{F3*} m_{F3}^*$ was confirmed by the observation of 12 spin zeros in dHvA experiments at 12T as [405] well as by SdH measurements at 22.5T[11] [399]. The interpretation of the $g_* m^*$ in the class of organic CT salts is controversial. Some groups assume a renormalisation of m^* by electron-phonon interaction [406,407,393], whereas other groups (e.g., [200,408,409]) assume that electron-electron interaction may renormalise *g* with respect to the $g_{F3} \approx 2$ value measured by electron spin resonance.
It should be noted that in the present material κ-(BEDT-TTF)$_2$I$_3$ up to now no spin zero could be detected for the QO frequency F_2 within an angular range $-70° \leq \Theta \leq +70°$. This suggests that g_{F2} may deviate considerably from $g \approx 2$.

It was described in Sec. 3.2.3, that the so-called Dingle temperature T_D is connected with the carrier relaxation time τ by Eq. (3.14) and a low T_D is therefore an indication as well as quantification for high crystal quality. In organic metals Dingle temperatures vary usually between 0.5K and about 3K (for an overview see, e.g., [83]). In ordinary metals finite Dingle temperatures generated by impurity scattering are of the order 10-100K per atomic % of impurities [87]. Usually T_D is obtained by the so-called Dingle plot, i.e., a plot of the implicit FFT amplitudes of QOs with a certain frequency F_j versus $1/B$ (see Eq. 3.15). For a number of organic metals reasonable T_D values are obtained by this procedure provided that system specific details as, e.g., magnetic break down, are considered. This shows that even in its standard 3D formulation the LK theory (Secs. 3.1-3.2) can be widely used to describe the field dependence of the QO amplitudes in quasi-2D organic metals.
It was however shown in [410] that under certain experimental conditions this standard procedure for the Dingle temperature determination cannot be used for the present material κ-(BEDT-TTF)$_2$I$_3$ due to the strong two-dimensionality of the material (see also Sec. 5.3). Instead, T_D was obtained in [410] via τ according to a method proposed in [164]. By this at

[10] Considerably different MB fields and therefore gap values of roughly 10meV are determined by different groups.

[11] The verification of $g_{F3*} m_{F3}^*$ at different fields will be of special importance for the discussion in Sec. 5.3.1.

least a lower limit of $\tau_{F3} > 10$ps was obtained for the carriers on the F_3 orbit, which corresponds to a $T_D < 0.12$K. In order to verify this result, τ and therefrom T_D are redetermined here by the simple condition that

$$\omega_{c,Fj} * \tau_{Fj} > 1. \tag{5.2}$$

This condition means that at the field where QOs with F_j may arise, a closed coherent electron motion must encircle at least one complete cyclotron orbit. In reverse, from the field where F_j arises, a lower limit for τ_{Fj} and in turn $T_{D,Fj}$ can be estimated for the successive QO frequencies F_2 and F_3. The results obtained from the observation of F_2 above 0.8T and F_3 above 2T the following values for τ and T_D are obtained (see Tab. 5.4).

κ-(BEDT-TTF)$_2$I$_3$	τ [ps]	T_D [K]	v_F [m/s]	λ [μm]
F_3 = 3883T (disreg. MB) F_3, considering MB	> 11 ≥ 28	< 0,11 ≤ 0,04	$1*10^5$	> 1,1 ≥ 2,8
F_2 = 570T	> 13	< 0,08	$8*10^4$	> 1

Tab. 5.4: A selection of fermiological data for κ-(BEDT-TTF)$_2$I$_3$: Lower limits for the carrier scattering times τ and the mean free paths λ, upper limits for T_D as well as Fermi velocities for the carriers contributing to F_2 and F_3, respectively.

It should be noted that finite temperature is not considered in Eq. (5.2). In consequence, τ_{Fj} may be markedly higher and $T_{D,Fj}$ considerably lower than the obtained values. Furthermore magnetic breakdown (MB) is likewise not considered in Eq. (5.2). This means that for F_3 the bare condition (5.2) may be fulfilled already at considerably lower fields, but only enhanced to 2T by the finite energy gap (see Fig. 5.10), which prevent the electrons from closing the orbit around A_3. This means that τ_{F3} may be even much higher and $T_{D,F3}$ even much lower than estimated here. Finally it has to be considered that the τ values in Tab. 5.4 were determined from interplane SdH experiments[12] so that the carrier motion contains an interplane component. In the pure intraplane direction however, τ_{F3} is expected to be considerably higher owing to the fact that scattering is minimised within the highly conducting planes.

At first, the estimations performed here on the simple, but fundamental condition (5.2) confirm the preceding data. They show that crystals of κ-(BEDT-TTF)$_2$I$_3$ can be grown very pure.

From the known Fermi wave vectors k_F given in Tab. 5.3 the corresponding Fermi velocities $v_{F,Fj}$ can be obtained via the quantisation of momentum $p = \hbar k_F = m^* v_F$ and with τ_{Fj} the mean free paths λ are found for the carriers on each of the orbits. The results are added to Tab. 5.4.

Finally, if desired, the effect of MB can be at least roughly considered by the argument, that the carriers move already coherently along an orbit corresponding to the full length of the F_3 orbit, as soon as a combination frequency of F_2 and F_3 arises. This is the case above 0.8T at 20mK. Therefrom the values τ, T_D and λ for F_3 are included in Tab. 5.4 for completeness.

[12] For an estimation of τ by Eq. (5.2) interplane measurements are favourable since the higher signal-to-noise ratio allows to extend the verification of Eq. (5.2) down to lower fields.

5.2.2 Quantification of the Two-Dimensionality

It was already mentioned in the preceding, structural aspects as well as a number of experiments hint to the strong two-dimensionality of the electronic system of the organic metal κ-(BEDT-TTF)$_2$I$_3$. They are collected here for an overview. In addition, the quantification of the two-dimensionality is given in terms of the ratio of transfer integrals perpendicular and parallel to the conducting (b,c) planes respectively, i.e., $t_\perp/t_{//}$. The following arguments identify κ-(BEDT-TTF)$_2$I$_3$ as a strongly 2DES:

1) Structure and band structure calculations with a high in-plane symmetry and an almost circular orbit (nearly vanishing gap) within the (k_b,k_c) plane (see Fig. 5.10).

2) A Strong interplane/in-plane anisotropy versus almost perfect in-plane isotropy of resistivity (see Fig. 5.2).

3) A Strong oscillatory content $\Delta\sigma/\sigma \approx 90\%$ of SdH oscillations in high fields (see Fig. 5.5) and a rich harmonic content.

4) The angular dependence of the QO frequency F_3 [395a,399], which follows up to at least $\Theta = 68°$ the $1/\cos(\Theta)$ law expected for the cylindrical FS of a 2D metal (see Fig. 3.5b).
The same $1/\cos(\Theta)$ dependence is found for the effective mass $m^*_{F3}(\Theta)$ at low fields (see [411,402] and Sec. 5.3). A statement on the two-dimensionality would require the verification of the $1/\cos(\Theta)$-law of F_j or m^* up to angles closest possible to 90°, but unfortunately QOs disappeared above 68° in the experiments at 0.4K.

All these aspects are clear indications for the two-dimensionality of the system, but not very suited to *quantify* the 2D character (the reasons for this are already discussed partly Sec. 5.1). The following experiments are much more suitable for this purpose.

5) The anisotropy of B_{c1} and B_{c2} reported in Ref. [59] allows experiments up to $\Theta = 90°$. The results reproduced in Fig. 5.11 show the angular dependence of B_{c2}. The main part of the figure shows the observed B_{c2} values at different temperatures. The inset shows that the data around the crucial angle $\Theta = 90°$ (i.e., $\boldsymbol{B}$ // to the conducting planes) deviate significantly from the fit according to the 3D anisotropic Ginzburg-Landau formula

$$1 = \left(\frac{B_{c2}(\theta)\cos\theta}{B_{c2,\perp}}\right)^2 + \left(\frac{B_{c2}(\theta)\sin\theta}{B_{c2,//}}\right)^2, \tag{5.3}$$

which is represented by a dashed line. Instead, the data can be fitted perfectly by the so-called Tinkham formula for 2D superconducting thin films [412], which follows the equation

$$1 = \left|\frac{B_{c2}(\theta)\cos\theta}{B_{c2,\perp}}\right| + \left(\frac{B_{c2}(\theta)\sin\theta}{B_{c2,//}}\right)^2 \tag{5.4}$$

and is plotted as a solid line in Fig. 5.11. These results show that the organic superconductor κ-(BEDT-TTF)$_2$I$_3$ behaves almost as a 2D thin film but *not* as a bulk 3D system. From the results in Ref. [59] the ratio of transfer integrals can be estimated as $t_\perp/t_{//} \lesssim 5.3 * 10^{-4}$.

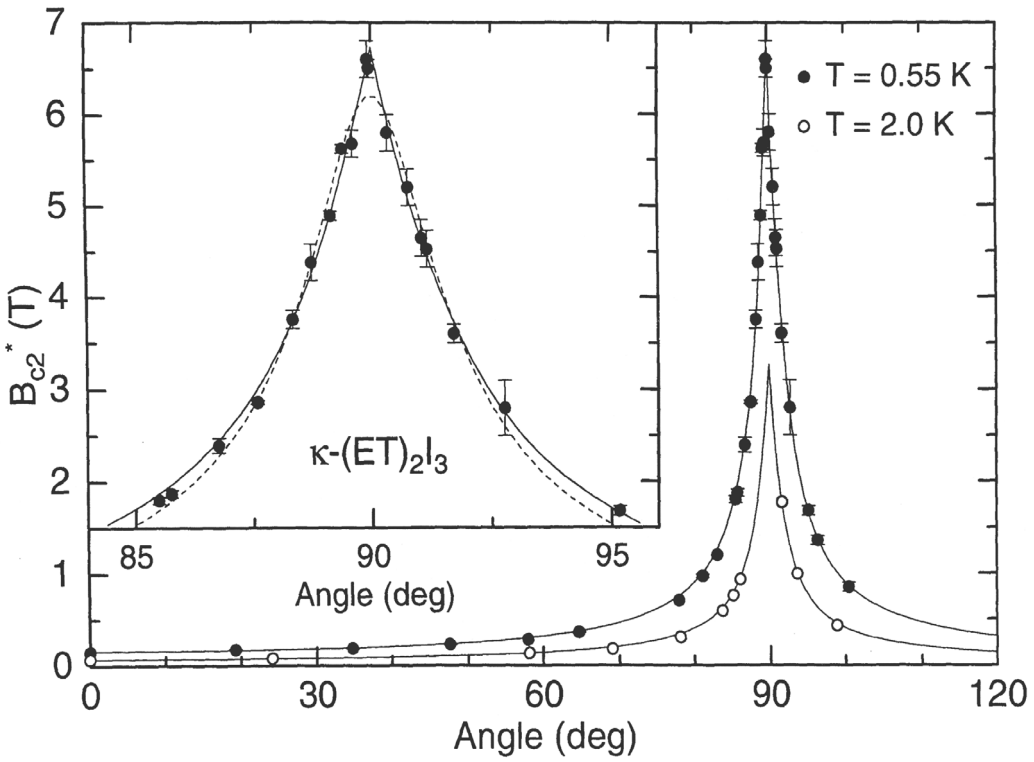

Fig. 5.11: Angular dependence of the upper critical field B_{c2} in crystals of the organic superconductor κ-(BEDT-TTF)$_2$I$_3$ according to Ref. [59] (B_{c2} was obtained by AC-susceptibility measurements; BEDT-TTF is abbreviated as 'ET'). Dashed lines in the **inset** represent a fit of the data according to the anisotropic Ginzburg-Landau model, whereas the full line shows the fit according the Tinkham formula for 2D thin films.

6) One favourable consequence of the very high crystal quality is the fact that QOs can be observed in κ-(BEDT-TTF)$_2$I$_3$ beginning from very low fields, i.e., in a wide field window. Owing to this the so-called warping (i.e., corrugation) of the Fermi surface can be estimated as described in Sec. 3.4.3 by the search for so-called *beating nodes* in the envelope of the QOs (see simulation in Fig. 3.6). From the estimated warping (i.e., $\delta F/F$) the ratio of transfer integrals $t_\perp/t_{//}$ as a measure for the electronic anisotropy can be obtained directly when beating nodes are indeed present. In cases where such nodes are absent, at least upper limits for $\delta F/F$ and $t_\perp/t_{//}$, respectively, can be estimated from the total field window covered by QO experiments (this was used in Ref. [146] for a first estimation of the warping).
As already mentioned, the QO frequency F_2 is observed at dilution temperatures already above 0.8T, while F_3 arises at about 1.13T. In the entire field region from this minimum field B_{min} up to the maximum field B_{max} = 52.5T, no beating nodes were observed in κ-(BEDT-TTF)$_2$I$_3$ [13] and even no saturation of the QO amplitudes is indicated at high fields. These facts illustrate that above 52.5T no further beating node may occur (conf. Fig. 3.6). This means that the last node must be located at fields below 1.13T and 0.8T, respectively. In such special cases the upper limit for the warping can be determined by the relation $\delta F = (3/4)B_{node}$ [14] if the last node is indeed observed at $B_{min}=B_{node}$. In the present case where $B_{\min} \geq B_{node}$, this relation is used as limiting condition

[13] In order to avoid needless repetition, the absence of beating nodes is illustrated later in Sec. 5.5, where field dependent QO measurements are discussed especially in connection with results of the two-dimensionality of the system.
[14] This relation can be easily derived from Eq. (3.9) by superposition of the contributions from two frequencies (F, $F+\delta F$) with the different phases $+\pi/4$ for a minimum and $-\pi/4$ for a maximum orbit.

$$\delta F \leq (3/4) B_{\min}\,, \tag{5.5}$$

which allows to estimate an upper limit for the beating frequency δF from the field B_{min} where QOs arise. From this an upper limit for the warping $\delta F/F = t_\perp/t_{//}$ is obtained and by considering that in a 2DES $t_{//} = E_F/4$, both transfer integrals can be determined.
At a first glance this would reveal $\delta F/F < 2.2{*}10^{-4}$ for the QO frequency F_3 itself. However it should be recalled that the minimum field at which F_3 arises is limited by both, the MB as well as the strong temperature dependence of the F_3 amplitudes. This complication can be overcome by considering the fundamental fact that all beating node positions B_{node} are prescribed solely by the QO frequency difference δF *itself*, but not by the involved QO frequency values F_j. This means that if, e.g, between 0.8T and 1.13T, a beating node is absent in the amplitudes of one of the frequencies (here F_2), it is also absent in those of the other QO frequencies (thus F_3), which 'contain' the corresponding orbit (i.e., A_2, see Fig. 5.10). From this general fact it can be deduced that above 0.8T no further node is present in the amplitudes of both, F_2 and F_3, so that according to Eq. (5.5) $\delta F \leq 0.6$T. The corresponding results for the upper limit the warping $\delta F/F$ and the anisotropy $t_\perp/t_{//}$ are given in Tab. 5.5.

	'warping' $\boldsymbol{\delta F/F}$	$\boldsymbol{t_\perp / t_{//}}$
κ-(BEDT-TTF)$_2$I$_3$	$< 1{,}5{*}10^{-4}$	$< 1{,}5{*}10^{-4}$

Tab. 5.5: Estimates for the two-dimensionality of the electronic system of κ-(BEDT-TTF)$_2$I$_3$ by values for the warping and the corresponding ratio of transfer integrals $t_\perp / t_{//}$ perpendicular an parallel to the conducting (b,c) planes. The results are obtained by quantum oscillation experiments.

It should be noted that both, finite temperature and the steep background magnetoresistance above the superconducting transition make the observation of QOs at low fields quite difficult, so that certainly $B_{\min} \geq B_{node}$. This asks to consider that the warping $\delta F/F$ may be may be even lower i.e., the two-dimensionality may be even more pronounced than estimated here.
By these results, κ-(BEDT-TTF)$_2$I$_3$ is identified as the to date strongest two-dimensional electronic system within the class of organic CT salts (see, e.g., [25,37,83] for comparison).

5.3 Strong Anomalies in the Quantum Oscillation Amplitudes at High Fields, Low Temperatures and $\boldsymbol{B} \perp$ (b,c) ≡ Θ = 0° as a Result of Two-Dimensionality

During the investigations of κ-(BEDT-TTF)$_2$I$_3$ single crystals by QO experiments it turned out that, regardless of the strong two-dimensionality of its electronic systems, the standard Lifshitz-Kosevich (LK) description for QOs in 3D metals (Eq. (3.9) ff.) applies very well in the entire field, temperature and angular range covered by the experiments. Minor deviations can be understood by considering oscillations of the chemical potential with the QO frequency F_3 (as reported in [91,215] and discussed in Sec. 5.3.1). However at high fields, low temperatures and the special field orientation $\boldsymbol{B} \perp$ (b,c), i.e., Θ = 0° strong deviations

from LK behaviour are observed, which manifest themselves as a dramatic reduction of the SdH amplitudes under these conditions. Since these damping effects influence (or may even prohibit) the estimation of the effecting mass m^*, they are illustrated concomitant to the discussion of m^* in the following.

Determination of the Carrier Effective Masses m^* by Quantum Oscillation Experiments

Within the scope of dHvA and SdH experiments underlying to this work, the effective masses m^*_{Fj} of the carriers contributing to F_2 and F_3, respectively, were estimated. The values for m^*_{Fj} were obtained by a fit of the temperature dependence of the FFT amplitudes[15] of F_j to the temperature damping factor R_T of the LK formula, as discussed with Eq. (3.10). The data obtained by this standard procedure are shown in Tab. 5.6. The m^*_{F3} value estimated by both, dHvA and SdH experiments is in agreement with data obtained by dHvA experiments at $\Theta = 0°$ and B = 11T reported in [395a]. From $m^*_{F3} = 3.90$ the value for the Fermi energy was determined by Eq. (3.2). The obtained $E_F = 0.114$eV corresponds very well to the value of 0.113eV calculated from structure data. For F_2 $m^*_{F2} = 1.90$ and a Fermi energy of 35meV was found.

These results show that dHvA and SdH experiments give access to very reasonable values for m^* and it shows in reverse that in general the standard 3D LK formalism applies very well for the description of QOs even in such 2DES.

κ-(BEDT-TTF)$_2$I$_3$	**m*** ($\Theta = 0°$) [m_e]	Fermi Energy **E_F** [eV]
F_3 = 3883T	3,90 3,80 *)	0,114 0,113 **)
F_2 = 570T	1,9	0,035

Tab. 5.6: Effective masses m^* of the carriers contributing to the F_2 and F_3 orbit, respectively (*) is the value from Ref. [395a]). The values obtained from dHvA and SdH experiments at different angles Θ were rescaled to $\Theta = 0°$ by the 1/cosΘ-law given for a 2D system. The Fermi energy values for the two corresponding bands are obtained from the frequency values and Landau level spacing (**) is E_F as obtained from structure data).

However, comparative dHvA and SdH studies of the temperature dependence of the QO amplitudes at various fields revealed decisive peculiarities, as shown in the following.

[15] It is noted, that for the SdH effect the QO amplitudes have to be rescaled by the non-oscillating background (see Eq. (3.22)). However this may generate artefacts, since the estimation of the background is not straightforward to carry out in a 2DES and is therefore a point of controversial discussion in the quasi-2D organics. However in the present material, the background is very weakly temperature dependent in the investigated temperature region. Therefore both, the rescaled SdH amplitudes just as those from the raw data, yield consistent results within the error bars plotted in Figs. 5.12 and 5.13.

Application and Limits of the Lifshitz-Kosevich Formula

For the present 2DES the application and the limits of the standard 3D description of QOs in metals can be best illustrated by the investigation of the *temperature* as well as the *field* dependence of the QO amplitudes (the latter is discussed in Secs. 5.4 ff.).
At first, investigations of the temperature dependence of the QO amplitudes (i.e., m^*) were performed by SdH and dHvA experiments under various experimental conditions and the results are discussed in the following. Figure 5.12 shows as an example the values for m_{F3}^* obtained by SdH and dHvA experiments at different fields and angles. First, SdH measurements were carried out at $\Theta = 0°$ between 8 and 10T and the data reported in Ref. [395a] were reproduced (see Tab. 5.6). Further m_{F3}^* determinations were continued to higher fields by SdH experiments at 0°, since the amplitudes were found to be maximal at this angle. Surprisingly, it turned out that the fit of the temperature dependence of the SdH amplitudes to the LK formula (Eq. (3.10) suggested a strong decrease of m_{F3}^* with increasing field (see lower curve of Fig. 5.12). This was interpreted as an indication for a field dependent m_{F3}^* [397].
Subsequent experiments focused on the invoked questions, whether **i)** m_{F3}^* is indeed field dependent or, whether **ii)** SdH experiments might be *on principle* not suited to determine m_{F3}^* (since they are transport experiments and might be afflicted by scattering) or, whether **iii)** this effect occurs only at $\Theta = 0°$.

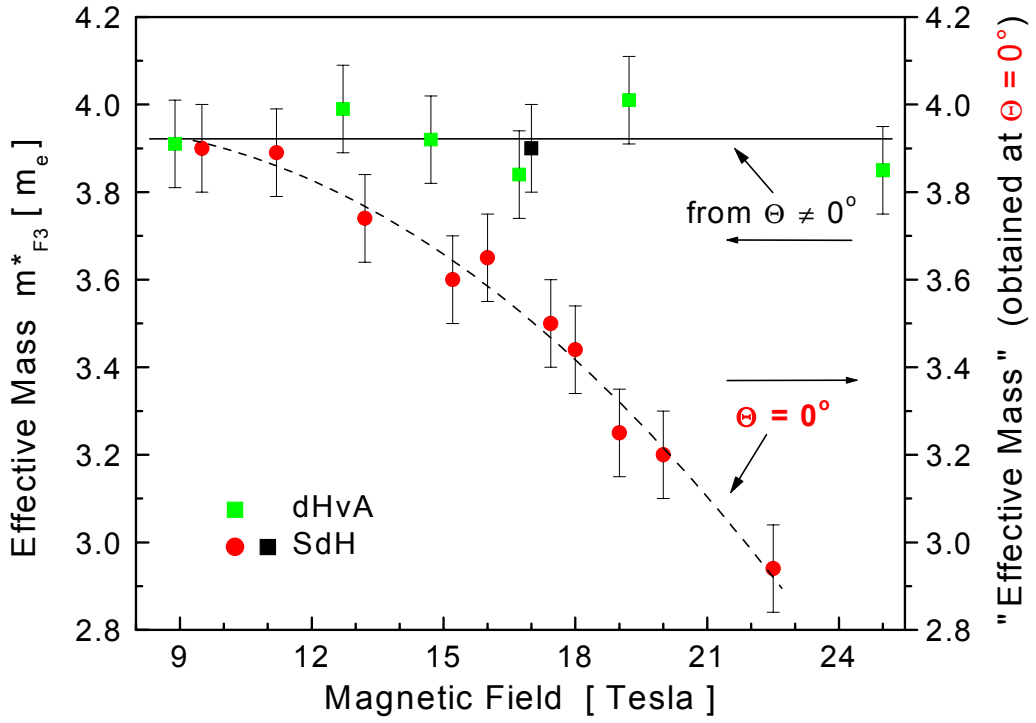

Fig. 5.12: Values for the carrier effective mass m_{F3}^* in κ-(BEDT-TTF)$_2$I$_3$. The filled circles represent estimates obtained by SdH experiments at $\Theta = 0°$. The green squares are results from dHvA experiments at various angles Θ. The black filled square is obtained by the set of angle-dependent SdH and dHvA measurements shown in Fig. 5.13. The m_{F3}^* values estimated at $\Theta \neq 0°$ are rescaled to 0° by the 1/cosΘ - law valid for 2D systems. The right *y*-axis illustrates the *apparent* decrease of m^* at 0° (the scale of the right *y*-axis is no real quantity, but is only applied to show the magnitude of the effect). For discussion see text.

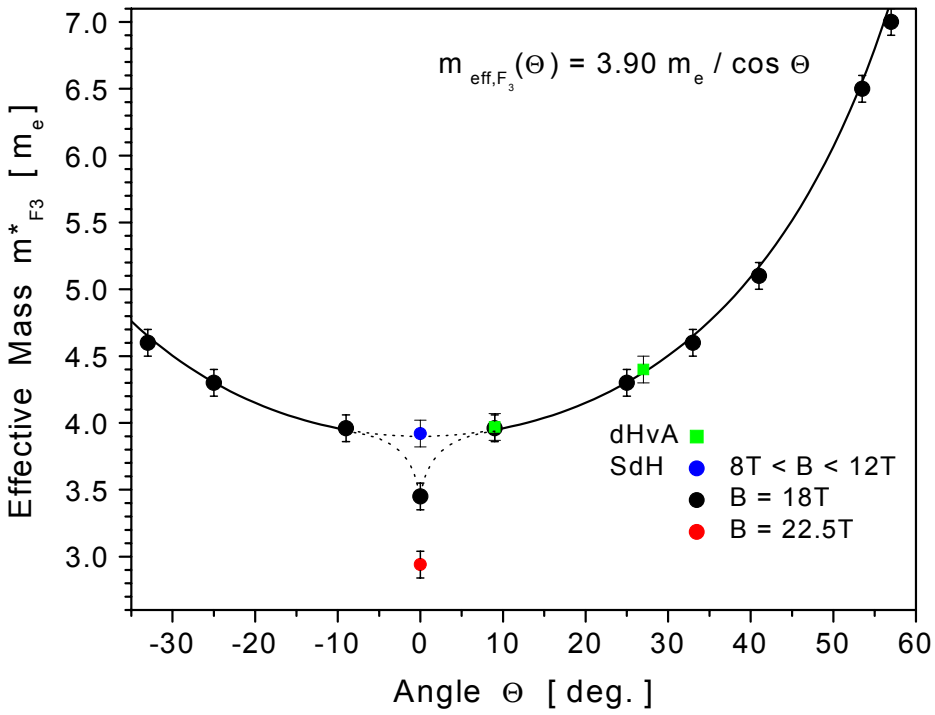

Fig. 5.13: The angular dependence of m_{F3}* in κ-(BEDT-TTF)$_2$I$_3$ is in perfect agreement with the 1/cosΘ - law (full curve) as expected for 2D systems. SdH and dHvA experiments show consistent results at $\Theta \neq 0°$ even at high fields.

Unfortunately dHvA torque experiments are a priori excluded at 0°, since the torque signal itself vanishes due to the symmetry of the FS at this angle[16]. Therefore a direct comparison between dHvA torque and SdH results at *exactly* 0° is not possible in this system. This problem was got round by comparative SdH and dHvA experiments at various tilted-field angles $0° < \Theta \leq 57°$, which were carried out at different fields. The results are shown in Fig. 5.13 and the obtained m_{F3}* values can be rescaled to 0° by the 1/cosΘ behaviour of m* in 2D systems. Fig. 5.13 shows that angle-dependent SdH and dHvA experiments follow this 1/cosΘ law and that both types of experiments reveal perfectly consistent results at $\Theta \neq 0°$. Rescaled to 0°, both types of experiments reveal m_{F3}* = 3.9 (see Fig. 3.13). This value is transferred to Fig. 5.12 (upper plot) and completed by dHvA measurements at various fields and different angles (full green squares). Rescaled to 0°, these measurements show that m_{F3}* in fact is *constant* within the error bars up to high fields. This is confirmed by the fact that the QO frequency values themselves (which are determined by m* via $\hbar\omega_c$, see Eq. (3.2)) remain constant up to 52T. From these detailed experiments it was concluded, that

- there is *no general* difference between the results obtained from dHvA (i.e., magnetisation) and SdH (i.e., transport) experiments[17] and
- m_{F3}* is not field dependent within the error bars of its determination.

These results prove, that this anomalous effect is clearly restricted to $\Theta = 0°$, which is the field orientation exactly perpendicular to the conducting (b,c) planes and, furthermore they

[16] In Eq. (3.9b) $\partial F/\partial\Theta$ and therefore the torque signal vanishes at $\Theta = 0°$.

[17] The situation at $\Theta \approx 0°$ at high fields is discussed in Sec. 5.3.1 by comparative dHvA and SdH measurements performed on the same sample at $\Theta = 0.07°$.

show, that the origin of the *apparent* decrease of m_{F3}* at 0° can be best found by thinking over the *way to determine* m_{F3}* from the temperature dependence of the QO amplitudes.
Apparently lower m* values mean that at low temperatures the QO amplitudes are *lower* than expected by LK theory. Furthermore, continual 'decreasing' m* values with increasing field mean, that this deviation from LK behaviour becomes stronger with increasing field. Considering this it was concluded that the results shown in Figs. 5.12 and 5.13 have to be understood in terms of strong field and temperature dependent *damping effects* of the SdH amplitudes at Θ = 0°, which lead to an apparent decrease of m_{F3}* as soon as the standard LK formalism is applied for its estimation [399,411,146].

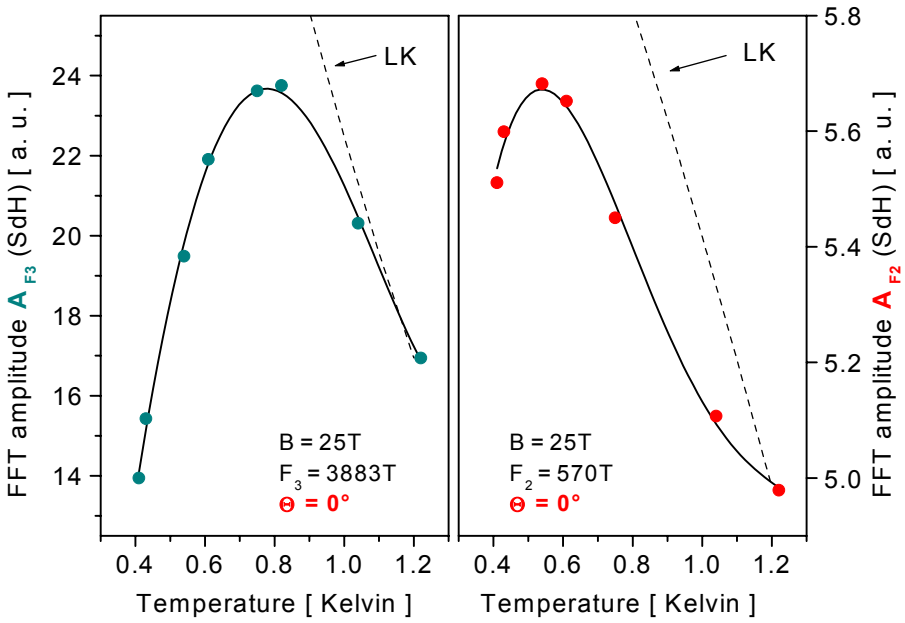

Fig. 5.14: Temperature dependence of the SdH amplitudes of F_2 and F_3 at 25T and Θ = 0°. The dashed lines show the expected behaviour according to the standard Lifshitz-Kosevich theory whereas the full lines are a guide to the eye.

This means that the LK formalism applies very well for the description of both, dHvA as well as SdH measurements[18] at Θ ≠ 0° and at 0° at B < 12T, but it cannot be applied for the description of SdH amplitudes at high fields, low temperatures at this special field orientation Θ = 0°.
As the field is further increased, the strong anomalous damping effects (DEs) at Θ = 0° become such dramatic, that the amplitudes even decrease with decreasing temperature (see Fig. 5.14). A comparison of the experimental results with the expected LK behaviour (dashed lines) shows the strength of the damping effects. They are observed in the amplitudes of both QO frequencies, F_2 and F_3, respectively.
Further SdH investigations were carried out concerning the field dependence of these damping effects. The results are plotted in Fig. 5.15, where the left part compares the measured SdH amplitudes with the expected field dependence according to LK theory (dashed line, according to Eqs. (3.12)-(3.15)). At high fields the observed QO amplitudes even decrease at Θ = 0°.

[18] Minor deviations from standard 3D LK behaviour at high fields and $0^o < \Theta \lesssim 20^o$can be understood by considering oscillations of the chemical potential with the QO frequency F_3. These effects are discussed in Sec. 5.3.1.

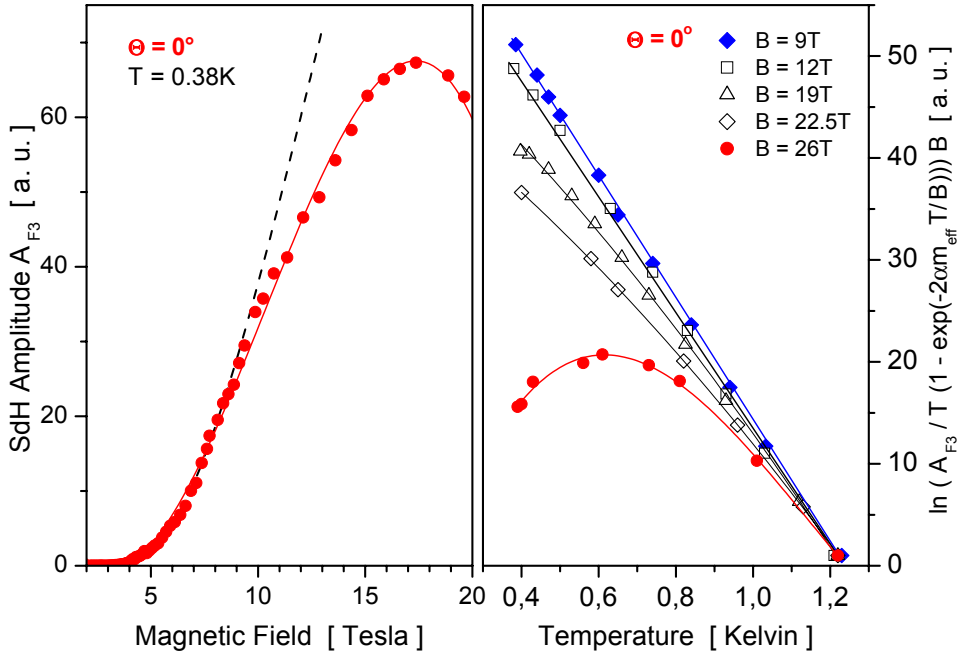

Fig. 5.15: Illustration of the anomalous damping effects of SdH oscillations in κ-(BEDT-TTF)$_2$I$_3$ at Θ = 0°. **left:** Field dependence of the SdH amplitudes (circles) compared to LK behaviour (dashed line). The amplitudes were determined by FFT from neighbouring narrow field windows. **right:** Temperature dependence of the SdH amplitudes A_{F3} at different fields (discussion see text).

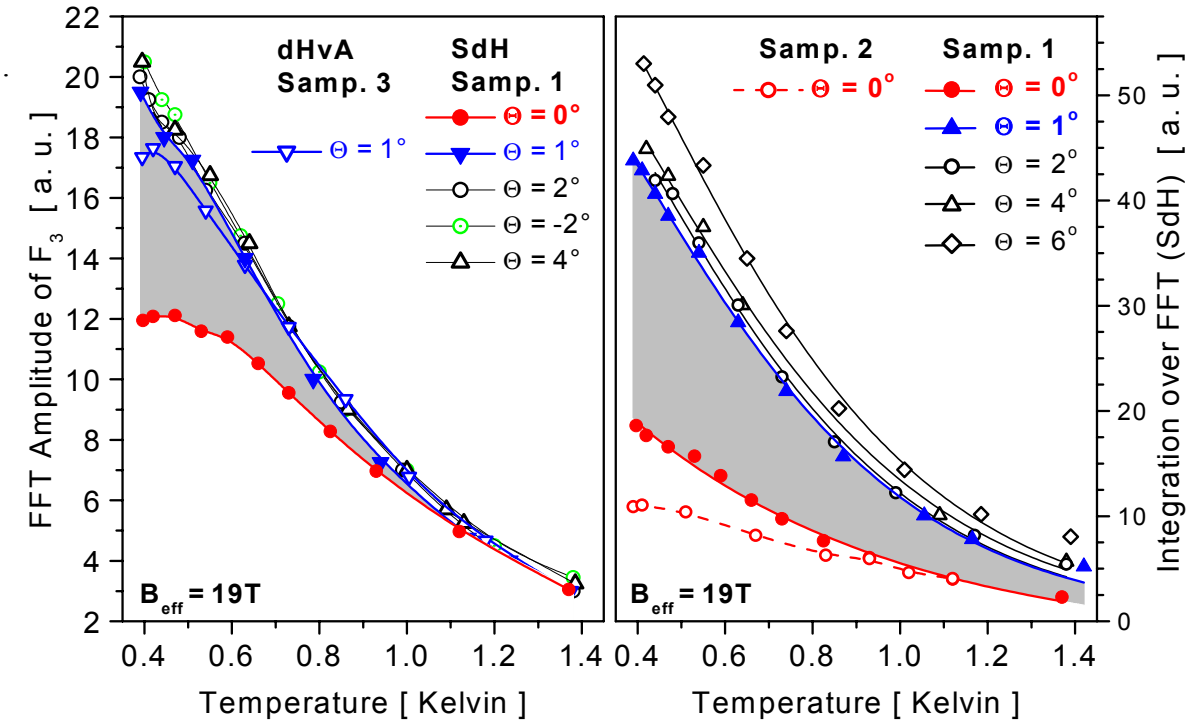

Fig. 5.16: left: Temperature dependence of the FFT amplitudes from SdH and dHvA oscillations at tilt angles -2° ≤ Θ ≤ 4° at 19T. The grey-shaded area illustrates how sharply the damping effects are restricted to Θ < 1°. **right:** The integration over the whole FFT represents the entire magnitude of QOs. The angular dependence of the SdH amplitudes below 6° illustrate the damping effects (grey-shaded area) and confirms their restriction to Θ < 1°.

The right part of the figure shows the temperature dependence of the SdH FFT amplitudes A_{F3} at 0° and different fields. According to LK theory this implicit plot should be a straight line whose gradient should be constant and should give access to m_{F3}* (see Eq. (3.11)). The gradient at 9T accounts for normal 3D LK behaviour and reveals m_{F3}* = 3.9. Every deviation from this line with increasing field illustrates the strong damping effects at low temperatures and Θ = 0° (note the logarithmic scale).
In a further set of experiments the angular dependence of the DEs was investigated in a narrow region around 0°. The left part of Fig. 5.16 shows the temperature dependence of the QO amplitudes at $|\Theta| \leq 4^o$. Between 4° and 1° the amplitudes show quite normal 3D LK behaviour (cons. Fn. [16]). It should be emphasised that comparative SdH and dHvA results at 1° are nearly congruent, even though they are obtained from different samples. As soon as the angle is switched from 1° to 0°, the anomalous DEs of SdH amplitudes set in (illustrated by the grey-shaded area)[19]. It is emphasised that these damping effects at 0° are also observed in the amplitudes of the harmonics $2*F_3$ and $3*F_3$ themselves [402]. This excludes already, that the amplitudes of the fundamental are simply reduced in favour of an amplification of those of the harmonics. Nevertheless, in order to account for the entire rich harmonic content of the QO amplitudes, the integration of the entire FFT was performed as a measure for the entire magnitude of QOs. It is plotted in the right part of Fig. 5.16 as a qualitative illustration of the anomalous DEs. The strong increase of the plots for 6° ≥ Θ ≥ 1° symbolise quite normal LK behaviour. The drastic deviation at 0° illustrates once again the strong amplitude reduction at this angle. By reproducing these results on a number of samples of different batches the experience was made that the higher the sample quality is, the stronger the damping effects at 0° are. The results for a further sample (open circles) are plotted for comparison.

In consequence, a number of well-known, i.e., 'conventional' effects were considered, asking whether they may explain the most prominent features of the observed damping effects, i.e. their increasing strength with increasing field and decreasing temperature, as well as their sharp restriction to 0°, the field orientation exactly perpendicular to the conducting planes. The results are summarised in the following (since a part of them is already reported in detail, they are not reproduced in all detail).

5.3.1 Possible Reasons For the Anomalous Damping Effects of the SdH Amplitudes of κ-(BEDT-TTF)$_2$I$_3$ at High *B* Low *T* and Θ = 0°

Spin Splitting and/or a Field Dependent *g*-Value

It is a typical observation in κ-(BEDT-TTF)$_2$I$_3$ at 0°, that spin splitting arises at high *B*, and low *T* leading to a double-peak structure of the QOs (see Fig. 5.5) and a strong representation of the second as well as all even harmonics in the FFT spectrum (see Fig. 5.7). This may give rise to the question, whether spin splitting can be the origin of the anomalous damping

[19] In the wide angular range of the sample rotation unit (about 330° in total) the absolute angle can be typically resolved with an error of about 0.5°-1° (depending on the angle itself). At the most interesting angles $|\Theta| \lesssim 2^o$ however, a very good angular resolution of $\delta\Theta \leq 0.04^o$could be realised. This was enabled by mounting the SdH sample on a torque platelet and tilting the angle within$|\Theta| \lesssim 2^o$. The exact reproduction of the vanishing torque signal at $\Theta \equiv 0^o$ provided the high resolution $\delta\Theta$. Furthermore it allowed **i)** the exact finding of this angle, it ensured that **ii)** the sample is not tilted into the direction perpendicular to the sample rotation axis and that **iii)** the sample is exactly in the magnetic field centre.

effects. However, from the obtained results this possibility has to be ruled out for the following arguments.

- From the finding that the spin zero positions do not shift between 11T and 22.5T it was concluded in Sec. 5.2.1 that gm^* and therefore the spin damping factor R_s of the LK formula (Eq. (3.17)) remains constant within this field range. This excludes a field dependent damping of the QOs by a change of R_s, i.e., by spin splitting.
- The magnitude of spin splitting increases with the tilting angle Θ and is maximal, e.g., at 15.5°. The assumption of spin splitting as an origin of the DEs would require, that these effects would become even stronger with increasing tilt angles and would be strongest just at the spin zero angles, e.g., at 15.5°. In contrast, at this angle and in the whole angular range , $0° < |\Theta| \leq 68°$, such DEs do not occur.
- The magnitude of spin splitting varies very smoothly (via gm^*) with the tilt angle. Therefore it cannot explain such a sharp angular dependence of the DEs as observed between 0° and 1°.

For these reasons spin splitting can be excluded as an origin of the anomalous DEs at 0°.

Magnetic Interaction

It is a matter of fact that magnetic interaction (MI) may influence the field and temperature dependence of QOs (see Sec. 3.4.1).

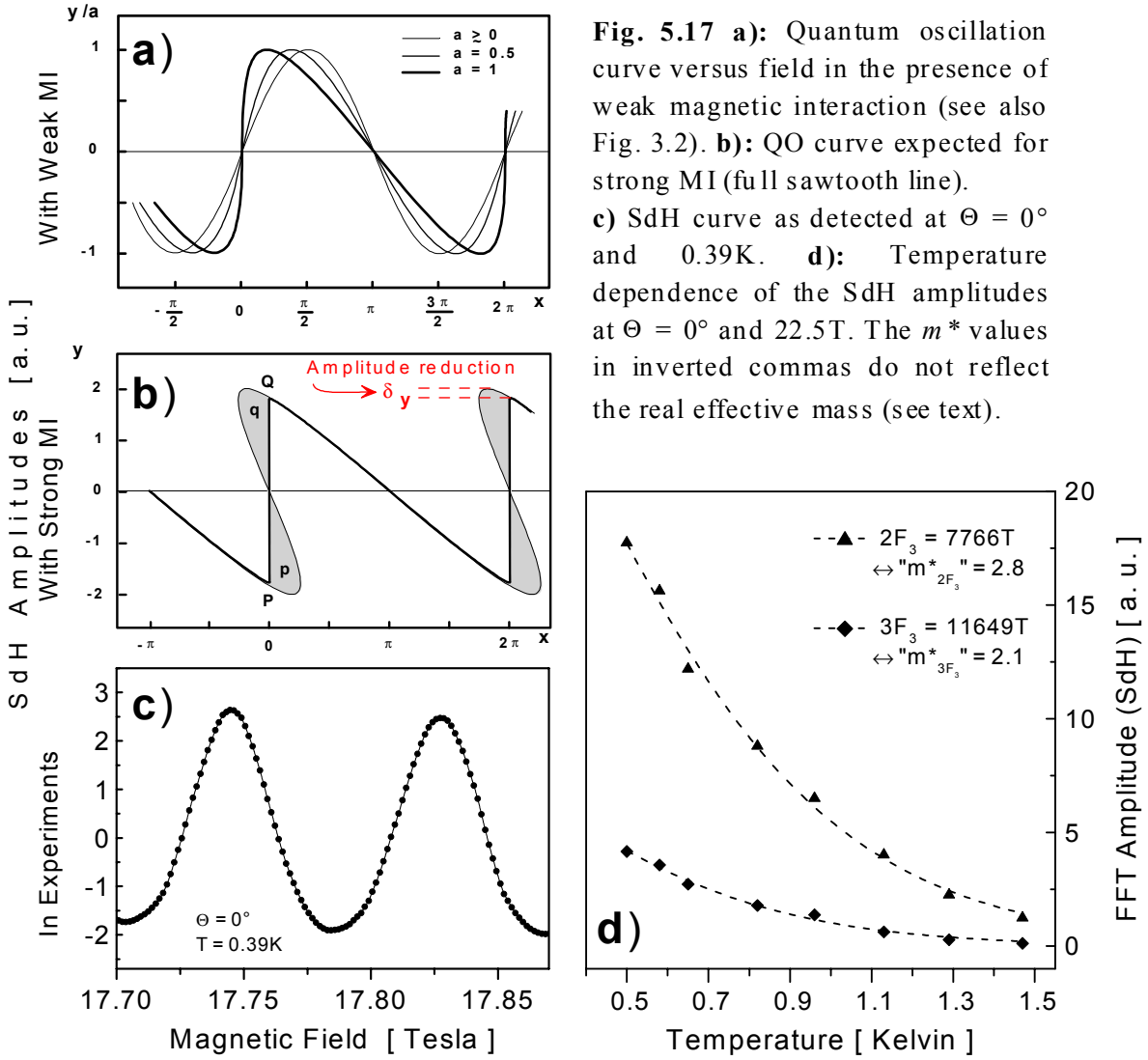

Fig. 5.17 a): Quantum oscillation curve versus field in the presence of weak magnetic interaction (see also Fig. 3.2). **b):** QO curve expected for strong MI (full sawtooth line). **c)** SdH curve as detected at Θ = 0° and 0.39K. **d):** Temperature dependence of the SdH amplitudes at Θ = 0° and 22.5T. The m^* values in inverted commas do not reflect the real effective mass (see text).

One of the characteristics of MI is that even in the presence of weak MI the QO amplitudes are considerably deformed (see Fig. 3.2.b, reproduced in Fig 5.17.a)), while for negligible MI the QO curve (dashed line) is symmetric.
In the case of strong MI an inverse sawtooth curve is expected (steep flank at the low-field side of the QO) and the amplitude of the fundamental frequency is reduced (see part b)). In comparison to this expectation, the measured SdH curve plotted in part c) of the figure does not show any indication for such an inverse sawtooth, even at $B > 17$T. This proves already that the role of MI is negligible in the SdH experiments.
Furthermore, the harmonic content of the QO amplitudes is indeed high, but if caused by MI, it should be much stronger temperature dependent as expected by the LK formula. Thus, an 'estimation' of m_{nF3}* from each of the observed harmonics $n*F_3$ should result in apparently *higher* m_{nF3}* values than the correct m_{F3}* = 3.9. Figure 5.17.d) shows that the opposite is the case in κ-(BEDT-TTF)$_2$I$_3$. The *lowered* values 'm_{nF3}*' illustrate that the amplitudes of the harmonics are damped at low T, which is in strong contrast to the behaviour expected for MI.
Moreover it was shown that the strong harmonic content itself can be explained completely by considering spin splitting as well as the oscillation of the chemical potential with the QO frequency F_3 [91] (see also end of this Sec.). This explanation applies for both, dHvA as well as SdH measurements, including those at 0°.
Finally it has to be considered that MI depends on the absolute field. Therefore effects of MI would be observable also at $\Theta > 0°$ at high fields and they would be least of all restricted to 0° in such a sharp manner as observed.

These arguments exclude magnetic interaction as an origin for the strong DEs of SdH oscillations at 0°.

Magnetic Breakdown

As next the possibility was followed that the strong damping effects might be a result of magnetic breakdown (MB). The following arguments were found to be crucial in this context.

i) The MB gap is overcome above a breakdown field of about 2T (see Sec. 5.2.1). Therefore with increasing field the electrons are more and more unimpeded on following the orbit corresponding to F_3, i.e., the higher the field is, the lower the influence of MB can be. This is in contrast to the observation that the damping effects in the F_3 oscillations just increase with field. Furthermore if ever MB itself would generate the damping effects, they would be also present in the closely related material κ-(BEDT-TTF)$_2$Cu(NCS)$_2$, which has an almost identical FS. More than this, the DEs would be expected to be even stronger there, since the MB itself occurs only at higher fields in that material. However such effects are absent in the Cu(NCS) salt.

ii) The energy gap $E_g \lessapprox 3$meV is much bigger than$k_B T \approx 1.7 * 10^{-3}$meV. Therefore thermal energy cannot contribute to tunnelling and Bragg reflection probabilities and thus the results of MB should be temperature independent (see Sec. 3.4.2). In contrast, the present DEs are found to be strongly temperature dependent.

iii) The MB probability (Eq. (3.25)) depends on the absolute field. Therefore effects of MB must be observable also at $\Theta > 0°$ at high fields and they would be least of all restricted to 0° in such a strict way as observed.

These arguments show that the strong DEs of SdH oscillations at 0° cannot be generated by magnetic breakdown. A further illustration of this finding is postponed to the discussion of Fig. 5.24 in Sec. 5.4, since appropriate.

Warping

On the search for a 'conventional' explanation for the anomalous damping effects of QOs at $\Theta = 0°$ the possibility was followed that they might be the result of a warping, i.e., a corrugation of the Fermi surface (as illustrated in Fig. 3.5a). However it was found that a warping cannot be the origin of these DEs. Since this feature is already set out in Refs. [402,146,410,413,414,216] the discussion is not carried out in detail here. Instead, two of the characteristics of a warping are selected, which show that it cannot be the origin of the DEs.
i) A warping is not temperature dependent, while the damping effects are found to be even strongly temperature dependent.
ii) A warping is not restricted to a certain field orientation, i.e., angle Θ. Its angular dependence is given by the angular dependence $\partial F/\partial\Theta$ of the participating QO frequencies. Since $\partial F/\partial\Theta$ even vanishes around $\Theta = 0°$ (see Refs. [395a,399]), an assumed warping would be only very smoothly angle dependent around 0° and therefore observable in a wide angular range $\Theta > 0°$. This consequence of a warping is in clear contrast with the restriction of the DEs to 0°.

This disagreement between the characteristics of the damping effects of QOs and those of a warping shows that the latter cannot be the origin of the DEs[20].

Quantum Interference

It was already pointed out in Sec. 3.4.7, that an unambiguous assignment between a certain Fourier spectrum and quantum interference (QI) or magnetic breakdown (MB) with or without an oscillation of the chemical potential $\tilde{\mu}$ is not given to date. However the FFT may give at last hints for the situation present, which have to be verified with additional arguments.
Therefore the FFT spectrum of SdH oscillations in κ-(BEDT-TTF)$_2$I$_3$ detected in the MB region (Fig. 5.18.a) and d)) was compared with the situations for $\tilde{\mu}$ and QI (see parts b) and c), taken from Fig. 3.10) as studied in the very closely related quasi-2D material κ-(BEDT-TTF)$_2$Cu(NSC)$_2$ [191]. The results of this comparison are the following.
It was found that the FFT spectrum of SdH oscillations in the I$_3$ salt (Fig. 5.18.a)) corresponds very well in a number of aspects to the dHvA spectrum just for the case of $\tilde{\mu}$ calculated for the Cu(NSC)$_2$ salt[21] , while it deviates clearly from the cases of pure MB (Fig. 3.10.a)) as well as QI (Fig. 5.18.c)). This turns out in several aspects.

[20] For completeness it is anticipated here that a further argument which excludes warping, is discussed in Sec. 5.5.

[21] This correspondence indicates moreover, that in the present I$_3$ salt the behaviour of *transport* properties (as SdH) at $\Theta = 0°$ and low fields is almost identical to the behaviour calculated for a *pure thermodynamic* property (i.e., dHvA). This supports the statement of general correspondence of dHvA and SdH results given in Sec. 5.3.

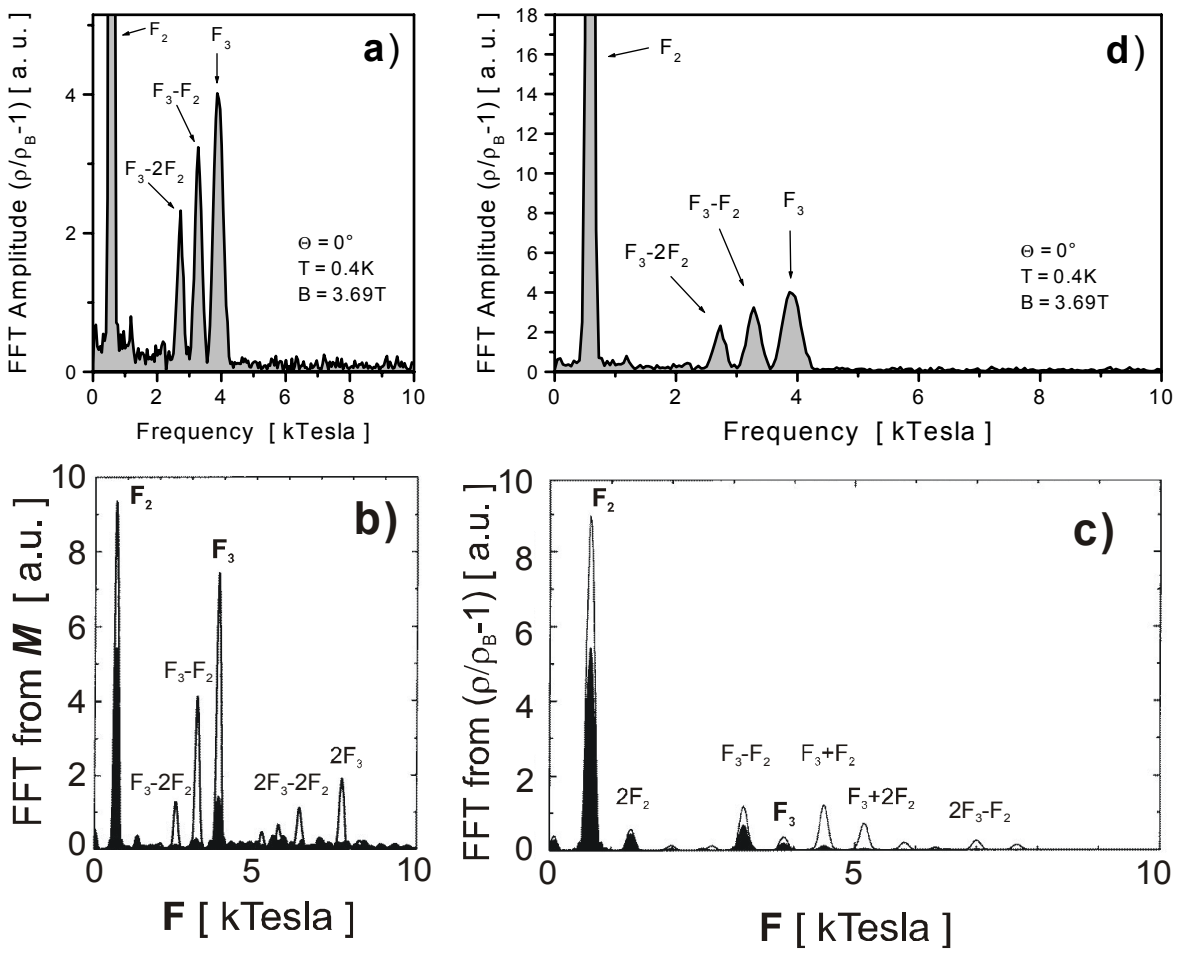

Fig. 5.18. a) and **d)**: FFT spectrum (SdH) of κ-(BEDT-TTF)$_2$I$_3$ detected in the MB region at Θ = 0° (with different *y*-scale). **b)** dHvA FFT spectrum of κ-(BEDT-TTF)$_2$Cu(NSC)$_2$ in the MB region as calculated for the case of an oscillating chemical potential. **c)** SdH spectrum of the latter material for the case of quantum interference (both, b) and c) are plots according to Ref. [191]). The black filled areas in b) and c) correspond to 1.4K, whereas the solid lines correspond to 0.4K.

- The *presence* of both forbidden difference frequencies F_3-F_2 and F_3-$2F_2$ in a decreasing spectral weight is found in the studies reported in [191] to be characteristic of the oscillating μ case, but not of the QI case.
- The *absence* of the allowed combination frequencies F_3+F_2 and F_3+$2F_2$ is, likewise, characteristic of the oscillating μ case (comp. Figs. 5.18. a) and b)), but in strong contrast to the QI case, where the combination frequencies F_3+F_2 and F_3+$2F_2$ are not only present, but even higher in magnitude as F_3 itself (Fig. 5.18.c)).
- Furthermore, in the case of QI (part c)), both, F_3-F_2 and F_3+F_2, should be observed even at high temperatures, where F_3-F_2 should have even a higher magnitude than F_3 itself. This is not observed in the present material (part d)).
- Moreover, in the case of present QI the combination frequencies F_3+F_2 and F_3+$2F_2$ should be not only present, but at 0.4K they should both even exceed the amplitude of F_3 itself (part c)). In contrast, these frequencies are completely absent in κ-(BEDT-TTF)$_2$I$_3$ (part d)).

These aspects hint to the fact that μ may oscillate in this 2D I_3-salt even at low fields (a fact which is meanwhile confirmed) and moreover, that QI is most likely not the origin of the anomalous damping of the SdH amplitudes at high field, low temperatures and 0°.
This latter indication is supported by further aspects.

- The difference frequencies are restricted to the MB region [402], as expected for the case of an oscillating μ in the MB region. If they were ever generated by QI and the underlying path differences (see Fig. 3.9.b), they would persist up to high fields, since the path differences are not restricted to the MB region. Thus, such a field dependent behaviour of the difference frequencies cannot be generated by QI.

- The mentioned path differences shown in Fig. 3.9.b are very weakly tilt-angle dependent, especially at 0°. This is due to the symmetry of the coupled network geometry with respect to this angle. Therefore, if an assumed QI were the origin of the anomalous DEs it would necessarily generate them in a wide angular range. This is in clear contrast, the observed restriction of the DEs to 0°.

These aspects show that the strong anomalous damping effects in the SdH amplitudes of κ-(BEDT-TTF)$_2$I$_3$ at high B, low T and $\Theta = 0°$ cannot be attributed to quantum interference.

Further Possibilities: Superlattice and FS Instability

In the scope of the present work further possibilities were followed which might modify the amplitudes of QOs in an anomalous way.
As already mentioned in the discussion of the structure in Sec. 5.1, superlattice spots in the X-ray structure investigations were not observed, so that the occurrence of a superlattice at low temperature can be excluded in the present I_3 salt. Therefore the anomalous DEs of the SdH amplitudes cannot be attributed to a superlattice effect.
Especially, indications for a superlattice structure as proposed for the isostructural quasi-2D organic superconductor κ-(BEDT-TTF)$_2$Cu[N(CN)$_2$]Br [415,416] are not observed in the present I_3 salt.
Furthermore, the linearity of the plot of the Landau levels versus $1/B$ in Fig. 5.8 shows, that the QO frequencies and thus also the Fermi surface are stable up to at least 52T, so that a field-induced Fermi surface instability can be excluded as an origin of the damping effects.

Eddy Currents

It has to be considered that especially in highly conductive metals as the present one, eddy currents might be induced during QO experiments owing to a finite $\partial B/\partial t$. Indeed, in pulsed field dHvA experiments indications for the presence of such currents were observed [215]. Their induction would be not surprising in view of the strong $\partial B/\partial t$ reaching even 10^3 T/s.
However it could not be clarified in the framework of those dHvA studies, whether eddy currents may influence SdH experiments and to which extent they might contribute to the strong damping effects at 0°. This question accompanied our later SdH measurements at high fields especially at 0°. In order to minimise a possible induction of eddy currents, SdH measurements with low field sweeping rates of typically $1.7*10^{-3}$ T/s were carried out in

steady resistive magnets and compared with results obtained at lowest sweeping rates of $2.3*10^{-4}$ T/s in superconducting coils (see also results discussed in Sec. 5.5).
It was not only found that the strong damping effects *persist* in experiments at lowest sweeping rates, even more, they can be excellently observed and they occur even at by far lower field values than in pulsed fields (at the same temperature 0.4K the DEs occur already at about 2T in resistive coils (see, e.g., Fig. 5.30) instead of more than 20-30T in pulsed fields).

In further comparative pulsed field/steady field SdH experiments at 0° it was confirmed that the pulsed field and the steady field SdH results are perfectly consistent in the sense that the magnitude of damping effects is neither influenced by the sweeping rate, nor, by the way, by a certain critical field or temperature value, but exclusively by the ratio of $\hbar\omega_c/k_BT$.

The consistence of results obtained in an order of magnitude of seven decades in the sweeping rate $\partial B/\partial t$ illustrate that the strong anomalous reduction of SdH amplitudes at $\Theta = 0°$ cannot be attributed to the occurrence of supposed field induced eddy currents.

Theory of the dHvA Effect in 2D Systems

In the frame of a search for a 'conventional' explanation for the origin of the above mentioned damping effects of QO amplitudes, the theory of the dHvA effect in 2DES proposed by *Vagner et al.* [88,89,90] (see Sec. 3.4.4) was taken up.
An estimate for the field dependence of the envelope of the dHvA amplitude as proposed in [90] was performed in order to probe whether the QO amplitudes of the 2DES of κ-(BEDT-TTF)$_2$I$_3$ can be at least roughly understood by this theory. Figure 5.19 shows the dHvA signal of this I_3 salt measured at 16°. Added to the figure is the envelope of the signal (grey curve) as expected by the initial theory for the dHvA effect in a 2DES. The estimate obtained by the system parameters as given in the figure caption shows rather disagreement with the measured data.

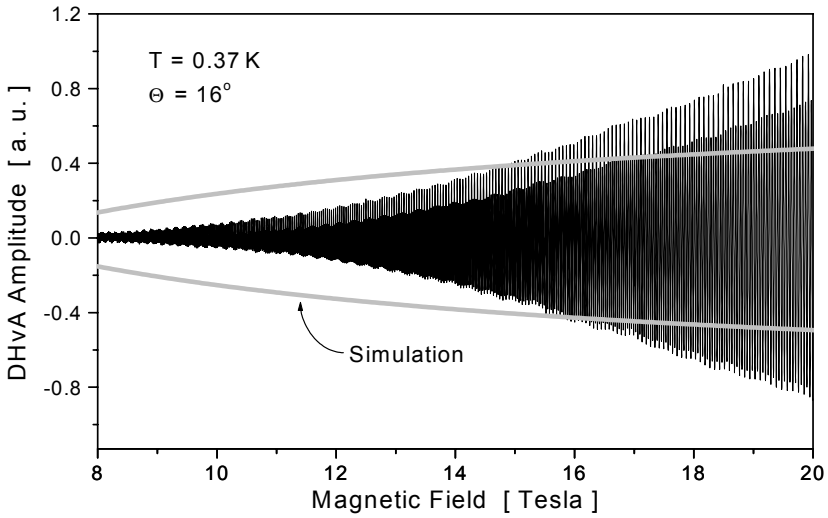

Fig. 5.19: DHvA signal of κ-(BEDT-TTF)$_2$I$_3$ detected at 0.37K and 16°. Simulation of the envelope (grey) as expected according to the theory for the dHvA effect in 2DESs [90] with the system parameters $m^* = 3.98$, $E_F = 0.114$eV and $T = 0.37$K.

Motivated by the very striking results obtained on this 2D organic metal, effort was put in the progress of a more appropriate theoretical description. The results are discussed in the following.

Oscillation of the Chemical Potential with the QO Frequency F_3

In order to improve the theoretical understanding of the complex behaviour of dHvA and SdH amplitudes in κ-(BEDT-TTF)$_2$I$_3$ at high magnetic fields, the system parameters were introduced in the simulations for the QO amplitudes in 2D systems.
In an analytical approach based on Refs. [88,90,92,417], the two-dimensionality of the electronic system of κ-(BEDT-TTF)$_2$I$_3$ was considered by an oscillating chemical potential [91]. For simplicity, only a μ oscillation with the QO frequency F_3, i.e., $\tilde{\mu}_{F3}$, was introduced and it was shown that $\tilde{\mu}_{F3}$ acts in a retrospective way onto the wave form of the actual QO with F_3. In contrast to a preceding approach for 2D systems proposed in [418,87], which was derived only for vanishing temperature and Dingle temperature, finite T and T_D was now considered in the improved description [91]. For a further refinement, the summation of the contribution of an arbitrary number of Landau levels was enabled, whereas the preceding approach in Refs. [88,90] accounts only for the main contribution of the two LLs lying closest to the Fermi cylinder (see Sec. 3.4.4).
Thus the retrospective action of $\tilde{\mu}_{F3}$ onto the wave form of the F_3 oscillations was analysed at high fields, low temperatures and different tilt angles. This approach [91] could identify the following experimental features as results of the two-dimensionality, i.e., an oscillating μ_{F3} in κ-(BEDT-TTF)$_2$I$_3$:
- The temperature dependence of the dHvA amplitudes could be perfectly reproduced down to 0.4K even at high fields (27T).
- The position of spin-split oscillations was shown to be *always midway* between the prominent oscillations, *independently* from the tilt angle Θ between B and the 2D conducting planes. This is a result of the pinning of the spin levels to $\tilde{\mu}_{F3}$ and is therefore in contrast to the behaviour in 3D systems, where the positions of spin-split amplitudes *vary* with the tilt angle (as discussed in Sec. 3.2.4).
- The oscillation of μ_{F3} in the 2D system leads to a sawtooth of the QOs whose steep flank is on the high-field part of a QO, whereas for the 3D system the sawtooth[22] is inversed, i.e., the steep flank is in the low-field part of a QO.

The properties found, can explain the dHvA amplitudes and the spectral weight in the FFT in the whole angular range $0 < \Theta \leq 40°$, where spin splitting was observed. The theoretical approach applies perfectly even at 0.4K and 27T, i.e., at fields, where the strong damping effects of SdH amplitudes are observed at 0°.
Later it was found that the description reproduces also the spectral weight of the SdH amplitudes at these angles, even including $\Theta = 0°$. This confirms the general correspondence of dHvA and SdH experiments and the general application of this approach to SdH results.

Thus, spin splitting of the QOs, spectral weight in the FFTs and minor deviations of the temperature dependence of the QO amplitudes are indeed understood by considering two-dimensionality, i.e., the oscillating $\tilde{\mu}_{F3}$. In contrast, the absolute SdH amplitudes i.e., the

[22] in an ideal 3DES at $T = 0$.

strong anomalous damping effects at Θ = 0° and especially their field and temperature dependence as well as their restriction to 0°, cannot be explained even by this special 2D approach.

In a further study the use of inductive technique (see, e.g., [87]) enabled dHvA experiments in pulsed fields up to 60T at Θ = 0° [215]. Figure 5.20 (left) shows the temperature dependence of the dHvA FFT amplitudes of F_3 and its harmonic $2*F_3$ at 40T.

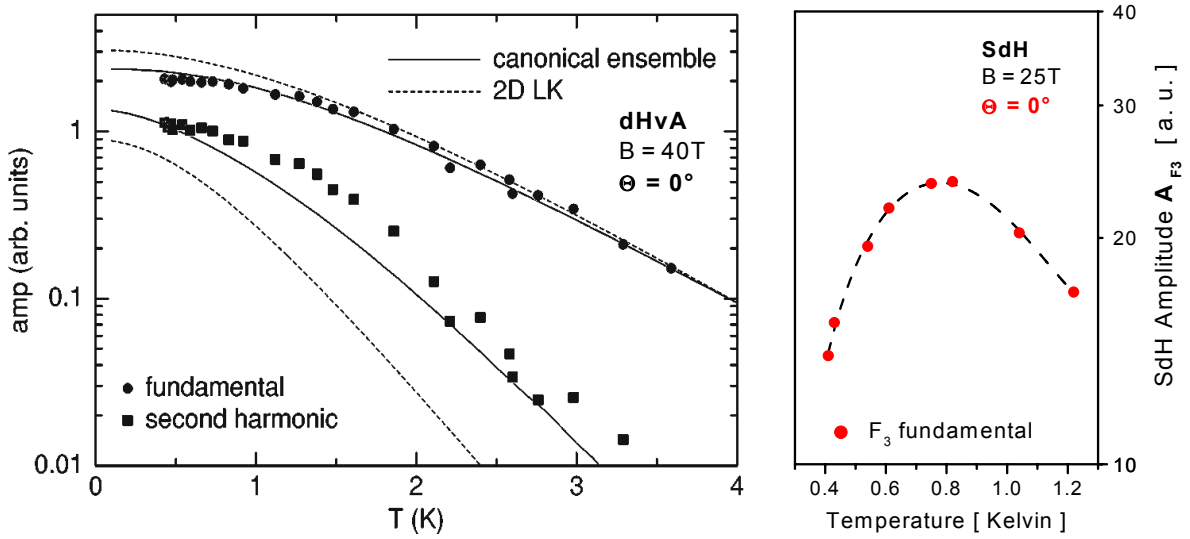

Fig. 5.20: Temperature dependence of QO amplitudes from different κ-(BEDT-TTF)$_2$I$_3$ single crystals at Θ = 0°. **left:** dHvA FFT amplitudes of F_3 and $2*F_3$ at 40T, including fits according to the 2D Lifshitz-Kosevich theory [87] and a numerical approach for a 2D canonical ensemble of electrons (from [215]). **right:** SdH FFT amplitudes at 25T (see also Fig. 5.14.a; the connecting line is a guide to the eye). Note the logarithmic *y*-scale in the figures.

In the left part of Fig. 5.20 the dHvA amplitudes recorded at 0° show minor but significant deviations from standard 3D LK behaviour by a sublinear behaviour i.e., a slight amplitude reduction at low temperatures. An improved approach to the experimental curve is achieved by the 2D Lifshitz-Kosevich theory (dashed line). A considerably better correspondence is reached by numerical calculations based on the 2D model introduced in Ref. [417], where the temperature dependence of dHvA oscillations was estimated including finite temperature, Dingle temperature and μ oscillations with F_3 [215]. The resulting full curve in Fig. 5.20 (left) shows a good agreement with the experimental data.
However it has to be emphasized that in dHvA studies at 0° only minor deviations from 3D LK behaviour are found (see Fig. 5.20, left), which do not compare to the dramatic damping effects found in SdH experiments at the same angle (right part of the figure).

Comparative dHvA and SdH Experiments at Θ = 0.07° on the Same Crystal

The finding illustrated in Fig. 5.20 indicates a discrepancy of SdH and dHvA experiments which is not general but occurs exclusively at 0°, high *B* and low *T*. In view of this it was unsatisfactory that the aforementioned two types of experiments were carried out on different crystals. In order to exclude possible influences by different crystal quality, comparative

dHvA and SdH experiments were performed in steady fields up to 26T on the same sample [419].

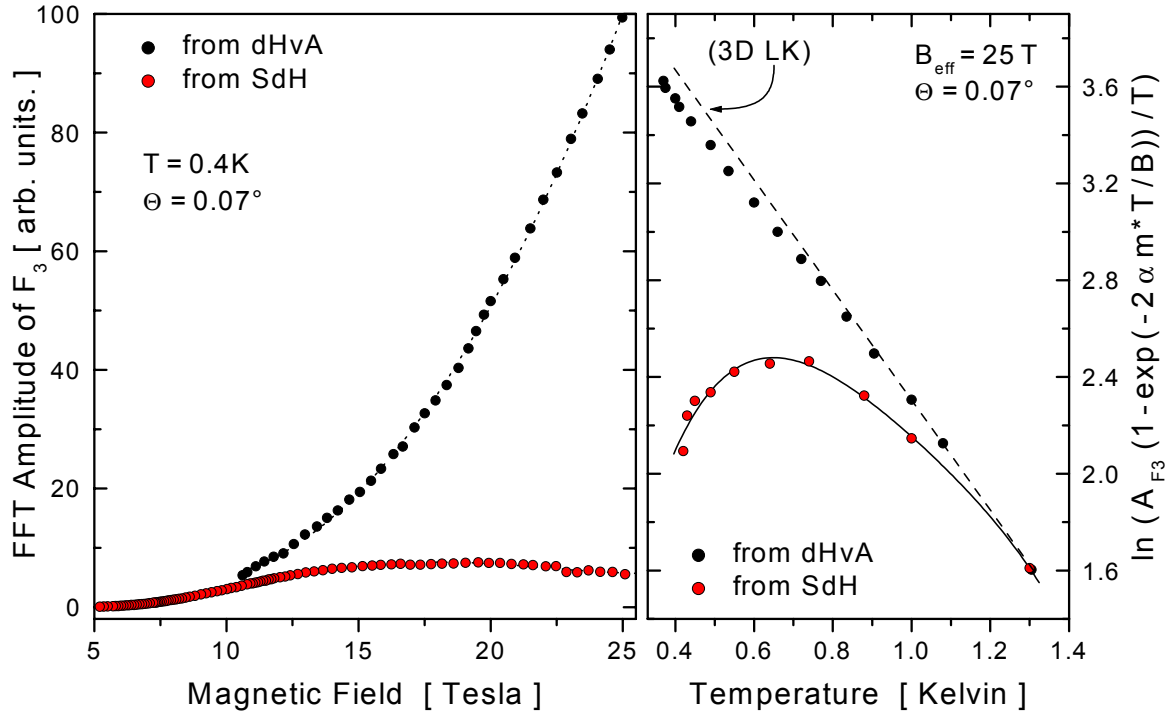

Fig. 5.21: Comparative dHvA and SdH studies on the same κ-(BEDT-TTF)$_2$I$_3$ single crystal at Θ = 0.07°. **left:** Field dependence of the FFT amplitudes taken from narrow field windows. **right:** Temperature dependence of the amplitudes at 25T in a logarithmic plot according to Eq. (3.11). The dashed line is a fit to the standard 3D LK theory, the full line is a guide to the eye.

For these experiments a special technique was used to reach best possible angular resolution. Therefore the sample as contacted for SdH experiments was mounted onto a dHvA torque cantilever. This allowed to take advantage from a property inherent to torque measurements, namely that the dHvA oscillations vanish at $\Theta \equiv 0^o$ due to the FS symmetry. This was used at highest field to find the exact 0° position. The vanishing of the signal at exactly 0° allowed not only **i)** the exact finding of this angle, but moreover it ensured that **ii)** the sample is not tilted into the direction perpendicular to the sample rotation axis and **iii)** the crystal is exactly in the magnetic field centre. Owing to the high crystal quality dHvA oscillations could be already observed by tilting the sample by 0.04°. Then the dHvA amplitudes were reproduced at angles $|\Theta| \lesssim 2^o$, passing the zero several times and an excellent reproducibility was found within a resolution $\delta\Theta \leq 0.04^o$. After this the crystal was turned to Θ = 0.07° and the set of SdH measurements were performed. In order to avoid any mechanical or inductive influences onto the subsequent dHvA experiments, the gold wires were disconnected from the sample, however leaving the sample on the torquemeter in its initial position. After reproducing the entire adjusting procedure, dHvA torque experiments were carried out at 0.07°. The results of the comparative dHvA and SdH experiments on the same sample are plotted in Fig. 5.21. The left part of the figure shows the field dependence of the QO amplitudes at 0.07° and 0.4K. Above about 11T the dHvA and SdH amplitudes (rescaled to the same values at low fields) show increasing discrepancy with increasing field. While the dHvA still increase strongly with field, the SdH amplitudes even decrease above about 20T. This dramatic damping is particularly anomalous, since according to the theory of the SdH effect, the SdH amplitude in

such a high-quality 2DES should rather tend to *diverge* at high fields instead of being reduced (see Sec. 3.3). Moreover, most of the known possible deviations of SdH amplitudes from dHvA amplitudes are given by the fact that, as a transport experiment, the SdH effect may be influenced by additional scattering. Such effects should be however minimised in intraplane transport, so that, again, strongest SdH amplitudes would be expected just at 0°.
In the right part of Fig. 5.21 the temperature dependence of the dHvA and SdH amplitudes is plotted in the standard 3D LK manner, where the plot according to Eq. (3.11) should result in the straight dashed line. The deviation of the dHvA amplitudes from this 3D behaviour is weak and can be clearly understood by the 2D approach described in the preceding section. In contrast, the dramatic magnitude of the damping effects in the SdH amplitudes is evident even in this logarithmic scale.

Interjection

The actual section comprised a number of 'conventional' fermiological possibilities, which were followed on the search for an explanation for the anomalous damping effects of SdH amplitudes at high B, low T and 0°. A partial success could be achieved by considering the general influence of two-dimensionality, i.e., $\tilde{\mu}_{F3}$ onto the QOs. It was found that a theoretical understanding is indeed reached for

a) the slight deviations from standard 3D LK theory, which are generated by $\tilde{\mu}_{F3}$ at high B and low T and which are observable in a wide range of the tilt angle Θ between field and 2D conducting planes.
b) the general correspondence of dHvA and SdH in the entire field, temperature and angular range covered by the experiments, except at 0°, high B and low T.
c) the shape and magnitude of dHvA amplitudes at 0° even at high B and low T.

However, by all these considerations the strong damping effects in the SdH amplitudes at high B, low T and 0° could not be explained and least of all their restriction to this angle.
After inclusion of $\tilde{\mu}_{F3}$ at both, finite T and T_D, the numerical and analytical treatments of QOs are in very good agreement with the experiments at high B and low T and $\Theta > 0°$, for dHvA measurements even including 0°. This shows that a pure thermodynamic property (i.e., dHvA effect) can be well described by the models used and confirms that the results of two-dimensionality, i.e., $\tilde{\mu}$ in principle have been considered in an appropriate way - at least at a first glance.
However, the fact that the behaviour of SdH amplitudes at 0° are still not understood, asked to find an *additional* mechanism, which

1) is inherent to 2D systems,
2) acts at high fields and low temperatures (as can be reflected by $\hbar\omega_c/k_BT$),
3) is restricted to $\Theta = 0°$,
4) influences only SdH, i.e., transport experiments.

One key of understanding is the restriction of the damping effects to 0°. A further stimulating aspect is the fact that the standard 3D LK theory and all corrections to it as discussed in the preceding, are based on the common assumption that the total number of carriers contributing to QOs in a system is constant. Both these features are taken up in the following.

5.3.2 The Very Special Experimental Conditions in a 2D Multilayer Metal at Θ = 0° Compared to Θ ≠ 0°

The restriction of the strong damping effects of the SdH amplitudes to Θ = 0° asks to think over the special role of this angle in a 2D multilayer metal.
It was described in Chap. 2, that most of the widely investigated 2D systems are based on semiconductors, where a 2DES is generated in one single 2D layer of finite thickness. By this the electron motion is naturally restricted to this 2D plane and a tilting of the external field with respect to the normal to this plane can be considered by replacing the absolute field value by the component normal to the plane.
However the situation in a 2D multilayer metal is fundamentally different. In order to illustrate this, a schematic cyclotron motion in real space is drawn for a 2D multilayer metal in Fig. 5.22 for tilt angles between field and conducting planes Θ ≠ 0° and Θ = 0°, respectively. The left part of the figure sketches an idealised cyclotron orbit at arbitrary angle Θ ≠ 0°. This situation leads to a competition between the intrinsic two-dimensionality of the system, which tends to keep the carriers within the 2D planes, and the perpendicular component of Lorentz force $F_{L,\perp}$, which compels the carriers to tunnel between the successive conducting layers. Therefore, when Θ ≠ 0°, the electrons of a multilayer metal will undoubtedly leave the conducting planes and follow a cyclotron orbit in the third dimension. This fact is proven by a *metallic*, relatively low interplane resistivity (see Fig. 5.1) as well as a by metallic, *low* thermopower in the interplane direction (see Fig. 5.2). This means that a finite potential gradient or even a low temperature gradient (of about < 0.5K) perpendicular to the planes is able to compel the electrons to leave their planes and therefore the same can be forced by the perpendicular component of Lorentz force. By the motion into the *third* direction the intrinsic two-dimensionality is clearly disturbed at all angles Θ ≠ 0° (or, at least at Θ ≥ 1°, as suggested by Fig. 5.16).

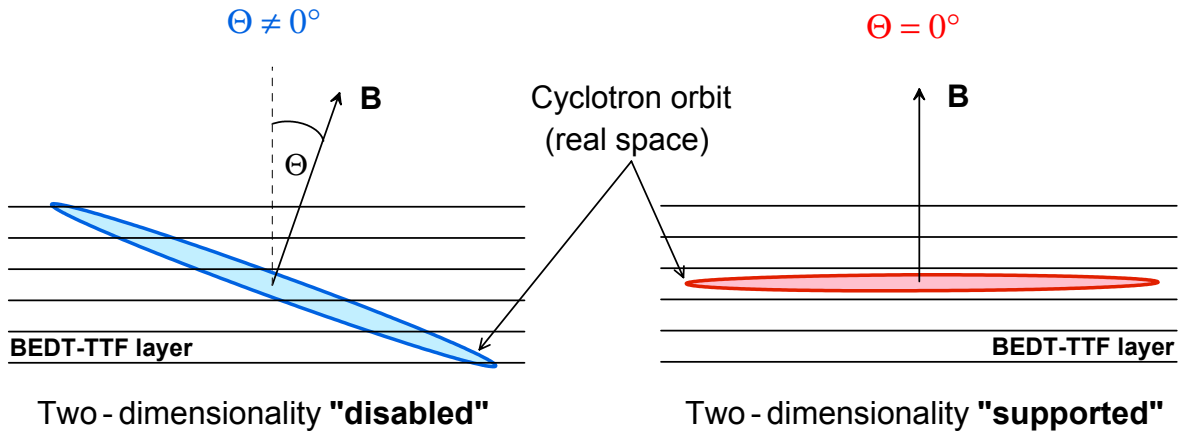

Fig. 5.22: Idealised cyclotron motion (real space) in a 2D multilayer metal as, e.g., κ-(BEDT-TTF)$_2$I$_3$. The horizontal lines indicate the successive 2D conducting BEDT-TTF layers. **left:** At Θ ≠ 0° the carriers leave the conducting planes (the real trajectory is of course more complex, but may be disregarded here). **right:** At Θ = 0° the carriers stay within their conducting planes.

However despite this 3D motion forced onto the system by the experimental conditions at Θ ≠ 0°, some of the typical 2D properties may be expected to survive: Since the interplane carrier motion is not only 'free' (metallic), but even coherent in κ-(BEDT-TTF)$_2$I$_3$ [420], the Fermi surface can be regarded as an almost perfect cylinder with free k_z motion (see Fig.

3.5.b). Therefore the main properties of a cylindrical FS persist even at $\Theta \neq 0°$. These are, e.g., the $1/\cos\Theta$ behaviour of both, m^* as well as the frequency values of F_j. In addition, μ oscillations of this Fermi cylinder may be observed also at angles $\Theta \neq 0°$. All these aspects are in full agreement with the experimental results of the preceding sections.
At $\Theta = 0°$, however, both, the intrinsic two-dimensionality as well as the field orientation keep the cyclotron motion of the carriers within the conducting planes. This point reveals a fundamental difference between a metallic multilayer 2D system and, e.g., a well-known single-layer semiconducting 2DES: It turns out that in a 2D *multilayer metal* $\Theta = 0°$ is the *exclusive* angle where the intrinsic two-dimensionality can take full effect, since the 2D character is not perturbed by the field orientation, but even 'supported' by it. Hence this angle is the exclusive field orientation, where a 2D multilayer metal has the chance to approach a 2D semiconductor in the possibility to realise its almost perfect two-dimensionality.

In view of this, the fact that the strong damping effects of the SdH amplitudes of a cyclotron motion at high B and low T are observed just at the exclusive field orientation, where the two-dimensionality of the system may take full effect, may be understood as a request: It asks to consider more subtle influences of two-dimensionality, going beyond 'merely' μ oscillations - effects which occur in such systems at high B and low T, i.e., electron correlation and electron localisation, as known from the quantum Hall effects. In this framework it was proposed that the strong damping effects in the SdH amplitudes at 0° may be understood in the sense that electron localisation at high B low T and 0° may cause a loss of mobile electrons which may contribute to magnetotransport, i.e., SdH amplitudes [399,411,146]. In consequence, the SdH amplitudes at 0° produced by the remaining mobile carriers must appear as strongly damped from the viewpoint of all 'conventional' descriptions of QOs, including corrections and the theories for 2D systems (see Chap. 3), since all of them assume that the total number of mobile carriers is constant.

When taking up this possibility, it was immediately outstanding, that the quantised Hall effects were observed experimentally only at low Landau level filling factors ν with typically $\nu \lesssim 5$ (as quoted in Ch. 4) and sometimes even only in the quantum limit ($\nu \approx 1$). This is in strong contrast to the known ν in κ-(BEDT-TTF)$_2$I$_3$ (e.g., $\nu_{F2} = 114$ at 10T, whereas $\nu_{F3} = 777$, both considering spin splitting). Even if in theories a clear statement on 'cutoff' filling factors for the quantised Hall effects is not found, the filling factors present here seemed to be very high.
In view of the fact that band structure calculations are only of finite resolution (see Sec. 5.2), especially *small* pockets on the FS might be disregarded. Therefore effort was put in detailed QO experiments on the search for low-frequency quantum oscillations, i.e., the presence of low LL filling factors in κ-(BEDT-TTF)$_2$I$_3$. The results are discussed in the following sections.

5.4 The Role of the Low Frequency QO With F_0 = 13T

The search for low-frequency oscillations requires to extend QO experiments at lowest possible fields, since for their identification widest possible field windows in $[1/B]$ are needed. On κ-(BEDT-TTF)$_2$I$_3$ such low-field experiments are enabled by the high crystal

quality and they were performed as SdH experiments, since this method is by far more sensitive as dHvA torque technique[23].

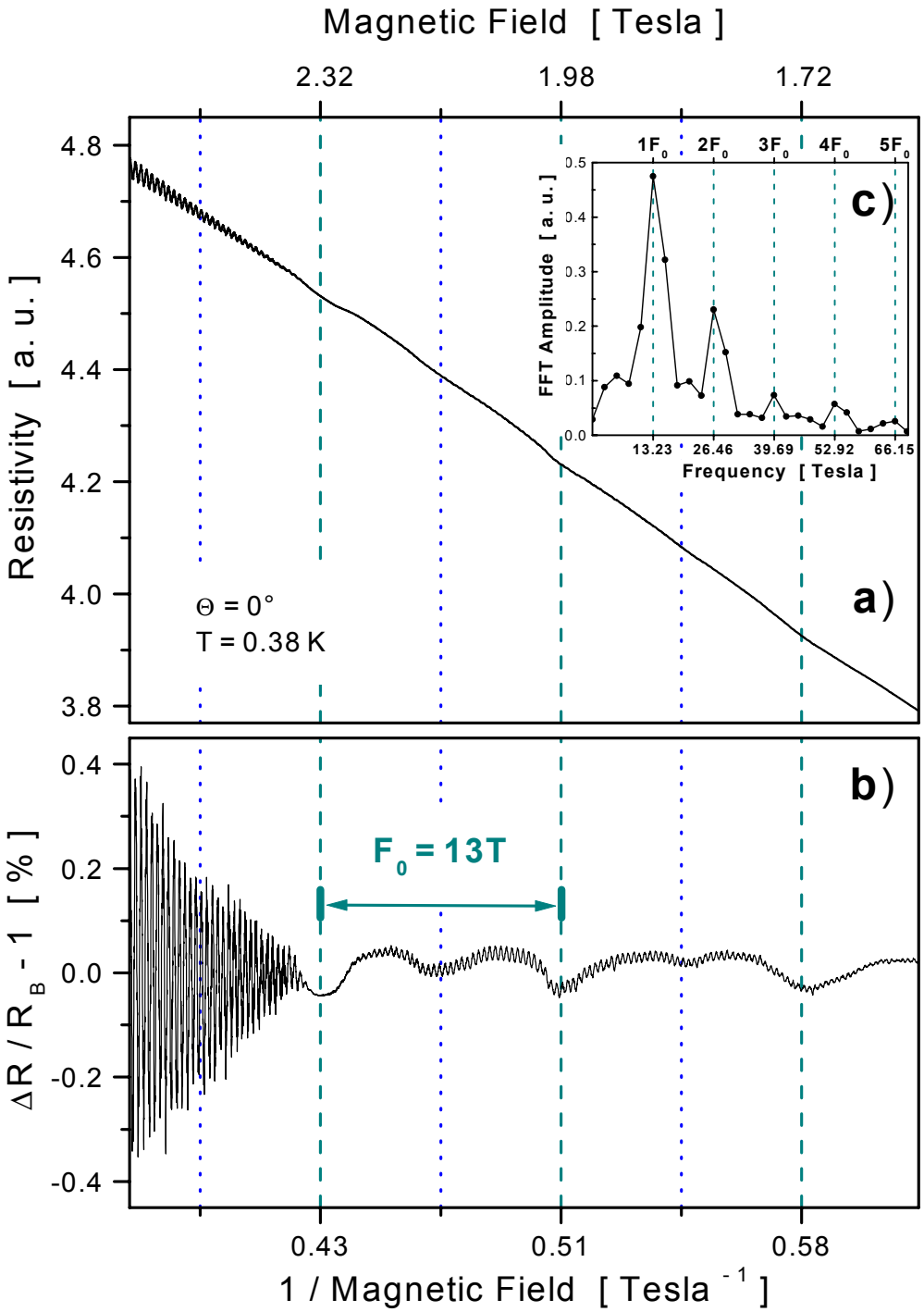

Fig. 5.23: Low-field SdH signal of a κ-(BEDT-TTF)$_2$I$_3$ single crystal at 0.38K and Θ = 0° [413]. **a)** Raw data versus 1/*B*, showing dips which correspond to F_0 = 13T. **b)** The same signal after division by the background. **c)** The Fourier transform of the signal shows F_0 = 13.23T and its harmonics [410].

Further aims of these measurements were **i)** the search for DEs of SdH amplitudes at low fields and **ii)** to extend their investigation to their *field* instead of their temperature dependence. In order to detect even the high-frequency SdH oscillations in best possible

[23] It is recalled that the torque cantilever itself provides a sensitivity which increases linearly with *B*.

resolution down to lowest possible fields, the experiments were carried out with very low field sweeping rates (in the order of 10^{-4} T/s) in steady resistive and superconducting magnets, respectively.
Figure 5.23 shows a low-field SdH experiment at 0° and 0.38K where part a) of the figure shows the raw data [413]. In the steep background resistivity significant dips are observed which occur equidistantly in 1/*B* (stressed by grid lines). This finding is more evident in part b) of the figure, where the signal is plotted after division by the background resistivity. The variation in the depth of the oscillations suggests to recognise a main frequency (blue dashes) which corresponds to F_0 = 13T as well as its spin-split oscillation[24] (green pointed grids). An FFT of the signal (part c)) confirms this finding and shows F_0 as well as its harmonics [410].
The relatively exact value F_0 = 13.23(±0.1)T obtained by the intercept of the dips in the low-field range and is confirmed by the FFT and the slope of the plot of the Landau level indices of F_0 versus 1/*B* [410]. From this value the fermiological data of Tab. 5.7 are obtained.

κ-(BEDT-TTF)$_2$I$_3$	A_{F0} [nm^{-2}]	k_F [nm^{-1}]	**Part of the FBZ**
F_0 = 13,2T	0,13	0,2	$3{,}4*10^{-3}$

Tab. 5.7: Fermiological data for the QO frequency F_0 in κ-(BEDT-TTF)$_2$I$_3$. A_{F0} is the extremal area in *k*-space, k_F is the corresponding Fermi wave vector.

These data illustrate that the closed area A_{F0} corresponding to F_0 represents only a very small pocket of the FS. In view of this it is not very surprising that this closed orbit might be beyond the resolution of standard band structure calculations. It should be mentioned, that a similar low frequency is not yet observed in isostructural organic compounds as, e.g., κ-(BEDT-TTF)$_2$Cu[N(CN)$_2$]Br or, respectively, the Cu(NCS)$_2$ salt. While the occurrence of such a low frequency in the Cu[N(CN)$_2$]Br salt might be a priori excluded by the formation of a superstructure below about 200K [415,416], the presence of such a low QO frequency as F_0 is not excluded in the Cu(NCS)$_2$ material. However, the relatively high B_{c2} value (≈ 6T, [57]) of this material restricts the available field window to about one single complete oscillation with a frequency as low as F_0. This might impede the search for an analogon of F_0 in the Cu(NCS)$_2$ salt.

In the present I$_3$ salt F_0 is observed at 0.4K above about 1.25T (see Fig. 5.24, right). At 2T the SdH amplitudes of F_0 reach about 0.04% of the background resistivity. Above about 2.4T the amplitudes of F_0 could not be observed directly, since the amplitudes of F_2 and F_3 increase strongly with field and dominate over those of F_0 (see Fig. 5.23.b).

[24] The observation of spin splitting shows that the *g*-value of the electrons on this orbit is finite.

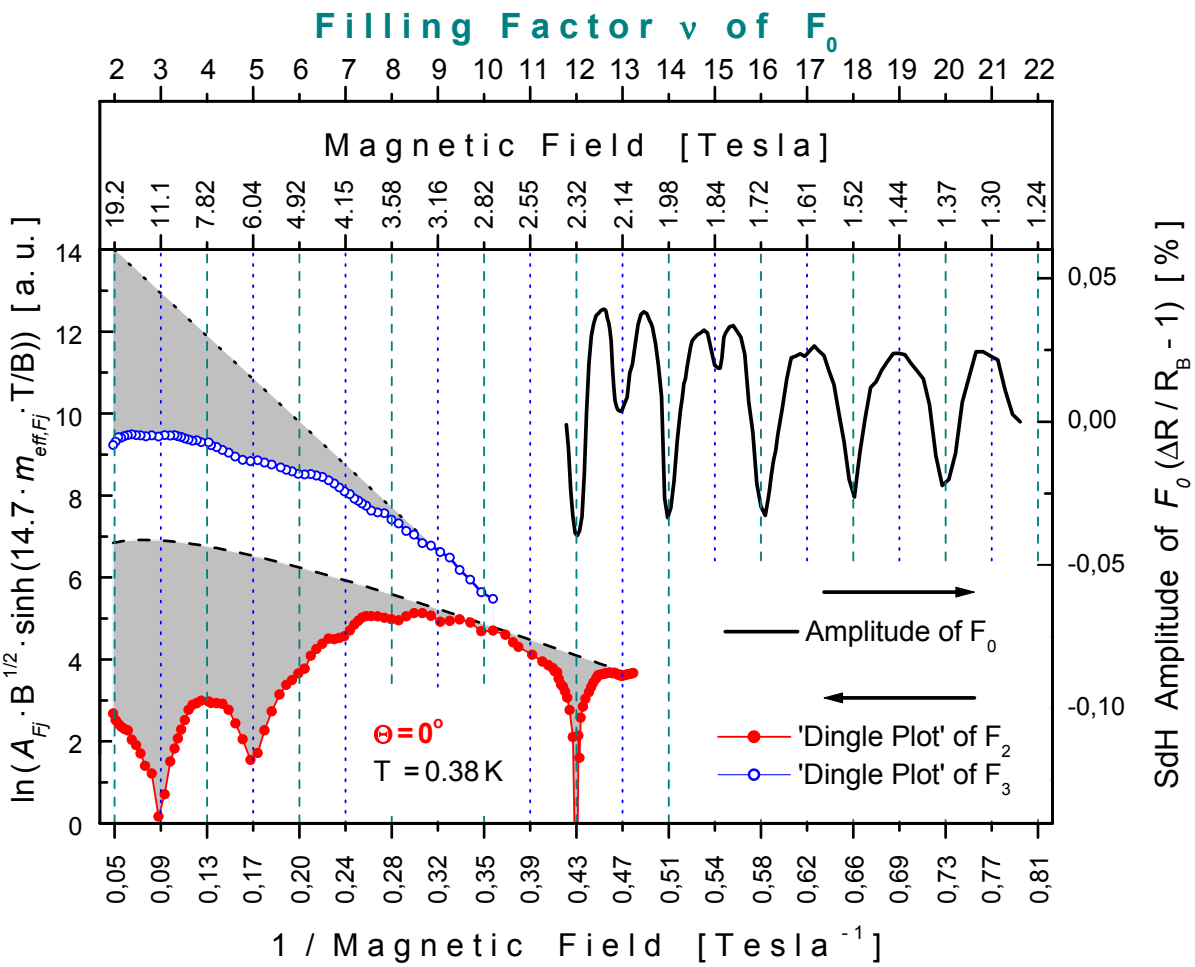

Fig. 5.24: right: SdH oscillations of F_0 in κ-(BEDT-TTF)$_2$I$_3$ single crystals [413]. The filling factor ν of F_0 is indicated on the top axis. **left:** 'Dingle plots' of F_2 and F_3, where A_{Fj} are the respective FFT amplitudes (taken from neighbouring narrow field windows). $m^*_{F2} = 1.9$ whereas $m^*_{F3} = 3.9$ is considered. The estimated dashed and dotted curves represent the expected amplitudes (accounting for magnetic breakdown). The grey-shaded areas represent the magnitude of the damping effects.

However the *action* of F_0 onto the amplitudes of F_2 and F_3 can be unambiguously observed up to high fields. This is illustrated by means of the so-called 'Dingle plots' (DPs) of the implicit values of the FFT amplitudes of F_2 and F_3 (see left y-axis in Fig. 5.24 and Eq. (3.15)) versus $1/B$. In the standard LK theory the slope of a DP should be linear and is a measure for the Dingle temperature T_D and the scattering time τ (see Eqs. (3.14) and (3.15)). In the present case of magnetic breakdown (MB) the LK theory has to be extended by the so-called 'coupled network description' (CND) to take account for the magnetic field dependence of the MB probabilities (see Sec. 3.4.2). According to the LK theory and the CND, the Dingle plot of F_2 should be sublinear, while that of the MB orbit F_3 is expected to be a straight line (the curves are determined by the Dingle temperatures and the magnetic breakdown field B_{MB}). Even though the low field region is least influenced by the anomalous damping effects, it can only hardly be fitted by taking an exaggerated $B_{MB} \approx 4$T and a by far too high $T_D \approx 0.4$K (see dotted curve in Fig. 5.24 for F_2 and dashed line for F_3). This indicates that already at low fields the behaviour of the QO amplitudes can be only hardly described by the LK theory and the CND. At higher fields the discrepancy becomes much stronger. Above 2T the DP of F_2 strongly deviates from the estimated curve (note the logarithmic scale). The DP of F_3 shows strong deviations from linearity above about 4T. At high fields both DPs show strong

damping effects (grey-shaded areas), which can neither be explained by MB, nor by the collection of effects summarised in Sec. 5.3.1.

The most important features in the DPs of both, F_2 and F_3, are revealed by the 'fine structure' of the DPs. These are the discontinuities in their curvature at high fields. For their understanding the field positions of the minima in the SdH signal of F_0 (where the Fermi energy E_F lies just between two successive spin-splitted Landau levels), are marked by grid lines and continued to high fields. The discontinuities and minima in the DP of F_2 show the same oscillatory structure as the oscillations with F_0. They occur just at the field values where the resistance minima of the F_0 oscillations are expected (i.e., where E_F lies between two adjacent spin levels of F_0). The same behaviour (even though weaker in magnitude) is present in the DP of F_3. An oscillatory structure with F_0 is observed in SdH experiments at $\Theta = 0°$ on several crystals [413,414]. By this, F_0 is identified to be directly involved in the damping of the amplitudes of F_2 and F_3. The filling factor ν_{F0} of F_0, as indicated on the top axis, turns out to be a controlling parameter for these effects [410,413]. While the amplitude of F_2 is already damped at $\nu_{F0} < 13$, that of F_3 is first demonstrably damped in the MB regime for $\nu_{F0} < 7$. The magnitude of the damping effects increases strongly with decreasing ν_{F0}. At the highest applied field, $\nu_{F0} = 2$ is reached with only two spin levels of the lowest Landau level of F_0 being occupied below the FS. While F_2 and F_3 are at fairly high filling factors when the damping effects in their amplitudes occur, F_0 is already close to the quantum limit (QL), i.e., at low ν. It is noted that the special situations at inverse field values $B^{-1} \approx 0.43$; 0.17 and 0.09 are discussed later in Secs. 5.5. ff.

The fact that the damping of the amplitudes of F_2 and F_3 are found to be equidistant in $1/B$ might give rise to the question, whether they may be attributed to warping nodes, i.e., a corrugation of the FS with a warping frequency corresponding to F_0. It can be anticipated here, that there are several arguments which clearly contradict to this possibility, so that F_0 has to be attributed to a low-frequency quantum oscillation. Since more appropriate, a discussion of this point is postponed to Sec. 5.5., where further aspects arising in that section can be included in the discussion.

The observation illustrated by Fig. 5.24, that the damping effects of the QO amplitudes of F_2 and F_3 show an oscillatory pattern just with F_0, proves that the electrons of all the corresponding subsystems (i.e., bands) are strongly correlated. This correlation persists even though the involved bands are at very different ν.
This established correlation means in reverse, that the carriers contributing to F_2 and F_3 on the one side are themselves sensitive to the conditions introduced by F_0 on the other side. This makes easier to understand why the filling factor ν_{F0} of F_0 becomes a controlling parameter of the *entire* system and why at high fields it is able to force quantum limit conditions on the entire correlated electronic system.
Two-dimensionality and the obvious presence of electron correlation ask to consider also their consequence, i.e., electron localisation around integer and noninteger low filling factors ν_{F0}. The correlation between the electrons of all orbits prove that such localisation effects may, accordingly, involve all carriers, not only those on the low-ν_{F0} orbit itself.

Based on this the damping effects of the QO amplitudes of F_2 and F_3 may be understood at this stage as a reduction of the carrier number contributing to these QOs, which is caused by

localisation effects, as generated by the low filling factors of F_0 [410,413]. However, before going into detail with the discussion of this point, further decisive results have to be included in the following sections.

Oscillation of the Chemical Potential with F_0

It was already shown in Sec. 5.3.1, that in view of the two-dimensionality of κ-(BEDT-TTF)$_2$I$_3$ oscillations of the chemical potential μ have to be considered. However due to the complexity of the system only those oscillations with the QO frequency F_3 could be treated in the numerical and analytical studies reported in Sec. 5.3.1. Therefore the subsequent, more intensive search for μ oscillations suggested to find a more direct and less lavish approach to $\tilde{\mu}$, whose results are described in the following.
One of the fundamental differences between a well-known semiconducting 2DES and the 2D organic metal κ-(BEDT-TTF)$_2$I$_3$ is the fact that in the former ones all electrons follow one single orbit, whereas in the latter they move on various orbits corresponding to very different QO frequencies. This condition can be excellently used to probe variations of μ with the successive QO frequencies. The huge difference between the frequency values of F_0, F_2 and F_3 themselves allow to use the high-frequency QOs as a 'high-resolution' sensor, which probes the actual position of μ as well as its low-frequency variations, if present.

In order to investigate the behaviour of μ in κ-(BEDT-TTF)$_2$I$_3$ more thoroughly, the successive field positions B_n were determined, at which the actually highest occupied n^{th} Landau cylinder (LC) of a certain frequency (here, e.g., F_3) passes the Fermi cylinder (see Fig. 5.25). The corresponding Landau level indices n_{F3} can be obtained as a result of Landau quantisation by a variation of Eq. (3.18), i.e.,

$$\frac{F_3}{B_{n,F_3}} = n_{F_3} + \tfrac{1}{2}. \qquad (5.6)$$

With the exact F_3 and n_{F3} values obtained from Fig. 5.8 and with

$$\mu = (n_{F_3} + \tfrac{1}{2})\left(\frac{e\hbar B_{n,F_3}}{m^* m_e}\right), \qquad (5.7)$$

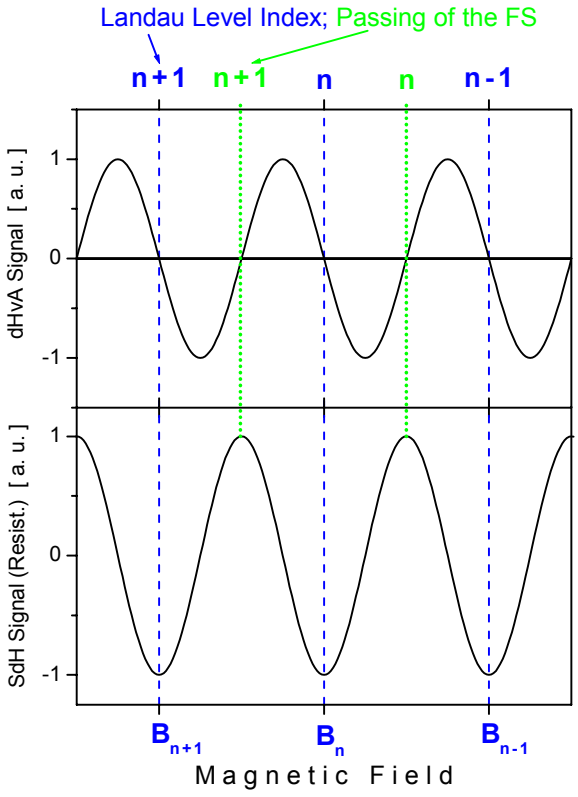

Fig. 5.25: Determination of the Landau level index n from a dHvA oscillation (**top**) and from a SdH oscillation (**bottom**). Both curves are simulations.

the actual position of μ can be obtained according to Eq. (5.7) simply by 'filling' the corresponding band by (n_{F3} + 1/2) Landau levels with a spacing of $\hbar\omega_c$. By this procedure, the QOs with F_3 as well as those with F_2 can be utilised as 'sensors' to probe the actual position of μ [414].

In a 3D system, where μ is practically fix, the sequence of B_n is prescribed to be exactly equidistant in 1/B (see, e.g., [87]). In a 2D system however, where μ itself oscillates, Landau quantisation directly connects these μ oscillations with a variation of the field positions of the successive B_n. In reversal of this, the detection of the successive B_n in a wide field range can be used to determine not only the actual position of μ but also its variation from the steady average value. In a system with several different QO frequencies this allows the use of the successive field positions of, e.g., a *high*-frequency QO as a 'sensor' in order to probe the actual position of μ and all its variations with frequencies *lower* than the 'sensor' frequency. Thus in our case the QOs of both, F_3 as well as F_2, can be used to investigate the low-frequency variations of μ by use of Eq. (5.7). In order to obtain μ with 'highest possible resolution', i.e., for most narrow field values, we started by using the F_3 oscillations as 'sensor', since these are most narrow to each other. By detection of the successive $B_{n,F3}$ over a wide field window, the field dependence of μ was obtained by Eqs. (5.6) and (5.7) and the result is plotted in Fig. 5.26 after normalization by the steady part $\mu_{St,F3}$ = 114 meV for F_3 (Tab. 5.6).

The curve obtained from SdH measurements at Θ = 0° (curve a)) shows pronounced sawtooth oscillations of μ above about 6 T with an oscillatory sequence corresponding just to the low QO frequency F_0 = 13 T (called $\tilde{\mu}_{F0}$ in the following) [414]. The filling factor ν_{Fo} and the corresponding magnetic field values are plotted on the top axes of the figure. At lower fields 6T ≥ B ≥ 3.8T even a further oscillatory structure of $\tilde{\mu}_{F2}$ with F_2 is indicated. However the discussion of this low field region would require the detailed consideration of the coincidence of $\tilde{\mu}_{F2}$ and magnetic breakdown and is therefore skipped here. After verification of being deep enough in the complete MB region [414], the subsequent measurements were focused on B ≥ 6T (i.e., above the MB) for further investigations of $\tilde{\mu}_{F0}$.

For comparison with the results in Fig. 5.26.a obtained with F_3 as a 'sensor', as next F_2 and its sequence $B_{n,F2}$ were used in the same way for the determination of μ. The high field part of the result above the MB is plotted in Fig. 5.26.b after rescaling by the steady part $\mu_{St,F2}$ = 35 meV (see Tab. 5.6). It confirms the behaviour shown in Fig. 5.26.a. The results in both parts a) and b) were obtained from SdH, i.e., transport measurements. In order to verify this finding, we investigated μ also by dHvA experiments, which directly probe the thermodynamics of the system [87]. As aforementioned, the dHvA torque signal vanishes at 0° itself for reasons of band structural symmetry. In the dHvA experiments best conditions for the detection of F_3 were given at 9° and for F_2 at 16°, respectively. The obtained results were rescaled to Θ = 0° by the 1/cosΘ - law valid for 2D systems. Figure 5.26.c shows the normalized $\tilde{\mu}$ from dHvA experiments at 9° determined by investigating the field positions $B_{n,F3}$ of the F_3 oscillations, while Fig. 5.26.d shows $\tilde{\mu}$ as obtained by the F_2 oscillations at 16°. Both show a low-frequency oscillatory structure $\tilde{\mu}_{F0}$.

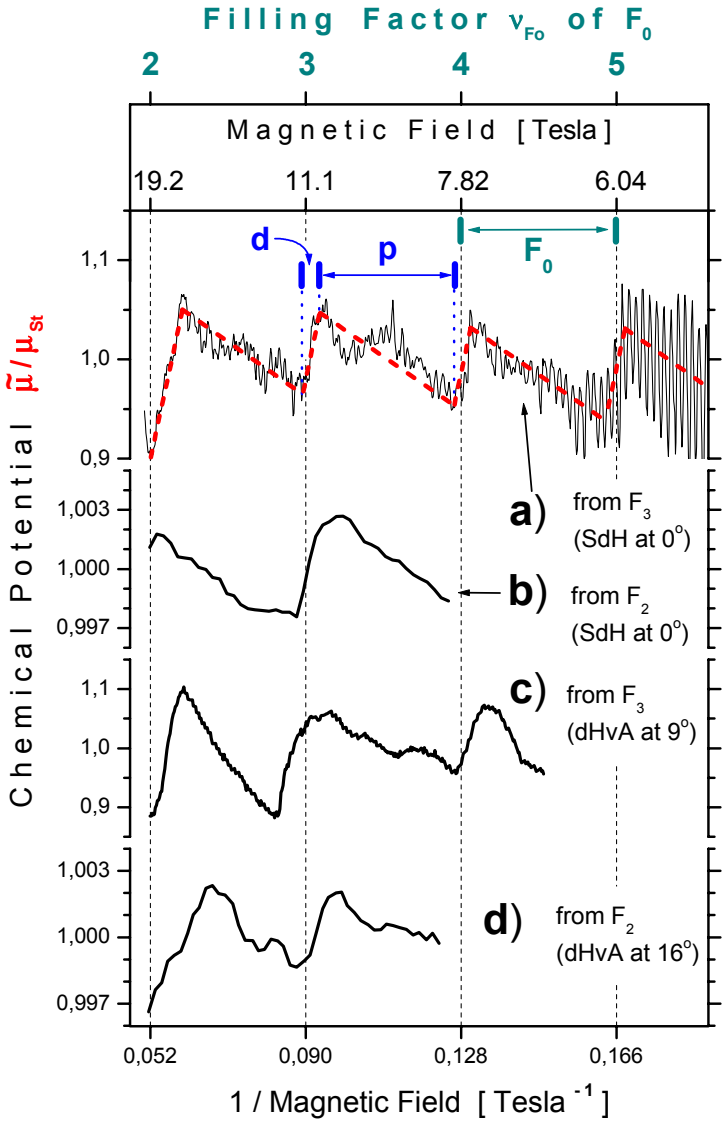

Fig. 5.26: Quantum oscillations of the chemical potential $\tilde{\mu}_{F0}$ with F_0 at 0.38K, where $\tilde{\mu}_{F0}$ is rescaled by the steady part μ_{St} (see text). $\tilde{\mu}_{F0}$ was obtained from SdH experiments at Θ = 0° (parts **a)** and **b)**), and from dHvA measurements at 9° and 16° (parts **c)** and **d)**), respectively [414]. The latter results were rescaled to Θ = 0° by the 1/cosΘ - law valid for 2D systems. The red dashed line in part **a)** is a guide to the eye. During the field window '**p**' μ is pinned to a Landau level of F_0, whereas during '**d**' it drops down to the very next occupied LL on the FS (discussion see Sec. 5.8.1).

At first these results show the power of the detection method introduced in [414]. By simply filling the corresponding band according to Eq. 5.7 with the n actual LLs as detected by the 'sensor' one obtains the correct values for the Fermi energies (113meV and 35meV, respectively), which means in reverse that both, n_{Fj} as well as m^*_{Fj} are obtained correctly by QO experiments. This shows that even in a rather complex system with several orbits present the method applied here is very sited to probe the actual position of the chemical potential as well as its variations with magnetic field.

At this point the results reveal further important aspects.
1) In Fig. 5.24, F_0 could not be detected above about 2.3T due to its low amplitude compared with the other QOs as well as the background resistivity [413]. In contrast, the μ oscillations

with F_0 shown in Fig. 5.26 represent the first detection of F_0 above 2.3T up to high fields, where the concomitant damping effects in the SdH oscillations are prominent.
2) The μ oscillations with F_0 prove the presence of both, a corresponding Landau cylinder structure and a closed orbit on the FS.
3) The results from both, transport (SdH) as well as thermodynamic (dHvA) measurements in Fig. 5.26 confirm the realisation of low ν and their importance in κ-(BEDT-TTF)$_2$I$_3$.
4) The fact that 'sensors' as the F_2 and F_3 oscillations, are able to probe results of F_0 confirms, that the electrons on the F_0, F_2 and F_3 orbits are correlated.
5) The very different filling factors of the 'sensors' F_2 and F_3 and the correlated 'object', i.e., F_0 proves that electron correlation (EC) bridges the very different ν and that EC is operative even at very high ν of F_2 and F_3.

Before going into further discussion, very recent investigations are included in the following. They are results of experiments motivated by an open question as invoked by Fig. 5.24: In the left part of the figure the Dingle plot of F_2 shows strongest damping effects at ν_{F0} = 3, 5 and 12. Even if at first glance they seem to be connected with the filling of F_0, they cannot be attributed in a simple way to this QO frequency, since they are by far stronger than the DEs at neighbouring filling factors ν_{F0}. At a first glance the DEs at ν_{F0} = 3 and 5 might be attributed to strong spin polarisation and proximity to quantum limit, but the strong amplitude reduction at ν_{F0} = 12 clearly contradicts to both these possibilities. The strength of these features gives rise to the question whether they may have a common origin. After vain attempts to find a conventional explanation, this latter possibility was taken up, i.e., that a further low-frequency QO might be present in κ-(BEDT-TTF)$_2$I$_3$, from which only the lowest LL may be observed at high fields.

5.5 The New Quantum Limit QO Frequency F_{new} = 3.8T

The pursue of the possibility that a further low-frequency oscillation might be present in κ-(BEDT-TTF)$_2$I$_3$, required to extend the SdH experiments far into the low-field range. They were enabled by decreasing T to dilution temperatures. It should be emphasised that this field region covers the magnetic breakdown between the closed F_2 orbit and the open F_3 orbit (see Fig. 5.10). For this reason the oscillations of the F_3 orbit are a priori excluded in the following investigations of the strong damping effects, since at these fields the F_3 orbit is not properly quantised and its investigation would be influenced by MB effects..
On several κ-(BEDT-TTF)$_2$I$_3$ single crystals field sweeps of very low sweeping rate were carried out at field orientation perpendicular to the conducting planes (i.e., 0°±0.04°) in superconducting and steady resistive magnets. The results are discussed in the present section. In Fig. 5.27 a typical result is confronted with the Dingle plot of F_2 from Fig 5.24.
At first the experiments on a number of crystals (as shown in the following) establish that the Dingle plots show consistently the patterns of strongest damping effects at certain field values and that these patterns have a common origin. At second, the low-field part of the detected DPs show a new oscillatory structure with a frequency of 3.8(±0.3)T, called F_{new} in the following (see also Figs. 5.28 - 5.30) [491]. The corresponding frequency is confirmed in the FFT of the SdH signal in the inset of Fig. 5.27. The results are confirmed on several additional single crystals from different batches of which a few are included in the subsequent figures. They show clearly that the strongest damping effects are governed by the

oscillatory structure with F_{new}. It is indicated that the discussion of the high field part of the signals is postponed to Sec. 5.8.

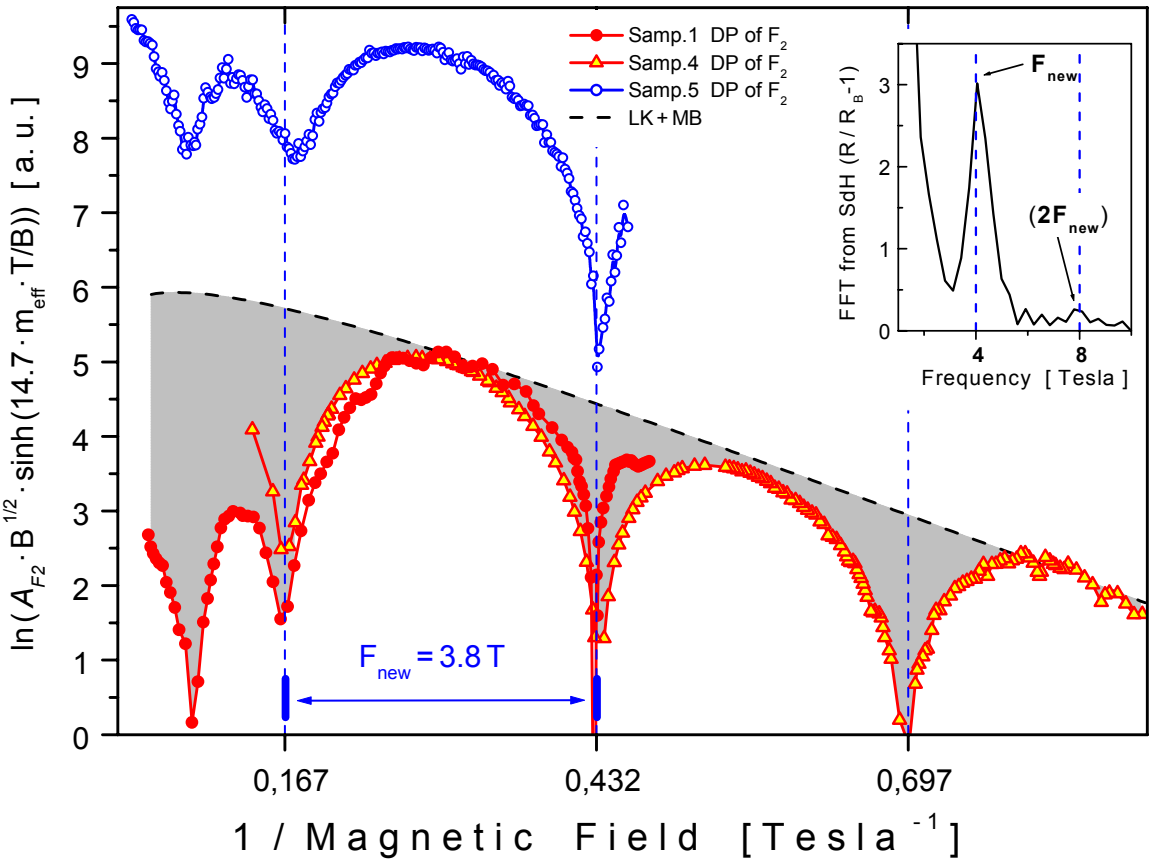

Fig. 5.27: Dingle plots of the F_2 FFT amplitudes A_{F2} of two κ-(BEDT-TTF)$_2$I$_3$ single crystals at Θ = 0° (the FFT amplitudes were obtained from SdH oscillations in narrow neighbouring field windows). The dashed line recalls the behaviour expected by standard LK theory including the magnetic breakdown by the coupled network description (CND). The parameters are T_D = 0.03K, B_{MB} = 2T, T = 380mK (Samp.1), 60mK (Samp. 4), 30mK (Samp. 5). The grey-shaded area illustrates the damping effects. The curve for Samp. 5 is offset for clarity. The inset shows the FFT of a SdH signal of Samp. 4 from a field window between 0.8T and 10T.

On the search for an angular dependence of the low-frequency oscillations F_{new} = 3.8T and F_0 = 13T, the whole angular range 0° < B ≤ 90° was examined with special focus on Θ = 90°. This was done in reminiscence to the Θ-phase of (BEDT-TTF)$_2$I$_3$, where a small pocket is likewise present (see Sec. 6.2.5). However in the latter material the low-frequency oscillation is also observed when B is aligned parallel to the conducting planes [421], which corresponds to 90° in the present notation. Therefore the low-frequency oscillation in Θ-(BEDT-TTF)$_2$I$_3$ was attributed to a 3D pocket of the FS. In contrast, in κ-(BEDT-TTF)$_2$I$_3$ the oscillatory structure with F_{new} and that with F_0 where observed exclusively at 0°. This means that the behaviour of both, F_{new} and F_0 in the present material is not that of a 3D pocket of the FS.

The further interpretation of the results of Secs. 5.4 and 5.5 in terms of the role of F_0 and F_{new} needs however the clarification of a decisive question, inserted in the following.

Could the Oscillations with F_0 = 13T and F_{new} = 3.8T be Generated by Warping

The search for an interpretation of the oscillatory structures with F_0 and F_{new} gives new rise to the question, whether they might be generated by a warping of the FS. In such a case the damping effects, showing structures of these frequencies, may be simply understood as warping nodes (see Fig. 3.6) as described in Sec. 3.4.3. This possibility is discussed in the following.

As shown in Fig. 3.5.a, a warping of the FS means that different extremal areas A_{Min}, A_{Max} are present on the FS. They correspond to distinct QO frequency values $F_{j,Min}$, $F_{j,Max}$ which differ just by the value of the warping frequency ΔF. Hence, assuming a warping, ΔF would be just 13T or 3.8T, respectively. In the case of a warping the total amplitude of a QO is a superposition of the contributions of $F_{j,Min}$ and $F_{j,Max}$, respectively, which enters into the LK formula (Eq. (3.9.a)). In consequence the field dependence of the QOs shows warping nodes with a field intercept (in $1/B$) which corresponds to ΔF.

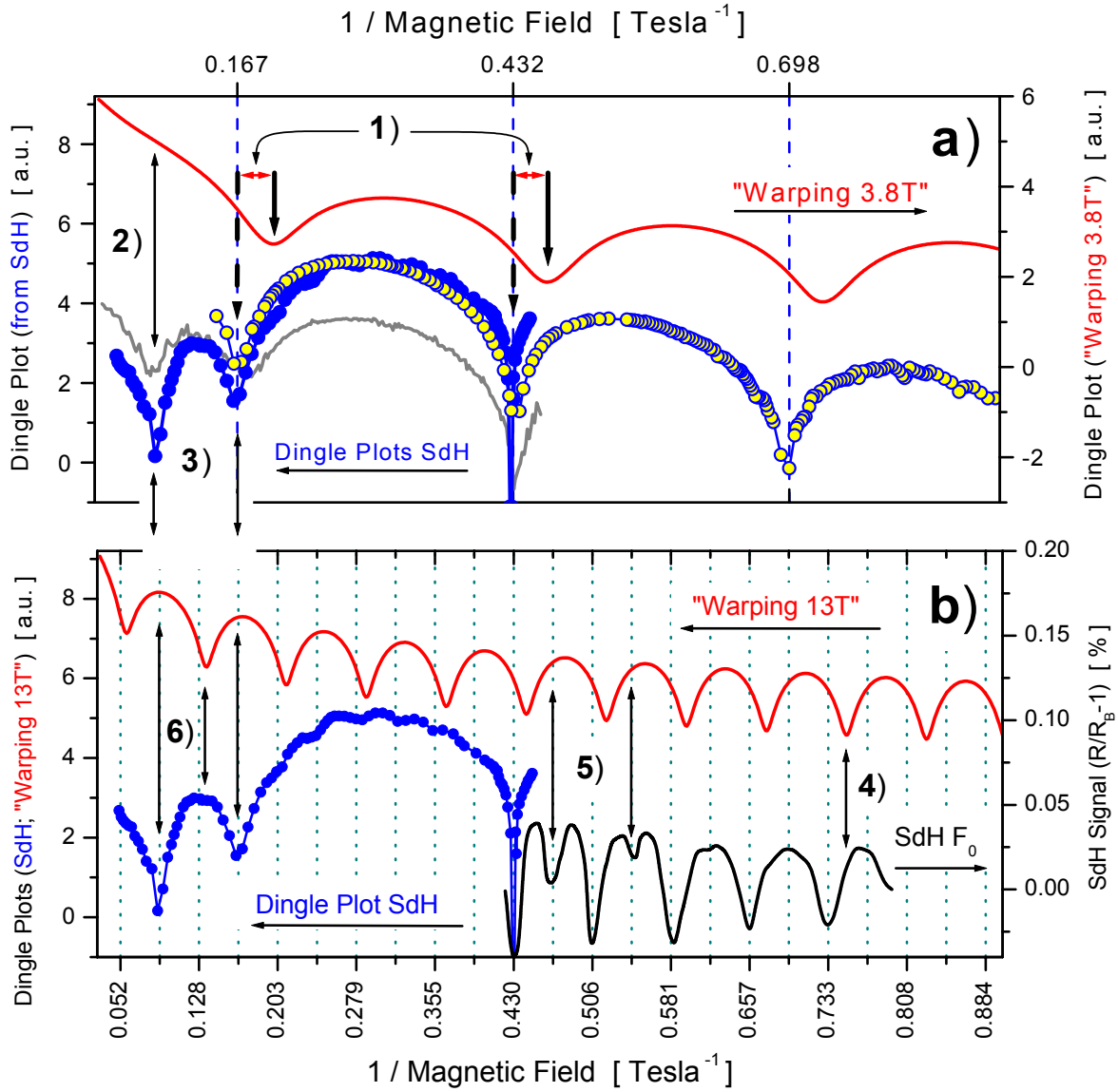

Fig. 5.28: Dingle Plots (DPs, blue and grey curves) and SdH oscillations (black curve) of κ-(BEDT-TTF)$_2$I$_3$ single crystals (from Figs. 5.24 and 5.27) at Θ = 0°. These experimental results are confronted with DPs of simulated quantum oscillations (red curves) with an assumed warping of 3.8T (**part a)**) and 13T (**part b)**). The vertical arrows show selected situations showing that experiments and simulations do not correspond. They show that the anomalous damping effects cannot be explained by warping (discussion see text).

In order to verify this, the general treatment for a warping shown in Fig. 3.6 was carried out in the present situation for all combinations, i.e., $F_j = F_2$ and F_3, whereas ΔF = 13T and 3.8T, respectively. The results are shown in Fig. 5.28. The two parts of Fig. 5.28 compare experimental results, i.e., Dingle plots and SdH oscillations at $\Theta = 0°$ (from Figs. 5.24 and 5.27) with DPs of simulated quantum oscillations, where a warping was assumed. Part a) of the Fig. 5.28 represents the situation for an assumed warping of 3.8T and part b) for 13T.
It can be anticipated that there are a number of arguments (going beyond those collected in Sec. 5.3.1), even each argument taken for itself, show that the strong damping effects of SdH oscillations at 0° cannot be explained by a warping of the FS by 3.8T and/or 13T, respectively. Some of these aspects are listed in the following and refer to the vertical arrows in the figure, which illustrate the discrepancies between simulations and experiments.
Before going into discussion, it might be necessary to recall that, according to Landau quantisation, the phase of a QO with a frequency F_j is prescribed except for an absolute phase, which may be regarded as a 'free' parameter in the simulations. This absolute phase may drift merely *within* one single oscillation of F_j itself [87]. This restriction persists in the case of warping and the involved maximum and minimum of the FS enter the LK formula (Eq. 3.9) only with a phase of $-\pi/4$ and $+\pi/4$ of a single oscillation of F_j. In consequence, the *field positions* of the warping nodes in the QOs (Fig. 3.6) and in the Dingle plots are prescribed a priori by the warping frequency ΔF and can only be varied *within* one oscillation of the fundamental frequency F_j itself, i.e., in a very narrow field window. This means that in Fig. 5.28 the field positions of the minima in the simulated Dingle plots are prescribed in x-direction by the assumed warping frequency ΔF except for a 'free' shift, which is however less than the thickness of a dashed grid line.

i) The simulated DP in Fig. 5.28.a with an assumed warping with ΔF = 3.8T (red curve) shows warping nodes at field positions, which clearly do not correspond to the observed minima in the measurements (see Pos. 1) in the figure). It should be emphasised that this shift exceeds the above mentioned limit by orders of magnitude.
ii) In high fields a strong damping minimum is observed in the experiments (see 2)), which contradicts to the continuously increasing DP as predicted by a warping with 3.8T.
iii) Warping nodes must be equidistant in $1/B$, whereas the observed DPs clearly break this sequence at high B. A warping with 3.8T forbids *any* node for $1/B < 0.2\text{T}^{-1}$ (see 2)).
iv) Likewise, the high field damping minima in the Dingle plots (see 3)) cannot be explained by an assumed warping with ΔF = 13T (red curve Fig. 5.28.b), which prescribe amplitude maxima at these field positions. This shows together with ii) and iii), that even a possible superposition, i.e., a double warping by 3.8T as well as 13T (which might be supposed on different parts of the FS), cannot explain the high-field damping minima in the detected DPs.
v) An assumed warping with 13T (red curve Fig. 5.28.b) shows also a significant phase shift (see 4)) with respect to the SdH oscillations (black curve), exceeding by far the above mentioned limit.
vi) A warping with 13T would not reproduce the spin splitting pattern of the SdH curve (see 5)).
vii) A 13T warping would place amplitude *maxima* just at the damping *minima* of the detected DPs and vice versa (see 6)).
viii) Moreover, an assumed warping with 3.8T would comprise about 1000 Landau levels of F_3 (whereas a 13T warping would include 300). This means that the warping is much bigger than LL spacing which itself is much bigger than k_BT (otherwise QOs with F_3 would be not

observable). Hence the assumed warping would exceed the thermal energy by orders of magnitude. Therefore such a warping could never influence the temperature dependence of the QO amplitudes so that it could never be the origin of the observed strong damping effects.

In addition to these arguments, the entire set of aspects collected in Sec. 5.3.1 apply also in the present situation. They all prove that the strong anomalous damping effects of the SdH amplitudes at high fields, low temperatures and $\Theta = 0°$ cannot be explained by a warping of the FS.
These results suggest to attribute the oscillatory structure with F_{new} = 3.8T to a new quantum oscillation. Comparative measurements on different crystals yield values F_{new} = 3.8(±0.08)T. The fermiological data corresponding to F_{new} are given in Tab. 5.8.

κ-(BEDT-TTF)$_2$I$_3$	A_{Fnew} [nm^{-2}]	k_F [nm^{-1}]	**Part of the FBZ**
F_{new} = 3,8T	0,036	0,11	$1*10^{-3}$

Tab. 5.8: Fermiological data for the QO frequency F_{new} = 3.8T in κ-(BEDT-TTF)$_2$I$_3$. A_{Fnew} is the extremal area in k-space, k_F is the corresponding Fermi wave vector [491].

These data show that the extremal area A_{Fnew} is very small, representing merely 10^{-3} of the first Brillouin zone (FBZ). In view of this it is not surprising that the small pocket corresponding to F_{new} is not yet found by band structure calculations.
Asking for a possible realisation for F_{new}, two aspects are briefly discussed here. At first, the fact that an oscillatory structure with F_{new} is observed at lowest field (actually $B \geq 0.8$T), where only F_2 is also present, shows that F_{new} cannot be understood as the result of a resonance effect between several present QO frequencies.
At second, the possibility was followed, whether F_{new} might be the result of a so-called geometrical resonance [32] between *open* orbits. This effect is generated in quasi-1D charge-transfer salts by electrons moving on the 1D wavy trajectory along $\boldsymbol{c}^*$ (see Fig. 5.10) As a result they oscillate in real space and may tunnel to the neighboring 1D trajectory at certain magnetic field values, where the amplitude of their oscillating motion in real space is commensurate with the lattice parameter. Such a geometrical resonance is discussed in connection with the quasi-1D CT-salt (TMTSF)$_2$ClO$_4$, where the respective trajectory in fact is an open orbit. In contrast to that, in κ-(BEDT-TTF)$_2$I$_3$ the trajectory along $\boldsymbol{c}^*$ is part of a closed orbit above about 3T, so that the above mentioned conditions are not given here, least of all at high fields. In addition it is argued that such a geometrical resonance would require a strong anisotropy *within* the 2D conducting plane. This requirement is not given in the case of the present I$_3$ salt, where nearly isotropic electronic properties are observed within the conducting (b,c)-planes (see Sec. 5.1 and [147]). Therefore a geometrical resonance has to be excluded as an explanation for F_{new} (and for the same reasons it was also excluded as an origin for F_0 in [410]). Hence the origin of the closed orbit corresponding to F_{new} remains to date an open question and gives motivation for refined band structure calculations.

A further argument which proves that F_{new} indeed corresponds to a quantised orbit, is given in the following section.

5.6 Oscillations of the Chemical Potential With the Quantum Oscillation Frequency F_{new} = 3.8T

In order to verify the presence of a Landau level structure corresponding to F_{new} by a thermodynamic property, the position of the chemical potential μ and its variation was probed by the method described in Sec. 5.4. For the same arguments as discussed there, the QOs with F_2 where taken as 'sensor' oscillations to probe μ. The results obtained on different crystals by SdH measurements at $\Theta = 0°$, are shown in Fig. 5.29.
The data in Fig. 5.29 show in very good agreement an oscillatory structure with F_{new}. This shows that F_{new} indeed corresponds to a thermodynamic quantity and confirms that F_{new} can be identified with a quantised orbit on the FS and a Landau level structure. It should be emphasised that the μ oscillations with F_{new} (called $\tilde{\mu}_{Fnew}$ in the following) draw a sharp sawtooth with its steep flank at the high-field side, as expected for μ oscillations in an almost ideal 2D system.
Questions arising on the high-field pattern in $\tilde{\mu}_{Fnew}$ are clarified in the following section.

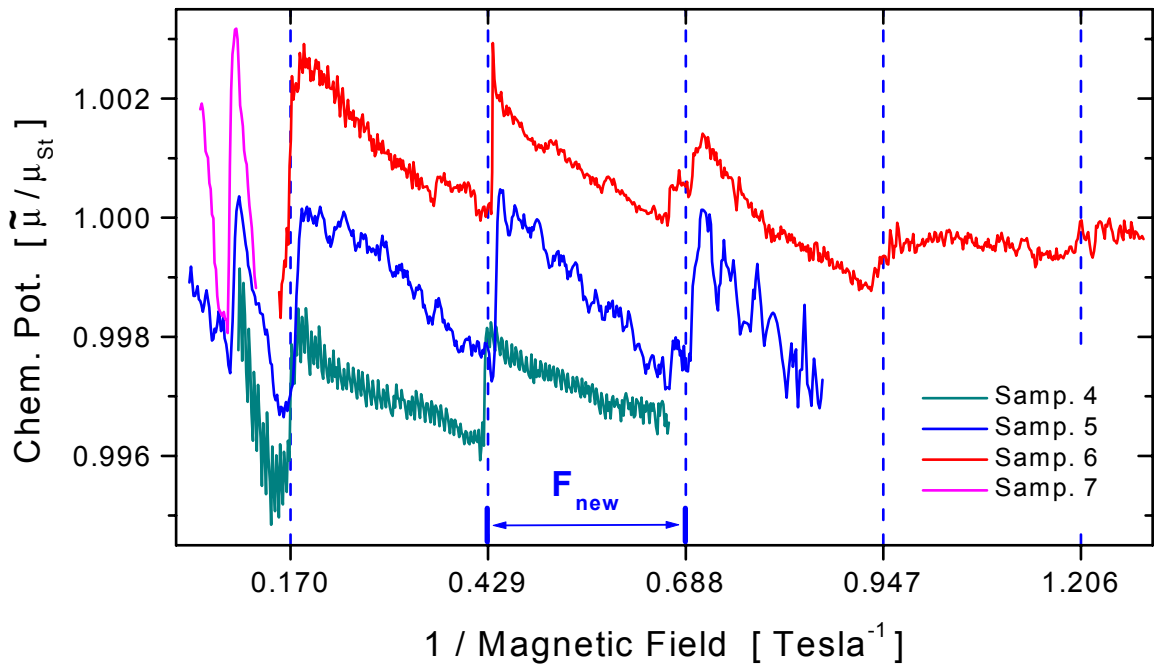

Fig. 5.29: Quantum oscillations of the chemical potential $\tilde{\mu}$ with F_{new} in κ-(BEDT-TTF)$_2$I$_3$ at $\Theta = 0°$ as observed by SdH experiments on different single crystals. (Sample 4: T = 60mK, Samp. 5: 30mK, Samp. 6: 60mK, Samp. 7: 400mK). The curves are rescaled by the steady part of μ (i.e., μ_{St}) and offset for clarity.

5.7 Connection Between the Damping Effects and the Filling Factors of F_{new}

In the following figure 5.30 the Landau level filling factors ν_{Fnew} are attributed to the QO frequency F_{new}, which is identified in Figs. 5.27-5.29 by SdH measurements at $\Theta = 0°$. The low frequency value of 3.8T itself and Eq. (3.18) make clear that quantum limit (i.e., $\nu_{Fnew} = 1$) is reached in available magnetic fields. Therefore $\nu_{Fnew} = 1, 2, 3, 4$ can be easily

related to the equidistant oscillatory pattern of $\tilde{\mu}_{Fnew}$. This relation is unambiguous, since no further Landau level can be placed between the field position of the innermost LL, i.e., $\nu_{Fnew} = 1$ and infinite field (i.e., $1/B = 0$) [491].

Part a) of Fig. 5.30 shows the attribution of the LL filling factors ν_{Fnew} of F_{new} to the sawtooth chemical potential oscillations discussed in Fig. 5.29. Quantum limit (QL), i.e., $\nu_{Fnew} = 1$ is reached at about 0.171T^{-1}, i.e., 5.85(±0.3)T (cons. Fn. [25]). The equidistant sawtooth track of μ_{Fnew} fits perfectly to the equidistant LL spacing of F_{new} between $\nu_{Fnew} = 1$ and 4.

However at higher fields, i.e., $\nu_{Fnew} < 1$, two fundamental circumstances preset the interpretation of this extreme quantum limit region. At first and as already mentioned, $\nu_{Fnew} = 1$ is unambiguously identified, since no further assumed LL can be placed equidistantly at higher fields, i.e., on the left-hand side of $\nu_{Fnew} = 1$ in Fig. 5.30.a.

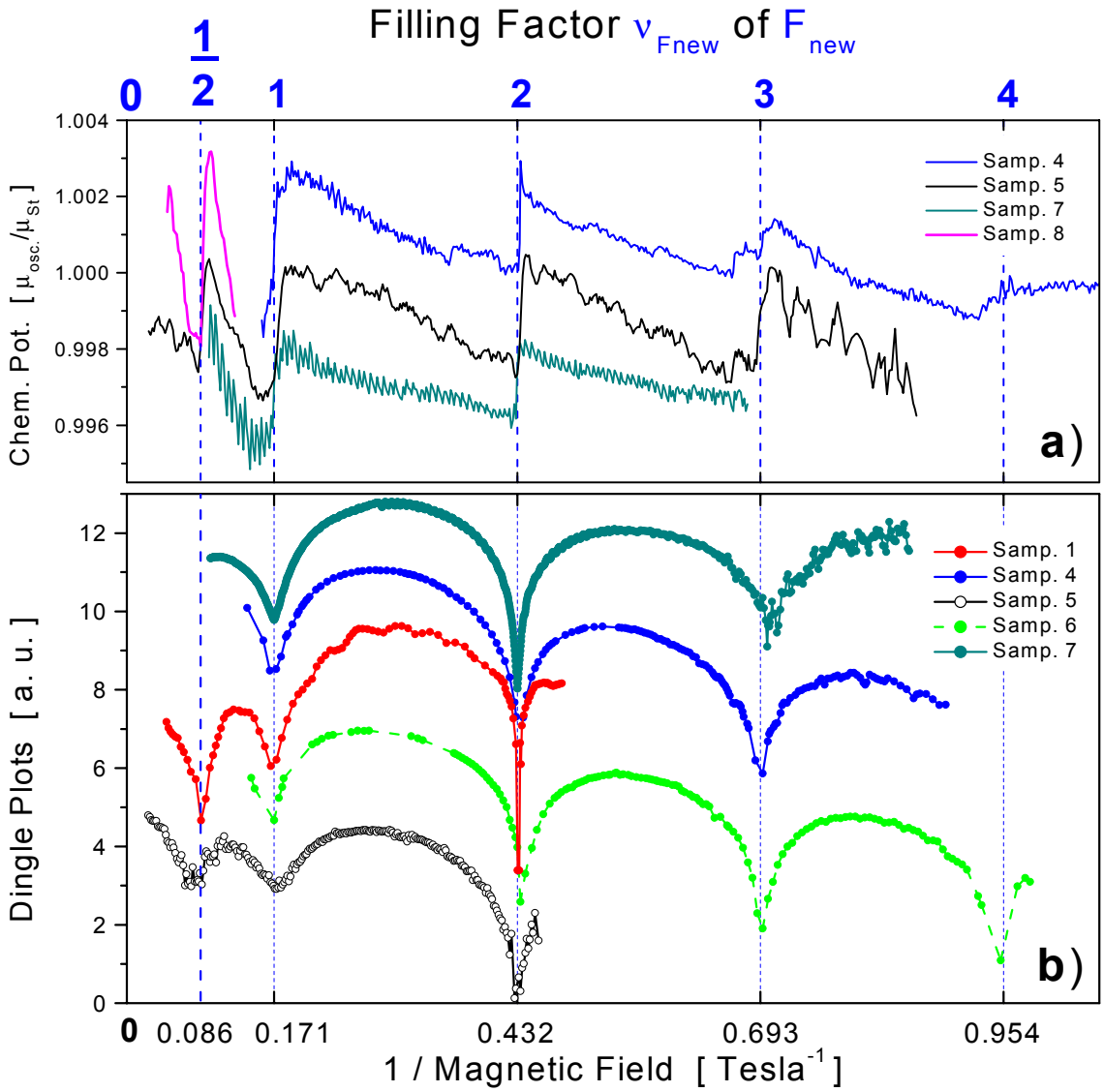

Fig. 5.30: Identification of Landau level filling factors ν_{Fnew} of F_{new} in the 2D multilayer organic metal κ-(BEDT-TTF)$_2$I$_3$. **a)** Chemical potential oscillations detected on different single crystals versus ν_{Fnew} (see Fig. 5.29). **b)** Dingle plots from different single crystals as obtained by SdH measurements at $\Theta = 0°$ (see also Figs. 5.27 and 5.28). Note that the *x*-axes of both, a) and b), end up at infinite magnetic field, i.e., $\nu \equiv 0$ [491].

[25] The error bar refers to the values obtained from different crystals.

At second, the left margin of Fig. 5.30 is given by $1/B = 0$, i.e., infinite field. This means according to Eq. (4.3) that $\nu \equiv 0$ there. These two definite circumstances require that in this extreme QL the LL filling ν_{Fnew} is to be defined in rational parts of this *remaining* field intercept between $\nu_{Fnew} = 1$ and 0, which covers $\Delta[1/B] = [0T^{-1}, 0.171T^{-1}]$. This reveals that the additional sawtooth oscillation at $1/B = 0.086T^{-1}$ (i.e., $B = 11.6(\pm0.5)$T) occurs at exactly $\nu_{Fnew} = ½$ in this multilayer 2D system [491]. The fact that the thermodynamic property μ oscillates at $\nu_{Fnew} = ½$ strongly indicates the existence of a thermodynamically stable state there. The presence of this state is also observed by strong damping effects of the SdH oscillations at $\Theta = 0°$ at $\nu_{Fnew} = ½$, as illustrated by the Dingle plots of several crystals in Fig. 5.30.b. Likewise, the integer $\nu_{Fnew} = 1$ - 4 can be identified in the Dingle plots as just those field regions where the damping effects of the SdH oscillations at 0° are strongest (note that strong DEs are observed even at $\nu_{Fnew} = 4$, i.e., at about 1T).
These results reveal that in the 2D multilayer organic metal κ-(BEDT-TTF)$_2$I$_3$ low integer ν and, moreover, $\nu_{Fnew} = ½$ are present. Furthermore the results show that the strongest damping effects in the SdH oscillations at 0° are correlated just with the low integer and fractional ν in this 2DES.

On the one hand, these most recent results and the rather detailed 'background' investigations discussed in the present section, ask for further extensive efforts for their detailed understanding. On the other hand, the preceding sections have certainly shown that κ-(BEDT-TTF)$_2$I$_3$ is in many fundamental aspects very different from the widely investigated semiconducting single-layer 2DES. The most unpleasant result of this is, that actually there is a very limited scope of theoretical descriptions, which may be applied for an at least qualitative understanding of the electronic properties of κ-(BEDT-TTF)$_2$I$_3$. This is one of the reasons, why the electronic properties of this 2DES in high magnetic fields is far from being completely understood to date.
However, the experimental results were found to be in agreement with a number of fundamental aspects found in experiments and theoretical descriptions for semiconducting 2DES. Therefore these properties may be understood even satisfactorily within this framework. A discussion of the most important results is given in the following section. Besides this, open questions are not concealed, where further experimental but especially theoretical work is required. It is attempted to include information which may be stimulating for this further work.

5.8 Indications for Fractional and Low Integer ν in the 2D Multilayer Organic Metal κ-(BEDT-TTF)$_2$I$_3$ and Its Consequences

The results of the preceding sections show the presence of the fractional filling factor $\nu_{Fnew} = ½$ as well as low integer filling factors $\nu_{Fnew} \leq 4$ and $\nu_{F0} \leq 12$ in the 2D multilayer organic metal κ-(BEDT-TTF)$_2$I$_3$.
One of the most exciting results in this context is the observation of the $\nu = ½$ state, whereas the single-layer fractional states of highest hierarchy, i.e., $\nu_{Fnew} = 1/3, 2/3, ...$ (see Fig. 4.10) are not observed here. This is however not surprising in view of the fact that κ-(BEDT-TTF)$_2$I$_3$ is a multilayer 2DES.
The present layered organic metal belongs undoubtedly to the category of coupled-multilayer systems with finite tunnelling (case c) in sec. 4.2.8). The existence of tunnelling is proven by,

interlayer thermopower (Fig. 5.2), interlayer metallic resistivity (Fig. 5.1) (for both see [145]) as well as coherent interlayer transport at field orientation parallel to the planes [420].
The results shown in the preceding sections agree with the behaviour expected for the case of coupled 2D layers with finite tunnelling in the following features:

1) The state of fractional quantisation at $\nu = ½$ is observed, as expected for such a multilayer semiconducting 2DESs (see, e.g., [366]).
2) Odd integer filling factors are present in this 2DES, as expected for the case of finite tunnelling (see, e.g., [283]).

It is noted that all ν_{Fj} of the different QO frequencies in κ-(BEDT-TTF)$_2$I$_3$ are undoubtedly *total* filling factors (i.e., they count the total filling of the bulk 2DES, not a 'single-layer' filling). This can be concluded, e.g., from the fact that the values for the QO frequencies F_2 and F_3 are quite identical with the values of their analogues in their κ-structured relatives (see, e.g., [83]). However these relatives of the present I$_3$ salt are quasi-2D systems with an amount of 3D dispersion, where ν clearly represents the total filling. This means that in the present material F_2, F_3 and their filling factors represent the number of electrons in the bulk material. Likewise, $\nu_{Fnew} = ½$ represents a total filling factor of the bulk, not the filling of a single layer[26]. The fact that the present ν_{Fj} are bulk multilayer filling factors, corresponds perfectly to the case of coupled 2D layers with finite tunnelling.
However one of the differences between semiconducting 2D coupled multiple layers and the metallic multilayer 2D system κ-(BEDT-TTF)$_2$I$_3$ is their different interlayer transport mechanism. While in the former one hopping mechanism is given, the present material shows metallic [145], even coherent interlayer transport [420], from which the latter is found by tilting the magnetic field *parallel* to the conducting planes. This may help to understand,
- why the results of two-dimensionality in κ-(BEDT-TTF)$_2$I$_3$ may take effect only in the field orientation *perpendicular* to the planes (i.e., 0°),
- why the fractional and low integer quantised states may only occur at 0° and
- why they can generate the strong damping effects of SdH amplitudes only at this angle.

All in all the results of the preceding sections show the presence of low integer filling factors as well as strong indications[27] for the presence of the fractional filling factor $\nu_{Fnew} = ½$ in the 2D multilayer organic metal κ-(BEDT-TTF)$_2$I$_3$. These low ν are brought into the system only by subsystems, i.e., the small pockets on the FS corresponding to F_{new} and F_0, respectively, while the rest of the system i.e., the F_2 as well as the F_3 orbit, is at fairly high ν. The fact that the low integer and fractional ν can be observed by their *action* on the electrons of the rest of the system, proves the presence of electron correlation which is sufficiently strong to bridge over very different ν, thus involving even electrons with very high kinetic energy.
Possible results of such correlation effects are discussed in the following.

[26] In a single layer, $\nu_{Fnew} = ½$ would be prohibited, since no stable ground state is possible at this filling. But, even if this law is put into question, an assumed *single*-layer filling factor $\nu_{Fnew} = ½$ multiplied by 10^5 layers would yield such a high total electron number in the bulk crystal, that charge neutrality could not be reached in the crystal.

[27] As discussed in the preceding sections, none of the current theories can explain the strong anomalous damping effects at 0° in high fields and especially at $B^{-1}=0.086T^{-1}$ accompanied by the sharp μ drop there. The interpretation of the $B^{-1}=0.086T^{-1}$ state as $\nu = ½$ is based on the proposition of such a state in 2D multilayer systems. However, especially in view of the complexity of the present system, it is of course not excluded that after theoretical treatment the understanding of this $\nu = ½$ state might turn out to be more complex than it appears to date.

5.8.1 Coexistence of Extended and Localised States

The fact that the 2DES of κ-(BEDT-TTF)$_2$I$_3$ brought into magnetic fields consists of a number of QO frequencies F_j, turns the attention to a further fundamental difference between the present material and a well-known semiconducting 2DES. This may be illustrated by help of Fig. 5.26, by focusing on a single sawtooth cycle of μ, where μ is pinned to a Landau level during the sequence '**p**' and drops sharply within a narrow field window '**d**'[28]. Normally in quantum Hall systems containing *one single* closed orbit corresponding to one QO frequency F, '**p**' represents the field window where extended states are at the FS. It is *well-separated* from '**d**', where only localised states are present. In contrast the situation is more complex in presence of *several, very different* F_j as, e.g., in the actual material. This means that even within the field window '**d**', where μ is situated within the region of those localised states defined by *one* of the frequencies (i.e., by F_0 or F_{new}), this window '**d**' is intersected by a number of more *narrow* LLs belonging to F_2 as well as F_3. Now these narrow LLs themselves introduce both, localised as well as extended states into this region '**d**'. In reverse, the region '**p**' of extended states of a low-frequency QO (e.g., of F_{new}) is intersected by an alternating series of both, extended and localised states of F_0, F_2 and F_3, respectively. Therefore in the present 2DES we find a *coexistence* of localised and extended states in a wide magnetic field region, with flowing borders between them. Thus sweeping the field generates alternating situations at the FS, where either the localised, or the extended states, respectively, dominate and thus determine the electronic properties at the FS.
This rather complex situation is one of the reasons, why a complete theoretical understanding of the actual results on κ-(BEDT-TTF)$_2$I$_3$ is not available to date.

5.8.2 Indications for Electron Localisation in κ-(BEDT-TTF)$_2$I$_3$ Around Fractional and Low Integer ν

It was shown in Secs. 5.4 - 5.7, that the strong damping effects of the SdH amplitudes in κ-(BEDT-TTF)$_2$I$_3$ at high B, low T and 0° are connected to a moderate extent to the integer ν_{F0} of F_0 (see Fig. 5.24) and to a much stronger extent to the integer and fractional ν_{Fnew} of F_{new} (see Fig. 5.30). The preceding section shows that the coexistence of very different QO frequencies F_j leads undoubtedly to a coexistence of extended and localised electronic states, from which the latter are mainly introduced by the low-frequency oscillations F_{new} and F_0. The fact that the quantum limit (QL) and extreme QL conditions, introduced by parts of the system, are best observed by their action onto the rest of the 2DES, proves the presence of electron correlation. This government of low ν over the entire rest of the system asks to consider that one of the main properties of a 2DES in the quantum limit, i.e., electron localisation, may likewise determine the rest of the system. This would involve even the high-frequency QOs in the coexistence of extended and localised states, thus localising a part of their electrons. These cannot contribute to QOs in transport any more, so that the amplitudes of the respective QOs (F_2 and F_3) appear as strongly damped owing to the reduction of contributing electrons. In consequence the Dingle plots would show strong damping effects in regions where localised states are present, since the theory beyond assumes a constant total number of electrons. This assumed constant total carrier number may be a also plausible reason why the considerations in Sec. 5.3.1, including oscillations of μ, cannot explain the strong damping effects.

[28] The same construction may be applied to F_{new} in Figs. 5.29 and 5.30, but was skipped there for clarity.

The results discussed in Secs. 5.4 and 5.5 provide a progress in the sense that they clearly attribute the structure in the magnitude of the damping effects (see Figs. 5.26 ff.) to low integer and fractional ν present in κ-(BEDT-TTF)$_2$I$_3$.

5.8.3 Localisation Lengths

On the search for an understanding of further peculiarities in connection with the strong damping effects of SdH amplitudes it turned out that a closer review of carrier localisation lengths may be very helpful. The occurrence of integer as well as fractional ν in κ-(BEDT-TTF)$_2$I$_3$ (see preceding sections) shows that the problem of electron localisation has to be considered in the single-particle picture (for integer ν) as well as in the correlated-particle picture (for fractional ν). This is performed in the following.

In Section 4.1.3 an insight into a microscopic understanding of electron localisation in the single-particle picture is discussed in connection with the IQHE. In this picture a non-interacting electron is assumed to be trapped to an impurity and the localisation length $\xi(\Delta E)$ is assumed to be described by the distance of the carrier's energy from the centre of the Landau band (see Eq. (4.4)). This description assumes a negligible spatial variation of the impurity potential on a scale of the magnetic length ℓ_0 (which is the carrier cyclotron radius, see Eq. (4.1)), so that an explicit consideration of ℓ_0 might be skipped in that picture, especially when all carriers have the same ℓ_0. However the situation is different in a 2D metal as κ-(BEDT-TTF)$_2$I$_3$. Here the electrons move on distinct orbits with *different* cyclotron radii $R_{c,Fj}$, corresponding to their QO frequencies F_j. In a metal these $R_{c,Fj}$ have a different field dependence from that of ℓ_0 in a semiconductor (comp. Eqs. (4.1) and (4.2)) and they may be considerably bigger than ℓ_0. For a better illustration ℓ_0 and the cyclotron radii of the carriers in κ-(BEDT-TTF)$_2$I$_3$ are plotted in Fig. 5.31 in comparison.

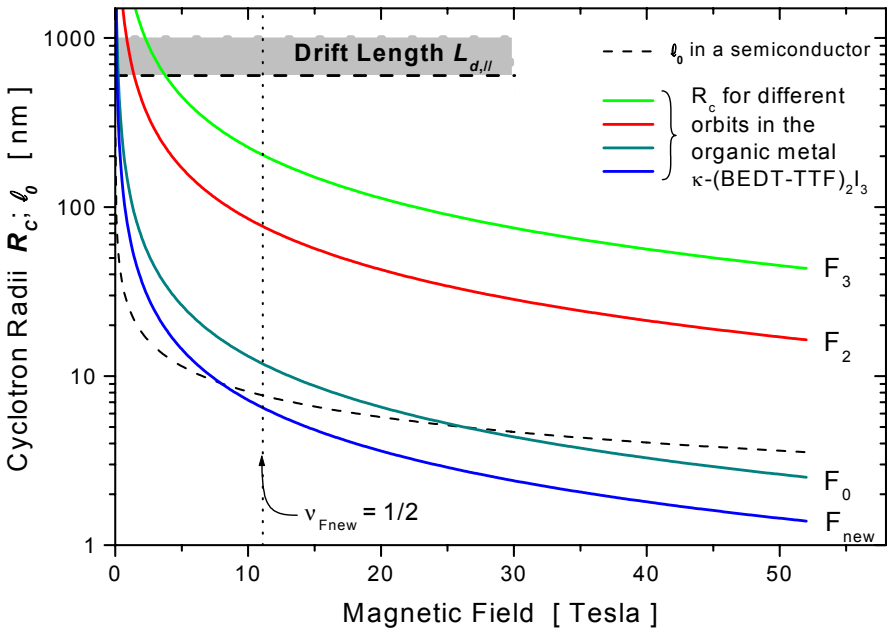

Fig. 5.31: Comparison between cyclotron radii $\ell_0$for a semiconducting 2DES (dashed line) and R_c for the organic metal κ-(BEDT-TTF)$_2$I$_3$, corresponding to the different QO frequencies F_j. The average intraplane drift length $L_{d,//}$ of magnetotransport at low temperatures is included in the figure (grey bar and dashed line; its variation with field can be disregarded in the present context). Discussion see text.

The figure shows that the cyclotron radii R_c of the big, i.e., high-frequency orbits F_3 and F_2 exceed the magnetic length (dashed line) by more than an order of magnitude over the entire available field region. In contrast, the $R_{c,Fj}$ of the low-frequency orbit F_{new} compare at least at low fields roughly to ℓ_0 in a semiconductor, falling below ℓ_0 at higher fields due to their $1/B$ dependence.
Now the fact that an electron has to feel the impurity potential $U(\boldsymbol{r})$ in order to get trapped by it, suggests to consider that all electrons in a distance within their own R_c may be concerned. In reverse, both the profile of $U(\boldsymbol{r})$ and $R_{c,Fj}$ would control, how far a carrier may move away from the impurity centre. Therefore both, localisation strength and localisation length might be determined by an interplay of the impurity potential profile and the successive $R_{c,Fj}$. Since the latter are different for the present orbits, localisation lengths may be also different for successive F_j. This may lead to a shorter localisation length for the carriers of F_2 owing to their smaller cyclotron radius.
This consideration may help to understand why the SdH oscillations F_2 are stronger damped (see Fig. 5.24), i.e., more influenced by localisation effects than those with F_3, since the carriers on F_2 are stronger localised than those on F_3.

Localisation Lengths Around Fractional ν_{Fnew}

A microscopic picture of carrier localisation in the fractional quantum Hall regime is given in Sec. 4.2.5. Unfortunately such a picture is not available for a *multilaye*r 2DES to date. However carrier localisation itself is a direct result of electron correlation. Therefore the picture of electron localisation at fractional ν should be - at least in its essential features - common in both, single layer as well as multilayer systems, so that this picture may allow at least a qualitative understanding of electron localisation in multilayer 2DESs.
According to Eq. (4.15) the size L_{QP} of a localised quasiparticle (QP) with fractional charge corresponds to its cyclotron radius ℓ_0. This quantity is understood likewise as the localisation length of a screening electron, since the QP size is defined by the screening electrons involved, which belong all to the same 'family' and their own cyclotron orbits are therefore of the same size ℓ_0. Therefore $\ell_0 = L_{QP}$ in such a 2DES. However the situation changes drastically in a 2D metal as κ-(BEDT-TTF)$_2$I$_3$, when various orbits with different $R_{c,Fj}$ come into play. The resulting modifications are similar as described above in the single-particle picture (see Fig. 5.31 for illustration). Now it has to be considered that, e.g., an electron moving on the F_3 orbit may already be trapped by the quasiparticle, when it is $R_{c,F3}$ away from it, since it couples necessarily with the QP when it continues its orbit. Hence its localisation length is $R_{c,F3}$ instead of ℓ_0 and, especially $R_{c,F3} > R_{c,F2} > ...$ (see Fig. 5.31).

A first consequence of this is that also in the correlated-paricle picture the SdH oscillations F_2 are stronger damped (see Fig. 5.24), i.e., more influenced by localisation effects than those with F_3, since the carriers on F_2 are stronger localised than those on F_3.

Drift Lengths in Magnetotransport

The drift length L_d in magnetotransport is the average distance which a carrier situated on the FS moves along an applied potential gradient during its average scattering time t.
The intraplane drift length $L_{d,//}$ can be estimated from resistivity measurements (see, e.g., [422]) and is obtained as $L_{d,//} \gtrsim 600$nm at low temperatures. This value is introduced in Fig. 5.31 (grey area with the dark dashed line as lower limit, given by the lower limit for the scattering time t). A comparison of the drift length $L_{d,//}$ with the cyclotron radii shows that all $R_{c,Fj}$ fall far below $L_{d,//}$ at high fields. This means that at high fields a number of carriers are localised on a scale of $R_{c,Fj} << L_{d,//}$. However a transport experiment to which as expected the total number of electrons on the FS may contribute, would require an average drift exceeding $R_{c,Fj}$ by far. Those electrons which are localised within $R_{c,Fj}$ may not provide this motion, so that the SdH oscillations appear as damped due to a loss of contributing carriers.
Furthermore $R_{c,F2} < L_{d,//}$ is reached at about 1.5T, while $R_{c,F3} < L_{d,//}$ is given at roughly 4T. These values may explain, why the F_2 oscillations are already damped at lower fields than the F_3 oscillations. Even more, the 'cut-off' field values estimated here correspond surprisingly well to those where damping effects of the QOs with F_2 and F_3 are indeed observed. Moreover $R_{c,F2} < R_{c,F3} << L_{d,//}$ at high fields, which may help to answer the question, why the oscillations of F_2 are much stronger damped as those of F_3 (see Figs. 5.23 and 5.26, respectively). Finally the competition of localisation length R_c and drift length L_d may also explain, why SdH amplitudes do not diverge at high fields - as expected in a 2D system (see Eq. 3.22) without localisation - but, instead, why they are strongly damped by the dominating localisation process.

This surprisingly good correspondence between the experiments and the localisation picture, as adapted to the special system conditions, shows that the proposed picture is at least reasonable. Therefore it may be used as an explanation for a further open question taken up in the following.

The Discrepancy Between Results of dHvA and SdH Experiments at High B Low T and $\Theta \approx 0°$

The discussion in Ch. 4 shows that electron localisation is a term which is relative to the length scale focused on. This means that a localised electronic state has to be regarded as *extended within* the length scale of its cyclotron radius, while it is localised on every length scale bigger than its R_c, since it is not allowed to leave an impurity (in the IQHE) or a localised quasiparticle excitation (in the FQHE).
Now if a 2D system as, e.g., κ-(BEDT-TTF)$_2$I$_3$, is exposed to high magnetic fields, all electrons are expected to follow a cyclotron radius around a practically fixed centre position. Considering this, a dHvA experiment is not expected to be able to distinguish between extended and localised states (possible different scattering rates disregarded), since in both states the electrons may follow the same cyclotron trace R_c around the *fixed* centre. The situation changes drastically when a *displacement* of the centre position is required by a transport, i.e., SdH experiment. As described above, in this case the electron is asked to leave the localised impurity (in the IQHE case) or the localised quasiparticle excitation (in the FQHE) and to bring about a drift of a certain average drift length L_d. This length can be regarded as relatively constant (due to a weak magnetoresistance), whereas R_c, i.e.,

localisation lengths strongly decrease with increasing B. At low fields where $R_c \geq L_d$ all electrons may contribute to the SdH experiment, so that its results are in line with those of the dHvA measurement. In contrast, at sufficiently high B where $R_c < L_d$, the SdH experiment is expected to probe only the extended states and hence the SdH amplitudes are expected to be damped owing to the 'loss' of contributing extended electrons.
Thus the inequality of localisation length R_c and drift length $L_{d,//}$ would lead to a discrepancy between dHvA and SdH experiments at high fields and this discrepancy increases with field in sympathy with the inequality of R_c and $L_{d,//}$. By this the localisation picture may explain the discrepancy between dHvA and SdH measurements at low T and 0° itself as well as its arising at high B and its strong amplification with B (see Fig. 5.21).

5.8.4 Questions on the Occurrence of Further Results of Two-Dimensionality

Edge States

At low integer Landau level filling edge states (ES) are found to play a considerable role in semiconducting 2DES under certain conditions (see Sec. 4.1.4). The experiments carried out on κ-(BEDT-TTF)$_2$I$_3$ may give rise to the question on the role of ES in this 2D organic metal. On a closer view several arguments listed below make clear that ES cannot explain the strong damping effects of SdH oscillations at high B, low T and 0°.

1) Edge states and resulting circular edge currents are 'necessary' to explain a non-vanishing Hall current around integer ν, i.e., in a region where the existence of extended states at the FS is prohibited. Even more, ES can only occur, when no electron may be transported from one sample edge to the other via the bulk of the sample. In contrast, in κ-(BEDT-TTF)$_2$I$_3$ in high B, we have practically always a coexistence of localised and extended states (see Sec. 5.8.1), from which the latter of course allow a conventional carrier transport via the bulk. This clearly prohibits the occurrence of ES.
2) Edge currents would exist even when no external voltage is applied and therefore their results must be observable in dHvA just as in SdH experiments. Therefore if the damping effects would be generated by ES, they would be inevitably observed also in dHvA experiments at $\Theta \approx 0°$ as well as $\Theta \neq 0°$. This contradicts clearly to the experimental results on κ-(BEDT-TTF)$_2$I$_3$ at $\Theta = 0.07°$.
3) Owing to the relatively high conductivity of organic metals dHvA field modulation technique probes especially the sample surface, since the contribution of the bulk is screened by skin effect. Thus, if generated by edge states, the strong damping effects of QO amplitudes would be even best observable by dHvA field modulation technique. In contrast no such effects are observed in such experiments [395a].
4) Edge currents are only weakly dependent on the tilt angle Θ between B and the 2DES. This is in clear contrast to the restriction of the damping effects to 0°.
5) A dependence of edge currents on even macroscopic magnetic field variation is not expected. This contradicts to the strongly increasing damping effects at high fields.
6) ES are able to transport currents merely below about 100nA. Above, their role is shown to be negligible. In contrast in the SdH experiments on the present material currents between 50 and 300μA where applied, which are by far above the critical currents of ES.

7) Furthermore a current transport by ES requires to place the contacts exactly at the sample edge (see. Fig. 4.7). For the SdH experiments discussed in the preceding the contacts where placed alternately at the edge and in the centre of the sample surface. The results were perfectly consistent, thus excluding an influence of edge states.

These arguments show in symphony that edge states most likely do not play any role in the generation of the strong damping effects of SdH amplitudes as present under the above mentioned conditions.

On the 1D Chiral Tomonaga-Luttinger Liquid

In section 4.1.4 the most important conditions for the occurrence of a 1D chiral Tomonaga-Luttinger liquid (TLL) at the sample edge were sketched. It was found that

i) The occurrence of a TLL requires ideal samples up to the sample edge without impurities, defects or carrier density fluctuations. This is necessary to provide that the Landau levels are *flat* up to the sample edge, i.e., that no charge/filling factor fluctuation is present there. This is not given on organic metals[29]. Their surfaces are generally covered by semiconducting donor molecules, so that stoichiometry and charge balance is far from being given at the sample edge.

ii) In the presence of a TLL, the system cannot be described by Fermi liquid theory, especially, a Fermi surface is absent and therefore cannot be investigated. In contrast, the present material shows a FS, it can be investigated (e.g., by QOs as shown in the preceding) and the results are in best agreement with those from band structure calculations.

These aspects show that a 1D Tomonaga-Luttinger liquid is most likely not the origin of the DEs of the SdH amplitudes, since it may not occur in this 2DES.

Wigner Crystallisation

As reported in Sec. 4.2.4 a so-called Wigner crystallisation is a process where electrons turn to be localised by forcing them to establish a stable, so-called Wigner lattice. Thus, such a process indeed would influence transport and therefore, in principle, a Wigner crystallisation would be a possible explanation for the damping effects of the SdH oscillations. However a Wigner crystallisation was found to be possible only below about $\nu = 1/10$. In κ-(BEDT-TTF)$_2$I$_3$ this condition is not even not fulfilled by F_{new}, but least of all by the other QO frequencies at $\nu = 10^1 \ldots 10^2$.
This shows that a Wigner crystallisation can be practically excluded in κ-(BEDT-TTF)$_2$I$_3$ at actually available fields.

[29] unless they would be cleaved in He atmosphere, however this was not done here.

Composite Fermions

The application of the composite fermion (CF) picture was reported in Sec. 4.2.7. It was developed to describe why a single-layer 2DES remains completely fermionic at, e.g., $\nu = ½$, instead of being completely bosonic, as expected by a direct application of Laughlin's theory at this filling factor.
In contrast the present 2DES of κ-(BEDT-TTF)$_2$I$_3$ does not meet the prerequisites for the occurrence of CFs in several senses:

a) The present material is a multilayer 2DES.
b) It shows indications for electron localisation, i.e., deviations from pure fermionic behaviour, around integer ν and in the same manner just at $\nu = ½$. This means that at $\nu = ½$, κ-(BEDT-TTF)$_2$I$_3$ shows aspects of both, fermionic as well as non-fermionic behaviour. This does not agree with a pure fermionic CF picture.
c) As a pure fermionic picture, the CF approach would not explain the strong damping effects of SdH amplitudes and least of all their restriction to 0°.

These arguments show, that the strong damping effects of SdH amplitudes at low T, 0° at integer and fractional ν_{Fnew} cannot be understood in the framework of the composite fermion picture.

Skyrmions

It was reported in Sec. 4.3 that skyrmions are charged spin texture excitations (see Fig. 4.15) in a 2DES, which reduce the total spin and lower the number of mobile charge carriers. They are a result of a competition between Coulomb energy and Zeeman energy in lowering the total system energy (se Eq. 4.21). In consequence, the formation of skyrmions is supported by a lowest possible g-value and their size is biggest around vanishing g.
In the present material the electrons are quantised on different orbits and may therefore have different g-values, owing to, e.g., spin-orbit interaction or many-particle effects as electron-electron or electron-phonon coupling. For the F_3 orbit $g = 2.27$ was found [395a,402], for the F_2 orbit g could not yet be investigated, whereas concerning the F_0 - orbit it was found that g is at least non-vanishing. In the case of the F_{new} orbit the quantum limit allows to identify the field position of the last LL and to use Eq. (3.18) in order to find the different possible values for g and the Onsager phase γ, which fulfill the equation. It was found that a vanishing g is one possible solution of the equation, so that the occurrence of skyrmions in κ-(BEDT-TTF)$_2$I$_3$ is not a priori excluded.
However, skyrmions are on principle possible only around odd ν from which only $\nu = 1$ is expected to provide a stable state. Therefore they cannot be the reason for the strong damping effect of SdH amplitudes at low T and 0°, since these occur (besides at $\nu = ½$) at both, odd just as even integer ν (see Fig. 5.30).

5.8.5 Further Aspects and Open Questions

The minima in the Dingle plots of SdH amplitudes of κ-(BEDT-TTF)$_2$I$_3$ at 0° show that at exactly ν_{Fnew} = ½, 1, 2, ... the damping effects (DEs) of SdH amplitudes are strongest (see Figs. 5.24, 5.27-5.30). This is not surprising, since carrier localisation is strongest around exact such filling factor values (see Discussion of Figs. 4.4 and 4.5).

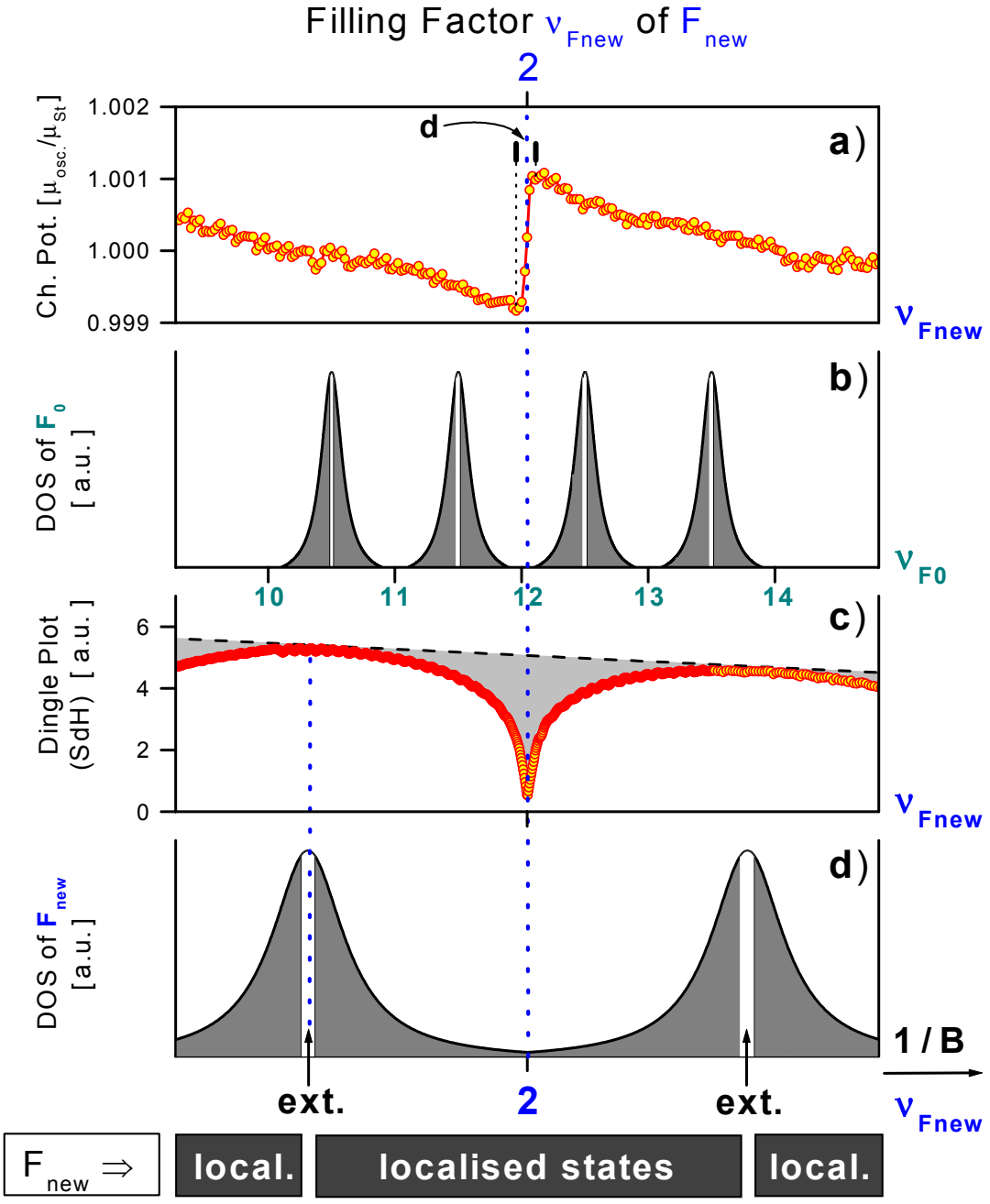

Fig. 5.32: Chemical potential oscillations (**a)**) and a typical Dingle Plot (**c)**) of κ-(BEDT-TTF)$_2$I$_3$ vs. ν_{Fnew} (from Fig. 5.30). The grey-shaded areas in **c)** illustrate the damping effects attributed to electron localisation. Distribution of the density of states (schematic) of F_0 (**b)**) and F_{new} (**d)**) with assumed localised states (grey shaded areas).

However a comparison with the chemical potential oscillations $\tilde{\mu}_{Fnew}$ in Figs. 5.26 and 5.29 arises a question, which is illustrated in Fig. 5.32. For this purpose the figure confronts typical SdH measurements on κ-(BEDT-TTF)$_2$I$_3$ as, e.g., shown in Fig. 5.30, with schematic illustrations of the density of states of F_0 and F_{new}. A closer view on the measurements shows that the chemical potential drops within a very narrow field window '**d**' in 1/B (see part a) of the figure)). In a 'simple' semiconducting 2DES with only *one single* closed orbit present, this would be just the region where IQHE plateaus would be expected and where localised states would be restricted to. The microscopic situation lying beyond is that μ drops to doping-induced states whose electrons are localised at the impurity sites.
Now, these field windows '**d**', being very narrow, arise the question whether the rather broad damping regions in the SdH amplitudes (shaded areas in c)) may be indeed reasonably connected with localised states. At a first glance the narrow localisation regions '**d**' seem to be in contradiction with the (roughly assumed) wide localisation region of F_{new} in part d) of the figure. However a key of understanding may be the following. The chemical potential is on principle defined by the highest occupied electronic state. As soon as a LL of F_{new} is emptied, μ would tend to drop either to the next lower LL of F_{new} (ideal crystal) or to an impurity site, provided that only this single orbit is present. However in the case of several orbits, as given in κ-(BEDT-TTF)$_2$I$_3$, μ drops to the very next occupied LL, which can belong to F_3 or F_2, respectively. Since these are *very narrow* the μ drop is restricted to a narrow field window and then, upon further field variation the LLs of the frequencies F_j define, i.e., keep the actual position of μ. They provide the FS with localised as well as extended states (illustrated in part c) exemplarily on F_0), despite that from the viewpoint of F_{new} only localised states would be possible and a broad Hall plateau would be expected. This consideration allows to understand at least qualitatively, why the damping region in the SdH oscillations (grey area in part c)) is much wider than suggested by the narrow drop of μ in part a). It is suggested to consider that the electrons may be influenced by this coexistence of localised and extended states over a much wider field region as suggested by '**d**'.

However, clearly, it is not claimed here that this is the ultimate understanding of the rather complex behaviour of κ-(BEDT-TTF)$_2$I$_3$. Instead, this picture is mainly drawn to illustrate that considerable - especially theoretical - work has to be done until this 2DES is really understood. In the framework of this challenge,

1) the role of the various correlated orbits corresponding to F_j with their very different filling factors,
2) multilayer effects, as coupling and tunnelling,
3) the very high electron density and high mobility

may be taken into account. Even further considerations may play a role:

4) Collective excited modes due to the inclusion of higher Landau levels (for a review see, e.g., [217]).
5) Filling factor fluctuations may be of importance which are caused by impurities and crystal defects in this 10^5-multilayer system.
6) Finally, in a semiconducting 2DES with a relatively low carrier concentration, the cyclotron radius corresponds approximately to the spacing between two electrons. In κ-(BEDT-TTF)$_2$I$_3$ the electron concentration is such high (about $1.1*10^{14}$/cm^2 per layer, see App. A), that the big R_c encircle a huge number of electrons (e.g., at ν_{Fnew} = ½ about 10^5

carriers are encircled by an electron on the F_3 orbit). It may have to be considered that these intersected cyclotron motions of neighbouring carriers may represent an interchange of particles and quasiparticles, so that influences on their statistics might play a role in this 2DES.

This task is beyond the scope of the present experimental work, so that a number of questions have to be left open.

Hall Effect Experiments

The presence of low integer and fractional ν in κ-(BEDT-TTF)$_2$I$_3$ raises the principle question on the presence of Hall plateaus at those ν. However the fundamental difference between, e.g., a 'well-known' semiconducting 2DES and the present metallic 2EDS brings out further interesting aspects of this question, which can be recognised by Fig. 5.32. Part d) of the figure would suggest the occurrence of even very broad Hall plateaus corresponding to a wide localised-state region introduced by F_{new}. On the other hand, part a) would propose merely narrow Hall plateaus of a width '**d**', where the chemical potential is situated between occupied LLs, i.e., extended states.
Motivated by this, Hall effect experiments at Θ = 0° where carried out in steady resistive as well as superconducting magnets on about 10 very thin single crystal platelets of typically $0.12*2.5*2.5mm^3$. Saying it right away, these results are unsatisfactory to date. In some of the experiments an oscillatory structure with F_{new} and furthermore narrow steps are indicated in R_{xy}. However, clearly spoken, these results have to be reproduced before any further interpretation. The latter task is afflicted with a number of difficulties, briefly sketched in the following:
- Hall contacts have to be applied on the edges of these rather thin crystals. Repeated cooling cycles for reproduction of the experiments in different setups led to contact cracks in several cases.
- The present metallic 2DES shows even at high fields a Hall signal of merely about 70nΩ. An increase of the signal-to-noise ration by enhancing the current is prohibited in view of possible sample heating as well as generation of further artefacts.
- In all examined contact arrangements a strong competition between the very low Hall and a huge SdH signal was found in κ-(BEDT-TTF)$_2$I$_3$.
- Compared to the rather low amplitudes of the low frequencies F_0 and F_{new} very strong amplitudes are contributed by F_2 and F_3, which - in addition - strongly increase with lowering the temperature. Therefore the presence of strong SdH and Hall components coming from F_2 as well as F_3 have to be accepted in all Hall experiments.
- The low Hall signals themselves and the relatively strong contributions from F_2 and F_3 make an extraction of the Hall component rather difficult. A decisive condition for this is a detection of the rather complex signal (including F_2 and F_3) as properly as possible. This resolution requires lowest sweeping rates of about 0.8T/h in order to avoid possible inductions. But even for a single set of two field-reversed Hall sweeps this requires a stability of the setup over about 24h with parasite signals below about 20nV (which is the actual order of magnitude of the indicated Hall steps in the signals).
These are the presumably most important experimental limiting conditions for successful Hall experiments. Despite of several attempts up to now, such a high stability of magnets, setups, and especially of power supplies for the experiments on such a long time scale, could

not yet be reached within the limited magnet time periods on high field magnets and may therefore not be guaranteed for such long Hall sweeps.
Therefore, the question on the occurrence of quantised Hall states of κ-(BEDT-TTF)$_2$I$_3$ must be left open to date. Especially the investigation of an exact shape of the Hall signal of this rather complex 2DES

- with fractional, low integer as well as very different high ν present,
- a very high electron number,
- a high carrier mobility,
- a coexistence of extended and localised states
- in a metallic system of correlated electrons,
- bound in a 10^5-layer bulk crystal
- with interlayer coupling as well as tunnelling

motivates for further improvement of the experimental conditions in order to achieve a progress in Hall experiments.
However the actual Hall experiments reveal the at least a clear result on R_{xx}. It is observed on all samples that R_{xx} remains finite even around integer ν as well as $\nu = ½$. This result is in line with those obtained, e.g., on the organic multilayer conductor (TMTSF)$_2$PF$_6$ where R_{xx} remains also finite even during clearly observable Hall steps in R_{xy} [101,102]. This is in clear contrast to the experience made with the IQHE in 'well-known' semiconducting 2DESs. This peculiarity is an additional motivation for a closer investigation of the IQHE in organic multilayer systems. Here special interest may be devoted to the role of the aforementioned *coexistence* of localised and extended states on different quantised orbits onto **i)** the behaviour of R_{xx} and R_{xy}, just as onto **ii)** the possibility (or not) to develop sawtooth quantum oscillations under such rather complex conditions.

5.9 Provisional Appraisal

In the present chapter it was shown that κ-(BEDT-TTF)$_2$I$_3$ is a 2D multilayer organic metal in which the intrinsic two-dimensionality requires magnetic field orientation exactly perpendicular to the conducting crystallographic (b,c) planes (i.e., 0°) in order to take full effect. In this field orientation strong anomalous damping effects of SdH oscillations are observed at high magnetic fields and low temperatures. These damping effects cannot be explained by the known 'classical' corrections to the 3D LK theory of quantum oscillations in metals, even when taking into account results of two-dimensionality as oscillations of the chemical potential.
It was found that low integer filling factors ν = 1,2,3,4 are present and ν = ½ is strongly indicated by experiments in κ-(BEDT-TTF)$_2$I$_3$ and that these ν couple with the rest of the correlated 2DES. Considering this, the fact that the *strength* of the damping effects is evidently controlled by the low integer and fractional ν and coincide with the regions of localised states, the strong damping effects of the SdH oscillations in κ-(BEDT-TTF)$_2$I$_3$ at 0° are proposed to be understood in terms of a loss of mobile carriers due to localisation of this part of the carriers, whereas the detected SdH signal is supposed to originate from the remaining mobile electrons in this 2D multilayer organic metal.

It is emphasised that considerable - especially theoretical - work has to be done until this 2DES is really understood. In the framework of this challenge,

1) the role of the various correlated orbits corresponding to F_j with their very different filling factors,
2) the coexistence of localised and extended states
3) the very high electron density and high mobility,
4) multilayer effects, as interlayer tunnelling, Coulomb coupling of the layers, as well as extension of localised excitations over more than one layer and their interlayer coupling

may be considered. In addition, more complex features play a role:

5) Collective excited modes due to the inclusion of higher Landau levels.
6) Filling factor fluctuations in this 10^5-multilayer system may be of importance.
7) Finally, in view of the high carrier concentration and the big R_c, it may have to be considered that the intersected cyclotron motions of neighbouring carriers may represent an interchange of particles and quasiparticles, so that influences on their statistics might play a role.

This task, however, is beyond the scope of the present experimental work, so that a number of questions have to be left open.
Instead, the work of the last years followed the aim to search for similar effects on related materials, to crystallise or to prepare further layered organic metals, which may provide the required conditions for similar effects and to investigate them. The results of these studies are discussed in the following chapter.

6. Search For Effects of Two-Dimensionality in Further Quasi-2D Organic Metals

The present chapter focuses on the possibility for the occurrence of electron correlation (EC), electron localisation (EL) and gives an insight to further results of pronounced two-dimensionality in quasi-2D organic metals.
It is anticipated that such direct indications for EC and EL as found in κ-(BEDT-TTF)$_2$I$_3$ (denoted as κ-I$_3$ in the following) are not yet reported on other organic CT salts. However the scope of investigations in this class of materials is very wide, whereas the conditions, under which indications for EL is found in κ-(BEDT-TTF)$_2$I$_3$, are very specific. Therefore, on the basis of the actual results the presence of electron localisation and electron correlation on other (quasi-)2D[1] organic metals is of course not excluded.

The possibility for the occurrence of electron localisation in further (quasi-)2D organic metals is taken up in the following by asking whether the main conditions for EL, i.e.,

1) sufficiently strong two-dimensionality, i.e., low intraplane anisotropy and high inter-/intraplane anisotropy,
2) low filling factors (i.e. proximity to quantum limit) and
3) high crystal quality

are given in other quasi-2D layered organic metals.
Since κ-structures themselves are known to provide most pronounced two-dimensionality to date, Sec. 6.1 examines the possibility of EL just in a series of κ-structured charge-transfer (CT) salts, which are isostructural to the present κ-I$_3$ salt. Section 6.2 resumes the experiments on (quasi-)2D organic metals with structures different from κ-type. Section 6.2.1 reports on QO experiments performed on (BEDT-TTF)$_4$[Ni(dto)$_2$], Sec. 6.2.2 is dedicated to β”-(BEDT-TTF)$_2$SF$_5$CH$_2$CF$_2$SO$_3$ Sec. 6.2.3 gives an insight to the Q2D α-phase salts α-(BEDT-TTF)$_2$*M*Hg(SCN)$_4$ (*M* = K, NH$_4$, Tl, Rb) and Sec. 6.2.4 introduces to the actual state of preliminary QO experiments on a stable high-T_c variation of β-(BEDT-TTF)$_2$I$_3$ at ambient pressure. The latter material was obtained by a preparation process different from the usual pressure-induced one.

6.1 κ-Phase Organic Metals with Quasi-2D Electronic Properties

The present section follows the question, whether indications for EL might be observed in κ-structure charge-transfer (CT) salts which are closest related to κ-I$_3$. These materials may be based either on BEDT-TTF or related donor molecules, from which κ-(BEDT-TTF)$_2$Cu(NCS)$_2$, as well as the Cu[N(CN)$_2$]Br and the Cu[N(CN)$_2$]Cl salts are the most intensively investigated ones.

[1] this means: with varying strength of two-dimensionality

κ-(BEDT-TTF)$_2$Cu(NCS)$_2$

The charge-transfer salt κ-(BEDT-TTF)$_2$Cu(NCS)$_2$ (referred to as κ-Cu(NCS)$_2$ in the following), was first synthesised by electrochemical methods[2] by *Urayama et al.* [43]. This compound is an organic superconductor with one of the to date highest transition temperatures within its class of materials ($T_c \approx 10.4$K at ambient pressure [214,44]). κ-Cu(NCS)$_2$ has a very similar structure and band structure [43,44] to that of the κ-I$_3$ salt [143,144]. First quantum oscillations on κ-Cu(NCS)$_2$ were recorded by SdH technique [214,423]. In these studies SdH oscillations with F_α[3] were detected at 0.55K above about 8.5T. In later experiments the magnetic breakdown frequency F_β was observed above about 16T. Due to its high crystal quality (Dingle temperature $T_D \approx 0.4$K), κ-Cu(NCS)$_2$ is meanwhile one of the most extensively investigated quasi-2D CT salt, on which a number of groups have carried out dHvA and SdH measurements (see, e.g., Refs. [403,424,198,425,426,427,404,428,406,407,429,201,191]). A selection of fermiological data is collected in the following table 6.1.

κ-(BEDT-TTF)$_2$Cu(NCS)$_2$	A_{Fj} [nm^{-2}]	Part of the FBZ [%]	m_{Fj}* [m$_e$]	$T_{D,Fj}$ [K]	τ_{Fj} [ps]
F_α = 599(±40)T	6,4 [1)]	18 [1)]	3,5 [1)]	0,4(±0,1) [2)]	3(±1) [2)]
F_β = 3872(±30)T	36,3 [3)]	100,9 [3)]	7,1 [4)]	0,64 [5)]	≈ 2

Tab. 6.1: Fermiological data of κ-(BEDT-TTF)$_2$Cu(NCS)$_2$ obtained from dHvA and SdH studies by different groups: [1)] [214]; [2)] [403]; [3)] [198]; [4)] [429,201]; [5)] [191].

These data show the close relation to the κ-I$_3$ salt by the very similar QO frequency values, the sizes A_{Fj} of the orbits in *k*-space and the part of the first Brillouin zone which they represent (comp. with Tabs. 5.3 and 5.4). However the values for the effective masses m_{Fj}* in κ-Cu(NCS)$_2$ are significantly higher than in the κ-I$_3$ salt (comp. with Tab. 5.6). Note that the average scattering times τ in κ-Cu(NCS)$_2$ are markedly lower than in the κ-I$_3$ salt (comp. with Tab. 5.4).

Within QO experiments a warping of the FS of κ-Cu(NCS)$_2$ is not reported. However to date QO experiments cover a rather limited field window of roughly [6T,50T], from which the absence of warping nodes allows merely a careful statement on the two-dimensionality of the system. Further clear indications for pronounced 2D properties are given by the angular dependence of the QO frequencies F_α [214], F_β [201] as well as $m_{F\alpha}$* [406,407]. These hints are confirmed by the angular dependence of the upper critical fields B_{c2} of the superconducting transition [57], which indicate an inter-/intraplane anisotropy of $B_{c2,\perp}/B_{c2,//} \approx 0.1$. However this anisotropy is considerably lower than that of κ-I$_3$, where $B_{c2,\perp}/B_{c2,//} < 0.028$ was found ([59], see Tab. 5.2 and Sec. 5.2.2). This means that the electronic system of κ-(BEDT-TTF)$_2$Cu(NCS)$_2$ has to be regarded as considerably less two-dimensional as that of the κ-I$_3$ salt discussed in Ch. 5. This finding identifies κ-(BEDT-TTF)$_2$Cu(NCS)$_2$ as a

[2] similar to those used for the synthesis of the κ-I$_3$ salt

[3] F_α and F_β correspond to F_2 and F_3, respectively, in Ch. 5.

quasi-2D system (i.e., with a considerable interplane transfer integral $t_\perp$) and arises the question whether its two-dimensionality is sufficiently high to generate effects as observed on the κ-I_3 salt.
Furthermore, in κ-$Cu(NCS)_2$ a presence of low frequency oscillations as found in the I_3-salt (i.e., F_0 and F_{new}, see Secs. 5.4. ff.) is not reported to date. The existence of such orbits in κ-$Cu(NCS)_2$ are not excluded in view of the close relation to κ-I_3, but might be put into question due to the slight structural differences between these materials. They manifest themselves also in the FS, e.g., by a considerably larger magnetic breakdown (MB) gap $E_g \approx 4.5$-6meV in κ-$Cu(NCS)_2$ (for comparison $E_g \leq 3$meV in κ-I_3, see Sec. 5.2.1).
From the absence of low-frequency oscillations in κ-$Cu(NCS)_2$ it may be concluded that low Landau level filling factors (i.e., proximity to quantum limit) are likewise absent in κ-$Cu(NCS)_2$. This would suggest that a further - possibly decisive - condition for the occurrence of such strong effects of two-dimensionality as observed in κ-I_3 is not fulfilled in κ-$Cu(NCS)_2$. But even further, more subtle influences may play a role. The large MB gap results in a high MB field of roughly $B_{MB} \approx 16$ - 30.5T[4] [198,199,404,426,201]. This means that even in high fields the carrier motions on both, the F_α and the F_β orbit may be influenced by both, tunnelling and Bragg reflection of the carriers on their trajectories. Moreover, significant influences of quantum interference on the magnetotransport of κ-$Cu(NCS)_2$ are reported ([191], see also Sec. 3.4.6). The influences of such effects on electron correlation effects in 2DESs are not yet studied.
Despite the less pronounced two-dimensionality of κ-$Cu(NCS)_2$ compared to κ-I_3, chemical potential oscillations with F_β are reported also in the former compound. Nevertheless, in κ-$Cu(NCS)_2$ the dHvA and SdH amplitudes of both, F_α and F_β are reported to follow perfectly the standard 3D theory. Indications for electron localisation, as present in κ-$(BEDT\text{-}TTF)_2I_3$, are not observed in κ-$Cu(NCS)_2$. In view of the less pronounced two-dimensionality of κ-$(BEDT\text{-}TTF)_2Cu(NCS)_2$ and the absence of quantum limit conditions, the presence of considerable electron localisation effects as a result of two-dimensionality can be put into question in this material.

κ-$(BEDT\text{-}TTF)_2Cu[N(CN)_2]Br$

The organic superconductor κ-$(BEDT\text{-}TTF)_2Cu[N(CN)_2]Br$ (hereafter referred to as κ-$Cu[N(CN)_2]Br$) reaches the to date highest ambient pressure transition temperature ($T_c \approx 11.6$K, [45,430]) within its class of materials. This material is supposed to belong to an universal phase diagram [431] with the unique κ-phase feature that the physical pressure and the 'chemical' pressure work in opposite directions. With respect to the pressure axis κ-$Cu[N(CN)_2]Br$ is supposed to be placed closer to the insulating state as κ-$Cu(NCS)_2$.
During the first years of syntheses, single crystals of κ-$Cu[N(CN)_2]Br$ produced by different groups showed significant differences in their temperature dependence of resistivity. In most cases a hump in $\rho(T)$ is observed at about 100K (see, e.g., [432] or [433]), while this hump is absent in measurements on crystals obtained by a slightly different synthesis [434]. This resistivity hump was suggested to be due to the generation of Cu(II) during the electrocrystallisation process [435], where Cu(II) may be regarded as paramagnetic impurity,

[4] These very different values are obtained by different groups.

thus influencing the low temperature properties of this compound. This idea was taken up in [436] and later confirmed in [437].
The calculated Fermi surface of κ-Cu[N(CN)$_2$]Br [45] is very similar to that of κ-I$_3$ ([143], see also Fig. 5.10). However first FS investigations by SdH experiments revealed confusing results. While at ambient pressure no QO signal could be found, SdH curves at high pressures (≥5kbar) showed a surprisingly low QO frequency $F_{\alpha'}$ [438,439] and at high fields the MB frequency F_β. The latter is indeed one of the expected frequencies. In later experiments F_β [440,436] and finally F_α itself [415] were found also at ambient pressure. A selection of fermiological data obtained by different groups [438,439,440,436,415,416,441,442] is collected in the following table 6.2.

κ-(BEDT-TTF)$_2$Cu[N(CN)$_2$]Br	p [kbar]	A_{Fj} [nm^{-2}]	Part of the FBZ [%]	m_{Fj}* [m$_e$]	$T_{D,Fj}$ [K]	τ_{Fj} [ps]
$F_{\alpha'}$ = 150T [1,2)]	≥ 5 [1,2)]	1,4	3,5-4 [1,2)]	≈ 1,3 [1,2,3)]	≈ 3,5 [1,2)]	≈ 3,4
F_α = 530T [4,5)]	≥ 0	5	14	3,1		
F_β = 3810T [6,7)]	≥ 0	36	100	5,4 [6)] 6,7 [7)]	3,4 [6)]	≈ 3,6

Tab. 6.2: Fermiological data of κ-(BEDT-TTF)$_2$Cu[N(CN)$_2$]Br obtained from dHvA and SdH studies by different groups: [1)] [438]; [2)] [439]; [3)] [416]; [4)] [441]; [5)] [442]; [6)] [436]; [7)] [440];. Note that $F_{\alpha'}$ is only observed above about 5kbar. Its fermiological data refer to 5kbar.

The fact that for a couple of years no QOs could be found at ambient pressure, was widely discussed and, e.g., low-temperature magnetic ordering with a field-induced magnetic phase transition or the presence of paramagnetic Cu(II) impurities were proposed as possible reasons. While the frequencies F_α and F_β correspond to the values expected by band structure calculations [45], $F_{\alpha'}$ is not represented in the initially proposed band structure. However the generation of $F_{\alpha'}$ at high pressures could be attributed in Refs. [416,415] to the presence of a superstructure which doubles the lattice constant in the *c*-direction [443].
Hints for pronounced 2D properties were found by a 1/cosΘ behaviour of $F_{\alpha'}$, F_α and F_β [438,439,442]. From angle-dependent B_{c2} measurements a ratio $B_{c2,\perp}/B_{c2,//} \approx 0.18$ was estimated [57]. This indicates that in κ-Cu[N(CN)$_2$]Br two-dimensionality is less pronounced than in both, κ-Cu(NCS)$_2$ ($B_{c2,\perp}/B_{c2,//} \approx 0.1$) and κ-I$_3$, where in the latter $B_{c2,\perp}/B_{c2,//} < 0.028$ was found ([59], see Tab. 5.2 and Sec. 5.2.2). In ambient pressure QO experiments on κ-Cu[N(CN)$_2$]Br no indications for beating nodes were found between 20T and 60T [416,436]. The search for possible beating nodes was extended to tilted angles, thus benefiting from the fact that the angle-dependence of beating frequencies push beating nodes from inaccessible fields to experimental field values. By this, such nodes could be indeed identified at tilted angles, and they allowed the crude estimation of the warping of the FS as $\delta A_{F3}/A_{F3} \approx 0.7\%$ ... 1.7%. This is considerably larger than estimated for κ-I$_3$ ($\delta A_{F3}/A_{F3} <$ 0.027%, see Tab. 5.5). By this, κ-(BEDT-TTF)$_2$Cu[N(CN)$_2$]Br is identified as a quasi-2D electronic system with less pronounced anisotropy as κ-Cu(NCS)$_2$ and by far less than κ-(BEDT-TTF)$_2$I$_3$.

A low-frequency oscillation, which may turn a part of the electronic system to quantum limit, is not reported in κ-Cu[N(CN)$_2$]Br. This suggests that two main conditions for the occurrence of strong electron localisation in 2DESs, i.e., sufficient two-dimensionality and low ν, are most likely not given in κ-(BEDT-TTF)$_2$Cu[N(CN)$_2$]Br.

κ-(BEDT-TTF)$_2$Cu[N(CN)$_2$]Cl

The layered organic superconductor κ-(BEDT-TTF)$_2$Cu[N(CN)$_2$]Cl (hereafter referred to as κ-Cu[N(CN)$_2$]Cl) held for several years the highest T_c = 12.8K [46] among the organics, however only under a moderate pressure of 0.3kbar. At ambient pressure the material undergoes a semiconductor/insulator transition at about 40K. It is supposed that the substitution of Br by Cl in the anion increases the 'chemical' pressure and drives the κ-Cu[N(CN)$_2$]Cl salt into the insulating region of the universal phase diagram for κ-structures [431]. Band structure calculations show that κ-Cu[N(CN)$_2$]Cl has practically the same band dispersion relation and FS as the related κ-phase salts (see [46] and Refs. therein). Indeed, both corresponding QO frequencies F_α and F_β have been observed by SdH experiments above about 3.8kbar [444]. The determined extremal areas in k-space correspond to the values calculated for κ-phases. At about 6kbar a beating node is observed in the amplitudes of F_β, proving a considerable warping of the FS. This reveals the presence of a notable 3D component to the dispersion and thus identifies κ-(BEDT-TTF)$_2$Cu[N(CN)$_2$]Cl as a quasi-2D electronic system.
A low-frequency oscillation, which may push a part of the electronic system to quantum limit, is not reported in κ-Cu[N(CN)$_2$]Cl. This suggests that two main conditions for the occurrence of electron localisation in 2DESs, i.e., sufficient two-dimensionality and low ν, are most likely not fulfilled in κ-(BEDT-TTF)$_2$Cu[N(CN)$_2$]Cl.

Further Organic κ-Phase Materials

κ-(BEDT-TTF)$_2$Ag(CN)$_2$H$_2$O is an organic superconductor with a $T_c \approx$ 5K [445] and a structure equivalent to κ-Cu(NCS)$_2$. Quantum oscillation experiments report on a clear beating of the amplitudes of F_α [446]. This proves a warping of the FS and indicates an even stronger interlayer integral $t_\perp$ than observed for the preceding κ-phase materials, so that strong two-dimensionality is certainly not given in this compound.
κ-(BEDT-TSF)$_2$Cu[N(CN)$_2$]Br is an organic metal based on BEDT-TSF which represents the modified donor (i.e., bis(ethylenedithio)tetraselenafulvalene, also abbreviated as BETS). This material is isostructural to κ-Cu[N(CN)$_2$]Br [447]. QO measurements on this compound report on beating nodes in the dHvA amplitudes of F_β, which show that the FS of this quasi-twodimensional material is considerably warped.
κ-(BEDT-TSF)$_2$C(CN)$_3$ is a quasi-twodimensional organic metal synthesised by [448]. Band structure calculations show that its FS is expected to be very similar to that of the related κ-phase materials. The main features of the FS were confirmed by dHvA and SdH experiments [449]. However in addition to the well-known QO frequencies F_α and F_β, lower-frequency oscillations F_λ = 120T and F_γ = 230T $\approx 2*F_\lambda$ were observed, whose realisation in k-space were not clear. It is pointed out that F_λ has very similar value to

F_1 ≈ 100T observed in the related κ-I_3 salt (see Tab. 5.3). QO studies on κ-(BEDT-TSF)$_2$C(CN)$_3$ [449] do not report any indication for pronounced two-dimensionality of the electronic system.

κ-(DMET)$_2$AuBr$_2$ is an organic superconductor with a T_c ≈ 1.9K [48] and is based on the electron donor molecule dimethyl-ethylenedithio-diselenedithiafulvalene. This compound is the first organic κ-phase material with a donor different from BEDT-TTF, where dHvA oscillations were observed. DHvA oscillations were detected above about 9T showing both frequencies F_α and F_β above this field [450]. From this it can be concluded that the MB gap (see Fig. 5.10) is smaller than, e.g., in κ-(BEDT-TTF)$_2$Cu(NCS)$_2$. Within the narrow field window where QOs are present, a statement on the two-dimensionality of the system cannot be given satisfactorily. However those measurements show a strong *inverse* sawtooth which reveals important details on the electronic properties of this material. Such an inverse sawtooth, whose steep flank is on the low-field part of a QO, is in strong contrast (i.e., just mirror-imaged) to the sawtooth shape expected in a strongly 2DES [88,90,91]. Such a sawtooth orientation can be explained, e.g., by the presence of a 1D electron reservoir with a carrier tunnelling between the closed quantised orbits and the open 1D reservoir orbit [417]. A similar inverse sawtooth with an electron reservoir supposed beyond was also found, e.g., in the organic metal β"-(BEDT-TTF)$_2$SF$_5$CH$_2$CF$_2$SO$_3$ [451].
The presence of such an 1D reservoir (whose corrugation is not known in κ-(DMET)$_2$AuBr$_2$) and the resulting carrier tunnelling to this reservoir are known to influence strongly the electronic properties of quasi-2D electronic systems.
In κ-(DMET)$_2$AuBr$_2$, but also in further κ-phase materials as, e.g., **κ-(BEDT-TTF)$_2$Cu(CN)[N(CN)$_2$]** and **κ-(BEDT-TTF)$_2$Cu$_2$(CN)$_3$** [452] indications of such strong two-dimensionality as realised in κ-I_3 are not reported.

It is emphasised that such low-frequency oscillations as F_0 and F_{new}, present in κ-(BEDT-TTF)$_2$I$_3$, are not reported to date in any other of the κ-phase materials. This suggests that among the κ-phase materials such strong two-dimensionality and/or quantum limit (and even fractionally quantised) conditions seem to be realised exclusively in κ-(BEDT-TTF)$_2$I$_3$ to date.

6.2 Quasi-2D Organic Metals with Structures Different from κ-Phase

Within the organic CT salts those with a κ-structure are known to be most promising candidates for pronounced 2D electronic properties, however two-dimensionality is not a priori restricted to these κ-phase materials. In view of the limited number of synthesisable κ-phase compounds, it was attempted to reach pronounced 2D properties in further structures by synthesis or by specific physical treatment of organic CT salts. The results of selected materials are briefly discussed in the following and further classes of CT salts are quoted.

6.2.1 The Quasi-2D Organic Metal (BEDT-TTF)$_4$[Ni(dto)$_2$]

The first charge transfer complex based on the electron donor BEDT-TTF and the acceptor Ni(dto)$_2$) (i.e., nickelbis(dithiaoxalate)) has been synthesised in a 2:1 stoichiometry by *Saito et al.* [453] and shows semiconducting behaviour. In contrast, the material discussed here is a 4:1 complex [545], showing metallic behaviour down to 20mK [419]. The resistivity ratio of $\rho_a : \rho_b : \rho_c : \approx 1 : 1 : 100$ indicates quasi-2D electronic properties of (BEDT-TTF)$_4$[Ni(dto)$_2$] single crystals. Tight-binding band structure calculations show the presence of a lens-shaped hole pocket A_α (14% of the FBZ) and a 1D open trajectory (see Ref. [455] and inset of Fig. 6.1).

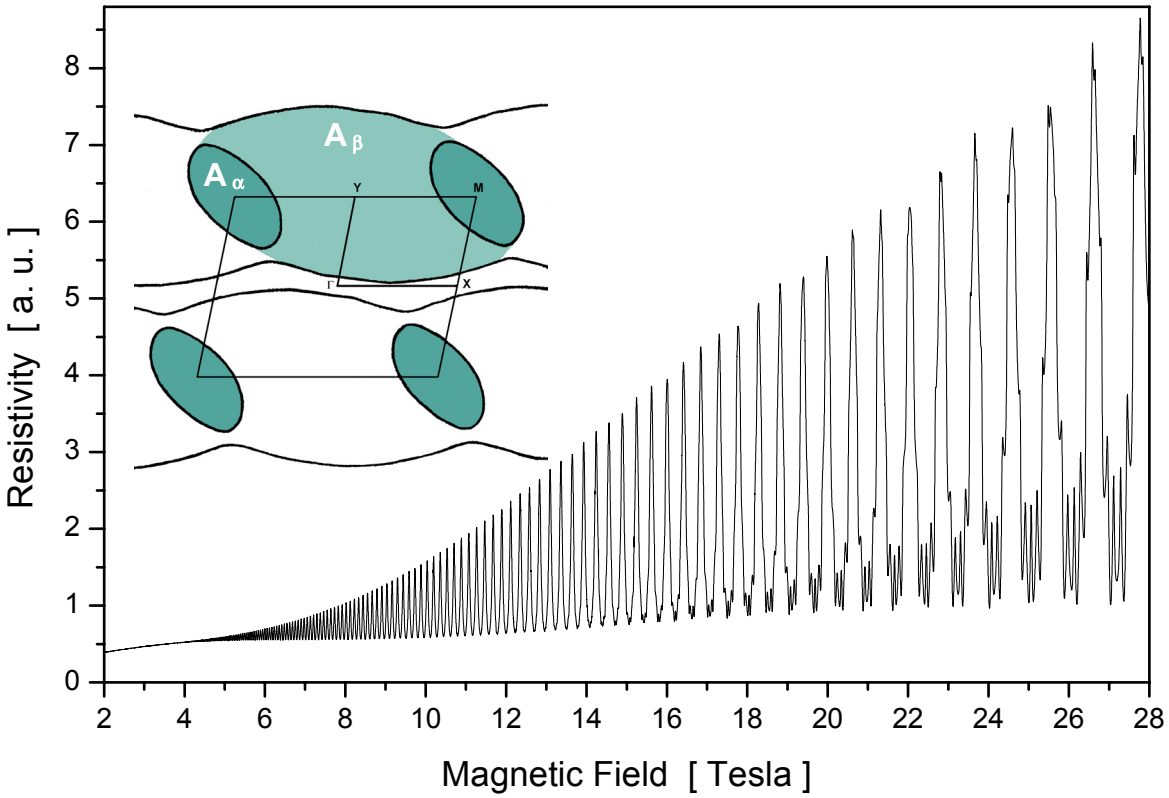

Fig. 6.1: SdH signal of a typical (BEDT-TTF)$_4$[Ni(dto)$_2$] single crystal at 0.38K and Θ = 0° [419]. **inset:** Fermi surface of the compound (according to [455]).

(BEDT-TTF)$_4$[Ni(dto)$_2$]	A_{Fj} [nm^{-2}]	Part of the FBZ [%]	m_{Fj}* [m$_e$]	$T_{D,Fj}$ [K]	τ_{Fj} [ps]
F_{low} = 179(±20)T	1,7	4,2			
F_α = 634(±10)T	6	15	2,1	0,3	4
F_β = 4245(±30)T	40,5	100	4,5	0,5	2,4

Tab. 6.3: Fermiological data of (BEDT-TTF)$_4$[Ni(dto)$_2$] obtained from dHvA and SdH studies (data for F_α and F_β see also [181,419,456], for F_{low} see [457].

The shape of the FS was confirmed by dHvA and SdH experiments carried out up to 28T and down to 20mK [181,456]. At 0.38K QOs are observed above about 2T. A typical result of a SdH field sweep is shown in Fig. 6.1. The two observed frequencies F_α and F_β correspond very well to the size of the extremal areas A_α and A_β in k-space. A collection of fermiological data obtained by QO experiments is shown in Tab. 6.3. The gap between the closed F_α orbit and the open part of the FS was found to be overcome above about the magnetic breakdown field of $B_{MB} \approx 9(\pm1)$T [181].

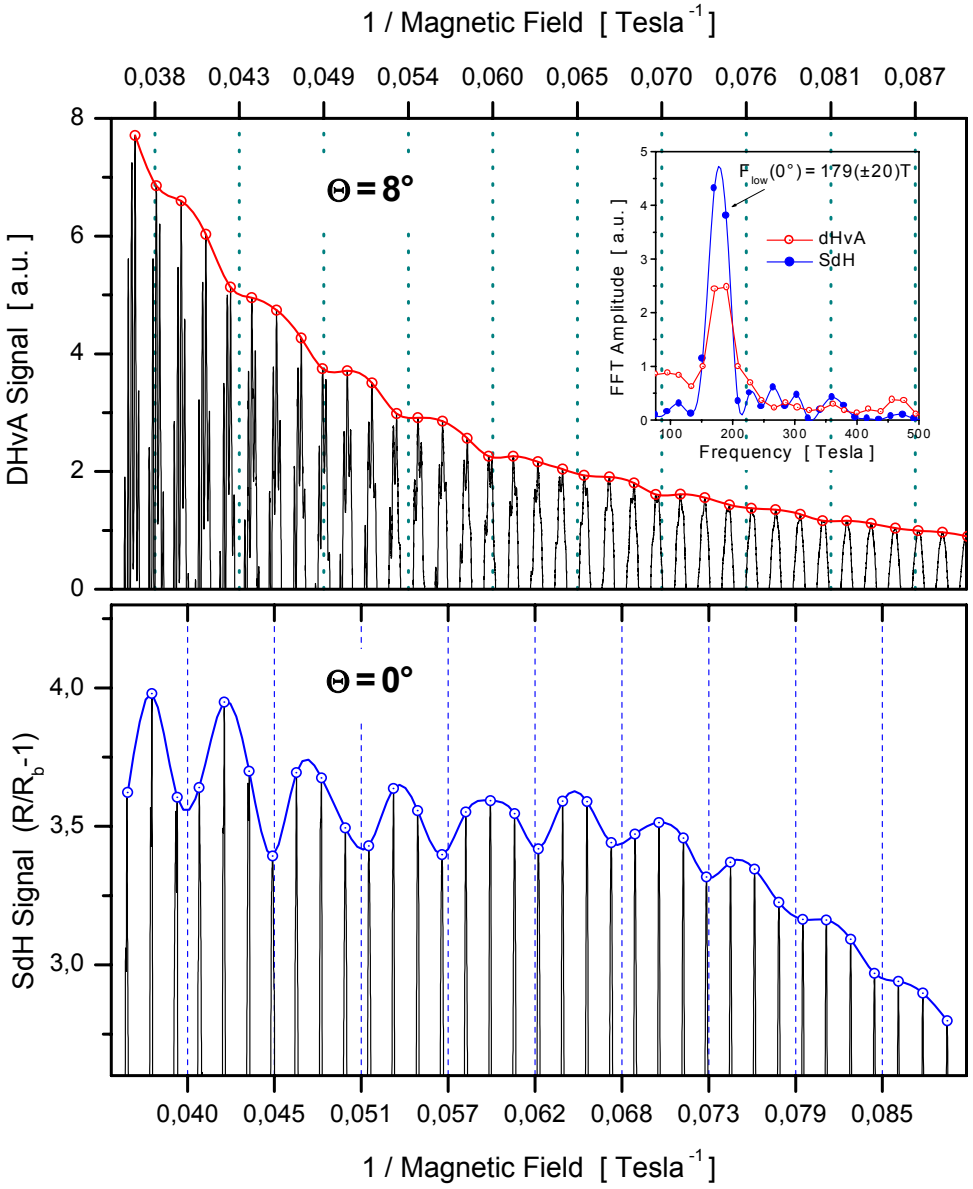

Fig. 6.2: DHvA torque signal (**top**, at Θ = 8° and 0.4K) and SdH signal (**bottom**, at 0° and 30mK) of $(BEDT\text{-}TTF)_4[Ni(dto)_2]$ single crystals. The new low-frequency F_{low} oscillation F_{low} is observable in the envelopes of both types of experiments (the slightly different oscillation period is due to the different tilt angle Θ). **inset:** FFT from both signals, where the FFT from the dHvA signal recorded at 8° was rescaled to 0° by the 1/cosΘ-law. F_{low} (Θ = 0°) = 179(±20)T is obtained.

The two main frequencies F_α and F_β as well as the effective carrier masses m_α* and m_β* were found to show a 1/cosΘ behaviour up to high Θ, which indicates pronounced 2D properties. However in angular dependent measurements beating nodes were observed in SdH as well as dHvA measurements, from which the warping of the FS was estimated for the

two orbits as $\delta F_{\alpha'}/F_\alpha \approx 0.007$ and $\delta F_\beta/F_\beta < 0.007$, respectively. This identifies (BEDT-TTF)$_4$[Ni(dto)$_2$] as quasi-2D electronic system.

Special focus was put on the search for low-frequency oscillations and deviations from standard LK theory in this compound. Indeed in more recent dHvA and SdH studies a low-frequency oscillation $F_{low} = 179(\pm 20)$T was observed (see Fig. 6.2). The presence of such a frequency F_{low} is not suggested by band structure calculations. The fact that F_{low} is observed in both, SdH (i.e., transport) as well as dHvA (i.e., 'pure thermodynamic') experiments, excludes quantum interference effects (discussed in Sec. 3.4.6) as an origin but indicates, that F_{low} is most likely generated by a further pocket on the FS.

It is well-known that the calculated Fermi surfaces of most organic CT salts correspond very well with the experimental results obtained, e.g., by QO experiments. However it is striking that in more and more cases additional oscillations are found, which are not suggested by band structure calculations (see, e.g., $F_{\alpha'}$ in κ-(BEDT-TTF)$_2$Cu[N(CN)$_2$]Br [438,439], Tab. 6.2; F_{new} and F_0 in κ-(BEDT-TTF)$_2$I$_3$, Tabs. 5.7 and 5.8, F_λ and F_γ in κ-(BEDT-TSF)$_2$C(CN)$_3$ [449], F_{low} in the present Ni(dto)$_2$ salt or a very low-frequency oscillation in Θ-(BEDT-TTF)$_2$I$_3$ [421], see also Sec. 6.2.5). In view of this it would be most desirable to succeed in a refinement of band structure calculations.

Owing to the presence of F_{low}, (BEDT-TTF)$_4$[Ni(dto)$_2$] reaches relatively low filling factors $\nu_{Flow} \approx 12$ [5)] at 28T. Despite its quasi-twodimensionality and the relatively low ν, both, dHvA and SdH amplitudes can be perfectly described by standard 3D LK theory under consideration of MB by the coupled network description (CND, see Sec. 3.4.2), except for a correction which is quoted in the following.

This correction to the 3D LK formula and the CND concerns not the absolute amplitudes themselves but the *position* of the beating nodes [181]. In the dHvA experiment the positions of these beating nodes in the oscillations of (BEDT-TTF)$_4$[Ni(dto)$_2$] single crystals were found to be *in line* with the field positions prescribed by the LK formula[6] for two contributing frequencies F_α and $F_{\alpha'}$, where the warping frequency $\Delta F_\alpha = F_\alpha - F_{\alpha'} \approx 4.5$T. However in the SdH signal detected on the same crystal at the same tilt angle, the beating nodes were found to be shifted by a phase of roughly π of the warping frequency ΔF_α. Any phase shift of these nodes is in contradiction with the standard LK formalism, which expects the beating nodes to be exactly at the same field positions in all types of QO experiments. It was shown in [181] that such a high phase shift cannot be explained by scattering processes as inherent to transport experiments [164]. A similar behaviour was suspected in κ-(BEDT-TTF)$_2$Cu[N(CN)$_2$]Br where a beating node was observed in the dHvA signal, while it was clearly absent in the SdH signal [441]. In a later study it was shown that such a phase shift in transport measurements may occur in quasi-2DES with a warped FS in the special case, where the cyclotron energy $\hbar\omega_c$ is comparable to the interlayer transfer integral $t_\perp$ [96]. It was found that the proposed description applies to the phase shift of beating nodes in the quasi-2D organic metal β-(BEDT-TTF)$_2$IBr$_2$, where however the shift between the nodes is much lower than in the Ni(dto)$_2$ salt. A further developed theory, which may explain even the drastic shift in the Ni(dto)$_2$ compound, is in progress [458].

This latter feature found on the Ni(dto)$_2$, the κ-[N(CN)$_2$]Br and the β-(BEDT-TTF)$_2$IBr$_2$ salts, turned out to be a peculiar property of the ratio $\hbar\omega_c/t_\perp$ i.e., the presence of a considerable $t_\perp$ as inherent to *quasi*-2D electronic systems.

Besides this peculiarity, (BEDT-TTF)$_4$[Ni(dto)$_2$] shows conventional 3D LK behaviour even despite of the low $\nu_{Flow} \approx 12$ at high fields for all angles Θ including 0°. This is striking since

[5] Spin splitting is considered in the counting of ν.

[6] For discussion see Secs. 3.4.3. and 5.5.

ν_{Flow} in Ni(dto)$_2$ is comparable to ν_{F0} found in κ-(BEDT-TTF)$_2$I$_3$, where already strong deviations from LK behaviour were found in the latter material (see Sec. 5.4). This suggests to consider that the *quasi*-twodimensionality of the Ni(dto)$_2$ salt may avoid more far-reaching results of two-dimensionality, e.g., electron localisation effects, as indicated in the κ-I$_3$ salt.

6.2.2 The Organic Superconductor β"-(BEDT-TTF)$_2$SF$_5$CH$_2$CF$_2$SO$_3$

The organic superconductor β"-(BEDT-TTF)$_2$SF$_5$CH$_2$CF$_2$SO$_3$ ($T_c \approx$ 4.4K, [459]; β"-SF$_5$CH$_2$CF$_2$SO$_3$ in short) shows quantum oscillations with a frequency $F \approx$ 200T [460]. Its angular dependence follows the 1/cosΘ-law as expected for 2DESs [451,461]. From the field window of observed QOs a warping of this part of the FS can be estimated as $\Delta F/F \lesssim 10^{-2}$, which shows the pronounced two-dimensionality of this system. As a result the material shows sawtooth QOs [451], where however the orientation of this sawtooth is inverse and hints to the presence of a 1D open trajectory, which acts as electron reservoir (as described, e.g., in [417]). The inverse sawtooth of the QOs illustrates how strongly the supposed 1D pocket determines the electronic behaviour at the FS. Information on a warping of this 1D reservoir (as, e.g., possible in the quasi-1D organics) could not yet be obtained.
In addition, β"-SF$_5$CH$_2$CF$_2$SO$_3$ shows a series of further unusual properties. At high B and low T the material undergoes a field-induced metal-insulator transition [462], which may influence, i.a., the interlayer transport of this material [420].
In this compound considerable deviations from standard LK behaviour are observed in magnetotransport. However after a careful extraction of the anomalous background magnetoresistivity, the rescaled QOs in transport can be perfectly described by the 2D dHvA theory [462,460].
Indications for electron localisation effects such as present in the κ-I$_3$ salt are not observed in β"-SF$_5$CH$_2$CF$_2$SO$_3$. Especially at Θ = 0°, the SdH signal up to 60T does not show comparable anomalies as in the κ-I$_3$ material. Nevertheless β"-(BEDT-TTF)$_2$SF$_5$CH$_2$CF$_2$SO$_3$ is a most promising system for the presence of localisation effects [461]. This may not only be assumed from the low ν at high fields, ($\nu \approx 6$ at 60T), but also from the fact that one *single* closed orbit is present at available fields. This means that a relatively wide Landau level spacing (i.e., a wide region of localised states) is present which is *not* intersected by further narrow Landau structures of additional QO frequencies, which would introduce extended states to this region. Thus the β"-SF$_5$CH$_2$CF$_2$SO$_3$ salt maintains expectations on electron localisation at high B and low T, where, if present, especially the metal-insulator transition arises the exciting question, whether the mechanism of possible EL may be similar to that in the κ-I$_3$ salt.

6.2.3 The Quasi-Twodimensional α-Phase Salts α-(BEDT-TTF)$_2$*M*Hg(SCN)$_4$

The Fermi surfaces of the Q2D α-phase salts α-(BEDT-TTF)$_2$*M*Hg(SCN)$_4$ (*M* = K, NH$_4$, Tl, Rb) consist of a closed 2D lens-shaped orbit from which 1D open trajectories are separated by a gap [445,463,464]. This gap is rather large and may be overcome by the magnetic breakdown effect only at very high magnetic fields. This coexistence of 2D and 1D FS sheets locates these materials between 1D and 2D systems. Influences of these different

dimensionalities manifest themselves not only by a competition of density-wave, metallic and superconducting behaviour at low temperatures, but also in high magnetic fields. It was found, e.g., by QO experiments and numerical calculations, that the 1D trajectory strongly influences the 2D part of the FS by acting as an electron reservoir, thus governing the behaviour of the chemical potential in high fields [417]. Besides this action of the 1D part of the FS, especially the behaviour of QOs at very high fields ($B \gtrsim 35$T) is attributed to possible effects of two-dimensionality. The presence of these effects is deduced in a subtle way from pulsed field QO experiments. The subtraction of the QO signals recorded in the very short pulse-up measurements and the longer pulse-down measurements are subtracted from each other and show a hysteresis in the QO signal [465,466]. This is attributed to the presence of eddy current 'resonances' in the crystal (as generated by the field pulse), which occur in conjunction with edge states as present in the IQHE. From this it was supposed that quantised Hall states may be present in some of these salts (M = Tl, K). In a later pulsed field experiment on α-(BEDT-TTF)$_2$TlHg(SCN)$_4$ strong SdH oscillations were found in ρ_{xy} with flat-top saturation effects at about 33T, i.e., at $\nu \approx 40$ [467]. Actually the question is open if these effects may be attributed to the IQHE [467], if other, more exotic explanations have to be considered [84] or whether they might be generated by spin splitting arising at high fields.

6.2.4 The Stable 8K Organic Superconductor β_T-(BEDT-TTF)$_2$I$_3$

β-(BEDT-TTF)$_2$I$_3$ is an organic superconductor with an ambient pressure $T_c \approx 1$K [468]. Application of a moderate pressure ($p \gtrsim 300$bar, [469]) suppresses a metal-metal transition at 175K and results in an enhancement of T_c to about 8.1K. This high-T_c phase is called β_H-(BEDT-TTF)$_2$I$_3$ [469,470] (or β_H-I$_3$ for short, whereas the low-T_c phase is also called β_L-I$_3$). β_H-I$_3$ is stable even when pressure is released unless temperature exceeds about 120K [471]. Quantum oscillations on β_H-I$_3$ were first reported in Ref. [472].

For a couple of years it was a challenge to find a method, which allows the preparation of such a high-T_c phase of β-I$_3$, which is stable not only at ambient pressure but even at room temperature. This aim was reached by a thermal treatment of β-I$_3$ [473]. For this procedure β-I$_3$ single crystals are locked in a glass ampoule under nitrogen or argon gas together with a few crystallites of pure I$_2$. The latter additive lowers evaporation of I$_3$ during annealing. The ampoule is heated up to about 390K for about 2h. The crystals treated by this, called β_T-(BEDT-TTF)$_2$I$_3$ (or simply β_T-I$_3$) in the following are stable at ambient pressure below 390K and after cooling they show a superconducting transition with $T_c \approx 8$K in resistivity (see Fig. 6.3.a). This transition temperature remembers to β_H-I$_3$.

DHvA torque experiments were carried out on β_T-I$_3$ crystals up to 28T at 1.3K < T < 30mK. A typical result is shown in Fig. 6.3. A collection of the fermiological data obtained from these preliminary experiments is given in Tab. 6.4. β_T-I$_3$ holds a series of striking results: The observed low-frequency oscillation F_{low} can be attributed to β_L-I$_3$ [474,475], while F_β is up to now only observed in β_H-I$_3$ [472], but not in β_L-I$_3$. Moreover $F_{\alpha'}$ is not known from band structure calculations, even if their results are supposed to be very similar for both, β_L-I$_3$ and β_H-I$_3$ (see, e.g. [476,477]).

It should be mentioned that first SdH experiments performed on β_T-I$_3$ show F_β, however only above about 26T. A rather low signal-to-noise ratio in these SdH experiments indicates that the thermally induced phase transition from β_L-I$_3$ to β_T-I$_3$ generates most likely crystal imperfections, so that the annealing process has to be further optimised.

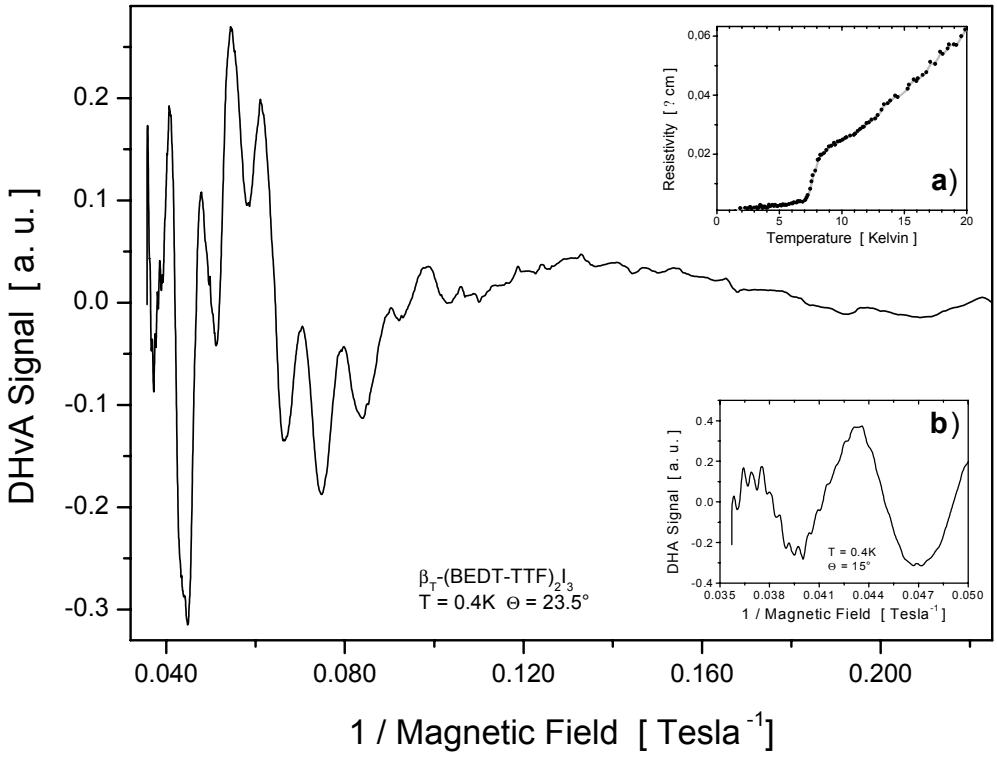

Fig. 6.3: a): Superconducting transition of the stable annealed phase β_T-(BEDT-TTF)$_2$I$_3$; (**main part**): Typical dHvA torque signal detected on β_T-(BEDT-TTF)$_2$I$_3$ crystals; **b)** High-field part of a dHvA signal ([473]).

β_T-(BEDT-TTF)$_2$I$_3$	A_{Fj} [nm^{-2}]	Part of the FBZ [%]	m_{Fj}* [m$_e$]	$T_{D,Fj}$ [K]	τ_{Fj} [ps]
F_{low} = 12(±2)T	0,1	0,3			
F_{low} = 115(±15)T	1,1	3			
$F_{\alpha'}$ = 1725(±25)T	16,6	45	1,2		
F_{β} = 3850(±20)T	37	100	≈ 5	1,2	1

Tab. 6.4: Fermiological data of β_T-(BEDT-TTF)$_2$I$_3$ obtained from dHvA experiments [473].

The QO frequencies F_{low}, $F_{\alpha'}$ as well as F_{β} show an 1/cosΘ-behaviour as expected for a pronounced 2D system. A further frequency F_{new} is observed in dHvA experiments, which is likewise not represented in band structure calculations. The fact that it is detected in a dHvA experiment excludes that it originates, e.g., from an interference process, since the latter would only influence transport. The angular dependence of F_{new} could not yet be determined, i.a., due to the presence of an angular dependent background signal as well as indications for spin zeros of F_{new}. Especially the latter finding suggests that F_{new} indeed originates from a very small closed pocket in *k*-space. In this case β_T-I$_3$ would reach quantum limit and even $\nu_{Fnew} < 1$ at high fields.

The actual results hint to a corrugation of the band connected with $F_{\alpha'}$ with a warping of $\Delta F_{\alpha'}/F_{\alpha'} \approx 3.7\%$. However it is stressed that $\Delta F_{\alpha'}/F_{\alpha'}$ could not be obtained as usual from the

intercept of two neighbouring beating nodes, since this low warping causes that only one node is indicated in the field range covered by the experiments. Therefore $\Delta F_{\alpha'}/F_{\alpha'}$ is estimated from the distance $\Delta F_{\alpha'}$ of a double-peak structure in the FFT of the entire signal, as present at certain tilt angles (e.g., at 9°). In view of the limited resolution of the FFT itself, it is emphasised that the actual $\Delta F_{\alpha'}/F_{\alpha'}$ estimation can be only rather crude. The warping frequency itself ($\Delta F_{\alpha'}(9°) = 65$T) indicated in β_T-I_3 remembers to the values $\Delta F_\beta = 74$T (at 0°) [472] and $\Delta F_\beta = 57.3$T (at 4°) [478] found in β_H-I_3 which, however, where found in F_β instead of $F_{\alpha'}$.
This indication of a warping hints to the presence of a notable interlayer transfer integral and thus to the fact that β_T-(BEDT-TTF)$_2I_3$ is a quasi-2D electronic system. Except for a considerable anharmonicity of the dHvA signals, no further signs for deviations from standard QO theories are found in this material. However in view of the facts that detailed SdH experiments at the special angle $\Theta = 0°$ could not yet be carried out and that crystal quality ($T_D = 1.2$K) has to be improved, β_T-(BEDT-TTF)$_2I_3$ might still remain a candidate for the occurrence of electron localisation effects especially at high fields, where $\nu_{Fnew} < 1$ might be reached in this material.

6.2.5 The Organic Superconductor Θ-(BEDT-TTF)$_2I_3$

Θ-(BEDT-TTF)$_2I_3$ is an organic superconductor with a $T_c \approx 3.6$K [479]. It is recalled that the correct stoichiometry of the first syntheses reads Θ-(BEDT-TTF)$_2(I_3)_{1-x}(AuI_2)_x$ with $x < 0.02$, since a small amount of AuI_2 was needed during the syntheses to succeed in the crystallisation of Θ-phase crystals. Initially there has been confusion on the crystal structure in the sense that an orthorhombic unit cell was found in first structure investigations [479], whereas a superstructure with a double-sized monoclinic unit cell was found later [480,481]. Correspondingly, different band structures and Fermi surfaces were proposed in Refs. [479,480,482]. Quantum oscillation experiments show two dominant oscillations with the frequencies $F_\alpha = 779$T and $F_\beta = 4234$T [482,483], which correspond very good to the latter of the proposed Fermi surfaces [482]. This agreement is confirmed by angular magnetoresistance oscillations, which in addition indicate a warped quasi-twodimensional FS [484]. However this latter finding is rather contradictory to the presence of a sharp sawtooth dHvA signal, which is interpreted in terms of even strong two-dimensionality [482,485].
In addition to F_α and F_β a further very low-frequency oscillatory structure was observed in magnetotransport with a frequency between 2T and 12T [421], which cannot be attributed to any of the band structure calculations quoted above. The very striking observation was that this oscillatory pattern is observed only below about 2T. A careful angular dependent investigation showed that this oscillation is present not only for field orientation perpendicular to the quasi-2D conducting planes (called 0° here), but even in the field orientation parallel to the planes (denoted as 90° here). From these results it was concluded that the oscillatory structure may be attributed to a 3D pocket on the Fermi surface.
Especially the presence of a low-frequency oscillation in the SdH signal was a motivation for our reproduction of this compound. The residual confusion on the structure of Θ-(BEDT-TTF)$_2(I_3)_{1-x}(AuI_2)_x$ asked to aspire to a synthesis without the use of AuI_2, which was indeed realised, so that the crystals have the stoichiometry Θ-(BEDT-TTF)$_2I_3$.
Our SdH experiments reproduce clearly the QO frequencies F_α and F_β as well as the very low-frequency oscillation. The presence of the latter was verified and confirmed in the field

orientations perpendicular and especially parallel to the conducting planes. Following the attribution of the low-frequency oscillation to a small 3D pocket on the FS, i.e., to a real quantised orbit, means that this Θ-phase salt would reach indeed quantum limit at available fields. In view of this and taking up the question on the strength of the electronic two-dimesnionality, we concentrated on the search for deviations in the temperature dependence of the SdH amplitudes especially at Θ = 0°. This was verified in order to find out whether this (quasi-)2D material might show similarly strong effects of two-dimensionality (i.e., damping effects of the QO amplitudes) as observed in the κ-phase of (BEDT-TTF)$_2$I$_3$ (see Sec. 5.3 ff.). By very recent SdH measurements it was found that the temperature dependence of the oscillation amplitudes of both, F_α and F_β, show the same behaviour at low fields (9T) and high fields (23T) [486]. Consequently for each of these frequencies the values m_α*(9T) = m_α*(23T) and m_β*(9T) = m_β*(23T) were obtained. The same behaviour was found for other tilt angles between field and conducting planes, i.e., Θ ≠ 0°. Hence, contrary to the behaviour of the 2D κ-phase salt, where this tilt angle plays a decisive role (see Sec. 5.3), in the Θ-phase no difference in the behaviour of the SdH oscillations were found for Θ = 0° and Θ ≠ 0°, respectively.
This means that despite its presumably low filling factors, the Θ-phase of (BEDT-TTF)$_2$I$_3$ does not show strong field dependent damping effects of the SdH amplitudes as present in κ-(BEDT-TTF)$_2$I$_3$ at 0°, which is however not surprising in view of the influence of the small 3D pocket on the Fermi surface. A more conclusive statement on the quasi-twodimensionality of Θ-(BEDT-TTF)$_2$I$_3$ cannot be given from the actual scope of results. However the proposed presence of the 3D small pocket on the FS suggests to consider that the electronic behaviour of this latter material may indeed be influenced by 3D properties.
In summary it was found that even though Θ-(BEDT-TTF)$_2$I$_3$ reaches most probably quantum limit, it does not show comparable effects of two dimensionality as observed in the κ-phase. Instead, the results on Θ-(BEDT-TTF)$_2$I$_3$ indicate the presence of a 3D pocket on the FS which might influence the (quasi-)2D electronic behaviour of this material.

In the present chapter a number of materials was examined, concentrating on the question whether the most important conditions, i.e.,

- strong two-dimensionality and
- low filling factors $\nu \lesssim 1$

are given, which may enable the occurrence of electron localisation effects as indicated in κ-(BEDT-TTF)$_2$I$_3$. This question was first followed within the κ-phase materials, which are known to be most promising for the realisation of 2DESs within the organics. In addition further compounds were synthesised, prepared, examined or reviewed, respectively, on the search for the realisation of the above mentioned conditions.
Actually it can be summarised that an electronic behaviour, which compares to that of κ-(BEDT-TTF)$_2$I$_3$, is not yet observed in any of the known quasi-2D organic conductors, least of all the presence of $\nu = 1/2$. Furthermore, among the organics, a material which meets *both* above mentioned requirements, is not available to date. This is the reason, why the present work had to be concentrated on the investigation of this most 2D organic metal κ-(BEDT-TTF)$_2$I$_3$ in its quantum limit and extreme quantum limit ($\nu \leq 1$).

Besides a number of open questions on the behaviour of κ-(BEDT-TTF)$_2$I$_3$ in high magnetic fields, further efforts have to be done on the synthesis of such multilayer 2DESs, which are in

many aspects very different from the ‘well-known’ semiconducting 2DESs. Of course this challenge includes also further possibilities which could not be discussed here as, e.g., the fabrication of thin films of 2D organic CT salts [487,488,489,490], the possibilities of their doping, but also the closer investigation of different classes of multilayer 2DESs as, e.g., high-T_c superconductors on the search for results of strong two-dimensionality.

7. Summary

This work presents quantum oscillation experiments in quasi-twodimensional multilayer organic metals. They show that low integer Landau level filling factors ν are present in the two-dimensional organic metal κ-(BEDT-TTF)$_2$I$_3$ and give strong indications for the existence of the fractional filling factor ν = ½ in this material. By this the work shows the presence of electron localisation and electron correlation in a bulk metallic two-dimensional system.
The underlying investigations had to be concentrated on the organic metal κ-(BEDT-TTF)$_2$I$_3$ since it meets the most important conditions for such effects, i.e., strongest two-dimensionality and the presence of quantised orbits (corresponding, e.g., to F_{new}), which impose extreme quantum limit to the entire electronic system.
κ-(BEDT-TTF)$_2$I$_3$ holds in many respects strongly different conditions compared to the well-known semiconducting single-layer 2D systems. The former material is metallic, it provides a very high electron density of 10^{19}/cm^2 and also a very high carrier mobility reaching $5*10^8$cm^2/Vs. It represents a system of 10^5 coupled metallic multilayers including interlayer tunnelling and it can be synthesised in very high purity as three-dimensional bulk single crystals. Despite of this, the material is found to show strongly two-dimensional electronic properties under certain experimental conditions, i.e., low temperatures and high magnetic fields applied perpendicular to the conducting planes. In contrast to the general situation in semiconducting two-dimensional systems, where (correlated) electrons move on one single quantised orbit, the carriers in κ-(BEDT-TTF)$_2$I$_3$ move on various quantised orbits with even very different filling factors, whose carriers are nevertheless strongly correlated. These are the main conditions under which the total filling factors ν_{tot} = ½ as well as 1, 2, 3, 4 are observed experimentally in κ-(BEDT-TTF)$_2$I$_3$.
Besides its very high electron number and mobility, its metallic properties, the correlation of different orbits, the very high number of coupled layers, κ-(BEDT-TTF)$_2$I$_3$ holds a number of further peculiarities, e.g., the coexistence of extended and localised electronic states or a field dependent dielectric constant. This combination of conditions may represent a challenge for the theoretical understanding of the ground states, which may be realised in bulk multilayer 2D electronic systems at high magnetic fields and low temperatures.

Besides this, the present work gives an insight to the power of quantum oscillation experiments in the investigations of influences of low-dimensionality onto the electronic properties of such materials. By this type of experiments, i.a., the electronic two-dimensionality can be probed and quantified in terms of the ratio of intra- and interlayer transfer integrals. The application of theories for quantum oscillations in 3D and 2D metals can be verified and their limits can be explored.
In addition, quantum oscillation measurements were found to be a very suited tool for the direct detection of the chemical potential and its variations - even under rather complex fermiological conditions.
The sensitivity of quantum oscillation experiments to electronic low-dimensionality as well as a series of further fermiological peculiarities was shown to reveal a number of surprising experimental results which may stimulate the progress and refinement of their theoretical description.

Acknowledgements

It is a pleasure to thank the following people for their contribution to this work!

Many thanks to Prof. Dieter Schweitzer for his supply with excellent crystals of a number of different organic conductors and superconductors, for very fruitful discussions, for his strong interest on the progress of this work and for the excellent collaboration;
Prof. Peter Wyder for the possibility to work during my postdoctoral fellowship at the Grenoble High Magnetic Field Laboratory (GHMFL), for very stimulating discussions, for his interest in the progress of this work and for the very fruitful and pleasant collaboration;
Prof. H.J.Keller, Dr. W.Strunz and I.Heinen for their long-standing efforts in the syntheses of low-dimensional organic conductors and for the supply with excellent crystals;
Prof. Louis (A.G.M.) Jansen (GHMFL / Centre d'Energie Atomique Grenoble), Dr. E.Steep as well as P.v.d.Linden (GHMFL) for very stimulating discussions, for the great support in a number of experimental questions and for the just as fruitful as very pleasant collaboration; Dr. E.Mossang, C.Warth-Martin and Dr. J.C.Vallier (GHMFL) for their very engaged support at the magnet sites; Drs. W.Joss, G.Martinez and M.Potemski (GHMFL) for their continuing interest in this work and for valuable discussions; Dr. D.K.Maude, Prof. J.C.Portal, Dr. S. de Brion (GHMFL) for all their spontaneous support with setup devices;
Drs. W.Biberacher and M.V.Kartsovnik, (Walther-Meissner-Institut Garching), Drs. A.Audouard and L.Brossard (Pulsed Field Laboratory LNCMP Toulouse) for very stimulating discussions, for their support in experimental questions and for the very pleasant collaboration; C.Proust (LNCMP) for his contribution in the framework of his PhD thesis;
Drs. T.Maniv, I.D.Vagner, M.A.Itskovsky (Technion-Israel-Institute of Technology Haifa) for very stimulating discussions and for the fruitful collaboration, T.Ziman (Institut Laue Langevin Grenoble), Prof. M.Lang and Prof. J.Wosnitza (Technische Universität Dresden) for very valuable discussions;
Prof. K. von Klitzing, Prof. A.M.Kosevich, Prof. B.I.Halperin, Prof. J.K.Jain, for very interesting and helpful discussions during meetings on the interpretation of the results;
Prof. J.Wrachtrup for the possibility to finish this work in the 3. Physikalisches Institut der Univesität Stuttgart;
All the colleagues from the workgroup of Prof. D. Schweitzer, especially those PhD students involved in the present work, i.e., A.Nothardt, M.Schiller and W.Schmidt for their contributions, for their support and for the very pleasant collaboration;
The members of the Max-Planck Institut für Festkörperforschung / Centre National de la Recherche Scientifique at the Grenoble High Magnetic Field Laboratory, especially the collaborating PhD students A.Gröger, R.Schleser and H.Weiss involved in the present work as well as in further subjects: thanks for all their contributions, for their support and for the very pleasant collaboration;
The members of the 3. Physikalisches Institut der Universität Stuttgart, for the agreeable working atmosphere.

Parts of this work were supported by the Training and Mobility of Researchers Programme of the European Community and, respectively, by the Deutsche Forschungsgemeinschaft.

Appendix A

Selected Characteristics of the 2D Multilayer Organic Metal κ-(BEDT-TTF)$_2$I$_3$

- typical single crystal size: $1 * 2 * 0.25 mm^3$
- layer spacing $d \approx 1.56$nm (centre - to - centre, see Fig. 2.5.a)
- number of layers in a crystal $N_L \approx 1.6 * 10^5$
- dielectric constant $\varepsilon \approx 8 \ldots 50$; indications for magnetic field dependence
- carrier mobility $\mu \approx 5 * 10^8 cm^2/Vs$
- electron density: $N_{e,bulk} \approx 7 * 10^{20}/cm^3$
  in detail on each of the correlated orbits:

κ-(BEDT-TTF)$_2$I$_3$	$n_{e,layer}$ [cm^{-2}] per single layer	$n_{e,sample}$ [cm^{-2}] per bulk sample surface	$n_{e,bulk}$ [cm^{-3}] per volume
$F_{new} = 3,8T$	$8 * 10^{10}$	$1,2 * 10^{16}$	$5 * 10^{17}$
$F_0 = 13,2T$ [1)]	$3 * 10^{11}$	$4,7 * 10^{16}$	$1.9 * 10^{18}$
$F_1 = 100T$ [1)]	$2,4 * 10^{12}$	$3,7 * 10^{17}$	$1,5 * 10^{19}$
$F_2 = 570T$ [1)]	$1,4 * 10^{13}$	$2,2 * 10^{18}$	$9 * 10^{19}$
$F_3 = 3883T$ [1)]	$9,5 * 10^{13}$	$1,5 * 10^{19}$	$6,1 * 10^{20}$
total $N_{e,QO}$ from QOs [1)]	$1,1 * 10^{14}$	$1,8 * 10^{19}$	$\approx 7 * 10^{20}$
total $N_{e,sto}$ from stoichiometry [2)]			$\gtrsim 2 * 10^{20}$

Tab. A1: Experimental values for the number of electrons n_e on each of the correlated orbits corresponding to the QO frequencies F_j.
$n_{e,layer}$ is given per single layer and cm^{-2},
$n_{e,sample}$ per cm^{-2} in a typical sample (thickness 0.25mm) and
$n_{e,bulk}$ per unit volume, respectively.

Lower lines: total number of carriers
[1)] $N_{e,QO}$ obtained from QO measurements, considering the Landau level degeneration factor.
[2)] $N_{e,sto}$ obtained from stoichiometry where 0.5 charge transfer per BEDT-TTF molecule, two molecules per unit cell and dimeristaion is considered.

——— * ———

References

[1] H.Akamatu, H.Inokuchi, Y.Matsunaga, Nature (London) **173**, (1954)

[2] H.Inokuchi, H.Akamatu, *Solid State Physics*, Vol. **12**, ed. by F.Seitz, D.Turnbull, Academic Press, New York, p. 93 (1961)

[3] D.S.Acker, R.J.Harder, W.R.Hertler, W.Mahler, L.R.Melby, R.E.Benson, W.R.Mochel, J. Am. Chem. Soc. **82**, 6408 (1960)

[4] D.L.Coffen, P.E.Garrett, E.J.Hufnagel, Tetrahedron Lett. 2043 (1969)

[5] F.Wudl, G.M.Smith, E.J.Hufnagel, Chem.Commun. 1453 (1970)

[6] **a)** L.B.Coleman, M.J.Cohen, D.J.Sandman, F.G.Yamagishi, A.F.Garito, A.J.Heeger, Sol. State Commun. **12**, 1125 (1973); **b)** L.B.Coleman, M.J.Cohen, A.F.Garito, A.J.Heeger, Phys. Rev. **B7**, 2122 (1973)

[7] J.Ferraris, D.O.Cowan, V.Walatka Jr., J.H.Perlstein, J. Am. Chem. Soc. **95**, 948 (1973)

[8] R.E.Peierls, *Quantum Theory of Solids*, Oxford Univ. Press, London (1955)

[9] H.Fröhlich, Proc. Roy. Soc. London, Ser. A **223**, 296 (1954)

[10] A.W.Overhauser, Phys. Rev. Lett. **4**, 462 (1960)

[11] For reviews especially on 1D conductors see, e.g.,: *Low-Dimensional Cooperative Phenomena,* ed. by. H.J.Keller, Plenum New York (1974); S.Kagoshima, H.Nagasawa, T.Sambongi, *One-Dimensional Conductors*, Springer Ser. Solid State Sci. Vol. **72**, Springer, Berlin, Heidelberg (1988)

[12] Yu.A.Bychkov, L.P.Gor'kov, I.E.Dzyaloshinskii, Sov. Phys. JETP Lett. **23**, 489 (1966)

[13] N.F.Mott, W.D.Twose, Adv. Phys. **10**, 107 (1961)

[14] L.D.Landau, Sov. Phys. JETP, **3**, 920 (1957)

[15] D.Pines, P.Nozières, *The Theory of Quantum Liquids I*, Benjamin, New York (1966)

[16] A.Tomonaga, Prog. Theor. Phys. **5**, 544 (1950)

[17] J.M.Luttinger, J. Math. Phys. **4**, 1154 (1963)

[18] D.Jérome, Science **252**, 1509 (1991)

[19] P.M.Chaikin, J.S.Brooks, S.T.Hannahs, W.Kang, G.Montambaux, L.Y.Chiang, in: *The Physics and Chemistry of Organic Superconductors*, ed. by. G.Saito, S.Kagoshima, Springer, Berlin, Heidelberg, p.81 (1990)

[20] W.Kang, S.T.Hannahs, P.M.Chaikin, Phys. Rev. Lett. **70**, 3091 (1993)

[21] S.K.McKernan, S.T.Hannahs, U.M.Scheven, G.M.Danner, P.M.Chaikin, Phys. Rev. Lett. **75**, 1630 (1995)

[22] R.Itti, H.Mori, K.Ikeda, I.Hirabayashi, N.Koshizuka, S.Tanaka, Physica C **185-189**, 2673 (1991)

[23] B.Dardel, D.Malterre, M.Gironi, P.Weibel, Y.Baer, J.Voit, D.Jérome, Europhys. Lett. **24**, 687 (1993)

[24] R.Liu, H.Ding, J.C.Campuzano, H.H.Wang, J.M.Williams, K.D.Carlson, Phys. Rev. B **51**, pp. 6155 and 13000 (1995)

[25] See proceedings of the *Vth International Symposium on Crystalline Organic Metals, Superconductors and Magnets (ISCOM),* 2003, to be published in J. Phys. IV, (2004) and Refs. therein

[26] W.A.Little, Phys. Rev. **134**, A1416 (1964)

[27] W.A.Little, Sci. Am. **212**, 21 (1965)

[28] J.Bardeen, L.N.Cooper, J.R.Schrieffer, Phys. Rev. **108**, 1175 (1957)

[29] D.Jérome, A.Mazaud, M.Ribault, K.Bechgaard, J. Phys. Lett. **41**, L95 (1980)

[30] D.Jérome, H.J.Schulz, Adv. Phys. **31**, 299 (1982)

[31] K.Bechgaard, K.Caneiro, M.Olsen, F.B.Rasmussen, C.S.Jacobsen, Phys. Rev. Lett. **46**, 852 (1981)

[32] R.L.Greene, P.M.Chaikin, Physica B **126**, 431 (1984)

[33] S.Kagoshima, H.Nagasawa, T.Sambongi, *One-Dimensional Conductors*, Springer Ser. Solid State Sci. Vol **72**, Springer, Berlin, Heidelberg (1988)

[34] T.Ishiguro, K.Yamaji, *Organic Superconductors*, Springer, Berlin, Heidelberg (1990)

[35] J.M.Williams, J.R.Ferraro, R.J.Thorn, K.D.Carlson, U.Geiser, H.H.Wang, A.M.Kini, M-.H.Whangbo, *Organic Superconductors: Synthesis, Structure, Properties and Theory*, Prentice Hall Enlewood Cliffs (1992)

[36] H.Mori, Int. J. Mod. Phys. B **8**, 1 (1994)

[37] See proceedings of the *International Conference on Synthetic Metals (ICSM),* 2002, published in Synth. Metals, **133-134** (2003)

[38] J.M.Williams, Science **252**, 1501 (1991)

[39] for a review see P.Cassoux, L.Valade, H.Kobayashi, A.Kobayashi, R.A.Clark, A.E.Underhill, Coord. Chem. Rev. **110**, 115 (1991)

[40] M.Mizuno, A.F.Garit SAI82o, M.P.Cava, J. Chem. Soc. Chem. Comm. **18**, (1978)

[41] G.Saito, T.Enoki, K.Torimuri, H.Inokuchi, Sol. State Commun. **42**, 557 (1982)

[42] S.S.P.Parkin, E.M.Engler, R.R.Schumaker, R.Lagier, V.Y.Lee, J.C.Scott, R.L.Greene, Phys. Rev. Lett. **50**, 270 (1983)

[43] H.Urayama, H.Yamochi, G.Saito, K.Nozawa, T.Sugano, M.Kinoshita, S.Sato, K.Oshima, A.Kawamoto, J.Tanaka, Chem. Lett. 55 (1988); H.Urayama, H.Yamochi, G.Saito, S.Sato, A.Kawamoto, J.Tanaka, T.Mori, Y.Maruyama, H.Inokuchi, Chem. Lett. 463 (1988)

[44] K.Oshima, H.Urayama, H.Yamochi, G.Saito, J.Phys. Soc. Jpn. **57**, 730 (1988); K.Nozawa, T.Sugano, H.Urayama, H.Yamochi, G.Saito, M.Kinoshita, Chem. Lett. 617 (1988)

[45] A.M.Kini, U.Geiser, H.H.Wang, K.D.Carlson, J.M.Williams, W.K.Kwok, K.G.Vandervoort, J.E.Thompson, D.L.Stupka, D.Jung, M.-H.Whangbo, Inorg. Chem. **29**, 2555 (1990)

[46] J.M.Williams, A.M.Kini, H.H.Wang, K.D.Carlson, U.Geiser, L.K.Montgomery, G.J.Pyrka, D.M.Watkins, J.M.Kommers, S.J.Boryschuk, A.V.S.Crouch, W.K.Kwok, J.E.Shirber, D.L.Overmyer, D.Jung, M.-H.Whangbo, Inorg. Chem. **29**, 3274 (1990)

[47] H.Taniguchi, M.Myashita, K.Uchiyama, K.Satoh, N.Mori, H.Okamoto, K.Myagawa. K.Kanoda, M.Hedo, Y.Uwatoko, proceedings of the *Vth International Symposium on Crystalline Organic Metals, Superconductors and Magnets (ISCOM),* (2003), to be published in J. Phys. IV, (2004)

[48] K.Kikuchi, M.Kikuchi, T.Namaki, K.Saito, I.Ikemoto, K.Murata, T.Ishiguro, K.Kobayashi, Chem. Lett. 931 (1987); K.Kikuchi, Y.Honda, Y.Ishikawa, K.Saito, I.Ikemoto, K.Murata, H.Anzai, T.Ishiguro, Sol. State Commun. **66**, 405 (1988)

[49] G.C.Papavassiliou, G.A.Mousdis, J.S.Zambounis, A.Terzis, A.Hountas, B.Hilti, C.W.Mayer, J.Peiffer, Synth. Met. **27**, B379 (1988)

[50] R.Kato, S.Aouna, Y.Okano, H.Sawa, M.Tamura, M.Kinoshita, K.Oshima, A.Kobayashi, K.Bun, H.Kobayashi, Synth. Met. **61**, 199 (1993)

[51] K.Oshima, H.Okuno, K.Kato, R.Murayama, R.Kato, A.Kobayashi, H.Kobayashi, Synth. Met. **70**, 861 (1995)

[52] S.Kahlich, D.Schweitzer, I.Heinen, S.E.Lan, B.Nuber, H.J.Keller, K.Winzer, H.W.Helberg, Sol. State Commun. **80**, 191 (1991)

[53] H.Kobayashi, H.Tomita, T.Naito, H.Tanaka, A.Kobayashi, T.Saito, J. Chem. Soc. Chem. Commun. 1225 (1995)

[54] R.Kleiner, F.Steinmeyer, G.Kunkel, P.Müller, Phys. Rev. Lett. **68**, 2394 (1992)

[55] P.Müller, *Advances in Solid State Physics,* **34**, Vieweg, Braunschweig (1994)

[56] F.Zuo, J.Hagel, S.Wanka, J.Wosnitza, E.Balthes, D.Schweitzer, W.Strunz, Physica **C 333** 79 (2000)

[57] M.Lang, F.Steglich, N.Toyota, T.Sasaki, Phys. Rev. B **49**, 15227 (1994)

[58] M.Lang, *Quasi-Twodimensional Organic Superconductors*, Supercond. Rev. Vol. **2**, 1 (1996)

[59] S.Wanka, D.Beckmann, J.Wosnitza, E.Balthes, D.Schweitzer, W.Strunz, H.J.Keller, Phys. Rev. **B 53**, 9301 (1996)

[60] L.C.Hebel, C.P.Schlichter, Phys. Rev. **113**, 1504 (1959)

[61] F.Creuzet, C.Bourbonnais, D.Jérome, D.Schweitzer, H.J.Keller, Europhys. Lett. **1**, 467, (1986); F.Creuzet, C.Bourbonnais, G.Creuzet, D.Jérome, D.Schweitzer, H.J.Keller, Physica B **143**, 363 (1986)

[62] Y.Maniwa, T.Takahashi, G.Saito, J. Phys. Soc. Jpn. **55**, 47 (1986); Y.Maniwa, T.Takahashi, M.Takigawa, H.Yasuoka, G.Saito, K.Murata, M.Tokumoto, H.Anzai, J. Phys. Soc. Jpn. **58**, 1048 (1989); T.Takahashi, T.Tokiwa, K.Kanoda, H.Urayama, H.yamochi, G.Saito, Physica C **153-155**, 487 (1988); Synth. Metals **27**, A319 (1988)

[63] S.M.DeSoto, C.P.Schlichter, H.H.Wang, U.Geiser, J.M.Williams, Phys. Rev. Lett. **70**, 2956 (1993)

[64] M.T.Béal-Monod, C.Bourbonnais, V.J.Emery, Phys. Rev. B **34**, 7716 (1986)

[65] D.J.Scalapino, E.Loh Jr., J.E.Hirsch, Phys. rev. B **35**, 6694 (1987)

[66] M.Takigawa, H.Yasuoka, G.Saito, J. Phys. Soc. Jpn. **56**, 873 (1987)

[67] I.J.Lee, M.J.Naughton, P.M.Chaikin, Physica B **294-295**, 413 (2001)

[68] M.J.Naughton, J.I.Oh, contribution the *Vth International Symposium on Crystalline Organic Metals, Superconductors and Magnets (ISCOM),* p. 20 (2003), to be published in J. Phys. IV, (2004), see also refs therein

[69] K.Kanoda, K.Akiba, K.Suzuki, T.Takahashi, Phys. Rev. Lett. **65**, 1271 (1990); T.Takahashi, K.Kanoda, K.Akiba, K.Sakako, M.Watabe, K.Suzuki, G.Saito, Synth. Metals **41-43**, 2005 (1991);

[70] S.Sridhar, B.Maheswaran, B.A.Willemsen, D.H.Wu, R.C.Haddon, Phys. Rev. Lett. **68**, 2220 (1992)

[71] L.P.Le, G.M.Luke, B.J.Sternlieb, W.D.Wu, Y.J.Uemura, J.H.Brewer, T.M.Riseman, C.E.Stornach, G.Saito, H.Yamochi, H.H.Wang, A.M.Kini, K.D.Carlson, J.M.Williams, Phys. Rev. Lett. **68**, 1923 (1992)

[72] D.Achkir, M.Poirer, C.Bourbonnais, G.Qiurion, C.Lenoir, P.Batail, D.Jérome, Phys. Rev. B **47**, 11595 (1993)

[73] M.Pinteric, S.Tomic, M.Prester, D.Drobac, O.Milat, K.maki, D.Schweitzer, I.Heinen, W.Strunz, Phys. Rev. B **61**, 7033 (2000)

[74] R.W.Giannetta, D.D.Lawrie, A.Carrington, R.Prozorov, J.A.Schlueter, A.M.Kini, J.Montasham, R.W.Winter, G.L.Gard, I.J.Bonalde, contribution the *Vth International Symposium on Crystalline Organic Metals, Superconductors and Magnets (ISCOM),* p. 52 (2003), to be published in J. Phys. IV, (2004)

[75] D.R.Harshman, R.N.Kleinman, R.C.Haddon, S.V.Chichester-Hicks, M.L.Kaplan, L.W.Rupp Jr., T. Pfitz, D.L.Williams, D..Mitzi, Phys. Rev. Lett. **64**, 1293 (1990); D.R.Harshman, A.T.Fiori, R.C.Haddon, M.L.Kaplan, T.Pfitz, E.KOster, I.Shikoda, D.L.Williams, Phys. Rev. B **49**, 12990 (1994)

[76] K.Holczer, D.Quinlivan, O.Klein, G.Grüner, F.Wudl, Sol. State Commun. **76**, 499 (1990); K.Holczer, O.Klein, G.Grüner, H.Yamochi, F.Wudl in: *Organic Superconductivity,* ed. by V.Z.Kresin, W.A.Little, Plenum, New York, p. 81 (1990);

[77] O.Klein, K.Holczer, G.Grüner, J.J.Chang, F.Wudl, Phys. Rev. Lett. **66**, 655 (1991)

[78] M.Lang, N.Toyota, T.Sasaki, H.Sato, Phys. Rev. Lett. **69**, 1443 (1992); M.Lang, N.Toyota, T.Sasaki, Physica B **186-188**, 1046 (1993)

[79] M.Lang, N.Toyota, T.Sasaki, H.Sato, Phys. Rev. B **46**, 5822 (1992)

[80] M.Dressel, S.Bruder, G.Grüner, K.D.Carlson, H.H.Wang, J.M.Williams, Phys. Rev. B **48**, 9906 (1993); M.Dressel, L.Degiorgi, O.Klein, G.Grüner, J. Phys. Chem. Solids **54**, 1411 (1993)

[81] M.Dressel, O.Klein, G.Grüner, K.D.Carlson, H.H.Wang, J.M.Williams, Phys. Rev. B **50**, 13603 (1994)

[82] For an overview see, e.g., J. Wosnitza, *Fermi Surfaces of Low-Dimensional Organic Metals and Superconductors,* Springer, Berlin, Heidelberg, New York (1995); M.Lang, *Quasi-Twodimensional Organic Superconductors*, Supercond. Rev. Vol. **2**, 1 (1996); proceedings of the *International Conference on Synthetic Metals (ICSM),*

2002, published in Synth. Metals, **133-134** (2003); proceedings of the *Vth International Symposium on Crystalline Organic Metals, Superconductors and Magnets (ISCOM),* p. 52 (2003), to be published in J. Phys. IV, (2004)

[83] J. Wosnitza, *Fermi Surfaces of Low-Dimensional Organic Metals and Superconductors,* Springer, Berlin, Heidelberg, New York (1995)

[84] J.Singleton, Rep. Prog. Phys. 63, 1111 (2000)

[85] I.M.Lifshitz, A.M.Kosevich; Dokl. Akad. Nauk. SSR **96**, (1954)

[86] I.M.Lifshitz, A.M.Kosevich; Zh. Eksp. Teor. Fiz. **29**, 730 (1955); Sov. Phys. JETP **2**, 636 (1956)

[87] D.Shoenberg; *Magnetic oscillations in metals*, Cambridge Univ. Press (1984)

[88] I.D.Vagner, T.Maniv, E.Ehrenfreund, Phys. Rev. Lett. **51**, 1700 (1983)

[89] I.D.Vagner, T.Maniv, Phys. Rev. **B 32**, 8398 (1985)

[90] K.Jauregui, V.I.Marchenko, I.D.Vagner, Phys. Rev. **B 41**, 18, 12922 (1990)

[91] M.A.Itskovsky, S.Askenazy, T.Maniv, I.D.Vagner, E.Balthes, D.Schweitzer, Phys. Rev. B **58**, R 13347 (1998).

[92] M.A.Itskovsky, T.Maniv, I.D.Vagner, Z.Phys. B **101**, 13 (1996)

[93] P.Grigoriev, I.D.Vagner, JETP Lett. **69**, 156 (1999)

[94] M.Itskovsty, T.Maniv, I.D.Vagner, Phys. Rev. B **61**, 14616 (2000)

[95] P.Grigoriev, J. Exp. Theor. Phys. **92**, 1090 (2001)

[96] P.Grigoriev, M.V.Kartsovnik, W.Biberacher, N.D.Kushch, P.Wyder, Phys. Rev. B **65**, R060403 (2002)

[97] R.H.McKenzie, P.Moses, Phys. Rev. Lett. **81**, 4492 (1998)

[98] P.Moses, R.H.McKenzie, Phys. Rev. B **60**, 7998 (1999)

[99] K.vonKlitzing, G.Dorda, M.Pepper, Phys. Rev. Lett. **45**, 494 (1980)

[100] J.F.Kwak, J.E.Schirber, R.L.Greene, E.M.Engler, Phys. Rev. Lett. **46**, 1296 (1981); J.F.Kwak, J.E.Schirber, R.L.Greene, E.M.Engler, Mol. Cryst. Liq. Cryst. **79**, 111 (1982)

[101] M.Ribault, D.Jérome, J.Tuchendler, C.Weyl, K.Bechgaard, J. Physique Lett. **44**, L953 (1983)

[102] P.M.Chaikin, M.-Y.Choi, J.F.Kwak, J.S.Brooks, K.P.Martin, M.J.Naughton, E.M.Engler, R.L.Greene, Phys. Rev. Lett. **51**, 2333 (1983)

[103] H.Schwenk, S.S.P.Parkin, R.Schumaker, R.L.Greene, D.Schweitzer, Phys. Rev. Lett. **56**, 667 (1986)

[104] J.R.Cooper, W.Kang, P.Auban, G.Montambaux, D.Jérome, K.Bechgaard, Phys. Rev. Lett. **63**, 1984 (1989)

[105] S.T.Hannahs, J.S.Brooks, W.Kang, L.Y.Chiang, P.M.Chaikin, Phys. Rev. Lett. **63**, 1988 (1989)

[106] W.Kang, J.R.Cooper, D.Jérome, Phys. Rev. B **43**, R11467 (1991)

[107] W.Kang, X.D.Shi, R.C.Yu, R.Upasani, L.Y.Chiang, S.T.Hannahs, P.M.Chaikin, Synth. Metals **41-43**, 1645 (1991)

[108] P.M.Chaikin, W.Kang, S.Hannahs,R.C.Yu, Physica B **177**, 353 (1992)

[109] K.Machida, Y.Hasegawa, M.Kohmoto, V.M.Yakovenko, Y.Hori, K.Kishigi, Phys. Rev. B **50**, 921 (1994)

[110] L.Balicas, G.Kriza, F.I.B.Williams, Phys. Rev. Lett. **75**, 2000 (1995)

[111] J.P.Ulmet, A.Narijs, S.Askenazy, M.J.Naughton, J.M.Fabre, Synth. Met. **86**, 2075 (1997)

[112] L.P.Gor'kov, A.G.Lebed, J. Physique Lett. **45**, L433 (1984)

[113] G.Montambaux, M.Héritier, P.Lederer, J. Physique Lett. **45**, L533 (1984)

[114] M.Héritier, G.Montambaux, P.Lederer, J. Physique Lett. **45**, L943 (1984)

[115] P.M.Chaikin, Phys. Rev. B **31**, 4770 (1985)

[116] K.Yamaji, J. Phys. Soc. Jpn. **54**, 1034 (1985)

[117] M.Ya.Azbel, P.Bak, P.M.Chaikin, Phys. Lett. A **117**, 92 (1986)

[118] K.Maki, Phys. Rev. B **33**, 4826 (1986)

[119] A.Virosztek, L.Chen, K.Maki, Phys. Rev. B **34**, 3371 (1986)

[120] G.Montambaux, D.Poilblanc, Phys. Rev. B **37**, 1913 (1988)

[121] M.Ribault, Mol. Cryst. Liq. Cryst. **119**, 91 (1985)

[122] N.Dupuis, V.M.Yakovenko, Europhys. Lett. **45**, 361 (1999)

[123] D.C.Tsui, H.L.Störmer, A.C.Gossard, Phys. Rev. Lett. **48**, 1559 (1982)

[124] R.B.Laughlin, Phys. Rev. B **23**, 5632 (1981)

[125] R.B.Laughlin, Phys. Rev. Lett. **50**, 1395 (1983)

[126] H.Aoki, J. Phys. C **10**, 2583 (1977)

[127] H.Aoki, Rep. Prog. Phys. **50**, 655 (1987)

[128] B.I.Halperin, Helv. Phys. Acta **56**, 75 (1983)

[129] M.Pepper, Contemp. Phys. **18**, 423 (1977)

[130] T.Ando, A.B.Fowler, F.Stern, Rev. Mod. Phys. **54**, 437 (1982)

[131] H.L.Störmer in *Advances in Solid State Physics,* ed. by P.Grosse, Vieweg, Braunschweig, vol. **24** (1984)

[132] H.L.Störmer, Rev. Mod. Phys. **71**, 875 (1999)

[133] C.C.Grimes, Surf. Sci. **73**, 379 (1978)

[134] S.Narita, S.Takeyama, W.B.Luo, S.Hyamizu, K.Nanbu, H.Hashimoto, Jap. J. App. Phys. **20**, L443 (1981)

[135] L.Esaki, R.Tsu, IBM J. Res. Develop. **14**, 61 (1970)

[136] R.Dingle, H.L.Störmer, A.C.Gossard, W.Wiegmann, Appl. Phys. Lett. **33**, 665 (1978)

[137] H.L.Störmer, R.Dingle, A.C.Gossard, W.Wiegmann, M.D.Sturge, Solid State Commun. **29**, 705 (1979)

[138] A.Cho, (Ed.) *Molecular Beam Epitaxy* (AIP Press, Woodbury, New York (1994)

[139] M.A.Herman, H.Sitter, *Molecular Beam Epitaxy: Fundamentals and Current Startus*, Springer, Berlin, (1998)

[140] E.F.Schubert, *Doping in III-IV Semiconductors*, Cambridge University Press, Cambridge (1993)

[141] K.Bender, I.Henning, D.Schweitzer, K.Dietz, H.Endres, H.J.Keller, Mol. Cryst. Liq. Cryst. **108**, 359 (1984)

[142] J.M.Williams, H.H.Wang A.M.Kini, D.Carlson, M.A.Beno, U.Geiser, M.H.Whangbo, D.Jung, M.Evain, J.J.Novoa; Mol. Cryst. Liq. Cryst. **181**, 59 (1990)

[143] K.Kajita, Y.Nishio, S.Moriyama,W.Sasaki, R.Kato, H.Kobayashi, and A.Kobayashi, *Sol. State Comm*. **64**, 10 1279 (1987)

[144] A.Kobayashi, R.Kato, H.Kobayashi, S.Moriyama, Y.Nishino, K.Kajita, W.Sasaki, Chem. Lett. 459 (1987)

[145] E.Balthes, A.Breining, S.Kahlich, J.Moldenhauer, D.Schweitzer, P.Bele, H.Brunner, I.Heinen, B.Nuber, H.J.Keller; Synth. Met. **55-57**, 2859 (1993)

[146] E.Balthes, C.Proust, A.Audouard, L.Brossard, D.Schweitzer, I.Heinen, H.J.Keller, W.Strunz, A.G.M.Jansen, E.Steep, Synth. Metals **94**, 3 (1998)

[147] E.Balthes, *Diploma Thesis*, 3. Phys. Inst. Universität Stuttgart, Stuttgart (1992)

[148] T.Klutz, I.Henning, U.Haeberlen, D.Schweitzer, Appl. Mag. Res. **2**, 441 (1991)

[149] T.Chakraborty in *Handbook of Semiconductors,* vol. 1, ed. by P.T.Landsberg, North-Holland, New York, (1992)

[150] D.Yoshioka, *The Quantum Hall Effect,* Springer, Berlin, Heidelberg, New York (2002)

[151] L.D.Landau Z. Phys. **64**, 629 (1930)

[152] V.Fock, Z. Phys. **47**, 446 (1928)

[153] L.M.Roth, Phys. Rev. **145**, 434 (1966)

[154] R.G.Chambers, Canad. J. Phys. **34**, 1395 (1956)

[155] A.V.Gold, *Solid State Physics*, Vol.1, *Electrons in Metals,* J.F. Cochran, R.R.Haering (ed.), The Simon Fraser University lectures, p. 39 (1968)

[156] L.Onsager; Pil. Mag. **43**, 1006 (1952)

[157] L.D.Landau (1939), see appendix to D.Shoenberg, Proc. Roy. Soc. A **170**, 341 (1939)

[158] A.B.Pippard, Phil. Trans. Roy. Soc. A **250**, 325 (1957)

[159] L.M.Falicov, H.Stachowiak, Phys. Rev. **147**, 505 (1966)

[160] M.Springford, *Electrons at the Fermi surface*, Cambridge Univ. Press (1980)

[161] E.H.Sondheimer, A.H.Wilson, Proc. Roy. Soc. **A 210**, 173 (1951)

[162] R.B.Dingle, Proc. Roy Soc., **A 211**, 500 (1952)

[163] L.W.Schubnikow[1], W.J. de Haas, Proc. Netherl. Roy. Acad. Sci. **33**, 130 und 163 (1930)

[164] E.N.Adams, T.D.Holstein, J. Phys. Chem. Solids **10**, 254 (1959)

[165] A.B.Pippard, *The Dynamics of Conduction Electrons*, Blackie & Son, Glasgow (1965); Proc. Roy. Soc. **A 287**, 165 (1965)

[166] D.Shoenberg, Phil. Trans. Roy. Soc. **A 255**, 85 (1962)

[167] R.D.Plummer, W.l.Gordon, Phys. Rev. Lett. **13**, 432 (1964)

[168] J.H.Condon; Phys Rev. **145**, 526 (1966)

[169] A.B.Pippard, Proc. Roy. Soc. **A 272**, 192 (1963)

[170] A.B.Pippard, *Electrons at the Fermi surface,* M.Springford (ed.), Cambridge Univ. Press, p. 124 (1980)

[171] D.Shoenberg, *The Fermi Surface,* W.A.Harrison, M.B.Webb (ed.), Wiley, New York, 74 (1960)

[172] M.G.Priestley, Proc. Roy. Soc. **A 276**, 258 (1963)

[173] M.H.Cohen, L.M.Falicov, Phys. Rev. Lett. **7**, 231 (1961)

[174] E.I.Blount, Phys Rev. **126**, 1636 (1962)

[175] A.B.Pippard, Proc. Roy. Soc. **A 270**, 1 (1962)

[176] A.B.Pippard, Phil. Trans. Roy. Soc. **A 256**, 317 (1964)

[177] A.B.Pippard, *The Physics of Metals 1. Electrons,* J.M.Ziman (ed.), Cambridge Univ. Press, 113 (1969)

[178] R.W.Stark, L.M.Falicov, *Progress in Low Temperature Physics*, C.J.Gorter (ed.), North-Holland, Amsterdam, **5**, 235 (1967)

[179] In a number of publications A_2 and F_2 are denoted as A_α and F_α, while A_3 and F_3 are called A_β and F_β, respectively. We followed the notation introduced in Ref. [HEI93a]by experiments on the present material κ-(BEDT-TTF)$_2$I$_3$.

[180] R.G.Chambers, Proc. Phys. Soc. **88**, 701 (1966)

[181] M.Schiller, W.Schmidt, E.Balthes, D.Schweitzer, H.-J. Koo, M.H.Whangbo, I.Heinen, T.Klausa, W.Strunz, P.Kircher, Europhys. Lett. **51,** 82 (2000)

[182] K.Yamaji, *J. Phys. Soc. Jpn.* **58**, 1520 (1989)

[1] at that time written in German spelling, later: L.W.Shubnikov

[183] R.Yagi, Y.Iye, T.Osada and S.Kagoshima, *J. Phys. Soc. Jpn.* **59**, 3069 (1990);

[184] K.Yamaji, *The Physics and Chemistry of Organic Superconductors,* G.Saito, S.Kagoshima (ed.), Springer-Verlag Heidelberg (1990), p. 216

[185] R.E.Peierls, Z.Phys **81**, 186 (1933)

[186] M.Lifshitz, A.M.Kosevich, Sov. Phys. JETP **2**, 636 (1956)

[187] I.D.Vagner, T.Maniv, W.Joss, J.M.v.Ruitenbeek, K.Jauregui, Synth. Metals **34**, 393 (1989)

[188] J.P.Eisenstein, H.L.Störmer, V.Narayanamurti, A.Y.Cho, A.C.Gossard, C.W.Tu, Phys. Rev. Lett. **55**, 875 (1985)

[189] S.A.J.Wiegers, M.Specht, L.P.Lévy, M.Y.Simmons, D.A.Ritchie, A.Cavanna, B.Etienne, G.Martienz, P.Wyder, Phys. Rev. Lett. **79**, 3238 (1997)

[190] F.A.Mayer, E.Steep, W.Biberacher, P.Christ, A.Lerf, A.G.M.Jansen, W.Joss, P.Wyder, K.Andres, Europhys. Lett. **32**, 681 (1995)

[191] N.Harrison, J.Caulfield, J.Singleton, P.H.P.Reinders, F.Herlach, W.Hayes, M.Kurmoo, P.Day, J. Phys. Cond. Mat. **8**, 5415 (1996)

[192] R.W.Stark, C.B.Friedberg, J. Low Temp. Phys. **14**, 111 (1974)

[193] R.W.Stark, R.Reifenberger, J. Low Temp. Phys. **26**, 763 and 819 (1977)

[194] M.I.Kaganov, A.A.Slutskin, Phys. Rep. **98**, 189 (1983)

[195] M.V.Kartsovnik, International Symposium on Organic Metals, Superconductors and Ferromagnets, Mittelberg, Austria (1995); M.V.Kartsovnik, G.Yu.Logvenov, T.Ishiguro, W.Biberacher, H.Anzai, N.D.Kushch, Phys. Rev. Lett. 77, 2530 (1996)

[196] J.W.Eddy, R.W.Stark, Phys. Rev. Lett. **48**, 257 (1982)

[197] S.Alexandrov, A.M.Bratkovsky, Phys. Rev. Lett. **76**, 1308 (1986)

[198] T.Sasaki, H.Sato, N.Toyota, Sol. State Commun. **76**, 507 (1990)

[199] C.P.Heidmann, H.Müller, W.Biberacher, K.Neumaier, C.Probst, K.Andres, A.G.M.Jansen, W.Joss, Synth. Metals **41-43**, 2029 (1991)

[200] J.Caulfield, J.Singleton, F.L.Pratt, M.Doporto, W.Lubczynski, W.Hayes, M.Kurmoo, P.Day, P.T.J.Hendriks, J.A.A.J.Perenboom, Synth. Metals **61**, 63 (1993)

[201] F.A.Meyer, E.Steep, W.Biberacher, P.Christ, A.Lerf, A.G.M.Jansen, W.Joss, P.Wyder, K.Andres, Europhys. Lett. **32**, 681 (1995)

[202] K.Kishigi, M.Nakano, K.Machida, Y.Hori, J. Phys. Soc. Jpn. **64**, 3043 (1995)

[203] K.Machida, K.Kishigi, Y.Hori, Phys. Rev. B **51**, 8946 ()1995

[204] K.Machida, K.Kishigi, Y.Hori, Synth. Metals **70**, 853 (1995)

[205] S.Uji, M.Chaparala, S.Hill, P.S.Sandhu, J.Qualls, L.Seger, J.S.Brooks, Synth. Metals **85**, 1573 (1997)

[206] K.Kishigi, J. Phys. Soc. Jpn. **66**, (1997)

[207] M.Nakano, J. Phys. Soc. Jpn. **66**, 19 (1997)

[208] J.-Y.Fortin, J.Bellissard, Miguel Cusmão, T.Ziman, Phys. Rev. B **57**, 1484 (1998)

[209] J.-Y.Fortin, T.Ziman, Phys. Rev. Lett. **80**, 3117 (1998)

[210] Ju.H.Kim, S.Y.Han, J.S.Brooks, Phys. Rev. B **60**, 3213 (1999)

[211] E.Steep, L.H.Nguyen, W.Biberacher, H.Müller, A.G.M.Jansen, P.Wyder, Physica B **259-261**, 1079 (1999)

[212] S.Y.Han, J.S.Brooks, Ju.H.Kim, Phys. Rev. Lett. **85**, 1500 (2000)

[213] V.M.Gvozdikov, Yu.V.Pershin, E.Steep, A.G.M.Jansen, P.Wyder, Phys. Rev. B **65**, 165102 (2002)

[214] K.Oshima, T.Mori, H.Inokuchi, H.Urayama, H.Yamochi, G.Saito, Phys. Rev. B **38**, 938 (1988)

[215] N.Harrison, C.H.Mielke, D.G.Rickel, J.Wosnitza, J.S.Qualls, J.S.Brooks, E.Balthes, D.Schweitzer, I.Heinen, W.Strunz, Phys. Rev. B **58**, 10248 (1998)

[216] E.Balthes, P.Wyder, D.Schweitzer, Sol. State Commun., **124**, 141 (2002)

[217] T.Chakraborty, P.Pietiläinen, *The Quantum Hall Effects,* 2nd edition, Springer, Berlin, Heidelberg, New York (1995)

[218] T.Ando, Y.Matsumoto, Y.Uemura, J. Phys. Soc. Jpn. **39**, 279 (1975)

[219] T.Englert, K.v.Klitzing, Surf. Sci. **73**, 70 (1978)

[220] J.Wakabayashi, S.Kawaji, Surf. Sci. **98**, 299 (1980)

[221] B.N.Taylor, Physics Today, **42**, 23 (1989)

[222] T.Quinn, Metrologia **26**, 69 (1989)

[223] R.Kubo, J. Phys. Soc. Jpn. **12**, 570 (1957)

[224] R.Kubo, S.J.Miyake, N.Hashitsume, Solid State Phys. **17**, 269 (1965)

[225] H.Aoki, T.Ando, Solid State Commun. **38**, 1079 (1981)

[226] R.E.Prange, Phys. Rev. B **23**, 4802 (1981)

[227] D.J.Thouless, J. Phys. C **14**, 3475 (1981)

[228] G.F.Giuliani, J.J.Quinn, S.C.Ying Phys. Rev. B **28**, 2969 (1983)

[229] B.I.Halperin, Phys. Rev. B **25**, 2185 (1982)

[230] P.W.Anderson, Phys. Rev. **109**, 1492 (1958)

[231] E.Abrahams, P.W.Anderson, D.C.Licciardello, T.V.Ramakrishnan, Phys. Rev. Lett. **42**, 673 (1979)

[232] S.V.Iordanski, Solid State Commun. **43**, 1 (1982)

[233] R.F.Kazarinov, Phys. Rev. B **25,** 7626 (1982)

[234] S.Luryi, R.F.Kazarinov, Phys. Rev. B **27**, 1386 (1982)

[235] S.A.Trugman, Phys. Rev. B **27**, 7539 (1983)

[236] R.Joynt, R.E.Prange, Phys. Rev. B **29**, 3303 (1984)

[237] S.M.Apenko, Yu.E.Lozovik, Sov. Phys. JETP **62**, 328 (1984)

[238] R.Zallen, H.Scher, Phys. Rev. B **4**, 4471 (1971)

[239] T.Ando, J. Phys. Soc. Jpn. **52**, 1740 (1983)

[240] T.Ando, J. Phys. Soc. Jpn. **53**, 3101, 3126 (1984)

[241] Y.Ono, J. Phys. Soc. Jpn. **51**, 237 (1982)

[242] A.H.MacDonald, P.Streda, Phys. Rev. B **29**, 1616 (1984)

[243] A.H.MacDonald, Phys. Rev. B **29**, 6563 (1984), Phys. Rev. B **30**, 4392 (1984), Phys. Rev. B **30**, 3550 (1984)

[244] L.Smrcka, J. Phys. C **17**, L63 (1984)

[245] T.Ando, in *Transport Phenomena in Mesoscopic Systems,* p. 185, H.Fukuyama, T.Ando (Eds.), Springer, Berlin, Heidelberg, New York, (1992)

[246] B.J.vanWees, E.M.M.Willems, C.J.P.M.Harmans, C.W.J.Beenacker, H.vanHouten, J.G.Williamson, C.T.Foxon, J.J.Harris, Phys. Rev. Lett. **62**, 1181 (1989)

[247] G. Müller, D. Weiss, S. Koch, K. von Klitzing, H. Nickel, W. Schlapp, R. Lösch, Phys. Rev. B **42**, 7633 (1990)

[248] C.W.J.Beenacker, H.vanHouten, Solid State Phys. **44**, 1 (1991)

[249] R.Haug, Semicond. Sci. Technol. **8**, 131 (1993)

[250] M.Ya.Azbel, Solid State Commun. **53**, 147 (1985)

[251] K.vonKlitzing, Adv. Solid State Phys. **30**, 25 (1990), Physica B **184**, 1 (1993)

[252] D.B.Chklovskii, B.I.Shlovskii, L.I.Glazmann, Phys. Rev. B **46**, 4026 (1992)

[253] H.Hirai, S.Komiyama, Phys. Rev. B **49**, 14012 (1994)

[254] D.J.Thouless, Phys. Rev. Lett. **71**, 1879 (1993)

[255] V.T.Dolgopolov, A.A.Shashkin, N.B.Zhitenev, S.I.Dorozhkin, K.vonKlitzing, Phys. Rev. B **46**, 12560 (1992)

[256] A.Luther, I.Peschel, Phys. Rev. B **9**, 2911 (1974)

[257] E.Wigner, Phys. Rev **46**, 1002 (1934)

[258] R.Willett, J.P.Eisenstein, H.L.Störmer, D.C.Tsui, A.C.Gossard, J.H.English, Phys. Rev. Lett. **59**, 1776 (1987)

[259] F.D.M.Haldane, Phys. Rev. Lett. **51**, 605 (1983)

[260] D.Yoshioka, Prog. Theor. Phys. Suppl. **84**, 97 (1995)

[261] H.L.Störmer, A.M.Chang, D.C.Tsui, J.C.M.Hwang, A.C.Gossard, W.Wiegmann, Phys. Rev. Lett. **50,** 1953 (1983)

[262] D.C.Tsui, H.L.Störmer, IEEE J. Quantum Electron. QE-**22**, 1711 (1986)

[263] R.G.Clark, Phys. Scr. T **39**, 45 (1991)

[264] H.L.Störmer, Physica B **177**, 401 (1992)

[265] V.M.Pudalov, S.G.Semenchinsky, JETP Lett. **39**, 170 (1984)

[266] G.Garilov, Z.D.Kvon, I.V.Kukushkin, V.B.Timofeev, JETP Lett. **39**, 507 (1984)

[267] S.F.Nelson, K.Ismail, J.J.Nocera, F.F.Fang, E.E.Mendez, J.O.Chu, B.S.Meyerson, Appl. Phys. Lett. **61**, 64 (1992)

[268] M.Shayegan, J.K.Wang, M.Santos, T.Sayoto, B.B.Goldberg, Appl. Phys. Lett. **54**, 27 (1988)

[269] A.M.Chang, P.Berglund, D.C.Tsui, H.L.Störmer, J.C.M.Hwang, Phys. Rev. Lett. **53**, 997 (1984)

[270] G.Ebert, K.vonKlitzing, J.C.Maan, G.Remenyi, C.Probst, G.Weimann,W.Schlapp, J. Phys. C **17**, L775 (1984)

[271] E.E.Mendez, L.L.Chang, M.Heiblum, L.Esaki, M.Naughton, K.Martin, J.Brooks, Phys. Rev. B **30**, 7310 (1984)

[272] G.S.Boebinger, A.M.Chang, H.L.Störmer, D.C.Tsui, Phys. Rev. B **32**, 4268 (1985)

[273] R.G. Clark, R.J.Nicholas, A.Usher, C.T.Foxon, J.J.Harris, Surf. Sci. **170**, 141 (1986)

[274] V.J.Goldman, M.Shayegan, D.C.Tsui, Phys. Rev. Lett. **61**, 881 (1988)

[275] R.L.Willett, H.L.Störmer, D.C.Tsui, A.C.Gossard, J.H.English, K.W.Baldwin, Sol. State Commun. **196**, 257 (1988)

[276] J.R.Mallett, R.G.Clark, R.J.Nicholas, R.Willett, J.J.Harris, C.T.Foxon, Phys. Rev. B **38**, 2200 (1988)

[277] J.P.Eisenstein, H.L.Störmer, L.Pfeiffer, K.W.West, Phys. Rev. Lett. **62**, 1540 (1989)

[278] H.W.Jiang, R.Willett, H.L.Störmer, D.C.Tsui, L.Pfeiffer, K.W.West, Phys. Rev. Lett. **65**, 633 (1990)

[279] T.Sajoto, Y.W.Suen, L.W.Engel, M.B.Santos, M.Shayegan, Phys. Rev. B **41**, 8449 (1990)

[280] T.Cakraborty, P.Pietiläinen, Phys. Rev. Lett. **59**, 2784 (1987)

[281] T.Cakraborty, P.Pietiläinen in *Recent Progress in Many-Body Theories*, (Eds.) A.Kallio, E.Pajane, R.F.Bishop, Plenum, New York, p.113 (1988)

[282] J.P.Eisenstein, G.S.Boebinger, L.N.Pfeiffer, K.W.West, S.He, Phys. Rev. Lett. **68**, 1383 (1992)

[283] S.Q.Murphy, J.P.Eisenstein, G.S.Boebinger, L.N.Pfeiffer, K.W.West,Phys. Rev. Lett. **72**, 728 (1994)

[284] D.Yoshioka, B.I.Halperin, P.A.Lee, Phys. Rev. Lett. **50,** 1219 (1983)

[285] D.Yoshioka, Phys. Rev. B **29**, 6833 (1984)

[286] D.Yoshioka, P.A.Lee, Phys. Rev. B **27**, 4986 (1983)

[287] M.Dressel, G.Grüner, J.P.Pouget, A.Breining, D.Schweitzer, J.Phys. I France **4**, 579 (1994)

[288] R.B.Laughlin, Surf. Sci. **142**, 163 (1984)

[289] R.E.Prange, S.M.Girvin, (Eds.): *The Quantum Hall Effect,* 2nd edition, Springer, Berlin, Heidelberg, New York (1989)

[290] R.B.Laughlin, Rev. Mod. Phys. **71**, 863 (1999)

[291] J.M.Caillol, D.Levesque, J.J.Weis, J.P.Hansen, J. Stat. Phys. **28**, 325 (1982)

[292] D.Levesque, J.J.Weis, A.H.MacDonald, Phys. Rev. B **30**, 1056 (1984)

[293] F.D.M.Haldane, E.H.Rezayi, Phys. Rev. Lett. **54**, 237 (1985)

[294] F.D.M.Haldane, E.H.Rezayi, Phys. Rev. B **31**, 2529 (1985)

[295] R.Morf, B.I.Halperin, Phys. Rev. B **33**, 2221 (1986)

[296] R.Morf, B.I.Halperin, Z. Phys. B **68**, 391 (1987)

[297] S.M.Girvin, *Interfaces, Quantum Wells and Superlattices,* ed. by C.R.Leavens, R.Taylor, Plenum, New York, p.333 (1987)

[298] S.A.Trugman, S.Kivelson, Phys. Rev. B **31**, 5280 (1985)

[299] V.L.Pokrovskii, A.L.Talapov, J. Phys. C **18**, L691 (1985)

[300] R.Morf, N.d'Ambrumenil, B.I.Halperin, Phys. Rev. B **34**, 3037 (1986)

[301] G.Fano, F.Ortolani, E.Colombo, Phys. Rev. B **34**, 2670 (1986)

[302] S.Kawaji, J.Wakabayashi, J.Yoshino, H.Sakaki, J. Phys. Soc. Jpn. **53**, 1915 (1984)

[303] G.S.Boebinger, A.M.Chang, H.L.Störmer, D.C.Tsui, Phys. Rev. Lett. **55**, 1606 (1985)

[304] G.S.Boebinger, A.M.Chang, H.L.Störmer, D.C.Tsui, J.C.M.Hwang, A.Y.Cho, C.W.Tu, G.Weimann, Surf. Sci. **170**, 129 (1986)

[305] R.L.Willett, H.L.Störmer, D.C.Tsui, A.C.Gossard, J.H.English, Phys. Rev. B **37**, 8476 (1988)

[306] E.Mendez, Surf. Sci. **170**, 561 (1986)

[307] J.Wakabayashi, S.Kawaji, J.Yoshino, H.Sakaki, J. Phys. Soc. Jpn. **55**, 1319 (1986)

[308] G.S.Boebinger, H.L.Störmer, D.C.Tsui, A.M.Chang, J.C.M.Hwang, A.Y.Cho, C.W.Tu, G.Weimann, Phys. Rev. B **36**, 7919 (1987)

[309] Y.Guldner, M.Voos, J.P.Vieren, J.P.Hirtz, M.Heiblum, Bhys. Rev. B **36**, 1266 (1987)

[310] R.G.Clark, J.R.Mallett, S.R.Haynes, J.J.Harris, C.T.Foxon, Phys. Rev. Lett. **60**, 1747 (1988)

[311] K.Maki, X.Zotos, Phys. Rev. B **28**, 4349 (1983)

[312] E.Mendez, M.Heiblum, L.L.Chang, L.Esaki, Phys. Rev. B **28**, 4886 (1983)

[313] P.K.Lam, S.M.Girvin, Phys. Rev. B **30**, 437 (1984)

[314] J.Wakabayashi, A.Fukano, S.Kawaji, K.Hirakawa, H.Sakaki, Y.Koike, T.Fukase, J. Phys. Soc. Jpn. **57**, 3678 (1988)

[315] D.P.Arovas, J.R.Schrieffer, F.Wilczek, A.Zee, Nucl. Phys. B **251** [FS13], 117 (1985)

[316] A.H.MacDonald, Science, Feb. 17th '95, p.p. 977 (1995)

[317] G.P.Collins, Physics Today, Nov. '97, p.p. 17 (1997)

[318] P.W.Anderson, Physics Today, Oct. '97, p.p. 42 (1997)

[319] B.Daviss, New Scientist, Jan. '98, p.p. 36 (1998)

[320] J.A.Simmons, H.P.Wei, L.W.Engel, D.C.Tsui, M.Shayegan, Phys. Rev. Lett. **63**, 1731 (1989)

[321] L.C.Kane, M.P.A.Fisher, Phys. Rev. Lett. **72**, 724 (1994)

[322] V.J.Goldman, B.Su, Science **267**, 1010 (1995)

[323] V.J.Goldman, Surf. Sci. **361**, 1 (1996)

[324] R.dePicciotto, M.Reznikov, M.Heiblum, V.Umansky, G.Bunin, D.Mahalu, Nature **389**, 162 (1997)

[325] L.Saminadayar, D.C.Glatti, Y.Jin, B.Etienne, Phys. Rev. Lett. **79**, 2526 (1997)

[326] D.Arovas, J.R.Schrieffer, F.Wilczek, Phys. Rev. Lett. **53**, 722 (1984)

[327] B.I.Halperin, Phys. Rev. Lett. **52**, 1583, 2390(E) (1984)

[328] J.M.Leinaas, J.Myrheim, Nuovo Cimento B **37**, 1 (1977)

[329] F.Wilczek, Phys. Rev. Lett. **49**, 957 (1982)

[330] F.Wilczek, *Fractional Statistics and Anyon Superconductivity,* World Scientific, Singapore (1990)

[331] S.S.Chern, C.W.Chu, C.S.Ting, (Eds.) *Physics and Mathematics of Anyons*, World Scientific (1991)

[332] V.L.Pokrovskii, A.L.Talapov, JETP Lett. **42**, 80 (1985)

[333] V.L.Pokrovskii, A.L.Talapov, JETP Lett.**63**, 455 (1986)

[334] F.C.Zhang, V.Z.Vulovic, Y.Guo, S.dasSarma, Phys. Rev. B **32**, 6920 (1985)

[335] E.H.Rezayi, F.D.M.Haldane, Phys. Rev. B **32**, 6924 (1985)

[336] W.Duncan, E.E.Schneider, Phys. Lett. **1**, 23 (1963)

[337] J.P.Hansen, D.Levesque, J. Phys. C **14**, L603 (1981)

[338] J.G.Zabolitzky, Adv. Nucl. Phys. **12**, 1 (1981)

[339] B.Jancovici, Phys. Rev. Lett. **46**, 386 (1981)

[340] T.Chakraborty, F.C.Zhang, Phys. Rev. B **29**, 7032 (1984)

[341] F.C.Zhang, T.Chakraborty, Phys. Rev. B **30**, 7320 (1984)

[342] F.D.M.Haldane, in: *The Quantum Hall Effect,* 2nd edition, R.E.Prange, S.M.Girvin, (Eds.), Springer, Berlin, Heidelberg, New York (1989)

[343] R.B.Laughlin, in: *Proceedings of the 17th Int. Conf. on the Physics of Semiconductors,* ed. by D.J.Chadi, W.A.Harrison, Springer, Berlin, Heidelberg, New York, p. 255 (1985)

[344] J.K.Jain, Phys. Rev. B **41**, 7653 (1990)

[345] R.G.Clark, R.J.Nicholas, J.R.Mallett, A.M.Suckling A.Usher, J.J.Harris, C.T.Foxon, in: *Proc. of the Eightennth Int. Conf. on the Phys. of Semicond.,* ed. by O.Engstrom, World Scientific, p. 393 (1987)

[346] Y.Kuramato, R.R.Gerhardts, J. Phys. Soc. Jpn. **51**, 3810 (1982)

[347] T.Chakraborty, P.Pietiläinen, Phys. Rev. B **38**, 10097 (1988)

[348] S.-C.Zhang, H.Hansson, S.Kivelson, Phys. Rev. Lett. **62**, 82 (1989); **62**, 980 (1989)

[349] J.K.Jain, Phys. Rev. Lett. **63**, 199 (1989); Phys. Rev. B **40**, 8079 (1989)

[350] A.López, E.Fradkin, Phys. Rev. B **44**, 5246 (1991)

[351] D.H.Lee, S.-C.Zhang, Phys. Rev. Lett. **66**, 1220 (1991)

[352] S.-C.Zhang, Int. J. Mod. Phys. B **6**, 1, 25 (1992)

[353] B.I.Halperin, P.A.Lee, N.Read, Phys. Rev. B **47**, 7312 (1993)

[354] O.Heinonen, (Ed.), *Composite Fermions,* World Scientific, Singapore, (1998)

[355] See, e.g., *Proceedings of the International Symposium on the Quantum Hall Effect,* Max-Planck-Institut für Festkörperforschung Stuttgart, Stuttgart, (2003)

[356] P.B.Visscher, L.M.Falicov, Phys. Rev. B **3**, 2541 (1971)

[357] W.L.Bloss, E.M.Brody, Sol. State Commun. **43**, 523 (1982)

[358] S.DasSarma, J.J.Quinn, Phys. Rev. B **25**, 7603 (1982); Phys. Rev. B **27**, 6516(E) (1983)

[359] T.Chakraborty, C.E.Campbell, Phys. Rev. B **29**, 6640 (1984)

[360] E.H.Rezayi, F.D.M.Haldane, Bull. Am. Phys. Soc. **32**, 892 (1987)

[361] H.C.AOji, A.H.MacDonald, S.M.Girvin, Phys. Rev. Lett. **58**, 824 (1987)

[362] D.Yoshioka, A.H.MacDonald, S.M.Girvin, Phys. Rev. B **39**, 1932 (1989)

[363] G.S.Boebinger, H.W.Jiang, L.N.Pfeiffer, K.W.West, Phys. Rev. Lett. **64**, 1793 (1990)

[364] A.H.MacDonald, P.M.Platzmann, G.S.Boebinger, Phys. Rev. Lett. **65**, 775 (1990)

[365] D.Yoshioka, A.H.MacDonald, J. Phys. Soc. Jpn. **59**, 4211 (1990)

[366] S.He, X.C.Xie, S.DasSarma, F.C.Zhang, Phys.Rev. B **43**, 9339 (1991)

[367] D.H.Lee, C.L.Kane, Phys. Rev. Lett. **64**, 1313 (1990)

[368] S.L.Sondhi, A.Karlhede, S.A.Kivelson, E.H.Rezaji, Phys. Rev. B **47**, 16419 (1993)

[369] H.A.Fertig, L.Brey, R.Côté, A.H.MacDonald, Phys. Rev. B **50**, 11018 (1994)

[370] R.Ladbury, Physics Today **48**, 19 (1995)

[371] J.K.Jain, X.G.Wu, Phys. Rev B **49**, 5085 (1994)

[372] A.Schmeller, J.P.Eisenstein, L.N.Pfeiffer, K.W.West, Phys. Rev. Lett. **75**, 4290 (1995)

[373] R.K.Kamilla, X.G.Wu, J.K.Jain, Sol. State Commun. **99**, 289 (1996)

[374] D.K.Maude, M.Potemski, J.C.Portal, M.Heini, L.Eaves, G.Hill, M.A.Pate, Phys. Rev. Lett. **77**, 4604 (1996)

[375] M.J.Manfra, B.B.Goldberg, L.Pfeiffer, K.West, Physics E **1**, 28 (1997)

[376] E.Gornik, R.Lassnig, G.Strasser, H.L.Störmer, A.C.Gossard, W.Wiegmann, Phys. Rev. Lett. **54**, 1820 (1985)

[377] J.K.Wang, J.H.Campbell, D.C.Tsui, A.Y.Cho, Phys. Rev. B **38**, 6174 (1988)

[378] J.K.Wang, D.C.Tsui, M.B.Santos, M.Shayegan, Phys. Rev. B **45**, 4384 (1992)

[379] V.Bayot, E.Grivei, S.Melinte, M.B.Santos, M.Shayegan, Phys. Rev. Lett. **76**, 4584 (1996)

[380] S.Melinte, E.Grivei, V.Bayot, M.Shayegan, Phys. Rev. Lett. **82**, 2764 (1999)

[381] I.V.Kukushkin, K.v.Klitzing, K.Eberl, Phys. Rev. B **60**, 2554 (1999)

[382] S.A.Vitkalov, C.R.Bowers, J.A.Simmons, J.L.Reno, J. Phys.: Cond. Matter **11**, L407 (1999)

[383] S.E.Barrett, G.Dabbagh, L.N.Pfeiffer, K.W.West, R.Tycko, Phys. Rev. Lett. **74**, 5112 (1995)

[384] S.Melinte, N.Freytag, M.Horvatic, C.Berthier, L.P.Lévy, V.Bayot, M.Shayegan, Phys. Rev. B **64**, 085327 (2001)

[385] P.Christ, *Diplomarbeit*, Walther-Meißner Institut Garching, Germany (1993); P.Christ, *Dissertation*, Hieronymus-Verlag, München, Germany (1998)

[386] R.Kato, H.Kobayashi, A.Kobayashi, S.Moriyama, Y.Nishino, K.Kajita, W.Sasaki, Chem. Lett. 507 (1987)

[387] H.Kobayashi, K.Kawano, T.Naito, A.Kobayashi, J. Mat. Chem. **5**, 1681 (1995)

[388] A.Nothardt, *Thesis*, 3.Physikalisches Institut, Universität Stuttgart, Stuttgart / Germany (2000)

[389] M.Weger, M.Tittelbach, E.Balthes, D.Schweitzer, H.J.Keller, J. Phys.: Cond. Matter **5**, 5869 (1993)

[390] H.C.Montgomery, J. Appl. Phys. **42**, 2971 (1971)

[391] M.Tittelbach, *Diploma Thesis*, 3.Physikalisches Institut, Universität Stuttgart, Stuttgart / Germany (1993)

[392] P.M.Chaikin, J.F.Kwak, Rev. Sci. Instrum. **46**, 218 (1975)

[393] For a review see, e.g., J.Wosnitza, Int. J. Mod. Phys. **B 7**, 2707 (1993)

[394] K.Oshima, H.Yamazaki, K.Kato, Y.Maruyama, R.Kato, A.Kobayashi, H.Kobayashi, Synth. Metals **55-57**, 2334 (1993)

[395] **a)** For dHvA field an temperature modulation experiments: M.Heinecke, K.Winzer, D.Schweitzer, Z. Phys. **B 93**, 45 (1993);
b) For SdH and dHvA torque experiments: E.Balthes, I.Heinen, H.J.Keller, D.Schweitzer, W.Strunz, W.Biberacher, A.G.M.Jansen, *Proceedings of the DPG Conference on Solid State Physics*, Regensburg, (1993).

[396] A.Audouard, Service National de Champs Magnetiques Pulsées INSA Toulouse/France, private communication

[397] E.Balthes, D.Schweitzer, I.Heinen, H.J.Keller, W.Biberacher, A.G.M.Jansen, E.Steep, Synth. Metals **70**, 841 (1995); D.Schweitzer, E.Balthes, S.Kahlich, I.Heinen, H.J.Keller, W.Strunz, W.Biberacher, A.G.M.Jansen, E.Steep, Synth. Metals **70**, 857 (1995)

[398] E.Balthes, D.Schweitzer, I.Heinen, H.J.Keller, W.Biberacher, A.G.M.Jansen, E.Steep, Acta Phys. Pol. **87**, 767 (1995)

[399] E.Balthes, D.Schweitzer, I.Heinen, H.J.Keller, W.Strunz, W.Biberacher, A.G.M.Jansen, E.Steep, Z. Phys. **B 99**, 163 (1996)

[400] In Ref. [146] F_1 = 100(±30)T was found in pulsed fields. On different samples values for F_1 between 89T and 119T were found at low fields provided by resistive or superconducting magnets.

[401] In our first studies on the present material [398,397,399]the 571T frequency was denoted as F_1 and the 3883T frequency as F_2, respectively, following the notation introduced in Ref. [395a]. The finding of a further QO frequency with F_1 = 100T required to rename the higher frequency oscillations into F_2 and F_3, respectively.

[402] E.Balthes, *Doktorarbeit,* 3.Physikalisches Institut, Universität Stuttgart, Stuttgart, Germany, (1997)

[403] N.Toyota, T.Sasaki, K.Murata, Y.Honda, M.Tokumoto, H.Bando, N.Kinoshita, H.Anzai, T.Ishiguro, Y.Muto, J. Phys. Soc. Jpn. **57**, 2616 (1988)

[404] K.Andres, C.-P.Heidmann, H.Müller, S.Himmelsbacher, C.Probst, W.Joss, Synth.Metals **41-43**, 1893 (1991)

[405] W.Biberacher, Walther-Meissner Institut, Garching, Germany, private communication

[406] J.Wosnitza, G.W.Crabtree, H.H.Wang, K.D.Carlson, M.D.Vashon, J.M.Williams, Phys. Rev. Lett. **67**, 263 (1991)

[407] J.Wosnitza, G.W.Crabtree, H.H.Wang, U.Geiser, J.M.Williams, K.D.Carlson, Phys. Rev. B **45**, 3018 (1992)

[408] J.Singleton, F.L.Pratt, M.Doporto, J.Caulfield, W.Hayes, I.Deckers, G.Pitsi, F.Herlach, T.J.B.M.Janssen, J.A.A.J.Perenboom, M.Kurmoo, P.Day, Synth. Met. **55-57**, 2198 (1993)

[409] J.Caulfield, W.Lubczynski, F.L.Pratt, J.Singleton, D.Y.K.Ko, W.Hayes, M.Kurmoo, P.Day, J. Phys. Condens. Matter, **6**, 2911 (1994).

[410] E.Balthes, M.Schiller, D.Schweitzer, I.Heinen, W.Strunz, E.Steep, A.G.M.Jansen P.Wyder, Physica C **317-318**, 108 (1999)

[411] E.Balthes, D.Schweitzer, I.Heinen, H.J.Keller, W.Strunz, A.G.M.Jansen, E.Steep, Synth. Metals **85,** 1549 (1997)

[412] M.Tinkham; Phys. Rev **129**, 2413 (1963); M.Tinkham; *Introduction to Superconductivity,* McGraw-Hill, New York (1975)

[413] E.Balthes, M.Schiller, D.Schweitzer, I.Heinen, W.Strunz, E.Steep, A.G.M.Jansen P.Wyder, Europhys. Lett. **47**, 70 (1999)

[414] E.Balthes, P.Wyder, D.Schweitzer, J. Phys. Chem. Sol. **63** 1249 (2002)

[415] H.Weiss, M.V.Kartsovnik, W.Biberacher, E.Steep, E.Balthes, A.G.M.Jansen, N.D.Kushch, Synth. Metals **103**, 1998 (1999)

[416] H.Weiss, M.V.Kartsovnik, W.Biberacher, E.Steep, E.Balthes, A.G.M.Jansen, K.Andres, N.D.Kushch, Phys. Rev. B **59**, 12370 (1999)

[417] N.Harrison, R.Bogaerts, P.H.P.Reinders, J.Singleton, S.J.Blundell, F.Herlach, Phys. Rev. B **54**, 9977 (1996)

[418] D.Shoenberg, J. Low Temp. Phys. **56**, 417 (1984)

[419] M.Schiller, *Thesis*, 3.Physikalisches Institut, Universität Stuttgart, Stuttgart, Germany (2000)

[420] J.Wosnitza, J.Hagel, J.S.Qualls, J.S.Brooks, E.Balthes, D.Schweitzer, J.A.Schlueter, U.Geiser, J.Mohtasham, R.W.Winter, G.L.Gard, Phys. Rev. B **65** R180506 (2002)

[421] T.Terashima, S.Uji, H.Aoki, M.Tamura, M.Kinoshita, M.Tokumoto, Sol. State. Commun. **91**, 595 (1994)

[422] N.W.Ashcroft, N.D.Mermin, *Solid State Physics*, Harcourt Brace College Publishers, New York (1976)

[423] K.Oshima, T.Mori, H.Inokuchi, H.Urayama, H.Yamochi, G.Saito, Synth. Met. **27**, A165 (1988)

[424] M.V.Kartsovnik, P.A.Konovich, V.N.Laukhin, R.B.Lyubovskii, S.I.Pesitskii, Zh. Eksp. Teor. Fiz. **98**, 708 (1990) [Sov. Phys. JETP **71**, 396 (1990)]

[425] A.G. Swanson, J.S.Brooks, H.Anzai, N.Kinoshita, M.Tokumoto, K.Murata, Sol. State Commun. **73**, 353 (1990)

[426] C.-P.Heidmann, W.Biberacher, H.Müller, W.Joss, K.Andres, in: *Lower-Dimensional Systems and Molecular Electronics*, ed. by R.M.Metzger, P.Day, G.C.Papavassiliou, NATO ASI series B, Vol. **248**, Plenum New York, p. 233 (1991)

[427] F.L.Pratt, J.Singleton, M.Kurmoo, S.J.R.M.Spermon, W.Hayes, P.Day, in: *The Physics and Chemistry of Organic Superconductors,* ed. by G.Saito, S.Kagoshima, Springer, Berlin, Heidelberg, p.200 (1990)

[428] F.L.Pratt, M.Doporto, W.Hayes, J.Singleton, T.Janssen, M.Kurmoo, P.Day, Synth. Metals **41-43**, 2195 (1991)

[429] N.Toyota, T.Sasaki, Physica B **186-188**, 1056 (1993); T.Sasaki, N.Toyota, Synth. Metals **55-57**, 2303 (1993)

[430] J.M.Williams, A.M.Kini, U.Geiser, H.H.Wang, K.D.Carlson, W.K.Kwok, K.G.Vandervoort, J.E.Thompson, D.L.Stupka, D.Jung, M.-H.Whangbo, in *Proceedings of the International Conference on Organic Superconductors South Lake Tahoe, CA, 1990*, Plenum New-York, pp. 33-44 (1990)

[431] K.Kanoda, Hyperfine Interact. **104**, 235 (1997)

[432] H.H.Wang, A.M.Kini, L.K.Montgomery, U.Geiser, K.D.Carlson, J.M.Williams, J.E.Thompson, D.M.Watkina, W.K.Kwok, U.Welp, K.G.Vandervoort, Chem. Mater. **2**, 482 (1990).

[433] See proceedings of the *Ist International Symposium on Crystalline Organic Metals, Superconductors and Magnets (ISCOM),* Hirschegg, Austria (1995)

[434] B.Thoma *Diploma Thesis*, 3.Physikalisches Institut, Universität Stuttgart, Stuttgart / Germany (1996)

[435] D.Schweitzer, *Ist International Symposium on Crystalline Organic Metals, Superconductors and Magnets (ISCOM),* Hirschegg, Austria (1995)

[436] C.H.Mielke, N.Harrison, D.G.Rickel, A.H.Lacerda, R.M.Vestal, L.K.Montgomery, Phys. Rev. B **56**, R4309 (1997)

[437] L.K.Montgomery, R.M.Vestal, K.P.Starkey, B.W.Fravel, M.J.Saminde, D.G.Pelers, C.H.Mielke, J.D.Thompson, Synth. Metals **103**, 1878 (1999)

[438] M.V.Kartsovnik, G.Yu.Logvenov, H.Ito, T.Ishiguro, G.Saito, Phys. Rev. B **52**, R15715 (1995)

[439] M.V.Kartsovnik, G.Yu.Logvenov, W.Biberacher, P.Christ, E.Steep, A.G.M.Jansen, Synth. Metals **86**, 2061 (1997)

[440] H.Weiss, M.V.Kartsovnik, W.Biberacher, E.Steep, A.G.M.Jansen, N.D.Kushch, Pis'ma Zh. Eksp. Teor. Fiz. **66**, 190 (1997) [JETP Lett. **66**, 202 (1997)]

[441] H.Weiss, M.V.Kartsovnik, W.Biberacher, E.Balthes, A.G.M.Jansen, N.D.Kushch, Phys. Rev. B **60**, R16259 (1999)

[442] H.Weiss, M.V.Kartsovnik, W.Biberacher, E.Balthes, A.G.M.Jansen, N.D.Kushch, Synth. Metals **120** 837 (2001)

[443] Y.Nogami, J.P.Pouget, H.Ito, T.Ishiguro, G.Saito, Solid State Commun. **89**, 113 (1994)

[444] M.V.Kartsovnik, W.Biberacher, K.Andres, N.D.Kushch, Pis'ma Zh.Eksp. Teor. Fiz. **62**, 890 (1995) [JETP .Lett. **62**, 905 (1995)]

[445] H.Mori, I.Hirabayashi, S.Tanaka, T.Mori, H.Inokuchi, Sol. State Commun. **76**, 35 (1990)

[446] K.Oshima, K.Araki, H.Yamazaki, K.Kato, Y.Maruyama, K.Yakushi, T.Mori, H.Inokuchi, H.Mori, S.Tanaka, Physica C **185-189**, 2689 (1991); K.Oshima, T.Doi, Y.Tokuoka, H.Yamazaki, K.Kato, Y.Maruyama, H.Mori, S.Tanaka, Synth. Metals **55-57**, 2339 (1993)

[447] N.Harrison, C.H.Mielke, D.G.Rickel, L.K.Montgomery, T.Burgin, Phys. Rev. B **56**, 12905 (1997)

[448] B.Zh.Narymbetov, N.D.Kushch, L.V.Zorina, S.S.Khasanov, R.P.Shibaeva, T.G.Togonidze, A.E.Kovalev, M.V.Kartsovnik, L.I.Buravov, E.B.Yagubskii, E.Canadell, A.Kobayashi, H.Kobayashi, Eur. Phys. J. B **5**, 179 (1998)

[449] T.G.Togonidze, M.V.Kartsovnik, J.A.A.J.Perenboom, N.D.Kushch, H.Kobayashi, Physica B **294-295**, 435 (2001)

[450] K.Kanoda, K.Kato, A.Kawamoto, K.Oshima, T.Takahashi, K.Kikuchi, K.Saito, I.Ikemoto, Synth. Metals **55-57**, 2309 (1993)

[451] J.Wosnitza, S.Wanka, J.Hagel, E.Balthes, N.Harrison, J.A.Schlueter, A.M.Kini, U.Geiser, J.Mohtasham, R.W.Winter, G.L.Gard, Phys. Rev. B **61**, 7383 (2000)

[452] H.Yamochi, T.Komatsu, N.Matsukawa, G.Saito, T.Mori, M.Kusunoki, K.Sakaguchi, J. Am. Chem. Soc. **115**, 11319 (1993)

[453] G.Saito, K.Yoshida, M.Shibata, H.Yamochi, N.Kojima, M.Kusunoki, K.Sakaguchi, Synth. Metals **70**, 1205 (1995)

[454] T.Klausa, Thesis, Anorganisch-Chemisches Institut, Universität Heidelberg (1999)

[455] M.H.Whangbo, R.Hoffmann, J. Am. Chem. Soc. **100**, 6093 (1978)

[456] E.Balthes, M.Schiller, W.Schmidt, D.Schweitzer, A.G.M.Jansen, P.Wyder, *"Molecular Low Dimensional and Nanostructured Materials for Advanced Applications",* Eds.: A.Graja, B.R.Bulka and F.Kajzar, NATO Science Series (Kluwer Academic Publishers) II Mathematics, Physics and Chemistry, Vol. 59, 1-12 (2002).

[457] E.Balthes, D.Schweitzer, to be published

[458] M.V.Kartsovnik, private communication, to be published

[459] U.Geiser, J.A.Schlueter, H.H.Wang, A.M.Kini, J.M.Williams, P.P.Sche, H.I.Zakowicz, M.L.VanZile, J.D.Dudek, P.G.Nixon, R.W.Winter, G.L.Gard, J.Ren, M.-H.Whangbo, Am. Chem. Soc. **118**, 9996 (1996)

[460] J.Wosnitza, S.Wanka, J.Hagel, J.S.Qualls, J.S.Brooks, N.Harrison, E.Balthes, D.Schweitzer, J.A.Schlueter, U.Geiser, J.Mohtasham, R.W.Winter, G.L.Gard, Physica B, **294-295** 442 (2001)

[461] J.Hagel, S.Wanka, J.Wosnitza, E.Balthes, J.A.Schlueter, A.M.Kini, U.Geiser, J.Montasham, R.W.Winter, G.L.Gard, Synt. Metals **120** 813 (2001)

[462] J.Wosnitza, S.Wanka, J.Hagel, H.v.Löhneysen, J.S.Qualls, J.S.Brooks, E.Balthes, J.A.Schlueter, U.Geiser, J.Mohtasham, R.W.Winter, G.L.Gard, Phys. Rev. Lett. **86** 508 (2001)

[463] M.V.Kartsovnik, A.E.Kovalev, N.D.Kushch, J.Physique I France, **3**, 1187 (1993)

[464] N.Harrison, E.Rzepniewski, J.Singleton, P.J.Gee, M.M.Honold, P.Day, M.Kurmoo, J. Phys. Cond. Matter **11**, 7227 (1999)

[465] N.Harrison, A.House, M.V.Kartsovnik, A.V.Polisski, J.Singleton, F.Herlach, W.Hayes, N.D.Kushch, Phys. Rev. Lett. **77**, 1576 (1996)

[466] M.M.Honold, N.Harrison, J.Singleton, H.Yaguchi, C.Mielke, D.G.Rickel, I.Deckers, P.H.P.Reinders, F.Herlach, M.Kurmoo, P.Day, J.Phys. Cond. Mat. **9**, L533 (1997)

[467] N.Harrison, M.M.Honold, M.V.Kartsovnik, J.Singleton, S.T.Hannahs, D.G.Rickel, N.D.Kushch, Phys. Rev. B **55**, R16005 (1997)

[468] É.B.Yagubskii, I.F.Schegolev, V.N.Laukhin, P.A.Kononovich, M.V.Kartsovnik, A.V.Zvarykina, L.I.Buravov, Pis'ma Zh. Eksp. Teor. Fiz. **39**, 12 (1984) [JETP Lett. **39**, 12 (1984)]

[469] F.Creuzet, G.Creuzet, D.Jérome, D.Schweitzer, H.J.Keller, J. Physique Lett. **46**, L1079 (1985)

[470] H.Veith, C.-P.Heidmann, F.Gross, A.Lerf, K.Andres, D.Schweitzer, Sol. State Commun. **56**, 1015 (1985); K.Murata, M.Tokumoto, H.Anzai, H.Bando, G.Saito, K.Kajimura, T.Ishiguro, J. Phys. Soc. Jpn. **54**, 1236 and 2084 (1985); V.N.Laukhin, E.É.Kostyuchenko, Y.V.Sushko, I.F.Schegolev, É.B.Yagubskii, Pis'ma Zh. Eksp. Teor. Fiz. **41**, 68 (1985) [JETP Lett. **41**, 81 (1985)]

[471] V.B.Ginodman, A.V.Gudenko, P.A.Kononovich, V.N.Laukhin, I.F.Schegolev, Pis'ma Zh. Eksp. Teor. Fiz. **44**, 523 (1986) [JETP Lett. **44**, 673 (1986)]; I.F.Schegolev, Jpn. J. Appl. Phys. **26**, Suppl. 26-3, 1972, (1987); W.Kang, D.Jérome, C.Lenoir, P.Batail, Synth. Metals **27**, A353 (1988)

[472] W.Kang, G.Montambaux, J.R.Cooper, D.Jérome, P.Batail, C.Lenoir, Phys. Rev. Letters **62**, 2559 (1989)

[473] W.Schmidt, E.Balthes, D.Schweitzer, to be published

[474] M.V.Kartsovnik, P.A.Kononovich, V.N.Laukhin, S.I.Pestoskii, I.F.Schegolev, Eksp. Teor. Fiz. **49**, 453 (1989) [JETP Lett. **49**, 519 (1989)]

[475] V.N.Laukhin, M.V.Kartsovnik, S.I.Pestoskii, P.A.Kononovich, I.F.Schegolev, Synth. Metals **41-43**, 2453 (1991)

[476] J.Kuebler, M.Weger, C.B.Sommers, Sol. State Commun. **62**, 801 (1987)

[477] T.Mori, A.Kobayashi, Y.sasaki, H.Kobayashi, G.Saito, H.Inokuchi, Chem. Lett. **957**, (1984)

[478] J.Wosnitza, G.Goll, D.Beckmann, S.Wanka, D.Schweitzer, W.Strunz, J. Phys. I France **6**, 1597 (1996)

[479] H.Kobayashi, R.Kato, A.Kobayashi, Y.Nishio, K.Kajita, W.Sasaki, Chem. Lett. **1986**, pp. 789 and 833 (1986); K.Kajita, Y.Nishio, S.Moriyama, W.Sasaki, R.Kato, H.Kobayashi, A.Kobayashi, Sol. State Commun. **64**, 1297 (1987)

[480] H.Kobayashi, R.Kato, A.Kobayashi, S.Moriyama, Y.Nishio, K.Kajita, W.Sasaki, Chem. Lett. **1986**, 2017 (1986); H.Kobayashi, R.Kato, A.Kobayashi, T.Mori, H.Inokuchi, Y.Nishio, K.Kajita, W.Sasaki, Synth. Metals **27**, A289 (1988)

[481] K.Kajita, Y.Nishio, T.Takahashi, W.Sasaki, R.Kato, H.Kobayashi, A.Kobayashi, Sol. State Commun. **70**, 1181 (1989)

[482] M.Tokumoto, A.G.Swanson, J.S.Brooks, M.Tamura, H.Tajima, H.Kuroda, Sol. State. Commun. **75**, 439 (1990)**;** M.Tokumoto, A.G.Swanson, J.S.Brooks, C.C.Agosta, S.T.Hannahs, N.Kinoshita, H.Anzai, M.Tamura, H.Tajima, H.Kuroda**,** A.Ugawa, K.Yakushi Physica B **184**, 508 (1993)

[483] T.Terashima, S.Uji, H.Aoki, M.Tamura, N.Kinoshita, M.Tokumoto, Sol. State Commun. **91**, 595 (1994); Synth. Metals **70**, 847 (1995)

[484] T.Terashima, S.Uji, H.Aoki, M.Tamura, N.Kinoshita, M.Tokumoto, Synth. Metals **70**, 847 (1995)

[485] M.Tokumoto, A.G.Swanson, J.S.Brooks, C.C.Agosta, S.T.Hannahs, N.Kinoshita, H.Anzai, M.Tamura, H.Tajima, H.Kuroda, J.R.Anderson in: *Organic Superconductivity,* ed. by V.Z.Kresin, W.A.Little, Plenum New York, p167 (1990); M.Tokumoto, N.Kinoshita, H.Anzai, A.G.Swanson, J.S.Brooks, S.T.Hannahs, C.C.Agosta, M.Tamura, H.Tajima, H.Kuroda, A.Ugawa, K.Yakushi, Synth. Metals **41-43**, 2459 (1991)

[486] A.Nothardt, E.Balthes, D.Schweitzer, to be published

[487] J. Moldenhauer, U.Niebling, T.ludwig, B.Thoma, D.Schweitzer, W.Strunz, H.J.Keller, P.Bele, H.Brunner, Mol. Cryst. Liq. Cryst. Vol. **284**, 161 (1996)

[488] U.Niebling, *Doktorarbeit,* 3.Physikalisches Institut, Universität Stuttgart, Stuttgart, Germany, (1999)

[489] J.Fraxedas, S.Molas, A.Figueras, I.Jimenes, R.Gago, P.Auban-Senzier, M.Goffman, J. Sol. State. Chem. **168**,384 (2002)

[490] J.Fraxedas, contribution the *Vth International Symposium on Crystalline Organic Metals, Superconductors and Magnets (ISCOM),* p. 76 (2003), to be published in J. Phys. IV, (2004)

[491] E.Balthes, A.Nothardt, P.Wyder, D.Schweitzer, Mat. Science Poland, **22**, 285 (2004).

——— * ———

Zusammenfassung

Im Folgenden ist eine deutschsprachige Zusammenfassung der vorliegenden Arbeit gegeben. Sie umreißt in einem Leitfaden die wichtigsten Schwerpunkte bzw. Ergebnisse der einzelnen Kapitel. Dadurch und mit Hilfe einiger ausgesuchter Bilder soll der Einblick in die Arbeit erleichtert werden[1].

Übersicht

Die vorliegende Arbeit konzentriert sich auf Quantenoszillationsexperimente in quasi-zweidimensionalen kristallinen Vielschichtstrukturen organischer Metalle. Die hier vorgestellten Experimente belegen das Auftreten von niedrigen ganzzahligen Landauniveau-Füllfaktoren ν = 1-4 im zweidimensionalen (2D) organischen Metall κ-(BEDT-TTF)$_2$I$_3$. Darüber hinaus ergeben sich aus diesen Messungen starke Anzeichen für das Auftreten des sehr speziellen Füllfaktors ν = ½ im vorliegenden Material. Damit belegen die hier diskutierten Ergebnisse das Auftreten von Elektronenlokalisierung und Elektronenkorrelationen in einem makroskopischen metallischen zweidimensionalen Elektronensystem. Diese Effekte treten im normalleitenden Zustand des organischen Supraleiters κ-(BEDT-TTF)$_2$I$_3$ auf.
Die revolutionäre Entdeckung des ganzzahligen sowie des fraktionierten Quanten-Hall-Effekts (QHE bzw. FQHE) in zweidimensionalen halbleitenden Einschichtsystemen (auf Basis von Si/SiO$_2$-Feldeffekttransistoren bzw. GaAs/AlGaAs-Heterostrukturen) in den 80er Jahren warf u.a. die Frage auf, ob derartige Effekte auch in anderen Materialklassen auftreten könnten und ob sie auch in dreidimensionalen Systemen, d.h. in makroskopischen Kristallen auftreten könnten. Große Anstrengungen wurden zunächst unternommen, um auf Basis von Halbleitern zweidimensionale *Zweischicht*systeme herzustellen, die Kopplung der einzelnen Schichten und das Tunneln von Elektronen zwischen den beiden Schichten zu kontrollieren. Später wurde nach und nach die Anzahl der Schichten erhöht. Diese Entwicklung war motiviert durch die Ergebnisse von theoretischen Arbeiten Mitte der 80er Jahre, wonach die Quanten-Hall-Effekte auch in 2D Zwei- bzw. sogar in Vielschichtsystemen als stabiler Grundzustand eines zweidimensionalen Elektronensystems (2DES) vorhanden sein könnte.
Seither wird mit beachtlichem Aufwand das experimentelle Ziel verfolgt, diese theoretischen Vorhersagen zu überprüfen und möglichst den QHE und den FQHE in Zwei- und schließlich in Vielschichtsystemen nachzuweisen. Das würde nicht nur die beiden Hall-Effekte aus dem Bereich der extremen Zweidimensionalität „befreien“, sondern sehr viele neue Aspekte zu deren Verständnis einbringen und sogar grundlegende neue Fragen aufwerfen.
κ-(BEDT-TTF)$_2$I$_3$ ist in seinem normalleitenden Zustand metallisch und weist eine sehr hohe Elektronendichte ($2*10^{19}$/cm^2) und Elektronenbeweglichkeit (ca. $5*10^8$cm^2/Vs) auf. Diese Werte liegen deutlich über denjenigen, welche 2DES auf Halbleiterbasis erzielen (derzeit ca. 10^{11}/cm^2 bzw. 10^7cm^2/Vs). Ein typischer κ-(BEDT-TTF)$_2$I$_3$-Einkristall besteht aus ca. 10^5 gekoppelten metallischen zweidimensionalen Schichten und kann in exzellenter Qualität als makroskopischer dreidimensionaler Einkristall (ca. 1x2x0.25mm^3 und größer) hergestellt werden. Dennoch zeigt dieses Material zweidimensionale elektronische Eigenschaften unter bestimmten experimentellen Bedingungen, wie im Rahmen der vorliegenden Arbeit gezeigt wird. Im Gegensatz zur charakteristischen Situation in einem 2DES auf Halbleiterbasis, in

[1] Dort wo es keine oder keine gängige Übersetzung für englischsprachige Fachbegriffe gibt, werden auch in der deutschsprachigen Zusammenfassung die englischen Fachbegriffe verwendet.

welchem die (korrelierten) Elektronen sich *alle auf einer einzigen* quantisierten Ladungsträgerbahn im *k*-Raum bewegen, verfolgen die stark korrelierten Ladungsträger in κ-(BEDT-TTF)$_2$I$_3$ eine Reihe von *verschiedenen* Bahnen welche dementsprechend verschiedene, sogar sehr unterschiedliche Landauniveau-Füllfaktoren ν aufweisen. Dies sind die wichtigsten charakteristischen Bedingungen, unter welchen in κ-(BEDT-TTF)$_2$I$_3$ die oben erwähnten Füllfaktoren ν experimentell beobachtet werden.
Darüber hinaus birgt das hier vorwiegend untersuchte organische Metall als durchaus komplexes elektronisches System eine Reihe weiterer Besonderheiten. Sie stellen eine Herausforderung dar für die theoretische Beschreibung eines makroskopischen Systems mit zweidimensionalen elektronischen Eigenschaften, in welchem Quantenlimes ($\nu \approx 1$) und möglicherweise sogar fraktionierte ν auftreten.
Schließlich umfasst die vorliegende Arbeit Experimente zum Einfluss der Quasi-Zweidimensionalität auf die elektronischen Eigenschaften einer Reihe von niederdimensionaler organischer Leiter. Die Auswahl der dabei diskutierten Substanzen beschränkt sich auf solche, die vielversprechend für das Auftreten von vergleichbaren Effekten wie in κ-(BEDT-TTF)$_2$I$_3$ erschienen.

Organische Leiter und zweidimensionale Elektronensysteme

Ein Einblick in die Historie organischer Leiter ist in Kapitel 1 gegeben. Darin werden u.a. die wichtigsten verwendeten Elektronen-Donormoleküle vorgestellt und die auf dem Wege der Elektrokristallisation hauptsächlich auftretenden Strukturen (s. Fig. 1.2) gezeigt. Ausgangspunkt für die hier diskutierten Substanzen ist der Donor **B**is(**e**thylen**d**ithiolo)**t**etra**t**hio**f**ulvalen (BEDT-TTF; s. Fig. 1.1).
Das zweite Kapitel gibt einen Einblick in die verschiedenen Möglichkeiten, ein zweidimensionales Elektronensystem zu realisieren. Die mit Abstand bekanntesten Methoden zur Herstellung von zweidimensionalen Einschichtsystemen basieren auf halbleitenden Ausgangsmaterialien und treten z.B. an Si/SiO$_2$-Grenzschichten von Feldeffekttransistoren bzw. In GaAs/AlGaAs-Heterostrukturen auf (s. Fig. 2.1-2.3). Das metallische Vielschichtsystem κ-(BEDT-TTF)$_2$I$_3$ unterscheidet sich jedoch grundlegend von derartigen Systemen. Ein typischer κ-(BEDT-TTF)$_2$I$_3$-Einkristall ist aufgebaut aus ca. 10^5 alternierenden BEDT-TTF- bzw. I$_3$-Schichten. Eine dieser leitfähigen Ebenen ist in Fig. 2.4.a dargestellt.
Die Seitenansicht in Fig. 2.5 verdeutlicht, dass die höchsten Elektronendichten innerhalb dieser leitfähigen Ebenen um die zentrale C=C Bindung der BEDT-TTF-Moleküle auftreten. Dies verleiht zahlreichen Vertretern dieser organischen Leiter quasi-zweidimensionale elektronische Eigenschaften. κ-(BEDT-TTF)$_2$I$_3$ erhält seine *ausgeprägt* zweidimensionalen Eigenschaften aufgrund seiner hohen elektronischen Anisotropie (ausgedrückt durch das niedrige Verhältnis der Transferintegrale t senkrecht bzw. parallel zu den Ebenen $t_\perp / t_\parallel < 1.5*10^{-4}$). Durch diesen geringen Wert gilt κ-(BEDT-TTF)$_2$I$_3$ als extremstes 2DES in der Klasse der organischen Metalle.

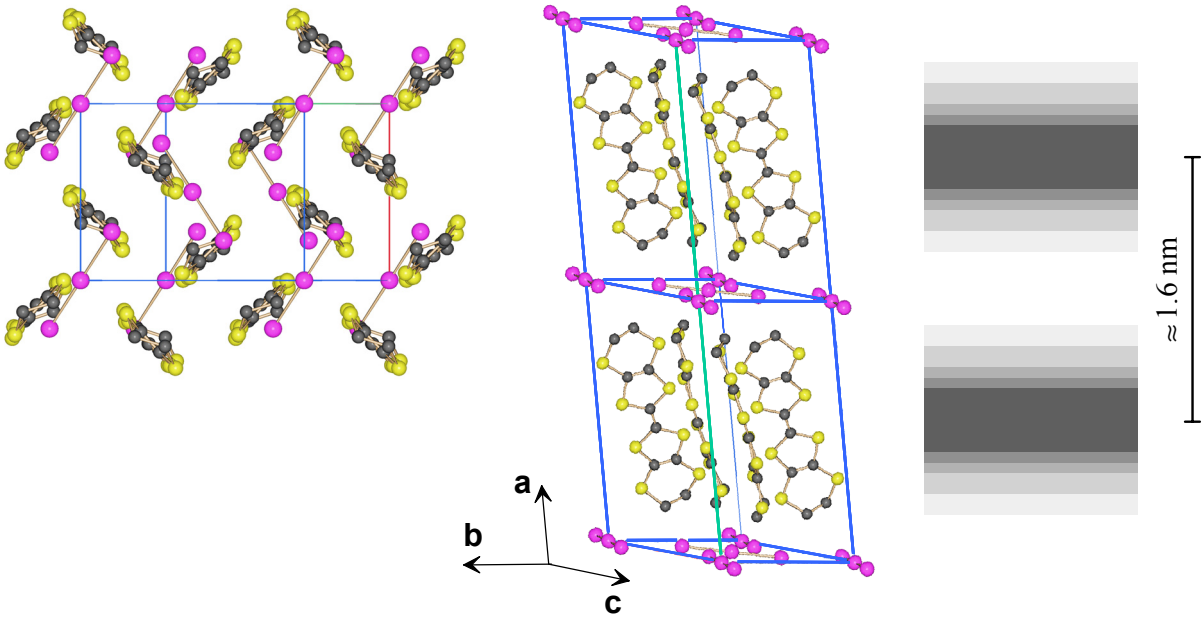

Fig. 2.4.a (links): Blick auf eine einzelne leitfähige (b,c)-Ebene von κ-(BEDT-TTF)$_2$I$_3$. C- (grau) bzw. S-Atome (gelb) des BEDT-TTF-Moleküls mit jeweils darüber bzw. darunter liegender I$_3$-Ebene (magenta).
Fig. 2.5a (Mitte): Seitenansicht auf zwei leitfähige BEDT-TTF-Ebenen von κ-(BEDT-TTF)$_2$I$_3$.
Fig. 2.5b (rechts): Schematische Darstellung der Elektronendichte (steigend mit steigender Graustufe) zur Veranschaulichung der zweidimensionalen Elektronenstruktur.

Theoretische Grundlagen: Beschreibung von Quantenoszillationen in Metallen, ganzzahligem sowie fraktioniertem Quanten-Hall-Effekt (QHE bzw. FQHE)

Der überwiegende Teil der Ergebnisse wurde aus Quantenoszillationsexperimenten, d.h. de Haas-van Alphen- (dHvA) sowie Shubnikov-de Haas- (SdH)-Experimenten an organischen Metallen gewonnen. Dies erfordert eine Einführung in die so genannte Lifshitz-Kosevich- (LK)-Theorie von Quantenoszillationen (s. Kap. 3). Sie beschreibt die zu erwartenden Quantenoszillationsamplituden in Metallen mit dreidimensionalen (3D) elektronischen Eigenschaften (s. Gl. 3.9).
Nachdem sich der experimentelle Teil der Arbeit auf die Diskussion von Anomalien in Oszillationsamplituden verschiedener organischer Materialien konzentriert, werden in den theoretischen Kapiteln (3 und 4) eine Reihe von Effekten besonders hervorgehoben, die Abweichungen bzw. Anomalien in Quantenoszillationen generieren können und den in Kap. 5 diskutierten sehr spezifischen experimentellen Befund an κ-(BEDT-TTF)$_2$I$_3$ erklären könnten. Auf dem Gebiet der Quantenoszillationen in Metallen sind dies insbesondere die in Kap. 3.4 angeführten Effekte:

- **Magnetische Wechselwirkung ('magnetic interaction', MI):**
  Sie beschreibt die Modifikation des externen Magnetfeldes auf Grund der Rückwirkung des magnetischen Moments der Elektronen während einer Quantenoszillation (s. Kap. 3.4.1). Im Falle eines Auftretens von MI entspräche das effektive Magnetfeld nicht mehr dem externen Feld und würde zusätzlich während einer Quantenoszillation nichtlinear variieren. Dies würde zu feld- und temperaturabhängigen Anomalien bzw. Dämpfungen in Quantenoszillationsamplituden führen (s. Fig. 3.2).

- **Magnetischer Zusammenbruch ('magnetic breakdown', MB):**
  Dieser Effekt beschreibt den Durchbruch bzw. das Tunneln von Ladungsträgern zwischen zwei benachbarten Trajektorien im *k*-Raum, welche durch einen endlichen Potentialwall voneinander getrennt sind (s. Fig. 3.3). Die resultierende Variation der Ladungsträger*zahl* auf jeder Bahn führt daher zu Anomalien in den Oszillationsamplituden (s. Kap. 3.4.2).

- **Effekte der Quasi-Zweidimensionalität ('warping' der Fermifläche):**
  Ein quasi-zweidimensionales (Q2D) elektronisches System ist durch eine Fermifläche charakterisiert, welche einem eingeschnürten Zylinder entspricht (s. Kap. 3.4.3). Dies führt zum Auftreten von verschieden großen Extremalflächen auf der Fermifläche, welche mit entsprechend unterschiedlichen Oszillationsfrequenzen zu Quantenoszillationen beitragen (s. Fig. 3.5.a). Die Superposition dieser Beiträge führt zu einer Modifikation der Gesamtamplitude und ist als Einschnürungsknoten (sog. 'warping'-Knoten) erkennbar (s. Fig. 3.6).

- **Effekte ausgeprägter Zweidimensionalität: Oszillationen des chemischen Potentials μ:**
  Die o.g. Standard-LK-Theorie wurde für 3D elektronische Systeme mit einer sphärischen Fermifläche entwickelt. In Gleichung 3.9 ist leicht zu erkennen, dass die verschwindende Krümmung *A"* einer zylindrischen Fermifläche eines 2DES zu einer Divergenz der Quantenoszillationsamplituden *M* führen würden und diese Theorie auf 2DES so nicht mehr anwendbar sein kann. In Kapitel 3.4.4 wird die Modifikation der LK-Theorie für 2DES angerissen. Den größten Einfluss hat dabei die zu erwartende sägezahnartige Oszillation des chemischen Potentials μ in einem 2DES. Sie tritt in einem 2DES (im Gegensatz zum 3DES) deshalb auf, weil die Landauzylinder *die im 2DES ebenfalls zylindrische Fermifläche 'instantan' verlassen*, so dass μ innerhalb eines engen Magnetfeldbereichs auf das nächst niedrigere Landau- d.h. Energieniveau springt (s. Fig. 3.5.b). Dies führt zu sägezahnartigen Sprüngen von μ die u.a. daran von anderen Effekten zu unterscheiden sind, dass die steile Flanke des Sägezahns in μ auf der Hochfeldseite einer solchen Sägezahnoszillation liegt. Im experimentellen Teil werden derartige Sägezahnoszillationen von μ an κ-(BEDT-TTF)$_2$I$_3$ vorgestellt und diskutiert (s. Fig. 5.26, 5.29-30). Ihr Auftreten belegt, dass es sich bei dieser Substanz tatsächlich um ein sehr ausgeprägt zweidimensionales Elektronensystem handelt.

- **Quanteninterferenzen (QI):**
  Quanteninterferenzen können auftreten, wenn im *k*-Raum Knotenpunkte auftreten, die durch unterschiedliche Trajektorien verbunden sind (s. Fig. 3.9). Die Interferenzen der Beiträge dieser unterschiedlichen Trajektorien werden als QI bezeichnet und können Oszillationsamplituden bzw. deren Fourierspektrum modifizieren (s. Kap. 3.4.6).
  Insbesondere in Kap. 3.4.7 werden eine Reihe von charakteristischen Unterscheidungsmerkmalen ausführlich diskutiert, die es erlauben, aus den experimentell gefundenen Fourierspektren die tatsächlich zu Grunde liegenden Effekte zu identifizieren bzw. auszuschließen.

Beschreibung des Ganzzahligen Quanten-Hall-Effekts (QHE)

In Kapitel 5 werden Messungen an κ-(BEDT-TTF)$_2$I$_3$ diskutiert, die u.a. starke Dämpfungen von Quantenoszillationsamplituden im Bereich niedriger ganzzahliger Landauniveau-Füllfaktoren zeigen. Sie werden dort als Anzeichen für eine Elektronenlokalisierung interpretiert, wie sie in 2DES bei hohen Magnetfeldern auftreten kann und im Zusammenhang mit dem QHE bekannt sind. Zum Verständnis dieses Lokalisierungsmechanismus' wird in Kap. 4 die Beschreibung des QHE wiedergegeben. Dabei wird besonders betont, dass der QHE im Einteilchenbild verstanden werden kann, d.h. dass in der Beschreibung des QHE Elektronenkorrelationen nicht berücksichtigt sind.

In Kapitel 4.1.4 wird eine modernere Methode zur Beschreibung des QHE über sog. 'Edge States' bzw. 'Edge Stripes' wiedergegeben. Es sei hier noch einmal hervorgehoben, dass in 'gängigen' d.h. halbleiterbasierten 2DES (z.B. MOSFETS sowie GaAs/AlGaAs-Heterostrukturen) die Fermifläche eine einzige geschlossene Ladungsträgerbahn aufweist, auf der sich alle Ladungsträger bewegen. Im jeweiligen Zentrum eines Landauniveaus liegen nun die mobilen Ladungsträgerzustände (s. Fig. 4.5), während an den Flanken der verbreiteten Landauniveaus die durch Potentiale von Verunreinigungen modifizierten Energiezustände liegen. Die Bewegung dieser Ladungsträger ist wegen des Pauli-Prinzips im Bereich der Verunreinigungen beschränkt, d.h. aus der Sicht einer makroskopischen Längenskala lokalisiert. Liegt nun die Fermienergie in diesem Bereich und ist nur eine einzige Landauniveau-Struktur im System vorhanden (s.o.), so existieren in diesem Bereich (es ist exakt der Bereich des Hall-Plateaus im QHE) keinerlei mobile Ladungsträger, die einen Hall-Strom zwischen den Probenkanten transportieren könnten. Aus dieser Erklärungsnotwendigkeit für das Auftreten eines nicht verschwindenden Hall-Stroms wurde vorgeschlagen, dass im Bereich des Hall-Plateaus der Ladungstransport entlang der Probenkanten mittels 'Edge States' bzw. Edge Stripes' stattfindet (s. Fig. 4.7).
Schließlich wird in diesem Zusammenhang das mögliche Auftreten einer eindimensionalen chiralen Tomonaga-Luttinger-Flüssigkeit an der Probenkante eines 2DES angerissen.

Beschreibung des Fraktionierten Quanten-Hall-Effekts (FQHE)

Nachdem sich herausgestellt hat, dass κ-(BEDT-TTF)$_2$I$_3$ bei hohen Magnetfeldern ein hochgradig korreliertes 2DES bei niedrigen Füllfaktoren darstellt, in welchem ein Teil der Fermifläche sogar den Quantenlimes erreicht (s. Kap. 5.4-5.8), muss zum Verständnis der dort diskutierten Ergebnisse die theoretische Beschreibung des FQHE berücksichtigt werden (s. Kap. 4.2). Der FQHE beschreibt bekanntlich Das Verhalten eines korrelierten 2D Elektronensystems im Bereich des Quantenlimes' und illustriert den Mechanismus, der dort zu Elektronenlokalisierung führen kann (Auftreten von Quasiteilchen mit fraktionierter Statistik, s. Fig. 4.13). Diese Stichworte beschreiben die Schwerpunkte der in Kap. 4.2 wiedergegebenen Beschreibung des FQHE. Es sei hervorgehoben, dass bislang lediglich für den FQHE in Einschicht-2DES eine detaillierte Beschreibung existiert.
Auf Basis der Laughlin'schen Beschreibung des FQHE-Grundzustandes am Beispiel von $\nu = 1/3$ werden die bekanntesten Hierarchie-Modelle für das Auftreten weiterer stabiler Grundzustände diskutiert. Diese Modelle erlauben das Auftreten des FQHE bei sehr viel mehr Füllfaktoren als bisher beobachtet und schließen letztlich sogar das Auftreten beliebiger Füllfaktoren und das Verlassen des unmittelbaren Quantenlimes' nicht aus (s. Kap. 4.2.6).
Die oben erwähnten Quasiteilchen mit fraktionierter Statistik (QTFS) werden als Elementaranregungen eines korrelierten Elektronensystems beschrieben, welches sich selbst wie eine inkompressible 'Laughlin'-Flüssigkeit verhält (s. Kap. 4.2.5). Diese QTFS treten aus energetischen Gründen im Bereich von Verunreinigungen auf und sind dort lokalisiert. Es konnte gezeigt werden, dass das Gesamtsystem seine Gesamtenergie dadurch minimieren kann, dass es diese geladenen Quasiteilchenanregungen durch Elektronen abschirmen lässt, welche dadurch selbst lokalisiert werden. Es kommt also im FQHE zu einer *Koexistenz von mobilen und lokalisierten Elektronenzuständen.*
Trotz der oben erwähnten Hierarchien, die eine Reihe weiterer Füllfaktoren erlauben, stellte sich heraus, dass in einem 2D Einschichtsystem der spezielle Füllfaktor $\nu = ½$ *kein* stabiler Grundzustand ist und der FQHE dort nicht auftreten darf. Stattdessen bleibt das 2DES bei $\nu = ½$ fermionisch und kann sehr elegant mit Hilfe des sog. 'Composite Fermion'-Bildes beschrieben werden. Beim Übergang von Elektronen zu 'Composite Fermions' mittels einer

statistischen Transmutation wird einem Elektron eine bestimmte Anzahl magnetischer Flussquanten angeheftet, die gerade bewirkt, dass sich das so zusammengesetzte Gebilde beim entsprechenden Magnetfeld (d.h. Füllfaktor) gerade wie ein Elektron verhält (s. Kap. 4.2.7). Einfach ausgedrückt gesagt: 'Composite Fermions' zeigen, warum sich ein 2D Einschichtsystem bei $\nu = ½$ wie ein normales Fermi-Gas verhält. Dieses Bild ist daher nicht geeignet um zu zeigen, warum ein 2D Vielschichtsystem dies nicht tut, sondern einen nichtfermionischen Grundzustand einnimmt.

Die Stabilitätskriterien für den FQHE und damit die erlaubten Füllfaktoren ändern sich drastisch beim Übergang von einem Einschicht- zu einem 2D Zwei- bzw. Vielschichtsystem (s. Kap. 4.2.8).
Erste Ansätze für die theoretische Beschreibung eines 2D Zweischichtsystems wurden Mitte der 80er Jahre veröffentlicht. Sie beschränkten sich zunächst auf die Behandlung entkoppelter und dann gekoppelter Schichten, ohne Elektronentunneln zwischen den Schichten zuzulassen. Einer der Gründe für diese Restriktionen sind die Probleme bei der Diagonalisierbarkeit der entsprechenden Hamiltonian. Es stellte sich heraus, dass sowohl QHE als auch FQHE weiterhin auftreten dürfen, wobei die Auswahl der erlaubten Füllfaktoren sich ändert. Insbesondere wird der FQHE bei einem Füllfaktor von jeweils ½ in jeder Schicht möglich. Sobald Tunneln zwischen den Schichten zugelassen ist, wird das Gesamtsystem mit dem totalen Füllfaktor des Gesamtsystems beschrieben. Dieser kann nun den Wert ½ annehmen, so dass FQHE und Elektronenlokalisierung bei $\nu = ½$ auftreten können. Der $\nu = ½$-Grundzustand wird dadurch stabil, dass die aus Einschichtsystemen bekannten innerhalb der Ebenen vorhandenen Elektronenkorrelationen zusätzlich durch Korrelationen *zwischen* den Ebenen stabilisiert werden. Damit wird der im 2D Einschichtsystem verbotene $\nu = ½$-Zustand im Zwei- und auch im Vielschichtsystem nicht nur erlaubt, sondern seine Stabilität steigt sogar mit dem Grad des Tunnelns, d.h. der Ebenenkopplung.
Diese theoretischen Vorhersagen haben seit Mitte der 80er Jahre die sehr intensive Suche nach dem QHE und insbesondere nach dem FQHE und dem $\nu = ½$-Zustand in 2D Zwei- und Vielschichtsystemen stimuliert. Dabei hat sich bisherige Suche auf stetig optimierte halbleiterbasierte 2DES konzentriert.

Experimenteller Teil: Elektronische Eigenschaften verschiedener quasi-zweidimensionaler organischer Metalle

Der Schwerpunkt der in Kap. 5 und 6 vorgestellten experimentellen Untersuchungen liegt beim Vielschichtsystem κ-(BEDT-TTF)$_2$I$_3$ (s. Kap. 5), da es zurzeit die ausgeprägtesten zweidimensionalen elektronischen Eigenschaften innerhalb dieser Substanzklasse aufweist. Die Fermifläche dieses Materials besteht aus zwei bislang durch Bandstrukturrechnungen nachgewiesenen Extremalbahnen um A_2 bzw. A_3 mit den dazugehörigen Quantenoszillationsfrequenzen $F_2 = 570$T und $F_3 = 3883$T (s. Fig. 5.10).
Neben einer Auswahl allgemeiner elektronischer sowie supraleitender Eigenschaften von κ-(BEDT-TTF)$_2$I$_3$ werden am Anfang von Kap. 5 u.a. die wichtigsten aus Quantenoszillationsexperimenten ermittelten fermiologischen Daten zusammengestellt und mit den Ergebnissen von Bandstrukturrechnungen verglichen. Es sind dies z.B. die effektiven Massen m^*_{Fj} der Ladungsträger auf den Umlaufbahnen zu den Frequenzen F_2, F_3, sowie einer neu gefundenen Frequenz $F_1 = 100$T, die Streuzeiten und die damit verbundenen sog. Dingle-Temperaturen T_D sowie Streulängen τ, die Fermi-Wellenvektoren k_F, -Geschwindigkeiten v_F sowie die Flächeninhalte der zugehörigen Extremalbahnen A_j auf der Fermifläche.

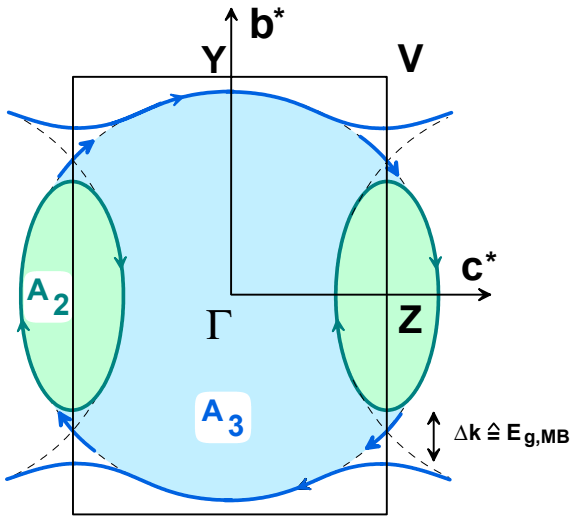

Fig. 5.10: Fermifläche von κ-(BEDT-TTF)$_2$I$_3$. Die elliptische geschlossene Bahn um A_2 entspricht der Oszillationsfrequenz F_2 = 570T, während die kreisförmige Bahn der Fläche A_3 erst geschlossen wird, sobald die Energielücke zwischen V und Z durch den MB überwunden wird. A_3 entspricht der Frequenz F_3 = 3883T.

Weiterhin werden die *g*-Faktoren bestimmt und die Energielücke $E_{g,MB}$ abgeschätzt, die durch den magnetischen Zusammenbruch überwunden wird. Als Quantifizierung der Zweidimensionalität wird das 'warping' $\equiv t_\perp / t_\parallel$, d.h. die prozentuale Abweichung der Fermifläche vom perfekten Zylinder eines idealen 2DES bestimmt. Der sehr niedrige ermittelte Wert $t_\perp / t_\parallel < 1.5*10^{-4}$ identifiziert κ-(BEDT-TTF)$_2$I$_3$ als das derzeit ausgeprägteste zweidimensionale System in der Klasse der organischen Metalle.
Dieses Ergebnis erfordert die Überprüfung der Gültigkeit und Grenzen der an sich für 3D Metalle entwickelten LK-Theorie der Quantenoszillationen (s. Kap. 5.3). Es stellte sich heraus dass in diesem Zusammenhang der *Winkel* Θ zwischen der externen *Magnetfeldrichtung* und den *leitfähigen Ebenen* der κ-(BEDT-TTF)$_2$I$_3$-Einkristalle *ausschlaggebend* ist. Dabei bezeichnet Θ = 0° die Feldorientierung *genau senkrecht* zu den leitfähigen Ebenen und ist im Folgenden besonders wichtig (s. Fig. 5.22).
Umfangreiche Untersuchungen der Temperatur- Feld- und Winkelabhängigkeit der Quantenoszillationsamplituden haben gezeigt, dass die LK-Theorie der Quantenoszillationen im gesamten untersuchten Winkelbereich Θ ≠ 0° sehr gut anwendbar ist, obwohl das hier untersuchte Material ein nahezu perfektes 2DES ist (s. Kap. 5.3). Geringere Abweichungen der Oszillationsamplituden von deren LK-Werten können durch die Einflüsse der Oszillation von μ auf Grund der Zweidimensionalität erklärt werden.
Bei Θ = 0° hingegen treten anomale starke Dämpfungen der SdH-Amplituden auf, die mit steigenden Feld (≥12T) und sinkender Temperatur (≤1K) extrem zunehmen (s. Fig. 5.14-16). Die Diskussion möglicher Ursachen kommt zu dem Schluss, dass es derzeit keine theoretische Erklärung (z.B. aus den Bereichen Fermiologie, Quantenoszillationen in 3D und 2DES, Phasenübergänge, Interferenzeffekte) gibt, die derartig drastische Dämpfungen und insbesondere ihre starke Beschränkung auf die spezielle Feldorientierung Θ = 0° erklären könnte.
Der Schlüssel zu einem möglichen Verständnis deren Ursache ist die Veranschaulichung dessen, was die Feldorientierung Θ = 0° gegenüber allen anderen Orientierungen Θ ≠ 0° auszeichnet (s. Fig. 5.22). Diese schematische Darstellung zeigt, dass Θ = 0° die *einzige Magnetfeldorientierung* darstellt, bei der in einem *metallischen Vielschichtsystem* die Ladungsträger auf ihren *Zyklotronbahnen innerhalb der leitfähigen Ebenen* verbleiben, bis sie gestreut werden. Das bedeutet, dass ausschließlich bei Θ = 0° die intrinsische Zweidimensionalität des Systems ungestört zum Tragen kommen kann.

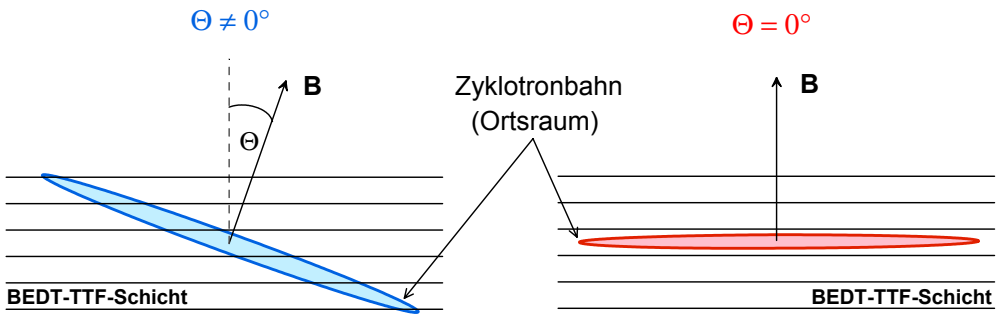

Fig. 5.22: Zyklotronbahn im Ortsraum (schematisch) in einem 2D Vielschicht-Metall wie z.B. κ-(BEDT-TTF)$_2$I$_3$. Die waagerechten Linien deuten die einzelnen leitenden BEDT-TTF-Schichten an. **Links:** Bei $\Theta \neq 0°$ verlassen die Ladungsträger die leitfähigen Ebenen (hier: idealisierte Bahn) **rechts:** Bei $\Theta = 0°$ verbleiben die Ladungsträger in der jeweiligen Ebene.

Die Tatsache, dass elektronische Zweidimensionalität bei hohen Magnetfeldern zu Elektronenlokalisierung führen kann, warf die Frage auf, ob die starken Dämpfungen der SdH-Amplituden von κ-(BEDT-TTF)$_2$I$_3$ im Hochfeld als ein Verlust von Elektronen durch Lokalisierung eines Teils der Ladungsträger verstanden werden könnte. Die Diskussion von Fig. 5.22 veranschaulicht, warum dieser Effekt der Zweidimensionalität in einem derartigen Vielschicht-Metall nur bei $\Theta = 0°$ zu erwarten ist.
Die Überprüfung dieser Idee warf die Frage nach den Füllfaktoren auf: Währen die quantisierten Hall-Effekte und die damit verbundene Elektronenlokalisierung bislang lediglich bei niedrigen Füllfaktoren (ca. $\nu \leq 5$) beobachtet wurde, wiesen die bislang bekannten Extremalbahnen in κ-(BEDT-TTF)$_2$I$_3$ Füllfaktoren von ca. 50 bis über 100 auf. Diese Extremalbahnen beruhten jedoch auf Bandstrukturrechnungen aus den 80er Jahren, die mit geringen Rechnerleistungen und unter erheblichen vereinfachenden Annahmen durchgeführt wurden, so dass die Möglichkeit besteht, dass dabei kleine Taschen auf der Fermifläche unberücksichtigt blieben. Dies motivierte zur experimentellen Suche nach niedrigen Füllfaktoren in κ-(BEDT-TTF)$_2$I$_3$ also niedrigen Oszillationsfrequenzen und in der Tat konnte nach aufwändigen Messungen eine neue Frequenz F_0 = 13T gefunden werden (Fig. 5.23-24).
Mehr noch, nach weiteren detaillierten Messungen stellte sich heraus, dass tatsächlich F_0 unmittelbar für die Dämpfungen in den Amplituden von F_2 und F_3 verantwortlich war und zwar in der Weise, dass die Dämpfungen besonders stark bei ganzzahligen ν von F_0 waren.
Die Tatsache, dass F_0 offensichtlich dazu in der Lage ist, seine eigenen Eigenschaften (Füllfaktoren) dem Gesamtsystem aufzuzwingen, d.h. das Verhalten *aller* Elektronen zu bestimmen, beweist das Auftreten starker Elektronenkorrelationen in diesem 2D Material. Im Hochfeld bringt F_0 mit $\nu = 2$ das Gesamtsystem sogar in die Nähe des Quantenlimes'. Dies und der Zusammenhang der Dämpfungen mit den ganzzahligen ν von F_0 bestätigte die Vermutung, dass die starken Dämpfungen in den Amplituden von F_2 und F_3 bei $\Theta = 0°$ tatsächlich mit der Lokalisierung eines Teils der Elektronen zu tun haben können.
Es konnte zwar gezeigt werden, dass diese neue niedrige Frequenz F_0 nicht auf fermiologische Effekte (wie z.B. ein 'warping' der Fermifläche oder aber Interferenzeffekte) zurückzuführen ist, dennoch blieb auf Grund des indirekten Nachweises von F_0 zunächst die Frage offen, ob F_0 mit einer tatsächlich existierenden Umlaufbahn und einer entsprechenden Landauniveau-Struktur identifiziert werden kann. Auf der Suche nach einer thermodynamischen Größe, welche die Existenz von F_0 überprüfen könnte, wurde im Rahmen dieser Arbeit eine zwar aufwändige aber dennoch im Prinzip sehr einfache Methode entwickelt und erfolgreich eingesetzt,

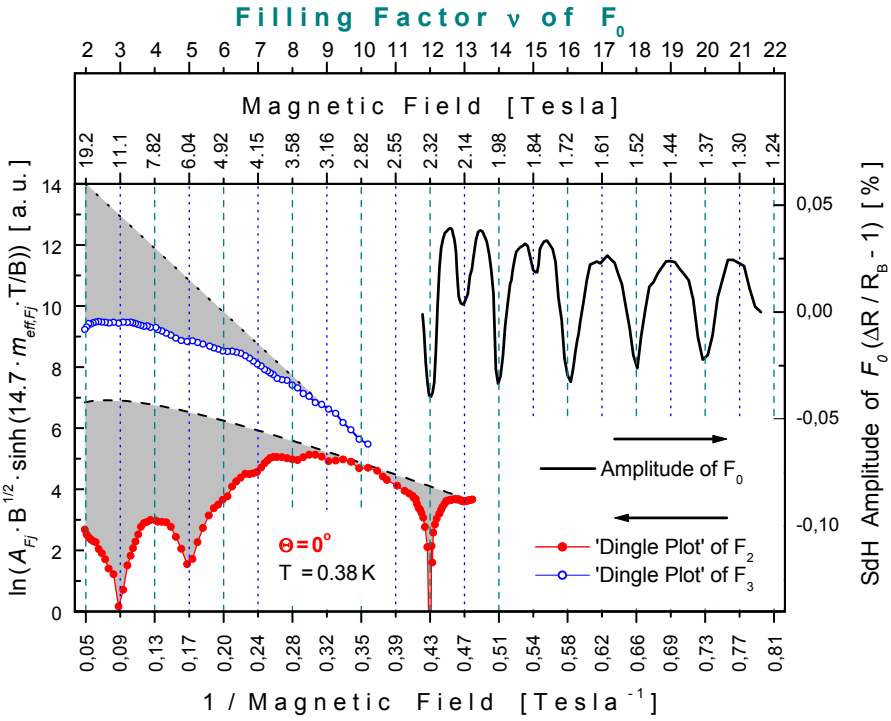

Fig. 5.24: rechts: SdH-Oszillationen mit F_0 in κ-(BEDT-TTF)$_2$I$_3$-Einkristallen bei 0°. Obere Abszisse: Füllfaktor ν von F_0. **links:** 'Dingle plots' (vgl. Kap. 3.2.3) der FFT-Amplituden A_{Fj} von F_2 und F_3 (A_{fj}-Werte stammen jeweils aus engen benachbarten Feldfenstern). Die effektiven Massen m^*_{F2} = 1.9 bzw. m^*_{F3} = 3.9 wurden berücksichtigt. Die gestrichelte und gepunktete Kurve markiert jeweils den erwarteten Amplitudenverlauf. Die grau unterlegten Flächen illustrieren die starken Dämpfungen im Hochfeld bei 0°.

die Position des chemischen Potentials μ und seine Variation mit dem Magnetfeld mit sehr hoher Auflösung unmittelbar zu detektieren (s. Fig. 5.25). Mit den so detektierten sägezahnartigen Oszillationen von μ mit F_0 (s. Fig. 5.26) konnte die Existenz von F_0 mit Hilfe einer thermodynamischen Größe eindeutig nachgewiesen werden. Darüber hinaus sind sowohl die scharfe Sägezahnform der μ-Oszillationen, als auch die Orientierung des Sägezahns (steile Flanke zur Hochfeldseite) weitere anschauliche Belege für die extreme Zweidimensionalität des Systems, einschließlich des zu F_0 gehörenden Teils.
Dennoch blieb die Frage zunächst offen, warum bei den bestimmten Feldwerten B^{-1} = 0.09T^{-1}, 0.17T^{-1}, 0.43T^{-1} die Dämpfungen besonders drastisch sind. Nachdem auch dafür keinerlei konventionelle Erklärung gefunden werden konnte, wurde der Möglichkeit nachgegangen, dass eine zusätzliche, noch niedrigere Frequenz im System vorhanden sein könnte. Unter weiter erhöhtem Aufwand wurden SdH-Messungen ins Niedrigfeld ausgedehnt. Tatsächlich konnte damit die Existenz einer neuen, sehr niedrigen Oszillationsfrequenz F_{neu} = 3.8T nachgewiesen werden, inklusive sägezahnartiger Oszillationen von μ mit F_{neu} (s. Fig. 5.30). Diese Messungen erlauben eine eindeutige Zuordnung der ganzzahligen Füllfaktoren ν_{Fneu} = 4,3,2,1. Insbesondere ν_{Fneu} = 1 ist dadurch eindeutig festgelegt, dass bei endlichen Feldern (also $\nu \geq 0$) kein weiteres niedrigeres Landauniveau platziert werden kann, ohne dass die Äquidistanz der einzelnen Landauniveaus verletzt werden müsste (s. Kap. 5.7). Damit ist B^{-1} = 1.71T^{-1} als ν_{Fneu} = 1 ≡ Quantenlimes identifiziert. Der untere Teil des Bildes zeigt, dass gerade diese niedrigen ν_{Fneu} für die extremsten Dämpfungen der Oszillationsamplituden verantwortlich sind und bestätigt erneut die Vermutung von Elektronenlokalisierung als deren Ursache. Unterhalb von ν_{Fneu} = 1 tritt jedoch eine weitere starke Dämpfung auf, die mit keinem ganzzahligen ν_{Fneu} identifiziert werden kann.

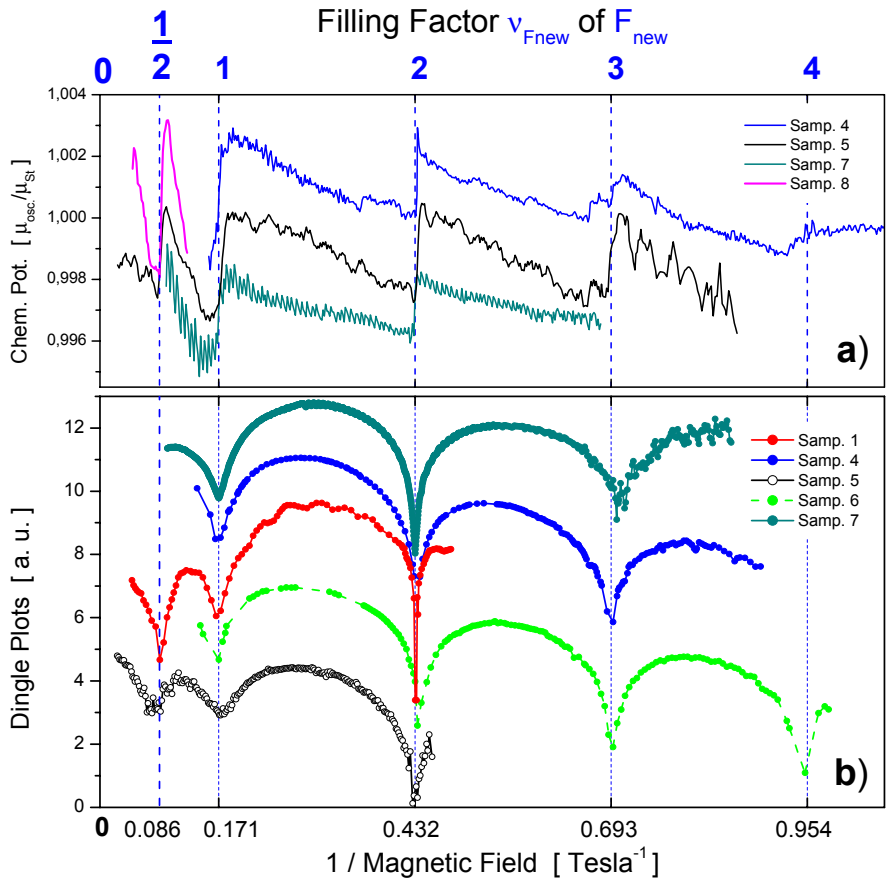

Fig. 5.30: Identifizierung der Füllfaktoren ν_{Fneu} von F_{neu}=3.8T im organischen 2D Vielschicht-Metall κ-(BEDT-TTF)$_2$I$_3$. **a)** Sägezahn-Oszillationen des Chemisches Potentials (an verschiedenen Proben) aufgetragen über ν_{Fnew} (vgl. Fig. 5.29). **b)** 'Dingle plots' aus SdH-Messungen an verschiedenen Einkristallen bei Θ = 0° (vgl. Fig. 5.27-28). Es ist zu beachten dass die x-Achsen in a) und b) bei unendlichem Magnetfeld d.h. ν ≡ 0 enden.

Das Bild zeigt, dass diese Dämpfung genau zwischen $\nu_{Fneu} = 1$ und $\nu_{Fneu} \equiv 0$ liegt und weist damit klar darauf hin, dass hier tatsächlich $\nu_{Fneu} = ½$ vorliegt. Die Oszillation von μ bei $\nu_{Fneu} = ½$ im oberen Bild bestätigt, dass bei diesem Füllfaktor tatsächlich ein thermodynamisch stabiler Grundzustand vorliegt [491]. Dies entspricht den theoretischen Vorhersagen, wonach in 2D Vielschichtsystemen $\nu_{Fneu} = ½$ im Gegensatz zu Einschichtsystemen auftreten könnte.

Die im Rahmen dieser Arbeit vorgestellten Experimente belegen das Auftreten von niedrigen ganzzahligen Landauniveau-Füllfaktoren ν im zweidimensionalen (2D) organischen Metall κ-(BEDT-TTF)$_2$I$_3$. Darüber hinaus ergeben sich aus diesen Messungen starke Anzeichen für das Auftreten des seit nunmehr fast zwei Jahrzehnten gesuchten sehr speziellen fraktionierten Füllfaktors ν = ½ im vorliegenden Material. Dadurch belegen die hier diskutierten Ergebnisse das Auftreten von Elektronenlokalisierung und Elektronenkorrelationen in einem makroskopischen metallischen zweidimensionalen Elektronensystem. Vergleichende Untersuchungen mir einigen anderen vielversprechenden quasi-zweidimensionalen Vertretern dieser Substanzklasse (s. Kap. 6) haben gezeigt, dass die komplexen Bedingungen (z.B. Zweidimensionalität, niedrige Füllfaktoren und hohe Kristallqualität) für derartige Effekte bislang wahrscheinlich noch nur im 2D organischen Metall κ-(BEDT-TTF)$_2$I$_3$ vereinigt sind.

——— * ———